



VNIVERSITATIS VALÈNCIA

Tests of the Electroweak model  
in the presence of two Higgs doublets

**Paula Tuzón Marco**

IFIC, Departament de Física Teòrica

Tesi Doctoral, 2011

Director: Antonio Pich Zardoya



ANTONIO PICH ZARDOYA, Catedrático del Departamento de Física Teòrica de la Universitat de València,

CERTIFICA:

Que la presente memoria “TESTS OF THE ELECTROWEAK MODEL IN THE PRESENCE OF TWO HIGGS DOUBLET” ha sido realizada bajo su dirección en el Departamento de Física Teórica de la Universitat de València, por PAULA TUZÓN MARCO y constituye su Tesis para optar al grado de Doctor en Física.

Y para que así conste, en cumplimiento de la legislación vigente, presenta en el Departamento de Física Teórica de la Universitat de València la referida Tesis Doctoral, y firma el presente certificado.

València, a 30 de Juny de 2011.

Antonio Pich Zardoya



*Als meus pares,  
a Carlos,  
i clarament, a Pau.*



# Contents

<b>1</b>	<b>Introducció</b>	<b>1</b>
1.1	El Model Estàndard: Un breu repàs . . . . .	1
1.2	Dinàmica de Sabor en la teoria Electrofeble . . . . .	3
1.2.1	Determinació de $V_{ij}$ . . . . .	6
1.2.2	Perspectives . . . . .	10
<b>2</b>	<b>Introduction</b>	<b>13</b>
2.1	The Standard Model: Short overview . . . . .	13
2.2	Flavour dynamics in the Electroweak theory . . . . .	15
2.2.1	Determination of $V_{ij}$ . . . . .	18
2.2.2	Prospects . . . . .	21
<b>3</b>	<b>The two-Higgs-doublet model</b>	<b>23</b>
3.1	Introduction . . . . .	23
3.2	The general two-Higgs-doublet model . . . . .	24
3.2.1	The potential . . . . .	26
3.2.2	Gauge boson interactions . . . . .	31
3.2.3	Yukawa interactions . . . . .	33
<b>4</b>	<b>The general two-Higgs-doublet model: LFV tests</b>	<b>37</b>
4.1	Introduction . . . . .	37
4.2	The model discriminating power of $\mu \rightarrow e$ conversion in nuclei . . . . .	38
4.3	LFV effective interaction and the $\mu \rightarrow e$ conversion rate . . . . .	39
4.3.1	Effective Lagrangian . . . . .	39
4.3.2	Transition rates . . . . .	42
4.3.3	Sources of uncertainty . . . . .	43
4.4	Testing the single operator dominance hypothesis . . . . .	44
4.4.1	Dipole, Vector and Scalar models . . . . .	44
4.4.2	$\mu \rightarrow e\gamma$ vs $\mu \rightarrow e$ conversion . . . . .	46
4.4.3	Target dependence of $\mu \rightarrow e$ conversion . . . . .	47
4.5	Testing the two-operator dominance hypothesis . . . . .	49
4.5.1	Dipole-Scalar . . . . .	49
4.5.2	Dipole-Vector . . . . .	50

4.5.3	Scalar-Vector . . . . .	50
4.6	Application to a SUSY model . . . . .	51
4.7	Conclusions . . . . .	52
<b>5</b>	<b>The Aligned two-Higgs-doublet model</b>	<b>61</b>
5.1	Introduction . . . . .	61
5.2	The model . . . . .	62
5.3	Quantum corrections . . . . .	63
<b>6</b>	<b>Charged Higgs phenomenology in the Aligned two-Higgs-doublet model</b>	<b>67</b>
6.1	Introduction . . . . .	67
6.2	Inputs and statistical treatment . . . . .	68
6.3	Tree-level decays . . . . .	70
6.3.1	Lepton decays . . . . .	70
6.3.2	Leptonic decays of pseudoscalar mesons . . . . .	71
6.3.3	Semileptonic decays of pseudoscalar mesons . . . . .	75
6.3.4	Global fit to leptonic and semileptonic decays . . . . .	79
6.4	Loop-induced processes . . . . .	79
6.4.1	$Z \rightarrow b\bar{b}$ . . . . .	80
6.4.2	$B^0$ - $\bar{B}^0$ mixing . . . . .	82
6.4.3	$K^0$ - $\bar{K}^0$ mixing: $\epsilon_K$ . . . . .	84
6.4.4	$\bar{B} \rightarrow X_s \gamma$ . . . . .	84
6.5	CP Asymmetries in $B$ -systems . . . . .	89
6.5.1	$\bar{B} \rightarrow X_s \gamma$ . . . . .	90
6.5.2	$B^0$ - $\bar{B}^0$ . . . . .	93
6.6	Discussion . . . . .	96
<b>7</b>	<b>The two-Higgs-doublet model in the presence of an extra <math>U(1)</math> gauge boson</b>	<b>103</b>
7.1	Introduction . . . . .	103
7.2	The model . . . . .	104
7.3	Heavy gauge boson searches . . . . .	108
7.3.1	$Z'$ to fermions . . . . .	109
7.3.2	$Z'$ to bosons . . . . .	110
7.3.3	Results . . . . .	111
7.4	Conclusions . . . . .	112
	<b>Conclusions</b>	<b>118</b>
	<b>Conclusions</b>	<b>120</b>
<b>A</b>	<b>Higgs potential formulae</b>	<b>123</b>
A.1	Basis dependent potential parameters . . . . .	123
A.2	Higgs self-couplings . . . . .	124

---

<b>B <math>\Delta F = 2</math> effective Hamiltonian</b>	<b>127</b>
B.1 $\Delta B = 2$ . . . . .	127
B.2 $\Delta S = 2$ . . . . .	130
<b>Bibliography</b>	<b>131</b>
<b>Acknowledgements</b>	<b>151</b>

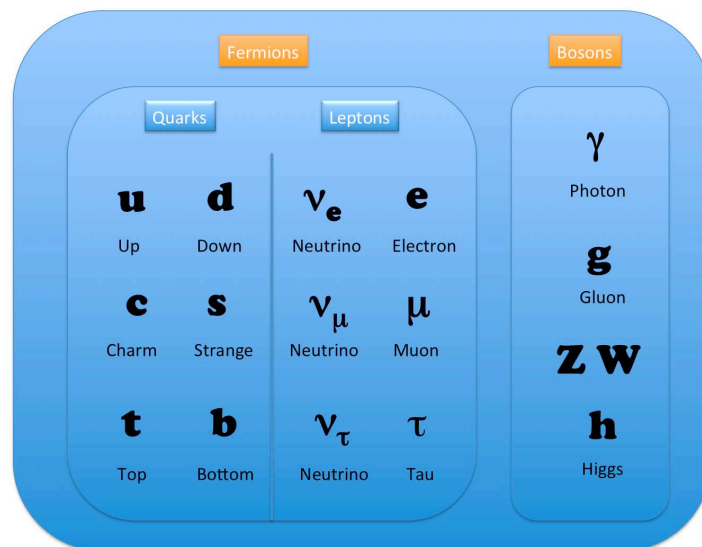


# Capítol 1

## Introducció

### 1.1 El Model Estàndard: Un breu repàs

De què està feta la matèria? Quin tipus de forces dominen l'Univers? Quines són les lleis fonamentals de la Natura? Aquestes grans preguntes han sigut de gran interès per a molts científics en la història. Un dels principals objectius sempre ha sigut entendre com es comporten els components bàsics de la matèria. De fet, quan a un conegut físic li van preguntar sobre què deixaria com a llegat a una hipotètica nova civilització intel·ligent, en cas de què el món fos destruït, ell va respondre que escriuria en un troç de paper menut que “*la matèria està feta d'àtoms*”. Açò se sap des de fa ja molts anys. Tots els àtoms presents en la natura s'han entès i organitzat en una taula d'acord a les seues propietats. Ara bé, també sabem que aquest no és el final, totes eixes espècies tenen una estructura *subatòmica* formada per les anomenades *partícules elementals*, considerades per ara els components més fonamentals de la matèria.



Què són aquestes partícules i com interaccionen són qüestions que el Model Estàndard de la Física de Partícules resol d'una manera prou exitosa. Les partícules elementals són molt petites ( $\sim h$ ) i molt ràpides ( $\sim c$ ), el que implica que tant la Mecànica Quàntica com la Relativitat Especial són necessàries alhora per tal de descriure el seu comportament,  $\lambda = h/p$ . Però, només ajuntant ambdues teories no és suficient, per a un bon enteniment de la “probabilitat”, la noció d'una teoria de camps també ha de ser introduïda. El Model Estàndard (SM) és aleshores una teoria quàntica de camps que descriu la interacció electrofeble i la forta (amb la teoria Electrofeble (EW) i la Cromodinàmica Quàntica (QCD) respectivament), existents entre els quarks i els leptons. Aquests són el contingut de matèria fermiònica i apareixen replicats en tres famílies (mireu la taula de dalt), amb l'única diferència essent la massa i el número quàntic de sabor. Només els quarks interaccionen fortament, ambdós, quarks i leptons, interaccionen dèbilment i, a més, els quarks i els leptons carregats interaccionen electromagnèticament. En teoria de grups, les partícules elementals són les representacions irreductibles del grup de Poincaré, que està format per translacions, rotacions i *boosts*; les càrregues conservades d'aquesta simetria caracteritzen a la perfecció les nostres partícules lliures, però no les interaccions. Per tant, és necessari altre tipus de simetria per tal d'introduir les forces en la teoria. Aquesta és la simetria de *gauge* local, la càrrega conservada de la qual és la càrrega de la interacció corresponent i els generadors donen el nombre de partícules intermediàries requerides, que són camps d'spin 1: huit gluons sense massa per a QCD, els massius  $W^\pm$  i  $Z$  per a la interacció dèbil, i un fotó sense massa per l'electromagnetisme. És per açò perquè el SM és una teoria de *gauge local* basada en el grup de simetria  $G \equiv SU(3)_C^{QCD} \otimes [SU(2)_L \otimes U(1)_Y]^{EW}$ .

Ara bé, els termes de massa per als camps en el Lagrangian trenquen aquesta simetria de *gauge* local, volent dir que el model necessita un mecanisme ad-hoc per a generar partícules massives, i.e. per a proporcionar resultats no simètrics en *gauge* però preservant la simetria a nivell del Lagrangian. Aquesta doble condició es realitza fent ús del mecanisme de Higgs-Kibble, que aplica el Teorema de Goldstone en el context de la teoria EW. El mecanisme introdueix la idea del trencament *espontani* de la simetria (SSB), assumint un Lagrangian simètric en *gauge* amb un buit no simètric que trenca la part EW del grup en el subgrup Electromagnètic,  $G \rightarrow SU(3)_C \otimes U(1)_{em}$ . Açò s'implementa amb l'existència d'un camp escalar doblet d' $SU(2)$  amb càrrega elèctrica zero i hipercàrrega 1 la interacció del qual amb el buit és no nul·la (adquireix un valor d'expectació en el buit),  $\langle 0|\phi^{(0)}|0 \rangle = v/\sqrt{2}$ . El camp escalar anomenat Higgs, després del trencament de la simetria *gauge*, es pot definir com una excitació del seu estat fonamental. La interacció del Higgs amb les partícules fermiòniques, amb els bosons de *gauge* intermediaris a través de la derivada covariant i amb ell mateix, és allò que proporciona les seues masses. Aquestes estan definides per l'acoblament d'eixos camps, a través de la interacció que acabem d'indicar, amb el valor d'expectació no nul del Higgs.

Amb aquesta descripció, el SM (per a una revisió mireu e.g. [1]) és capaç d'explicar la majoria de les observacions experimentals, algunes d'elles amb moltes xifres de precisió. A més, totes les partícules predites ja s'han observat, a excepció del Higgs. Nogensmenys, malgrat l'enorme èxit en explicar la fenomenologia, el SM deixa moltes preguntes sense

resposta, volent dir que encara que la teoria sembla correcta, està de segur incompleta. Hi ha alguns grans “problemes” sense resoldre, com ara la implementació de la Gravetat dins el mateix context de teoria *gauge*, la Gran Unificaió de totes les forces (no només de la dèbil i l’electromagnètica) o la descripció del  $\sim 96\%$  de l’Univers que no està compost per matèria ordinària (SM), sinó per matèria fosca ( $\sim 22\%$ ) i energia fosca ( $\sim 74\%$ ). Ara bé, a part d’aquestes, hi ha altres qüestions (potser relacionades amb elles o potser no) que afecten directament a l’estructura de sabor del model. Una primera qüestió seria per què *tres* és el nombre de famílies i no més, i si en són *més*, quantes. També, per què el patró de masses i mescles és com és, si totes elles venen de la mateixa interacció electrofeble amb el Higgs. Com que aquest patró està directament relacionat amb el trencament espontani de la simetria electrofeble, i.e. amb el sector escalar, està aquest sector escalar *ocult* ocultant alguna cosa més? És només la massa allò que diferencia cada família? Què hi ha de la massa dels neutrins? Pot existir una bona descripció dels fenòmens observats que violen CP? Quin és l’origen del sabor? El sector de sabor fermiònic és la font de paràmetres lliures més important en el SM, amb neutrins sense massa ja hi ha 9 masses, 3 angles de mescla i 1 fase complexa. Si a més tenim en compte que són, de fet, massius, el nombre de paràmetres augmenta almenys en 7. Mecanismes de nova física que puguen donar respostes a totes estes preguntes són, per tant, necessaris d’investigar.

En particular, en aquesta tesi tenim l’objectiu d’estendre el sector escalar (ocult) més enllà de la versió mínima donada al SM, ja que no hi ha res que no ho permeta, i analitzarem l’impacte en l’estructura de sabor i els corresponents nous fenòmens.

## 1.2 Dinàmica de Sabor en la teoria Electrofeble

El SM organitza els fermions observats en tres famílies, còpies de la mateixa estructura  $SU(2)_L \otimes U(1)_Y$ , essent l’única diferència la massa i el sabor. Els camps levogirs són doblats d’ $SU(2)_L$  mentre que els dextrogirs són singlets d’ $SU(2)_L$ ,

$$\left( \begin{array}{c} u' \\ d' \end{array} \right)_L, \quad \left( \begin{array}{c} \nu'_l \\ l' \end{array} \right)_L, \quad u'_R, \quad d'_R, \quad l'_R, \quad (1.1)$$

on  $u$ ,  $d$  i  $l$  són vectors de tres dimensions en l’espai de sabor i la primera indica que són autoestats de *gauge*. En el cas general d’ $N_G$  generacions de fermions,  $u = u, c, t, u_4, \dots, u_{N_G}$ ,  $d = d, s, b, d_4, \dots, d_{N_G}$  i  $l = e, \mu, \tau, l_4, \dots, l_{N_G}$ , el Lagrangiana de Yukawa més general ve donat per

$$\mathcal{L}_Y = - \left\{ (\bar{u}', \bar{d}')_L \left[ c_d \phi d'_R + c_u \tilde{\phi} u'_R \right] + (\bar{\nu}'_l, \bar{l}')_L c_l \phi l'_R \right\} + h.c., \quad (1.2)$$

on  $c_d$ ,  $c_u$  i  $c_l$  són matrius  $N_G \times N_G$  generals de Yukawa complexes corresponents a l’acoblament del doblet escalar  $\phi$  als sectors fermiònics *down*, *up* i leptònic, i  $\tilde{\phi} = i\sigma_2 \phi^*$ . Després del SSB electrofeble, el doblet escalar es pot escriure com

$$\phi = \left( \begin{array}{c} \phi^{(+)} \\ \phi^{(0)} \end{array} \right) \xrightarrow{\text{SSB}} e^{i\frac{\sigma_i}{2}\theta^i} \left[ \begin{array}{c} 0 \\ \frac{1}{\sqrt{2}}(v+h) \end{array} \right], \quad (1.3)$$

on  $\theta_i$  i  $H$  són quatre camps reals. Tres dels quatre graus de llibertat es poden eliminar per la invariància local d' $SU(2)_L$  del Lagrangia,  $\theta_i$ , que no són més que els *would-be* bosons de Goldstone associats amb el SSB. En aquest *gauge*, anomenat Gauge Unitary, el Lagrangia de Yukawa resulta

$$\mathcal{L}_Y = - \left( 1 + \frac{h}{v} \right) \left[ \bar{d}'_L M'_d d'_R + \bar{u}'_L M'_u u'_R + \bar{l}'_L M'_l l'_R \right] , \quad (1.4)$$

on  $M'_f \equiv \frac{v}{\sqrt{2}} c_f$  ( $f = u, d, l$ ). En la base dels autoestats de massa dels fermions

$$\begin{aligned} f_L &= S_f f'_L \\ f_R &= S_f U_f f'_R , \end{aligned} \quad (1.5)$$

on  $S_f$  i  $U_f$  són matrius unitàries, el Lagrangia de Yukawa obté la següent forma:

$$\mathcal{L}_Y = - \left( 1 + \frac{h}{v} \right) \left[ \bar{d}_L M_d d_R + \bar{u}_L M_u u_R + \bar{l}_L M_l l_R \right] , \quad (1.6)$$

on  $M_f = S_f M'_f U_f^\dagger S_f^\dagger$  són les matrius diagonals de massa corresponents als tres sectors fermiònics,

$$\begin{aligned} M_u &= \text{diag}(m_u, m_c, m_t, m_{u_4}, \dots, m_{u_{N_G}}) \\ M_d &= \text{diag}(m_d, m_s, m_b, m_{d_4}, \dots, m_{d_{N_G}}) \\ M_l &= \text{diag}(m_e, m_\mu, m_\tau, m_{l_4}, \dots, m_{l_{N_G}}) . \end{aligned} \quad (1.7)$$

El Lagrangia de Yukawa (1.6) posa de manifest que qualsevol acoblament del camp de Higgs als fermions és proporcional a les seues masses.

Quan anem des del Lagrangia d'autoestats de *gauge* al d'autoestats de massa en interaccions neutres, trobem en el model Electrofeble dos casos diferents:

- Interaccions neutres descrites per l'intercanvi de  $Z_\mu$  i  $A_\mu$  (vector): L'estructura en l'espai de sabor és necessàriament  $\bar{f}'_L f'_L$  (no hi ha cap altra matriu de sabor enmig) o  $\bar{f}'_R f'_R$ . En el Lagrangia d'autoestats de massa estes estructures corresponen directament a  $\bar{f}_L f_L$  i  $\bar{f}_R f_R$ , respectivament. Per tant, no hi ha corrents neutres amb canvi de sabor (FCNCs) a nivell arbre provinents d'interaccions vectorials.
- Interaccions neutres descrites per l'intercanvi d' $h$  (escalar): L'estructura en l'espai de sabor és sempre de la forma  $\bar{f}'_L X_f f'_R$ , on  $X_f$  és en el SM una única matriu de sabor  $N_G \times N_G$  no diagonal que ve de l'acoblament del doblec escalar al sector fermiònic  $f$ . En el Lagrangia d'autoestats de massa l'estructura de sabor esdevé  $\bar{f}_L X_f^D f_R$ , on  $X_f^D$  ha sigut diagonalitzada pel canvi de base. Per tant, tampoc hi ha corrents neutres amb canvi de sabor provinents de les interaccions escalars.

Amb tot, els fenòmens FCNC estan prohibits per l'estructura de sabor en el SM (mecanisme de GIM [2]), la qual cosa està totalment d'acord amb les dades experimentals.

Pel que fa a les interaccions carregades, només hi ha una possibilitat en el model Electrofeble:

- Interaccions carregades descrites per l'intercanvi de  $W_\mu$  (vector i vector-axial): Les estructures en l'espai de sabor tenen la mateixa forma  $\bar{u}'_L d'_L = \bar{u}_L S_u S_d^\dagger d_L = \bar{u}_L V d_L$ , on  $V \equiv S_u S_d^\dagger$  és una matriu de mescla no diagonal complexa i unitària (en general  $S_u \neq S_d$ ), coneguda com la matriu de Cabibbo-Kobayashi-Maskawa (CKM) [3, 4], la qual genera interaccions amb canvi de sabor en el sector carregat de quarks,

$$V = \begin{pmatrix} V_{ud} & V_{us} & V_{ub} & V_{ud_4} & \cdots & V_{ud_{N_G}} \\ V_{cd} & V_{cs} & V_{cb} & V_{cd_4} & \cdots & V_{cd_{N_G}} \\ V_{td} & V_{ts} & V_{tb} & V_{td_4} & \cdots & V_{td_{N_G}} \\ V_{u_4 d} & V_{u_4 s} & V_{u_4 b} & V_{u_4 d_4} & \cdots & V_{u_4 d_{N_G}} \\ \cdots & \cdots & \cdots & \cdots & \cdots & \cdots \\ V_{u_{N_G} d} & V_{u_{N_G} s} & V_{u_{N_G} b} & V_{u_{N_G} d_4} & \cdots & V_{u_{N_G} d_{N_G}} \end{pmatrix}. \quad (1.8)$$

Degut a l'absència de neutrins dextrogirs, els camps levogirs sempre es poden redefinir com  $\bar{\nu}_L = \bar{\nu}'_L S_l^\dagger$  i, conseqüentment, no hi ha una matriu de mescla anàloga a  $V$  en el sector leptònic carregat,  $\bar{\nu}'_{lL} l'_L = \bar{\nu}_{lL} l_L$ .

Les masses dels fermions i les mescles donades per  $V$  estan totes determinades pel Lagrangià de Yukawa (1.2), però els elements de les matrius generals complexes  $c_f$  són impredecibles a partir del model Electrofeble. Açò genera immediatament un fum de paràmetres lliures que apareixen a través de la matriu  $V$ . En general, una matriu unitària  $N_G \times N_G$  té  $N_G^2$  paràmetres reals,  $N_G(N_G - 1)/2$  mòduls i  $N_G(N_G + 1)/2$  fases. Ara bé, en el cas de  $V$ , no tots són rellevants, ja que està enmig de camps de quarks que sempre es poden redefinir per una fase; en total,  $2N_G - 1$  fases poden ser reabsorbides. Amb tot, el nombre de paràmetres lliures físics reals es redueix a  $(N_G - 1)^2$ , on  $N_G(N_G - 1)/2$  són mòduls i  $(N_G - 1)(N_G - 2)/2$  són fases.

Del comptatge, és fàcil veure com el cas de dues generacions implica directament zero fases, el que faria impossible per al SM explicar l'assimetria de CP observada, present, per exemple, en el sistema de  $K$ . És per això que fins i tot abans de què el  $b$  i el  $\tau$  foren detectats, es va assumir l'existència d'una tercera generació. Si  $N_G = 2$ , llavors  $V$  es caracteritza per un únic paràmetre real i es pot escriure en la notació de la matriu de rotació de Cabibbo [3] com

$$V = \begin{pmatrix} \cos \theta & \sin \theta \\ -\sin \theta & \cos \theta \end{pmatrix}. \quad (1.9)$$

En el SM ( $N_G = 3$ ),  $V$  té quatre graus de llibertat, tres angles i una fase, i normalment es

parametrizta com

$$V = \begin{pmatrix} c_{12}c_{13} & s_{12}c_{13} & s_{13}e^{-i\delta_{13}} \\ -s_{12}c_{23} - c_{12}s_{23}s_{13}e^{i\delta_{13}} & c_{12}c_{23} - s_{12}s_{23}s_{13}e^{i\delta_{13}} & s_{23}c_{13} \\ s_{12}s_{23} - c_{12}c_{23}s_{13}e^{i\delta_{13}} & -c_{12}s_{23} - s_{12}c_{23}s_{13}e^{i\delta_{13}} & c_{23}c_{13} \end{pmatrix}, \quad (1.10)$$

on  $c_{ij} \equiv \cos \theta_{ij}$  i  $s_{ij} \equiv \sin \theta_{ij}$  i  $i, j = 1, 2, 3$  es refereixen a cada generació de quarks.  $\delta_{13}$  és per tant l'única fase complexa en el SM. Els angles  $\theta_{ij}$  es poden elegir tal que pertanyen al primer quadrant, llavors  $s_{ij}, c_{ij} > 0$ . Experimentalment, hi ha una jerarquia manifesta en les entrades de la matriu  $V$ :  $s_{13} \ll s_{23} \ll s_{12} \ll 1$ , i.e. els elements diagonals són tots molt semblants a 1, els que connecten les dues primeres famílies són tots del mateix ordre  $\lambda \sim |V_{us}| = 0.2252 \pm 0.0009$  [5], la mescla entre la segona i la tercera generació és en comparació  $\sim \lambda^2$  i la primera i la tercera generació tenen una mescla  $\sim \lambda^3$ . Per tant, pareix convenient exhibir aquest patró utilitzant la parametrització de Wolfenstein [6] per a la matriu  $V$  com<sup>1</sup>

$$V = \begin{pmatrix} 1 - \lambda^2/2 & \lambda & A\lambda^3(\rho - i\eta) \\ -\lambda & 1 - \lambda^2/2 & A\lambda^2 \\ A\lambda^3(1 - \rho - i\eta) & -A\lambda^2 & 1 \end{pmatrix} + \mathcal{O}(\lambda^4), \quad (1.11)$$

on  $s_{12} = \lambda = |V_{us}|/\sqrt{|V_{ud}|^2 + |V_{us}|^2}$ ,  $s_{23} = A\lambda^2 = \lambda |V_{cb}/V_{cs}|$  i  $s_{13}e^{i\delta_{13}} = A\lambda^3(\rho + i\eta) = V_{ub}^*$  són les relacions per obtenir (1.11) a partir de (1.10) amb un desenvolupament de Taylor en  $\lambda$  i, també, la connexió amb els paràmetres originals de (1.8).

### 1.2.1 Determinació de $V_{ij}$

Els elements de la matriu  $V$  són paràmetres fonamentals del SM i, per tant, és molt important que es determinen amb precisió. Nogensmenys, aquesta tasca no és gaire fàcil perquè involucra l'estudi de les desintegracions hadròniques febles amb els corresponents elements de matriu hadrònics, l'evaluació dels quals és un problema no pertorbatiu de QCD i, necessàriament, introdueix errors teòrics. En [5] es pot trobar una discussió i revisió de l'actual determinació de  $V_{ij}$  a partir de diferents processos hadrònics. De la teoria, el fet que la matriu  $V$  siga unitària imposa

$$V_{ij}V_{il}^* = \delta_{jl}, \quad V_{ij}V_{kj}^* = \delta_{ik}, \quad (1.12)$$

on les sis combinacions que s'anul·len es poden representar per triangles en el pla complex. Les àrees d'eixos triangles són totes iguals, la meitat de l'invariant de Jarlskog  $J$ , una

<sup>1</sup>Com que  $V_{td}V_{ts} \sim \lambda^5$ , seria necessària una expansió de la part imaginària de  $V$  fins a  $\lambda^5$  per tal de tenir en compte la violació de CP. En eixe cas, per unitarietat,  $V$  té la mateixa forma que (1.11) amb excepció de tres elements que s'han de modificar:  $V_{13} = A\lambda^3(\rho - i\eta) + i\eta\lambda^2/2$ ,  $V_{22} = 1 - \lambda^2/2 - i\eta A\lambda^4$  i  $V_{23} = A\lambda^2(1 + i\eta\lambda^2)$  [6]. La parametrització fins a  $\lambda^5$  en ambdues parts, la real i la imaginària, de  $V$  es pot trobar a [5], *CP violation in meson decays*.

quantitat independent de convencions de fase i que mesura la “quantitat” de violació de CP. Es defineix com

$$\text{Im}[V_{ij}V_{kl}V_{il}^*V_{kj}^*] = J \sum_{m,n} \epsilon_{ikm}\epsilon_{jln} . \quad (1.13)$$

Les relacions d’unitarietat que inclouen productes de files o columnes veïnes són quasi degenerades, i.e. un costat és molt més curt que els altres. En el cas de les columnes,

$$\begin{aligned} V_{ud}^*V_{us} + V_{cd}^*V_{cs} + V_{td}^*V_{ts} &= 0 , \\ V_{us}^*V_{ub} + V_{cs}^*V_{cb} + V_{ts}^*V_{tb} &= 0 , \\ V_{ub}^*V_{ud} + V_{cb}^*V_{cd} + V_{tb}^*V_{td} &= 0 , \end{aligned} \quad (1.14)$$

podem veure com les dues primeres igualtats representen aqueix fet, les relacions entre els costats són  $\lambda : \lambda : \lambda^5$  en el primer i  $\lambda^4 : \lambda^2 : \lambda^2$  en el segon, posant de manifest una supressió en  $\lambda$  evident per a un dels costats. És per açò perquè la violació de CP és petita en sistemes de  $K$  i, també, perquè algunes de les assimetries predites en sistemes  $B_s$  són insignificants en el SM. En aquest sentit, el tercer triangle és més interessant, on tots els costats són  $\sim \lambda^3$ . Dividint cada costat per  $V_{cb}^*V_{cd}$  aquest triangle normalment es representa com en la Figura 1.1. Els vèrtex són  $(0,0)$ ,  $(1,0)$  i  $(\bar{\rho}, \bar{\eta}) \equiv (1 - \lambda^2/2)(\rho, \eta)$ . Moltes de les mesures en

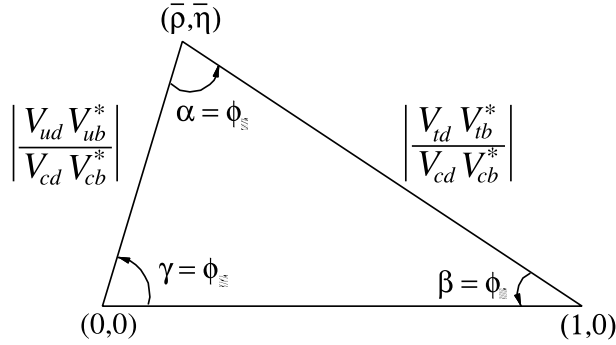


Figura 1.1: Triangle d’unitarietat.

física de sabor es poden representar en el pla  $(\bar{\rho}, \bar{\eta})$ , donant importants determinacions i restriccions als elements de  $V$ ; aquestes mesures poden ser, o bé amplades de desintegració i amplituds, o bé observables de violació de CP, relacionats amb els angles  $\alpha$ ,  $\beta$  i  $\gamma$ .

## Violació de CP

Encara que les interaccions febles violen les simetries discretes C i P separatament, la combinació de conjugació de càrrega i transformació de partit, CP, és encara una bona simetria. No només en la teoria, també en la majoria dels fenòmens de CP observats, sembla romandre conservada. Malgrat això, alguns processos donen senyals no trivials de violació de CP, com és el cas dels sistemes  $K$  i  $B$ . D’altra banda, hi ha una enorme

assimetria entre matèria i antimatèria en l'Univers, cosa que implica que el rol de la violació de CP és crucial a l'hora d'explicar la bariogènesi primordial.

La violació de CP està relacionada amb la presència de fases complexes entre amplituds d'interferència; el teorema CPT (on T es refereix a inversió temporal) assegura la conservació del producte d'aquestes tres simetries discretes en qualsevol teoria quàntica de camps invariant Lorentz (local) que preserve microcausalitat. Per tant, si es viola CP, aleshores també es viola T. En aquest sentit, essent T una transformació antiunitària, necessàriament han d'aparèixer fases relatives. Siguen dues amplituds d'interferència per a les transicions  $i \rightarrow f$  i  $\bar{i} \rightarrow \bar{f}$ ,

$$\begin{aligned}\mathcal{A}(i \rightarrow f) &= A_1 e^{i(\delta_1 + \phi_1)} + A_2 e^{i(\delta_2 + \phi_2)}, \\ \mathcal{A}(\bar{i} \rightarrow \bar{f}) &= A_1 e^{i(-\delta_1 + \phi_1)} + A_2 e^{i(-\delta_2 + \phi_2)},\end{aligned}\quad (1.15)$$

on la barra denota estats conjugats de CP,  $A_{1,2}$  són les parts reals de les amplituds,  $\delta_{1,2}$  són les fases febles (les úniques afectades per la conjugació de CP) i  $\phi_{1,2}$  fases fortes, qualsevol efecte de violació de CP es posarà de manifest en la següent quantitat

$$\frac{\Gamma(i \rightarrow f) - \Gamma(\bar{i} \rightarrow \bar{f})}{\Gamma(i \rightarrow f) + \Gamma(\bar{i} \rightarrow \bar{f})} = \frac{-2A_1 A_2 \sin(\delta_1 - \delta_2) \sin(\phi_1 - \phi_2)}{|A_1|^2 |A_2|^2 + 2A_1 A_2 \cos(\delta_1 - \delta_2) \cos(\phi_1 - \phi_2)}. \quad (1.16)$$

D'ací es poden deduir algunes condicions necessàries per a què esdevinga una asimetria de CP directa: i) Es necessiten almenys dues amplituds d'interferència, ii) es requereixen dues fases febles i fortes diferents i iii) per tal d'obtenir una asimetria significativa, ambdues amplituds han de ser de la mateixa grandària,  $A_1 \sim A_2$ .

En el SM l'única font de violació de CP és  $\delta_{13}$ , cosa que restringeix molt els fenòmens de violació de CP predits per la teoria, imposant alhora condicions en l'estructura del sector de sabor. Tal i com hem mencionat abans, són necessàries almenys tres generacions per a tenir una fase complexa, també, tots els elements de la matriu  $V$  han de ser distints de zero i els quarks de la mateixa càrrega no poden tenir la mateixa massa. Si qualsevol d'aquestes condicions no s'acompleix, llavors  $\delta_{13}$  pot ser reabsorbida pels camps dels quarks. És a dir, els efectes de violació de CP són proporcionals al producte de tots els angles de la matriu  $V$  i s'anul·len quan les masses de dos quarks amb la mateixa càrrega són degenerades. Tot açò es pot resumir en la següent condició: La violació de CP és possible en el SM si  $\text{Im}(\det[M'_u M_u'^{\dagger}, M'_d M_d'^{\dagger}]) \neq 0^2$ .

Aquesta simple anàlisi dóna pistes clares sobre com de grans i on poden haver asimetries de CP en el SM. D'altra banda, l'invariant de Jarlskog, que apareix en qualsevol observable de violació de CP, és en ordre de magnitud

$$J = c_{12} c_{23} c_{13}^2 s_{12} s_{23} s_{13} \sin \delta_{13} \sim A^2 \lambda^6 \eta < 10^{-4}, \quad (1.17)$$

el que vol dir que en el SM les violacions de CP són sempre menudes. Per a asimetries significatives, les amplades de desintegració deuen involucrar elements petits de la matriu

---

<sup>2</sup>Aquesta relació és per a un nombre imparell de famílies  $n_g$ . Per a  $n_g$  arbitrari la relació general és  $\text{tr}[M'_u M_u'^{\dagger}, M'_d M_d'^{\dagger}]^3 \neq 0$  [7].

$V$  (desintegracions suprimides). Les desintegracions de  $B$  són en aquest sentit molt bones candidates per exhibir violació de CP. A més a més, aquestos sistemes són els processos amb més baixa massa on els quarks de les tres generacions juguen un paper directe (no estan degenerats en massa).

## Ajust global

La unitarietat retringeix significativament el rang d'alguns dels elements de la matriu  $V$ . Nogensmenys, es poden determinar amb molta més precisió combinant aquestes restriccions del SM (unitarietat) amb totes les mesures i les prediccions teòriques dels elements de matriu hadrònics i els seus errors en un ajust global. Hi ha diferents propostes que implementen aquesta combinació, els freqüentistes CKMfitter [8,9] i [10], i UTfit [11,12], que utilitzen un mètode Bayesià. Ambdues propostes donen resultats similars. La Taula 1.1 mostra els valors per als paràmetres de Wolfenstein a partir de les propostes de CKMfitter i UTfit.

	$\lambda$	$A$	$\bar{\rho}$	$\bar{\eta}$
CKMfitter	$0.2253 \pm 0.0007$	$0.808^{+0.022}_{-0.015}$	$0.132^{+0.022}_{-0.014}$	$0.341 \pm 0.013$
UTfit	$0.2246 \pm 0.0011$	$0.832 \pm 0.017$	$0.130 \pm 0.018$	$0.350 \pm 0.013$

Taula 1.1: Resultats de l'ajust global de CKMfitter i UTfit per als paràmetres de Wolfenstein.

Els resultats per a les magnituds dels paràmetres de la matriu  $V$  a partir de l'ajust són [5],

$$V = \begin{pmatrix} 0.97428 \pm 0.00015 & 0.2253 \pm 0.0007 & 0.00347^{+0.00016}_{-0.00012} \\ 0.2252 \pm 0.0007 & 0.97345^{+0.00015}_{-0.00016} & 0.0410^{+0.0011}_{-0.0007} \\ 0.00862^{+0.00026}_{-0.00020} & 0.0403^{+0.0011}_{-0.0007} & 0.999152^{+0.000030}_{-0.000045} \end{pmatrix}, \quad (1.18)$$

i  $J = (2.91^{+0.19}_{-0.11}) \times 10^{-5}$ . Finalment, la Figura 1.2 mostra les restriccions de l'ajust global en el pla  $(\bar{\rho}, \bar{\eta})$  a partir de distintes mesures. Les regions amb color estan al 95% CL i es superposen consistentment, encara que es poden observar algunes tensions interessants. El valor de  $V_{ub}$  i  $\sin 2\beta$  posa de manifest una petita discrepància, deguda al valor actualitzat, un poc més gran, de  $\text{Br}(B^+ \rightarrow \tau^+\nu)$  i al valor un poc més petit de  $\sin 2\beta$  registrat en les factories de  $B$  [13]. També, una possible fase significativa en la mescla de  $B_s$  està sent de gran interès des que D0 va mesurar la *like-sign dimuon charge asymmetry* [14]. La raó d'aquestes tensions pot ser, o bé fluctuacions en les mesures experimentals, l'efecte dels errors de *lattice* QCD, o bé signes de nova física. En aquest sentit, la precisió en física de sabor resulta una bona estratègia per a mirar més enllà del SM; mentre que la cerca directa es fa al Tevatron i a l'LHC, efectes a baixa energia deuriem ser també visibles en els observables de sabor. Per tal d'això, és necessari tant un bon control dels errors com una millora dels experiments.



---

A banda del mecanisme de GIM, no hi ha res restringint l'estructura del sector de sabor, deixant molt d'espai per a propostes de nova física. Afegir una nova generació seria un possible pas a implementar, però cal anar amb cura de preservar unitarietat en el triangle estàndard, i.e. per a les tres primeres generacions. A més a més, LEP només ha observat tres neutrins lleugers, llavors, afegir una quarta generació necessita també un mecanisme que genere neutrins pesats. La modificació del sector escalar és igual de simple però més versàtil, l'apropiada ampliació del qual origina moltes possibilitats dinàmiques noves, tot i respectant les restriccions del SM. En aquesta tesi tenim l'objectiu d'implementar una anàlisi del model Electrofeble amb un sector escalar no mínim, en particular, estudiarem diferents aspectes del Model de Dos Doblets de Higgs.

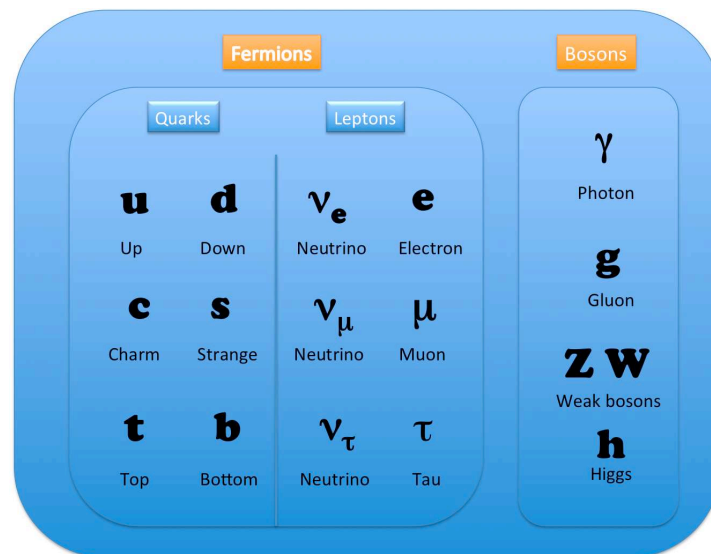


# Chapter 2

## Introduction

### 2.1 The Standard Model: Short overview

What is matter made of? Which kind of forces dominate the Universe? What are the fundamental laws of Nature? These big questions have been of great interest for many scientists in history. One of the most important aims have always been to understand how the basic contents of matter behave. Actually, when a famous physicist was asked about what he would leave as a legacy to a hypothetic new intelligent life civilization, just in case the world was destroyed, he answered that he would write in a small piece of paper “*matter is made of atoms*”. This is known already since many years ago. All the atoms present in nature are well understood and organized in a table according to their properties. However, we also know that this is not the end, all those species have a *subatomic* structure composed by what are called *elementary particles*, which are considered by now the most fundamental components of matter.



What these particles are and how they interact are questions that the Standard Model of Particle Physics addresses in a rather successful way. The elementary particles are very small ( $\sim h$ ) and very fast ( $\sim c$ ), which means that both Quantum Mechanics and Special Relativity are needed at the same time to describe their behaviour,  $\lambda = h/p$ . But just joining both theories is not enough, for a good understanding of “probability” the notion of a field theory needs to be introduced too. The Standard Model (SM) is then a quantum field theory that describes the electroweak and strong interactions (with the Electroweak (EW) theory and Quantum Chromodynamics (QCD) respectively) existing among quarks and leptons. These are the fermionic matter content and appear replicated in three families (see table above), with the only difference being the mass and the flavour number. Only quarks interact strongly, both quarks and leptons interact weakly and quarks and charged leptons also interact electromagnetically. In group theory, the elementary particles are the irreducible representations of the Poincaré group, which is formed by translations, rotations and boosts; the conserved charges of this symmetry perfectly characterize our free particles but not their interactions. Therefore, another kind of symmetry is needed in order to introduce the forces in the theory. This is the local gauge symmetry, whose conserved charge is the charge of the corresponding interaction and the generators give the number of the required intermediate particles, which are bosonic fields with spin 1: eight massless gluons for QCD, the massive  $W^\pm$  and  $Z$  for the weak interaction, and one massless photon for electromagnetism. That is why the SM is a *local gauge* theory based on the symmetry group  $G \equiv SU(3)_C^{\text{QCD}} \otimes [SU(2)_L \otimes U(1)_Y]^{\text{EW}}$ .

However, mass terms for the fields in the Lagrangian break this local gauge symmetry, meaning that the model needs an ad-hoc mechanism to generate massive particles, i.e. to provide gauge non-symmetric results but preserving the symmetry at the level of the Lagrangian. This is enforced by the Higgs-Kibble mechanism, which applies the Goldstone Theorem in the EW theory framework. This mechanism introduces the idea of *spontaneous* symmetry breaking (SSB), assuming a gauge symmetric Lagrangian with a non-symmetric vacuum that breaks the EW part of the group to the Electromagnetic subgroup,  $G \rightarrow SU(3)_C \otimes U(1)_{\text{em}}$ . This is implemented by the existence of an  $SU(2)$  scalar doublet field with zero electric charge and hypercharge 1 whose interaction with the vacuum is different from zero (it gets a vacuum expectation value),  $\langle 0|\phi^{(0)}|0 \rangle = v/\sqrt{2}$ . The scalar field called Higgs, after the gauge symmetry breaking, can be defined as an excitation of its ground state. The interaction of the Higgs with the fermionic particles, with intermediate gauge bosons through the covariant derivative and with itself, is what provides their masses. These are defined by the coupling of these fields, through the latter interaction, with the non-zero vacuum expectation value of the Higgs.

With such description the SM (for a review see e.g. [1]) is able to explain most of the experimental observations, some of them with many digits of precision. Moreover, all the predicted particles have already been observed, with the exception of the Higgs. Nevertheless, despite this enormous success explaining the phenomenology, the SM leaves unanswered many questions, meaning that, although the theory seems to be correct, it is for sure incomplete. There are some unresolved big “problems” like the implementation of

Gravity within the same gauge theory framework, the Grand Unification of all forces (not only the weak and electromagnetic) or the description of the  $\sim 96\%$  of the Universe which is not composed by ordinary matter (SM), but by dark matter ( $\sim 22\%$ ) and dark energy ( $\sim 74\%$ ). However, apart from those, there some other questions (maybe related to them or maybe not) that directly affect the flavour structure of the model. A first question would be why *three* is the number of families and not more, and if *more*, how many. Also, why the pattern of masses and mixing is like that, if they all come from the same electroweak interaction with the Higgs. Since this pattern is directly related with the electroweak SSB, i.e. with the scalar sector, is this *hidden* scalar sector hiding something else? Is only the mass what distinguishes each family? What about neutrino masses? Could it exist a good description of the observed CP violating phenomena? What is the origin of flavour? The fermionic flavour sector is the main source of free parameters in the SM, with massless neutrinos there are already 9 masses, 3 mixing angles and 1 complex phase. Taking into account that they are actually massive, the number of parameters increases at least by 7. New physics mechanisms that could give answers to all these questions are then necessary to investigate.

Particularly, in this thesis we aim to extend the (hidden) scalar sector beyond the minimal version given in the SM, since there is nothing that forbids it, and will analyze the impact in the flavour structure and the corresponding new phenomena.

## 2.2 Flavour dynamics in the Electroweak theory

The SM organizes the observed fermions in three families, which are copies of the same  $SU(2)_L \otimes U(1)_Y$  structure, with the only difference being the mass and flavour. The left-handed fields are  $SU(2)_L$  doublets while the right-handed ones are  $SU(2)_L$  singlets,

$$\begin{pmatrix} u' \\ d' \end{pmatrix}_L, \quad \begin{pmatrix} \nu'_l \\ l' \end{pmatrix}_L, \quad u'_R, \quad d'_R, \quad l'_R, \quad (2.1)$$

where  $u$ ,  $d$  and  $l$  are vectors of three dimensions in flavour space and the prime indicates that are gauge eigenstates. In the general case of  $N_G$  generations of fermions,  $u = u, c, t, u_4, \dots, u_{N_G}$ ,  $d = d, s, b, d_4, \dots, d_{N_G}$  and  $l = e, \mu, \tau, l_4, \dots, l_{N_G}$ , the most general Yukawa Lagrangian is given by

$$\mathcal{L}_Y = - \left\{ (\bar{u}', \bar{d}')_L \left[ c_d \phi d'_R + c_u \tilde{\phi} u'_R \right] + (\bar{\nu}'_l, \bar{l}')_L c_l \phi l'_R \right\} + h.c., \quad (2.2)$$

where  $c_d$ ,  $c_u$  and  $c_l$  are  $N_G \times N_G$  general complex Yukawa matrices corresponding to the coupling of the scalar doublet  $\phi$  to the down, up and lepton fermion sectors, and  $\tilde{\phi} = i\sigma_2\phi^*$ . After the electroweak SSB, the scalar doublet can be written as

$$\phi = \begin{pmatrix} \phi^{(+)} \\ \phi^{(0)} \end{pmatrix} \xrightarrow{\text{SSB}} e^{i\frac{\sigma_i}{2}\theta^i} \begin{bmatrix} 0 \\ \frac{1}{\sqrt{2}}(v+h) \end{bmatrix}, \quad (2.3)$$

where  $\theta_i$  and  $H$  are four real fields. Three of the four degrees of freedom are allowed to be rotated away by the local  $SU(2)_L$  invariance of the Lagrangian,  $\theta_i$ , which are nothing but the would-be Goldstone bosons associated with the SSB. In this gauge, called the Unitary Gauge, the Yukawa Lagrangian results in

$$\mathcal{L}_Y = - \left( 1 + \frac{h}{v} \right) [\bar{d}'_L M'_d d'_R + \bar{u}'_L M'_u u'_R + \bar{l}'_L M'_l l'_R] , \quad (2.4)$$

where  $M'_f \equiv \frac{v}{\sqrt{2}} c_f$  ( $f = u, d, l$ ). In the basis of fermion mass eigenstates

$$\begin{aligned} f_L &= S_f f'_L \\ f_R &= S_f U_f f'_R , \end{aligned} \quad (2.5)$$

where  $S_f$  and  $U_f$  are unitary matrices, the Yukawa Lagrangian takes the following form:

$$\mathcal{L}_Y = - \left( 1 + \frac{h}{v} \right) [\bar{d}_L M_d d_R + \bar{u}_L M_u u_R + \bar{l}_L M_l l_R] , \quad (2.6)$$

where  $M_f = S_f M'_f U_f^\dagger S_f^\dagger$  are the diagonal mass matrices corresponding to the three fermion sectors,

$$\begin{aligned} M_u &= \text{diag}(m_u, m_c, m_t, m_{u_4}, \dots, m_{u_{N_G}}) \\ M_d &= \text{diag}(m_d, m_s, m_b, m_{d_4}, \dots, m_{d_{N_G}}) \\ M_l &= \text{diag}(m_e, m_\mu, m_\tau, m_{l_4}, \dots, m_{l_{N_G}}) . \end{aligned} \quad (2.7)$$

The Yukawa Lagrangian (2.6) shows that any coupling of the Higgs field to fermions is proportional to their masses.

When going from the gauge eigenstates to the mass eigenstates Lagrangian in neutral interactions, two different cases are present in the Electroweak model:

- Neutral interactions described by the exchange of  $Z_\mu$  and  $A_\mu$  (vector): The structure in flavour space is necessarily  $\bar{f}'_L f'_L$  (there is no other flavour matrix in between) or  $\bar{f}'_R f'_R$ . In the mass eigenstate Lagrangian these structures directly correspond to  $\bar{f}_L f_L$  and  $\bar{f}_R f_R$  respectively. Therefore, there are no flavour-changing neutral currents (FCNCs) at tree level coming from vector interactions.
- Neutral interactions described by the exchange of  $h$  (scalar): The structure in flavour space is always of the form  $\bar{f}'_L X_f f'_R$ , where  $X_f$  is in the SM a single  $N_G \times N_G$  non-diagonal flavour matrix coming from the coupling of the scalar doublet to the fermion sector  $f$ . In the mass eigenstate Lagrangian the flavour structure becomes  $\bar{f}_L X_f^D f_R$ , where  $X_f^D$  has been diagonalized by the basis change. Thus, there are no flavour-changing neutral currents coming from scalar interactions either.

Therefore, FCNC phenomena are forbidden by the flavour structure in the SM (GIM mechanism [2]), which is in total agreement with the experimental data.

Regarding charged interactions only one possibility is present in the Electroweak model:

- Charged interactions described by the exchange of  $W_\mu$  (vector and axial-vector): The structures in flavour space have the same form  $\bar{u}'_L d'_L = \bar{u}_L S_u S_d^\dagger d_L = \bar{u}_L V d_L$ , where  $V \equiv S_u S_d^\dagger$  is a non-diagonal unitary complex mixing matrix (in general  $S_u \neq S_d$ ), known as the Cabibbo-Kobayashi-Maskawa (CKM) matrix [3, 4], which generates flavour-changing interactions in the charged quark sector,

$$V = \begin{pmatrix} V_{ud} & V_{us} & V_{ub} & V_{ud_4} & \cdots & V_{ud_{N_G}} \\ V_{cd} & V_{cs} & V_{cb} & V_{cd_4} & \cdots & V_{cd_{N_G}} \\ V_{td} & V_{ts} & V_{tb} & V_{td_4} & \cdots & V_{td_{N_G}} \\ V_{u_4 d} & V_{u_4 s} & V_{u_4 b} & V_{u_4 d_4} & \cdots & V_{u_4 d_{N_G}} \\ \cdots & \cdots & \cdots & \cdots & \cdots & \cdots \\ V_{u_{N_G} d} & V_{u_{N_G} s} & V_{u_{N_G} b} & V_{u_{N_G} d_4} & \cdots & V_{u_{N_G} d_{N_G}} \end{pmatrix}. \quad (2.8)$$

Due to the absence of right-handed neutrinos, the left-handed fields can always be redefined as  $\bar{\nu}_L = \bar{\nu}'_L S_l^\dagger$  and consequently there is no mixing matrix analog to  $V$  in the charged lepton sector,  $\bar{\nu}'_{lL} l'_L = \bar{\nu}_{lL} l_L$ .

The fermion masses and the mixings given by  $V$  are all determined by the Yukawa Lagrangian (2.2), but the elements of the general complex matrices  $c_f$  are unpredictable by the Electroweak model. This immediately generates a ‘‘bunch’’ of free parameters that appear through the  $V$  matrix. In general, a  $N_G \times N_G$  unitary matrix has  $N_G^2$  real parameters,  $N_G(N_G - 1)/2$  moduli and  $N_G(N_G + 1)/2$  phases. However, in the case of  $V$ , not all are relevant, since it is in between of quark fields that can always be redefined by a phase; in total,  $2N_G - 1$  phases can be reabsorbed. With this, the number of physical free real parameters is reduced to  $(N_G - 1)^2$ , where  $N_G(N_G - 1)/2$  are moduli and  $(N_G - 1)(N_G - 2)/2$  are phases.

From the counting, it is easy to see how the case of two generations directly implies zero phases, which would make it impossible for the SM to explain the observed CP asymmetry present, for instance, in the  $K$  system. This is why even before  $b$  and  $\tau$  were detected, a third generation was assumed to exist. If  $N_G = 2$ ,  $V$  is then characterized by only one real parameter and can be written in the notation of the Cabibbo rotation matrix [3] as

$$V = \begin{pmatrix} \cos \theta & \sin \theta \\ -\sin \theta & \cos \theta \end{pmatrix}. \quad (2.9)$$

In the SM ( $N_G = 3$ ),  $V$  has four degrees of freedom, three angles and one phase, and is usually parametrized as

$$V = \begin{pmatrix} c_{12}c_{13} & s_{12}c_{13} & s_{13}e^{-i\delta_{13}} \\ -s_{12}c_{23} - c_{12}s_{23}s_{13}e^{i\delta_{13}} & c_{12}c_{23} - s_{12}s_{23}s_{13}e^{i\delta_{13}} & s_{23}c_{13} \\ s_{12}s_{23} - c_{12}c_{23}s_{13}e^{i\delta_{13}} & -c_{12}s_{23} - s_{12}c_{23}s_{13}e^{i\delta_{13}} & c_{23}c_{13} \end{pmatrix}, \quad (2.10)$$

where  $c_{ij} \equiv \cos \theta_{ij}$  and  $s_{ij} \equiv \sin \theta_{ij}$  and  $i, j = 1, 2, 3$  refer to the each generation of quarks.  $\delta_{13}$  is therefore the only complex phase in the SM. The angles  $\theta_{ij}$  can be chosen to lie in the first quadrant, so  $s_{ij}, c_{ij} > 0$ . Experimentally, there is a manifest hierarchy for the entries of the  $V$  matrix:  $s_{13} \ll s_{23} \ll s_{12} \ll 1$ , i.e. the diagonal elements are all very close to 1, the ones connecting the first two families are all of the same order  $\lambda \sim |V_{us}| = 0.2252 \pm 0.0009$  [5], the mixing between the second and third generations is in comparison  $\sim \lambda^2$  and the first and third generations have a mixing  $\sim \lambda^3$ . Then, it seems convenient to exhibit this pattern using the Wolfenstein parametrization [6] for the  $V$  matrix as<sup>1</sup>

$$V = \begin{pmatrix} 1 - \lambda^2/2 & \lambda & A\lambda^3(\rho - i\eta) \\ -\lambda & 1 - \lambda^2/2 & A\lambda^2 \\ A\lambda^3(1 - \rho - i\eta) & -A\lambda^2 & 1 \end{pmatrix} + \mathcal{O}(\lambda^4), \quad (2.11)$$

where  $s_{12} = \lambda = |V_{us}|/\sqrt{|V_{ud}|^2 + |V_{us}|^2}$ ,  $s_{23} = A\lambda^2 = \lambda|V_{cb}|/|V_{cs}|$  and  $s_{13}e^{i\delta_3} = A\lambda^3(\rho + i\eta) = V_{ub}^*$  are the relations to obtain (2.11) from (2.10) by a Taylor expansion in  $\lambda$  and, also, the connection with the original elements of (2.8).

### 2.2.1 Determination of $V_{ij}$

The  $V$  matrix elements are fundamental parameters of the SM and, therefore, their precise determination is very important. However, this task is not easy because involves the study of hadronic weak decays with the corresponding hadronic matrix elements, whose evaluation is a non-perturbative QCD problem and necessarily introduces theoretical uncertainties. A discussion and review of the current determination of  $V_{ij}$  from different hadronic processes can be found in [5]. From theory, the unitarity of the  $V$  matrix imposes

$$V_{ij}V_{il}^* = \delta_{jl}, \quad V_{ij}V_{kj}^* = \delta_{ik}, \quad (2.12)$$

where the six vanishing combinations can be represented as triangles in the complex plane. The areas of those triangles are all the same, half of the Jarlskog invariant  $J$ , a quantity which is independent of phase conventions and measures the strength of CP violation. It is defined as

$$\text{Im}[V_{ij}V_{kl}V_{il}^*V_{kj}^*] = J \sum_{m,n} \epsilon_{ikm}\epsilon_{jln}. \quad (2.13)$$

---

<sup>1</sup>Since  $V_{td}V_{ts} \sim \lambda^5$ , an expansion of the imaginary part of the  $V$  matrix up to  $\lambda^5$  would be necessary for CP violation. In that case, by unitarity  $V$  requires the same form as (2.11) with the exception of three elements that are modified as follows:  $V_{13} = A\lambda^3(\rho - i\eta) + i\eta\lambda^2/2$ ,  $V_{22} = 1 - \lambda^2/2 - i\eta A\lambda^4$  and  $V_{23} = A\lambda^2(1 + i\eta\lambda^2)$  [6]. The parametrization up to  $\lambda^5$  in both real and imaginary parts of  $V$  can be found in [5], *CP violation in meson decays*.

The unitarity relations involving products of neighbouring rows or columns are almost degenerate, i.e. one side is much shorter than the others. In the case of columns,

$$\begin{aligned} V_{ud}^* V_{us} + V_{cd}^* V_{cs} + V_{td}^* V_{ts} &= 0, \\ V_{us}^* V_{ub} + V_{cs}^* V_{cb} + V_{ts}^* V_{tb} &= 0, \\ V_{ub}^* V_{ud} + V_{cb}^* V_{cd} + V_{tb}^* V_{td} &= 0, \end{aligned} \quad (2.14)$$

we can see how the two first equalities represent that fact, the relations among the sides are  $\lambda : \lambda : \lambda^5$  in the first one and  $\lambda^4 : \lambda^2 : \lambda^2$  in the second one, showing an evident  $\lambda$  suppression for one of the sides. This is why CP violation is very small in  $K$  systems and why some predicted asymmetries in  $B_s$  systems are tiny in the SM. In this sense, the third triangle is more interesting, where all the sides are  $\sim \lambda^3$ . Dividing each side by  $V_{cb}^* V_{cd}$  this triangle is usually represented as in Figure 2.1. The vertices are  $(0, 0)$ ,  $(1, 0)$

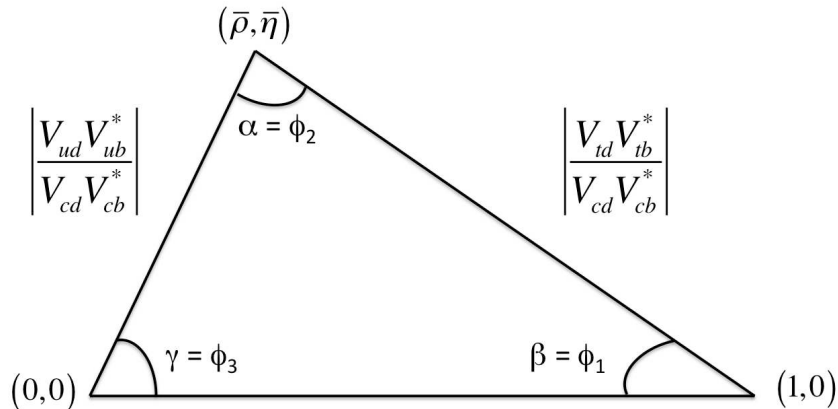


Figure 2.1: Unitarity triangle.

and  $(\bar{\rho}, \bar{\eta}) \equiv (1 - \lambda^2/2)(\rho, \eta)$ . Many measurements in flavour physics can be displayed in the  $(\bar{\rho}, \bar{\eta})$  plane, giving important determinations and constraints for the  $V$  elements; these measurements can be either decay rates and amplitudes or also CP violating observables related to the angles  $\alpha$ ,  $\beta$  and  $\gamma$ .

## CP violation

Although weak interactions violate the discrete symmetries C and P separately, the combination of charge conjugation and parity transformation, CP, is still a good symmetry. Not only in theory, but also in the majority of observed phenomena CP seems to be conserved. However, some processes give non trivial signals of CP violation, as is the case of  $K$  and  $B$  systems. Apart from that, there is a huge asymmetry between matter and antimatter in the Universe, which implies that the role of CP violation is crucial to explain the primordial baryogenesis.

CP violation is related to the presence of complex phases between interfering amplitudes; the CPT theorem (where T refers to time reversal) ensures the conservation of the product of those three discrete symmetries in any Lorentz invariant (local) quantum field theory that preserves micro-causality. Therefore, if CP is violated, the same happens with T. In this sense, being T an antiunitary transformation, relative phases need to be present. Given two interfering amplitudes for the transitions  $i \rightarrow f$  and  $\bar{i} \rightarrow \bar{f}$ ,

$$\begin{aligned}\mathcal{A}(i \rightarrow f) &= A_1 e^{i(\delta_1 + \phi_1)} + A_2 e^{i(\delta_2 + \phi_2)}, \\ \mathcal{A}(\bar{i} \rightarrow \bar{f}) &= A_1 e^{i(-\delta_1 + \phi_1)} + A_2 e^{i(-\delta_2 + \phi_2)},\end{aligned}\quad (2.15)$$

where the bar denotes CP conjugated states,  $A_{1,2}$  are the real parts of the amplitudes,  $\delta_{1,2}$  are weak phases (the only affected by the CP conjugation) and  $\phi_{1,2}$  strong phases, any CP violating effect can be accounted by the rate asymmetry as

$$\frac{\Gamma(i \rightarrow f) - \Gamma(\bar{i} \rightarrow \bar{f})}{\Gamma(i \rightarrow f) + \Gamma(\bar{i} \rightarrow \bar{f})} = \frac{-2A_1 A_2 \sin(\delta_1 - \delta_2) \sin(\phi_1 - \phi_2)}{|A_1|^2 |A_2|^2 + 2A_1 A_2 \cos(\delta_1 - \delta_2) \cos(\phi_1 - \phi_2)}. \quad (2.16)$$

From this, some necessary conditions for a direct CP asymmetry can be read: i) At least two interfering amplitudes are needed, ii) two different weak and strong phases are required and iii) for a sizeable asymmetry, both amplitudes have to be of the same size,  $A_1 \sim A_2$ .

In the SM, the only source of CP violation is  $\delta_{13}$ , constraining a lot the predicted CP violating phenomena and imposing necessary conditions in the structure of the flavour sector. As we mentioned before, at least three generations of quarks are necessary to have a complex phase, also, all the  $V$  matrix elements need to be different from zero and the quarks of the same charge cannot have equal masses. If any of these conditions is not accomplished, then  $\delta_{13}$  could be rotated away. That is, CP violation effects are proportional to the product of all angles of the  $V$  matrix and vanish when the masses of two quarks with the same charge are degenerate. All this is accounted by the following condition: CP violation is possible in the SM if  $\text{Im}(\det[M'_u M_u'^{\dagger}, M'_d M_d'^{\dagger}]) \neq 0^2$ .

This simple analysis gives clear hints on how big and where may be the predicted CP asymmetries in the SM. On the other hand, the Jarlskog invariant, which will appear in any CP violating observable, is in order of magnitude

$$J = c_{12} c_{23} c_{13}^2 s_{12} s_{23} s_{13} \sin \delta_{13} \sim A^2 \lambda^6 \eta < 10^{-4}, \quad (2.17)$$

meaning that in the SM violations of the CP symmetry are always small. For a sizeable asymmetry, the decay widths should involve small  $V$  matrix elements (suppressed decays).  $B$  decays are in this sense very good candidates to exhibit CP violation. Moreover, these systems are the lowest mass processes where the quarks of the three generations play a direct role (not mass degenerate).

---

<sup>2</sup>This relation is given for an odd number of families  $n_g$ . For an arbitrary  $n_g$  the general relation is  $\text{tr}[M'_u M_u'^{\dagger}, M'_d M_d'^{\dagger}]^3 \neq 0$  [7].

## Global fit

Unitarity significantly constraints the range for some of the  $V$  matrix elements. However those can be most precisely determined by combining these SM constraints (unitarity) with all the measurements and the theoretical predictions for the hadronic matrix elements and their uncertainties in a global fit. There are several approaches that perform such combination, the frequentists CKMfitter [8, 9] and [10], and UTfit [11, 12], that uses a Bayesian method. Both approaches give similar results. Table 2.1 shows the values for the Wolfenstein parameters from the CKMfitter and UTfit approach. The results for the

	$\lambda$	$A$	$\bar{\rho}$	$\bar{\eta}$
CKMfitter	$0.2253 \pm 0.0007$	$0.808^{+0.022}_{-0.015}$	$0.132^{+0.022}_{-0.014}$	$0.341 \pm 0.013$
UTfit	$0.2246 \pm 0.0011$	$0.832 \pm 0.017$	$0.130 \pm 0.018$	$0.350 \pm 0.013$

Table 2.1: CKMfitter and UTfit global fit results for Wolfenstein parameters.

magnitudes of the  $V$  matrix parameters from the fits are [5],

$$V = \begin{pmatrix} 0.97428 \pm 0.00015 & 0.2253 \pm 0.0007 & 0.00347^{+0.00016}_{-0.00012} \\ 0.2252 \pm 0.0007 & 0.97345^{+0.00015}_{-0.00016} & 0.0410^{+0.0011}_{-0.0007} \\ 0.00862^{+0.00026}_{-0.00020} & 0.0403^{+0.0011}_{-0.0007} & 0.999152^{+0.000030}_{-0.000045} \end{pmatrix}, \quad (2.18)$$

and  $J = (2.91^{+0.19}_{-0.11}) \times 10^{-5}$ . Finally, Figure 2.2 shows the global fit constraints on  $(\bar{\rho}, \bar{\eta})$  from different measurements. The coloured regions are at 95% CL and overlap quite consistently, although some interesting tensions are present. The value of  $V_{ub}$  and  $\sin 2\beta$  shows a slight discrepancy, which is due to the larger  $\text{Br}(B^+ \rightarrow \tau^+ \nu)$  updated value and the smaller  $\sin 2\beta$  reported by  $B$ -factories [13]. Also, a possible large phase in  $B_s$  mixing has been of great interest since D0 measured a like-sign dimuon charge asymmetry [14]. The reason for these tensions could be either fluctuations of the experimental measurements, the effect of lattice QCD uncertainties or a hint of new physics. In this sense, flavour precision data is a good strategy to look for physics beyond SM; while the direct search is performed at Tevatron and at the LHC, low energy effects should also be visible in flavour observables. For that, a good control of uncertainties and improved experiments are necessary.

### 2.2.2 Prospects

As was mentioned before, despite the successful description of the observed phenomena given by the SM, it leaves many questions unanswered, a big part of them related with the flavour structure itself. The gauge and scalar sectors have 4 free parameters,  $\alpha_{em}$ ,  $M_Z$ ,  $G_F$ , which are very well determined, and the mass of the Higgs,  $M_h$ . Anyway, a model with only 4 degrees of freedom permits to make rather good predictions. However, the fermionic flavour sector introduces 13 more, with 9 fermion masses, 3 mixings and 1 phase. And moreover, if one takes into account that neutrinos are actually massive, 3

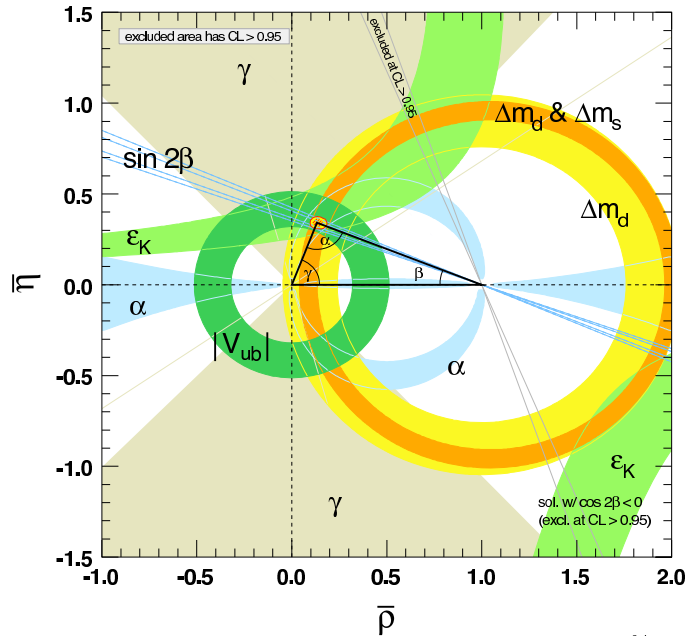


Figure 2.2: Constraints on the  $(\bar{\rho}, \bar{\eta})$  at 95% CL [5].

more masses need to be added, plus the corresponding mixing matrix for the lepton sector (other 4 parameters, plus 2 new phases if neutrinos are Majorana particles). The existence of all these degrees of freedom comes from the unknown Yukawa couplings, the origin and the structure of which conform an unresolved flavour puzzle. The scalar sector plays an important role in its structure, since the generation of masses is completely related with the electroweak SSB, the most obscure part of the SM Lagrangian. A CP violation mechanism is incorporated by the SM through a single phase in the  $V$  matrix. Although it explains (by now) all the observed CP violating phenomena in the laboratory, this mechanism is not enough to describe the matter-antimatter asymmetry of the Universe. Therefore, a fundamental explanation of the origin of CP violation is still absent. Neutrino oscillations are the first phenomenon towards the existence of *new* flavour physics; in this sense, lepton flavour violation opens a window to a new flavour dynamics lacking in the SM.

Apart from the GIM mechanism there is nothing constraining the structure of the flavour sector, giving a lot of space for new physics proposals. Adding one more generation would be a simple step to perform, but one should be worried about preserving unitarity in the standard triangle, i.e. for the three standard generations. Moreover, LEP has only observed three light neutrinos and, then, adding a fourth generation needs also a mechanism that generates heavy neutrinos. As simple but more versatile is the modification of the scalar sector, whose (appropriate) enlargement origins many new dynamical possibilities while respecting the SM constraints. In this thesis we aim to perform an analysis of the Electroweak model with a non-minimal scalar sector, in particular, we will study different aspects of the two-Higgs-doublet Model.

# Chapter 3

## The two-Higgs-doublet model

### 3.1 Introduction

The enlargement of the scalar sector is one of the most versatile extensions of the SM [7,15]. There is no theoretical principle constraining the Higgs sector to its minimal realization and, moreover, the extension results in a very *economical* choice; the idea of adding more scalar fields results simple and fruitful when one goes beyond, in the sense that the theoretical commitment is very low while the range of new dynamical possibilities it generates is very wide. Among these new dynamical features, the most relevant ones are i) the possibility of having Spontaneous CP violation, which cannot take place with only one Higgs doublet, ii) the discussion of the Strong CP problem, that requires the enlargement of the scalar sector in many of its solutions, including the Peccei-Quinn one, iii) the observed baryon asymmetry in the Universe, that cannot be explained by the SM; on one hand, because the electroweak phase transition is not strongly first order and, therefore, the baryon asymmetry created in the transition would be removed by unsuppressed baryon number violating processes in the broken phase; on the other hand, the SM Kobayashi-Maskawa mechanism provides CP violating effects that are too small. Thus, from Baryogenesis there is the need of having extra sources of CP violation and for that, the enlargement of the scalar sector is one of the simplest scenarios that could provide them. Finally, iv) within the context of multi-Higgs models, dark matter candidates can be also accommodated. Still in the motivations but as a more generic comment, it should be also noticed that many new-physics scenarios, including supersymmetry, can lead to a low-energy spectrum containing the SM fields plus additional scalar multiplets; in this sense, multi-Higgs models play the role of being a very convenient effective field theory where the low-energy effects of other high energy mechanisms can be studied.

There is a very important constraint in the way the scalar sector is enlarged, that is the well known relationship between the masses of the  $W^\pm$  and  $Z$  gauge bosons and the weak mixing angle  $\theta_w$ ,

$$M_W = \cos \theta_w M_Z . \tag{3.1}$$

In general, this holds at classical level if the added Higgs multiplets have isospin  $T$  and weak

hypercharge  $Y$  that accomplish  $T(T+1) = 3Y^2$  [7]. Therefore, the Higgs fields which get a vacuum expectation value (VEV) should be either  $SU(2) \otimes U(1)$  singlets or the neutral components of  $SU(2)$  doublets. Solutions apart from  $T = Y = 0$  and  $T = Y = 1/2$  are not usually considered because they correspond to large scalar multiplets without Yukawa interactions with fermions. Almost any other neutral scalars having a VEV will spoil (3.1) if these VEVs are not small enough.

In this thesis, we analyze the enlargement of the SM scalar sector by only one more doublet in different scenarios and the phenomenological implications.

## 3.2 The general two-Higgs-doublet model

In its minimal version, the 2HDM [16] is an  $SU(3)_C \otimes SU(2)_L \otimes U(1)_Y$  theory with the same fermion content as the SM (without right-handed neutrinos) and two scalar doublets  $\phi_a$  ( $a = 1, 2$ ) with hypercharge  $Y = \frac{1}{2}$ ,

$$\phi_a = \begin{bmatrix} \varphi_a^{(+)} \\ \varphi_a^{(0)} \end{bmatrix}, \quad (3.2)$$

whose charge-conjugated fields  $\tilde{\phi}_a \equiv i\sigma_2 \phi_a^*$  are also  $SU(2)$  doublets with  $Y = -\frac{1}{2}$ . After the EW SSB, the neutral<sup>1</sup> components of the scalar doublets acquire vacuum expectation values  $\langle 0 | \phi_a^T(x) | 0 \rangle = \frac{1}{\sqrt{2}} (0, v_a e^{i\theta_a})$ , and the eight real components can be parametrized as follows,

$$\phi_a = e^{i\theta_a} \begin{bmatrix} \varphi_a^+ \\ \frac{1}{\sqrt{2}}(v_a + \rho_a + i\eta_a) \end{bmatrix}. \quad (3.3)$$

Without loss of generality, we can enforce  $\theta_1 = 0$  through an appropriate  $U(1)_Y$  transformation, leaving the relative phase  $\theta \equiv \theta_2 - \theta_1$ . The gauge boson masses, which receive contributions from the two vacuum expectation values  $v_a$ , are given by the same expressions than in the SM, with  $v \equiv \sqrt{v_1^2 + v_2^2}$ .

The doublets  $\phi_1$  and  $\phi_2$  have identical flavour structures, so they are only distinguished by their self-interactions described in the Higgs potential. Therefore, they can always be redefined by an arbitrary complex transformation  $\phi_a \rightarrow \phi'_a = \mathcal{T}_{ab} \phi_b$ , with  $\mathcal{T}_{ab}$  being a matrix that depends on eight real parameters. Four of them can be used to transform the kinetic term of the scalar fields,

$$\mathcal{L}_K^{\phi_a} = c_{11} (D_\mu \phi_1)^\dagger D^\mu \phi_1 + c_{22} (D_\mu \phi_2)^\dagger D^\mu \phi_2 + [c_{12} (D_\mu \phi_1)^\dagger D^\mu \phi_2 + \text{h.c.}] , \quad (3.4)$$

where  $c_{11}$  and  $c_{22}$  are real while  $c_{12}$  is complex, into a canonical (renormalizable) form. This non-unitary transformation  $\mathcal{T}$  removes the four real degrees of freedom of  $c_{11}$ ,  $c_{22}$  and

---

<sup>1</sup>A vacuum preserving  $U(1)_{\text{em}}$  is assumed.

$c_{12}$ , setting  $c_{11} = c_{22} = 1$  and  $c_{12} = 0$ . Then, the most general transformation that leaves invariant the canonical kinetic term of the scalar doublets,

$$\mathcal{L}_K^{\phi_a} = (D_\mu \phi_1)^\dagger D^\mu \phi_1 + (D_\mu \phi_2)^\dagger D^\mu \phi_2, \quad (3.5)$$

is a global  $U(2)$  transformation  $\phi_a \rightarrow \phi'_a = \mathcal{U}_{ab} \phi_b$  in the scalar space  $(\phi_1, \phi_2)$  [17]. The fact that the doublets can be freely transformed (we say that we can *choose* the scalar basis) introduces a very important difference between the parameters in the model that are *invariant* under such basis transformations and those that are not. The physics cannot depend on the particular scalar basis that we choose, thus, only the parameters that remain invariant are physical quantities, observables. In general, the expressions for the mass matrix elements of the Higgs and their couplings will depend on this basis choice, in particular, the famous parameter  $\tan \beta$  that appears in the MSSM and in other types of 2HDMs, is not a physical quantity in the most general 2HDM. This is why one should take care about the real meaning of the bounds found for the parameters when analyzing this kind of models, and it is also why a basis-invariant technology has been developed by many authors, rewriting all the parameters in terms of scalar quantities (invariants) under these  $U(2)$  transformations. The need of describing the model with invariants was pointed out by [18, 19], references [7, 19] show how to construct invariants in a systematic way for different models including the 2HDM, work on basis invariance within the context of 2HDM has been deeply developed by [17, 20–23], and some alternative approaches can be found in [24–30]. Although this basis-invariant technology should be always kept in mind for a good understanding of the physical quantities, we present in the following the model in terms of the usual parameters for a clearer understanding of the reader.

There is a particular  $\mathcal{U}$  transformation that makes possible to define a basis for the scalar doublets such that only one has a non-zero vacuum expectation value, that is the so-called Higgs basis ( $\tan \beta \equiv v_2/v_1$ ):

$$\begin{pmatrix} \Phi_1 \\ -\Phi_2 \end{pmatrix} \equiv \begin{bmatrix} \cos \beta & \sin \beta \\ \sin \beta & -\cos \beta \end{bmatrix} \begin{pmatrix} \phi_1 \\ e^{-i\theta} \phi_2 \end{pmatrix}. \quad (3.6)$$

This has the advantage that the VEV and the three Goldstone fields  $G^\pm(x)$  and  $G^0(x)$  get isolated as components of  $\Phi_1$ , which resembles the SM Higgs doublet, while  $\Phi_2$  contains all the new fields:

$$\Phi_1 = \begin{bmatrix} G^+ \\ \frac{1}{\sqrt{2}}(v + S_1 + iG^0) \end{bmatrix}, \quad \Phi_2 = \begin{bmatrix} H^+ \\ \frac{1}{\sqrt{2}}(S_2 + iS_3) \end{bmatrix}.$$

The Higgs basis is also interesting because the expressions for the Lagrangian parameters are closely related to observables, as is demonstrated in [20]. The physical scalar spectrum has five degrees of freedom: two charged fields  $H^\pm(x)$  and three neutral scalars  $\varphi_i^0(x) = \{h(x), H(x), A(x)\}$ , which are related through an orthogonal transformation with the  $S_i$  fields:  $\varphi_i^0(x) = \mathcal{R}_{ij} S_j(x)$ . The form of the  $\mathcal{R}$  matrix is fixed by the scalar potential, which determines the neutral scalar mass matrix and the corresponding mass eigenstates.

### 3.2.1 The potential

The most general renormalizable scalar potential invariant under the EW symmetry group can be written as [7]

$$\mathcal{V} = \sum_{a,b,c,d=1}^2 [Y_{ab} \phi_a^\dagger \phi_b + Z_{abcd} (\phi_a^\dagger \phi_b) (\phi_c^\dagger \phi_d)] , \quad (3.7)$$

where  $Y_{ab}$  have dimensions of mass squared and  $Z_{abcd}$  are dimensionless.  $Z_{abcd}$  can be assumed to be equal to  $Z_{cdab}$  without loss of generality, and by hermiticity of  $\mathcal{V}$ ,  $Y_{ab} = Y_{ba}^*$  and  $Z_{abcd} = Z_{bacd}^*$ . In total, there are 14 independent real parameters. The extremes of the potential define the vacuum expectation values,

$$\left. \frac{\partial \mathcal{V}}{\partial \phi_1} \right|_{\phi_1 = \langle \phi_1 \rangle, \phi_2 = \langle \phi_2 \rangle} = 0 \quad \left. \frac{\partial \mathcal{V}}{\partial \phi_2} \right|_{\phi_1 = \langle \phi_1 \rangle, \phi_2 = \langle \phi_2 \rangle} = 0 , \quad (3.8)$$

where two different kind of solutions are possible: i) Both  $\langle \phi_a \rangle = 0$ , then the EW symmetry is preserved, and ii) the EW symmetry is spontaneously broken, either if  $\langle \phi_1 \rangle \neq 0$  and  $\langle \phi_2 \rangle = 0$ , or  $\langle \phi_1 \rangle = 0$  and  $\langle \phi_2 \rangle \neq 0$  (equivalent cases) or  $\langle \phi_1 \rangle \neq 0$  and  $\langle \phi_2 \rangle \neq 0$ . Therefore, any of the second kind of solutions must be taken. The condition for the extremum to become a minimum is that the eigenvalues of the mass squared matrix of the neutral Higgs in that point have to be non-negative.

The scalar potential in the Higgs basis is

$$\begin{aligned} \mathcal{V} = & \mu_1 \Phi_1^\dagger \Phi_1 + \mu_2 \Phi_2^\dagger \Phi_2 + [\mu_{12} \Phi_1^\dagger \Phi_2 + \text{h.c.}] \\ & + \lambda_1 (\Phi_1^\dagger \Phi_1)^2 + \lambda_2 (\Phi_2^\dagger \Phi_2)^2 + \lambda_3 (\Phi_1^\dagger \Phi_1) (\Phi_2^\dagger \Phi_2) + \lambda_4 (\Phi_1^\dagger \Phi_2) (\Phi_2^\dagger \Phi_1) \\ & + [(\lambda_5 \Phi_1^\dagger \Phi_2 + \lambda_6 \Phi_1^\dagger \Phi_1 + \lambda_7 \Phi_2^\dagger \Phi_2) (\Phi_1^\dagger \Phi_2) + \text{h.c.}] , \end{aligned} \quad (3.9)$$

where  $\mu_{12}$ ,  $\lambda_5$ ,  $\lambda_6$  and  $\lambda_7$  are in general complex parameters while  $\mu_1$ ,  $\mu_2$  and  $\lambda_{1-4}$  are real. In this basis, the stability point (3.8) of the potential arises when

$$\left. \frac{\partial \mathcal{V}}{\partial \Phi_1} \right|_{\Phi_1 = \frac{v}{\sqrt{2}}, \Phi_2 = 0} = 0 \quad \left. \frac{\partial \mathcal{V}}{\partial \Phi_2} \right|_{\Phi_1 = \frac{v}{\sqrt{2}}, \Phi_2 = 0} = 0 , \quad (3.10)$$

which gives the following relations between some of the parameters,

$$\mu_1 = -\lambda_1 v^2 , \quad \mu_{12} = -\frac{\lambda_6}{2} v^2 . \quad (3.11)$$

The corresponding masses for the Higgs fields can be easily obtained from the quadratic terms of the potential, taking (3.11) into account and rewriting (3.9) for the elements of the doublets, those terms are:

$$\mathcal{V} = \dots + M_{H^\pm}^2 H^+ H^- + \frac{1}{2} \begin{pmatrix} S_1 & S_2 & S_3 \end{pmatrix} \mathcal{M} \begin{pmatrix} S_1 \\ S_2 \\ S_3 \end{pmatrix} + \dots \quad (3.12)$$

$M_{H^\pm}^2 = \mu_2 + \frac{v^2}{2}\lambda_3$  corresponds to the mass of the charged Higgs and  $\mathcal{M}$  is a non-diagonal symmetric matrix mixing the neutral Higgs fields,

$$\mathcal{M} = \begin{pmatrix} 2v^2\lambda_1 & v^2\lambda_6^R & -v^2\lambda_6^I \\ v^2\lambda_6^R & M_{H^\pm}^2 + (\lambda_4 + 2\lambda_5^R)\frac{v^2}{2} & -v^2\lambda_5^I \\ -v^2\lambda_6^I & -v^2\lambda_5^I & M_{H^\pm}^2 + (\lambda_4 - 2\lambda_5^R)\frac{v^2}{2} \end{pmatrix}, \quad (3.13)$$

where  $\lambda_{5,6}^R$  and  $\lambda_{5,6}^I$  are the real and imaginary parts of the complex parameters respectively. For the neutral Higgs to be mass eigenstates,  $\mathcal{M}$  has to be diagonalized by an orthogonal matrix  $\mathcal{R}$ ,

$$\mathcal{D} = \mathcal{R}\mathcal{M}\mathcal{R}^T = \begin{pmatrix} M_1^2 & 0 & 0 \\ 0 & M_2^2 & 0 \\ 0 & 0 & M_3^2 \end{pmatrix}, \quad (3.14)$$

giving rise to the corresponding masses of the neutral scalars:  $M_1$ ,  $M_2$  and  $M_3$ .  $\mathcal{R}$  is sometimes written as the product of three rotational matrices,  $\mathcal{R} = \mathcal{R}_3\mathcal{R}_2\mathcal{R}_1$ , in terms of three Euler angles  $\alpha_i \in [0, \pi]$  such as,

$$\mathcal{R}_1 = \begin{pmatrix} c_1 & s_1 & 0 \\ -s_1 & c_1 & 0 \\ 0 & 0 & 1 \end{pmatrix} \quad \mathcal{R}_2 = \begin{pmatrix} c_2 & 0 & s_2 \\ 0 & 1 & 0 \\ -s_2 & 0 & c_2 \end{pmatrix}$$

$$\mathcal{R}_3 = \begin{pmatrix} 1 & 0 & 0 \\ 0 & c_3 & s_3 \\ 0 & -s_3 & c_3 \end{pmatrix}, \quad (3.15)$$

where  $s_i \equiv \sin \alpha_i$  and  $c_i \equiv \cos \alpha_i$ .

If CP is not an exact symmetry of the Lagrangian (general case), the CP-odd component  $S_3$  mixes with the CP-even fields  $S_{1,2}$  and the resulting mass eigenstates  $h_i$ ,

$$\begin{pmatrix} h_1 \\ h_2 \\ h_3 \end{pmatrix} = \mathcal{R} \begin{pmatrix} S_1 \\ S_2 \\ S_3 \end{pmatrix}, \quad (3.16)$$

do not have a definite CP quantum number. On the other hand, if CP is an exact symmetry of the Lagrangian, the imaginary parts of the complex parameters vanish and the admixture disappears. In this case  $A = S_3$  and therefore only  $\mathcal{R}_1$  is needed to implement the rotation, which can be conveniently written as

$$\begin{pmatrix} H \\ h \end{pmatrix} = \begin{bmatrix} \cos(\alpha - \beta) & \sin(\alpha - \beta) \\ -\sin(\alpha - \beta) & \cos(\alpha - \beta) \end{bmatrix} \begin{pmatrix} S_1 \\ S_2 \end{pmatrix}. \quad (3.17)$$

Finally, notice that the following relation for the masses,

$$M_1^2 + M_2^2 + M_3^2 = M_h^2 + M_H^2 + M_A^2, \quad (3.18)$$

is always accomplished because the trace of the matrix  $\mathcal{M}$  is invariant under unitary transformations.

### Theoretical constraints

The parameters of the Higgs potential have theoretical constraints coming from *positivity* and *minimum* conditions, tree-level unitarity and perturbativity. *Positivity* means that the potential must be positive (stable) for all values of the fields  $|\phi_a|$ . The *minimum* condition is the requirement for the extremum to be precisely a minimum. Both conditions give lower bounds on the parameters. On the other hand, to preserve tree-level unitarity, the quartic scalar self-interactions that contribute to different scattering amplitudes, scalar-scalar, scalar-gauge or gauge-gauge bosons s-waves, have to be such that the corresponding amplitude (partial wave) does not exceed the unitary limit. This condition gives upper and lower bounds. In general, all these constraints have been analyzed in the literature (for a review see [23] and references therein) for a CP conserving potential, where a  $\mathcal{Z}_2$ -type discrete symmetry enforces  $\mu_{12} = \lambda_5 = \lambda_6 = \lambda_7 = 0$ . There are some other studies where this symmetry is *softly* broken in the potential ( $\mu_{12} \neq 0, \lambda_5 \neq 0, \lambda_6 = \lambda_7 = 0$ ), and only for unitarity the study is extended for a general CP non-conserving potential [23]. These constraints are summarized in the following in terms of the parameters of the potential in the general basis (3.7),  $\mu'_i$  and  $\lambda'_i$  (the equivalences with  $Y_{ab}$  and  $Z_{abcd}$  and  $\mu_i$  and  $\lambda_i$  are given in the Appendix A).

- The positivity constraints in the case of soft  $\mathcal{Z}_2$  violation are analyzed in [23,31–35]. For the potential to be bounded from below, only the quartic terms have to be examined. Assuming that directions in the fields space where  $\mathcal{V} \rightarrow -\infty$  do not exist and neither flat directions for the quartic piece of the potential, the following conditions on  $\lambda'_i$  are easily obtained [34],

$$\begin{aligned} \lambda'_1 > 0, \quad \lambda'_2 > 0, \quad \lambda'_3 > -\sqrt{\lambda'_1 - \lambda'_2}, \\ \lambda'_3 + \lambda'_4 - |\lambda'_5| > \sqrt{\lambda'_1 \lambda'_2}. \end{aligned} \quad (3.19)$$

- The minimum constraints ensure that the extremum of the potential is a minimum for all directions in the scalar fields space. This happens if the mass matrix squared (3.13) is defined positive, i.e. its eigenvalues are positive,

$$M_{1,2,3}^2 > 0 \quad M_{H^\pm}^2 > 0. \quad (3.20)$$

- The tree-level unitarity constraint was first discussed by [36] in the SM framework. This kind of constraints can be derived by constructing the tree-level scattering matrices of all possible Higgs-Higgs,  $W_L$ - $W_L$ ,  $Z_L$ -Higgs, etc. states at very high energies, and diagonalizing them. Then the unitarity conditions are translated into limits to the eigenvalues of these matrices, which are given in terms of the Higgs potential parameters, as it is presented in [37], again in the SM. For a SM Higgs potential like  $\mathcal{V}_{SM} = (\lambda/2)(\phi^\dagger\phi - v^2/2)^2$  the condition arises as  $3\lambda \leq 8\pi$ , where the SM Higgs mass is  $M_h = v\sqrt{\lambda}$ . The decay rate of the Higgs  $\Gamma_h$  is basically dominated by the Higgs decay into the longitudinal components of the gauge bosons,  $W_L$  and  $Z_L$ , and grows

as  $M_h^3$ . Therefore, the unitarity limit is realized when  $\Gamma_h \sim M_h$ , where the physical Higgs boson disappears. Above this limit ( $\lambda \geq 8\pi$  at  $\sqrt{s} > v\sqrt{\lambda} \geq v\sqrt{8\pi} \sim 1.2$  TeV) the self-interaction of the Higgs boson and the  $W_L$  and  $Z_L$  interactions become strong (non-perturbative). The unitarity violation of a partial wave at tree-level in a gauge theory is protected by higher order diagrams that will come to the rescue, however, a strongly interacting field theory is an unresolved situation. The unitarity limit is therefore a boundary limit in  $\lambda$ 's space between this unlikely regime and the one that describes a physical Higgs boson with well known properties and no strong effects in the Higgs sector.

In the 2HDM, this was derived for a CP conserving potential enforced by an exact  $\mathcal{Z}_2$  symmetry in [38]. The cases of soft and complete  $\mathcal{Z}_2$  violation in the potential were analyzed in [35] and [39] respectively. We summarize below the unitarity conditions given for the eigenvalues of the scattering matrices arising in the latter cases [39]. The generic limit is

$$|\Lambda_{Y\sigma\pm}^{\mathcal{Z}_2}| < 8\pi, \quad (3.21)$$

where initial states  $\phi_a\phi_b$  with different  $\mathcal{Z}_2$  parity (even or odd), total hypercharge and weak isospin, give different cases that accomplish the upper limit:

$$\begin{aligned} \Lambda_{21\pm}^{\text{even}} &= \left( \lambda'_1 + \lambda'_2 \pm \sqrt{(\lambda'_1 - \lambda'_2)^2 + 4|\lambda'_5|^2} \right), \\ \Lambda_{21\pm}^{\text{odd}} &= \lambda'_3 + \lambda'_4, \\ \Lambda_{20\pm}^{\text{odd}} &= \lambda'_3 - \lambda'_4, \\ \Lambda_{01\pm}^{\text{even}} &= \left( \lambda'_1 + \lambda'_2 \pm \sqrt{(\lambda'_1 - \lambda'_2)^2 + 2|\lambda'_4|^2} \right), \\ \Lambda_{01\pm}^{\text{odd}} &= \lambda'_3 \pm 2|\lambda'_5|, \\ \Lambda_{00\pm}^{\text{even}} &= 3(\lambda'_1 + \lambda'_2) \pm \sqrt{9(\lambda'_1 - \lambda'_2)^2 + 2(2\lambda'_3 + \lambda'_4)^2}, \\ \Lambda_{00\pm}^{\text{odd}} &= \lambda'_3 + 2\lambda'_4 \pm 6|\lambda'_5|. \end{aligned} \quad (3.22)$$

Indirect constraints on the Higgs masses can be obtained from these unitarity conditions. All the masses are given in terms of  $\lambda$ 's and  $\mu_{12}^R$ . Although  $\mu_{12}^R$  does not get any limit from unitarity (only quartic couplings), some reasonable bounds on the masses can be derived for particular values of  $\mu_{12}^R$ . For example, for small values of this quantity [23, 39], the lightest Higgs can have a mass  $\sim 120$  GeV while the others have an upper bound of  $\sim 600$  GeV, without tree-level unitarity violation. For large values of  $\mu_{12}^R$ , all the Higgs particles except the lightest one, do not have any upper constraint on their masses coming from unitarity.

To end up with the theoretical constraints on the parameters of the potential, we make a small comment about custodial symmetry. A first ‘‘disadvantage’’ of the general 2HDM is that custodial symmetry could be broken by mass splittings between charged and neutral Higgs. This already happens at one-loop level ((3.1) holds at tree-level in the 2HDM) and

could be in conflict with electroweak precision data. Custodial symmetry is not an exact symmetry in the SM, it is violated by hypercharge gauge interactions and by the Higgs interactions with fermions in the Yukawa terms. However, the deviations generated by these terms are within the errors of the electroweak precision data. In order not to exceed these errors, further sources of custodial symmetry breaking apart from the latter should be necessarily very small. The Higgs potential in the SM has an “accidental” symmetry,  $SU(2)_L \times SU(2)_R$ , that avoids the possibility of adding one more source to this custodial symmetry violation, but it is not like that in the 2HDM anymore [40]. This problem can be solved in some restricted regions of the parameter space, which are either fine-tuned or implemented by imposing additional (discrete) symmetries on the potential. At the end, the condition for the custodial symmetry to be preserved in this context, results in a set of relations for the masses of the Higgs that need to be accomplished [40].

### Experimental constraints

The Particle Data Group [5] gives a collection of the current bounds on the scalar fields, in supersymmetric models and also in general 2HDM frameworks. For charged Higgs  $H^\pm$  searches, the process  $e^+e^- \rightarrow H^+H^-$  provides a very efficient way without referring to any specific Yukawa structure. Assuming that  $\text{Br}(H^+ \rightarrow c\bar{s}) + \text{Br}(H^+ \rightarrow \tau^+\nu_\tau) = 1$ , the combined LEP data constrain  $M_{H^\pm} > 78.6$  GeV (95% CL) [41]. The limit slightly improves if particular values of  $B_\tau \equiv \text{Br}(H^+ \rightarrow \tau^+\nu_\tau)$  are assumed. The weakest limit of 78.6 GeV is obtained for  $B_\tau \sim 0.4$ – $0.5$ , improving to 81.0 (89.6) for  $B_\tau = 0$  (1). These limits could be avoided by some types of 2HDMs (e.g. the *inert* model [42–45]) in some regions of the parameter space. In such a case, the charged scalar could be detected by the decay mode  $H^\pm \rightarrow W^\pm A$ , if it is kinematically allowed. Assuming a CP-conserving scalar potential, OPAL finds the (95% CL) constraints  $M_{H^\pm} > 56.5$  (64.8) GeV for  $12$  (15) GeV  $< M_A < M_{H^\pm} - M_{W^\pm}$  [46]. CDF [47] and D0 [48] have searched for  $t \rightarrow H^+b$  decays with negative results. CDF assumes  $\text{Br}(H^+ \rightarrow c\bar{s}) = 1$ , while D0 adopts the opposite hypothesis  $\text{Br}(H^+ \rightarrow \tau^+\nu_\tau) = 1$ . Both experiments find upper bounds on  $\text{Br}(t \rightarrow H^+b)$  around 0.2 (95% CL) for charged scalar masses between 60 to 155 GeV. Searches in  $e^+e^-$  collisions at and above the  $Z$  pole have ruled out the existence of a charged Higgs in the region  $M_{H^\pm} \leq 45$  GeV [5].

For neutral Higgs, the experiments in  $e^+e^-$  collisions mostly focus in the processes  $e^+e^- \rightarrow hZ, HZ$  (Higgs-strahlung) in the channels used for SM Higgs searches, and  $e^+e^- \rightarrow hA, HA$  with final states  $b\bar{b}b\bar{b}$  and  $b\bar{b}\tau^-\tau^+$ . In  $p\bar{p}$  collision experiments there are much more possibilities; the main Higgs production processes are the gluon fusion,  $gg \rightarrow h$ , the Higgs production with a vector boson,  $W^\pm h, Zh$ , or with a top quark pair,  $h\bar{t}t$ , and the vector boson fusion resulting in  $qqh$  or  $q\bar{q}h$ . These different processes together with a large integrated luminosity (LHC) provide a variety of search channels.

For a general 2HDM with CP violation the neutral sector is composed by  $h_1, h_2$  and  $h_3$ , which are mass eigenstates with no defined CP parity. The PDG [5] collects some mass limits for a “generic”  $h$  in extended Higgs models not necessarily belonging to a SUSY

framework. For example, a search for Higgs bosons decaying into  $\tau^+\tau^-$  [49] in 2HDMs in  $1.8 \text{ fb}^{-1}$  of  $p\bar{p}$  collisions at  $E_{\text{cm}} = 1.96 \text{ TeV}$  gives a lower bound for a neutral Higgs mass of 106 GeV at 95% CL. Apart from this, some other analysis are summarized in [5] (*Searches for Higgs Bosons*), all of them give lower bounds from different processes on a neutral Higgs boson mass around 100 GeV at 95%. Particular examples of this kind of analysis from D0, DELPHI and OPAL can be found in [50–54].

### A comment on Spontaneous CP violation

Spontaneous CP violation (SCPV) happens when a CP conserving Lagrangian becomes CP violating after the SSB, i.e. CP is a symmetry of the original Lagrangian but it is not for the vacuum. In the SM this phenomenon cannot occur because the complex VEV can always be redefined as a CP invariant number [7]. A natural framework for SCPV is the Weinberg model [55] when CP is assumed to be only spontaneously broken (Branco model [7]). This is a three-Higgs-doublet model where CP is imposed at the Lagrangian level through a discrete symmetry which is broken by the vacuum. In such a case, the  $V$  matrix is real and CP violation comes from scalar particles exchanges. SCPV can also be generated in a 2HDM. Provided that CP is imposed at the Lagrangian level, it can be spontaneously broken if no other discrete symmetry is present; this is called Lee’s model (see [7] for a complete review). The Yukawa couplings are real in the original Lagrangian, but the relative phase between the VEVs of the two scalars appears in the quark mass matrices generating a complex  $V$ .

### 3.2.2 Gauge boson interactions

The gauge structure in the 2HDM is the same as in the SM but just adding the interaction of the second doublet. Actually, the gauge sector structure of the SM is easily recovered by neglecting the interactions with the second doublet fields in the following formulation, where the Higgs basis is used and the first doublet resembles the SM one.

The kinetic term in the Lagrangian of the scalar doublets (3.5) defines their interaction with the gauge bosons through the covariant derivative,

$$D_\mu \equiv \partial_\mu + ig\widetilde{W}_\mu + ig'Y B_\mu, \quad (3.23)$$

where  $\widetilde{W}_\mu = \frac{\sigma^i}{2} W_\mu^i$ , being  $\sigma^i$  the Pauli matrices,  $g$  and  $g'$  are the usual weak coupling constants which are related to each other and to the electromagnetic coupling constant by the weak mixing angle:  $g \sin \theta_w = g' \cos \theta_w = e$ . All the possible interactions between the gauge and scalar fields can be written together as

$$\mathcal{L}_K + \mathcal{L}_\xi + \sum_a (D_\mu \Phi_a)^\dagger D^\mu \Phi_a = \mathcal{L}_{V^2} + \mathcal{L}_{\Phi^2} + \mathcal{L}_{\Phi V} + \mathcal{L}_{\Phi^2 V} + \mathcal{L}_{\Phi V^2} + \mathcal{L}_{\Phi^2 V^2}, \quad (3.24)$$

where  $V$  indicates a gauge (vector) boson,  $\mathcal{L}_K$  is the usual gauge boson kinetic Lagrangian,

$$\mathcal{L}_K = -\frac{1}{4} B_{\mu\nu} B^{\mu\nu} - \frac{1}{4} W_{\mu\nu}^i W_i^{\mu\nu} \quad (3.25)$$

with  $B_{\mu\nu} = \partial_\mu B_\nu - \partial_\nu B_\mu$  and  $W_{\mu\nu}^i = \partial_\mu W_\nu^i - \partial_\nu W_\mu^i - g\epsilon^{ijk}W_\mu^j W_\nu^k$ , and  $\mathcal{L}_\xi$  is the gauge fixing term, which is convenient to take it as follows ( $\xi = 1$ ),

$$\mathcal{L}_\xi = -\frac{1}{2}(\partial_\mu A^\mu)^2 - \frac{1}{2}(\partial_\mu Z^\mu + M_Z G^0)^2 - (\partial^\mu W_\mu^\dagger + iM_W G^+) (\partial_\nu W^\nu - iM_W G^-) . \quad (3.26)$$

The quadratic mixing terms between the gauge and Goldstone bosons generated by the covariant derivative are exactly cancelled by (3.26), making  $\mathcal{L}_{\Phi V} = 0$  and generating the Goldstone bosons with masses  $M_{G^\pm} = M_W = gv/2$  and  $M_{G^0} = M_Z = M_W/\cos\theta_w$ . The other quadratic terms are,

$$\mathcal{L}_{V^2} = -\frac{1}{2}(\partial_\mu A^\mu)^2 - \frac{1}{2}(\partial_\mu Z^\mu)^2 - \partial^\mu W_\mu^\dagger \partial_\nu W^\nu + \frac{1}{2}M_Z^2 Z_\mu Z^\mu + M_W^2 W_\mu^\dagger W^\mu , \quad (3.27)$$

and

$$\begin{aligned} \mathcal{L}_{\Phi^2} &= \frac{1}{2}(\partial_\mu H \partial^\mu H + \partial_\mu h \partial^\mu h + \partial_\mu A \partial^\mu A) + \partial_\mu H^+ \partial^\mu H^- \\ &+ \frac{1}{2}\partial_\mu G^0 \partial^\mu G^0 - \frac{1}{2}M_Z^2 (G^0)^2 + \partial_\mu G^+ \partial^\mu G^- - M_W^2 G^+ G^- . \end{aligned} \quad (3.28)$$

The interaction terms between the gauge and scalar fields are then cubic and quartic:

$$\begin{aligned} \mathcal{L}_{\Phi^2 V} &= ie(A^\mu + \cot(2\theta_w)Z^\mu) \left[ (H^+ \overleftrightarrow{\partial}_\mu H^-) + (G^+ \overleftrightarrow{\partial}_\mu G^-) \right] \\ &+ \frac{e}{\sin(2\theta_w)} Z^\mu \left[ (G^0 \overleftrightarrow{\partial}_\mu S_1) + (S_3 \overleftrightarrow{\partial}_\mu S_2) \right] \\ &+ \frac{g}{2} \left\{ W^{\mu\dagger} \left[ (H^- \overleftrightarrow{\partial}_\mu S_3) - i(H^- \overleftrightarrow{\partial}_\mu S_2) + (G^- \overleftrightarrow{\partial}_\mu G^0) - i(G^- \overleftrightarrow{\partial}_\mu S_1) \right] \right. \\ &\left. + \text{h.c.} \right\} , \end{aligned} \quad (3.29)$$

$$\begin{aligned} \mathcal{L}_{\Phi V^2} &= \frac{2}{v} S_1 \left( \frac{1}{2}M_Z^2 Z_\mu Z^\mu + M_W^2 W_\mu^\dagger W^\mu \right) \\ &+ (eM_W A^\mu - gM_Z \sin^2\theta_w Z^\mu) (G^+ W_\mu + G^- W_\mu^\dagger) , \end{aligned} \quad (3.30)$$

and

$$\begin{aligned} \mathcal{L}_{\Phi^2 V^2} &= \frac{1}{v^2} \left( \frac{1}{2}M_Z^2 Z_\mu Z^\mu + M_W^2 W_\mu^\dagger W^\mu \right) (H^2 + h^2 + A^2 + (G^0)^2) \\ &+ \left( e^2 [A^\mu + \cot(2\theta_w)Z^\mu]^2 + \frac{g^2}{2} W_\mu^\dagger W^\mu \right) (G^+ G^- + H^+ H^-) \\ &+ \frac{eg}{2} (A^\mu - \tan\theta_w Z^\mu) [S_1 (G^+ W_\mu + G^- W_\mu^\dagger) + S_2 (H^+ W_\mu + H^- W_\mu^\dagger)] . \end{aligned} \quad (3.31)$$

### 3.2.3 Yukawa interactions

The most general Yukawa Lagrangian is given by

$$\begin{aligned} \mathcal{L}_Y = & - \bar{Q}'_L(\Gamma_1\phi_1 + \Gamma_2\phi_2) d'_R - \bar{Q}'_L(\Delta_1\tilde{\phi}_1 + \Delta_2\tilde{\phi}_2) u'_R \\ & - \bar{L}'_L(\Pi_1\phi_1 + \Pi_2\phi_2) l'_R + \text{h.c.} , \end{aligned} \quad (3.32)$$

where  $Q'_L$  and  $L'_L$  denote the left-handed quark and lepton doublets and the prime indicates that they are gauge eigenstates. All fermionic fields are written as  $N_G$ -dimensional flavour vectors; i.e.,  $d'_R = (d'_R, s'_R, b'_R, \dots)$  and similarly for  $u'_R, l'_R, Q'_L$  and  $L'_L$ . The couplings  $\Gamma_a, \Delta_a$  and  $\Pi_a$  are  $N_G \times N_G$  complex matrices in flavour space. In the Higgs basis, the Lagrangian takes the form

$$\begin{aligned} \mathcal{L}_Y = & - \frac{\sqrt{2}}{v} \{ \bar{Q}'_L(M'_d\Phi_1 + Y'_d\Phi_2) d'_R + \bar{Q}'_L(M'_u\tilde{\Phi}_1 + Y'_u\tilde{\Phi}_2) u'_R \\ & + \bar{L}'_L(M'_l\Phi_1 + Y'_l\Phi_2) l'_R + \text{h.c.} \} , \end{aligned} \quad (3.33)$$

where  $M'_f$  ( $f = u, d, l$ ) are the non-diagonal fermion mass matrices, while the matrices  $Y'_f$  contain the Yukawa couplings to the scalar doublet with zero vacuum expectation value.

In the basis of fermion mass eigenstates (see equation (2.5)) the Yukawa Lagrangian can be written as

$$\begin{aligned} \mathcal{L}_Y = & - \{ \bar{u}_L M_u u_R + \bar{d}_L M_d d_R + \bar{l}_L M_l l_R \\ & + \frac{1}{v} (\bar{u}_L M_u u_R + \bar{d}_L M_d d_R + \bar{l}_L M_l l_R) S_1 \\ & + \frac{1}{v} \bar{u}_L Y_u u_R (S_2 - iS_3) - \frac{\sqrt{2}}{v} \bar{d}_L V^\dagger Y_u u_R H^- \\ & + \frac{\sqrt{2}}{v} \bar{u}_L V Y_d d_R H^+ + \frac{1}{v} \bar{d}_L Y_d d_R (S_2 + iS_3) \\ & + \frac{\sqrt{2}}{v} \bar{\nu}_L Y_l l_R H^+ + \frac{1}{v} \bar{l}_L Y_l l_R (S_2 + iS_3) \\ & + \text{h.c.} \} , \end{aligned} \quad (3.34)$$

where  $X_f = S_f X'_f U_f^\dagger S_f^\dagger$  but now  $X' = M', Y'$ , differently from the SM where  $X'$  was a single matrix. Again,  $V \equiv S_u S_d^\dagger$  corresponds to the usual Cabibbo-Kobayashi-Maskawa mixing matrix<sup>2</sup>. The unitary matrices  $S_f$  and  $U_f$  can be chosen such that  $M_f$  is a diagonal matrix whose elements correspond to the masses of the fermions; however,  $Y'_f$  are not necessarily diagonalized simultaneously by the same choice, therefore  $Y_f$  are in general non-diagonal matrices and unrelated to the fermion masses, introducing a mixing also in the neutral sector. In this way, flavour-changing neutral couplings are *naturally* generated by the model

<sup>2</sup>In the 2HDM there are not right-handed neutrinos either, thus the left-handed fields can also be redefined as  $\bar{\nu}_L = \bar{\nu}'_L S_l^\dagger$  and consequently there is no mixing matrix analog to  $V$  in the charged lepton sector.

(non-suppressed) without any dynamical restriction. This represents a contradiction with the experimental data, where FCNC phenomena appear strongly constrained, and therefore constitutes a second “disadvantage” of the general 2HDM: *unbounded flavour-changing interactions of the neutral scalars are allowed because the flavour structure of the model couples two different Yukawa matrices at the same time to a given right-handed fermion sector.*

As was argued for the custodial symmetry, the problem is solved in some regions of the parameter space, either fine-tuning those couplings or implementing ad-hoc dynamical restrictions in the Lagrangian to guarantee their suppression at the required level. To this aim, many models have been developed and can be classified in four main groups:

- Type III 2HDM

The use of some flavour symmetry generating a certain texture in the Yukawa matrices leads to a phenomenologically viable model [56–62]. The most famous example of this kind of approaches is the so-called *Sher-Cheng approximation* [57], where the off-diagonal elements of the Yukawa matrices are forced to be proportional to the mean of the fermion masses,

$$g_{ij} \propto \sqrt{m_i m_j}. \quad (3.35)$$

These models allow the discussion of suppressed FCNC phenomena, incorporating in some cases possible new CP violating sources generated by the complex numbers in the Yukawa matrices. The work developed in [63] shows the explicit form of a flavour symmetry for generating different textures.

- Decoupling limit

Another obvious possibility is to require the new scalar bosons to be heavy enough to suppress FCNCs at low energies. Although in this framework the phenomenological impact is reduced, it is considered the most “natural” scenario for the general 2HDM.

- $\mathcal{Z}_2$ -type models (I, II, X, Y and inert)

The standard way to avoid the FCNC problem is forcing one of the two Yukawa matrices to be zero; i.e., imposing that only one scalar doublet couples to a given right-handed fermion field [36]. This can be enforced implementing a discrete  $\mathcal{Z}_2$  symmetry, such that

$$\phi_1 \rightarrow \phi_1, \quad \phi_2 \rightarrow -\phi_2, \quad Q_L \rightarrow Q_L, \quad L_L \rightarrow L_L, \quad (3.36)$$

and selecting appropriate transformation properties for the right-handed fermion fields. There are four non-equivalent possible choices, giving rise to the so-called type I (only  $\phi_2$  couples to fermions) [64, 65], type II ( $\phi_1$  couples to  $d$  and  $l$ , while  $\phi_2$  couples to  $u$ ) [65, 66], leptophilic or type X ( $\phi_1$  couples to leptons and  $\phi_2$  to quarks) and type Y ( $\phi_1$  couples to  $d$ , while  $\phi_2$  couples to  $u$  and  $l$ ) models [67–73]. All these

cases make also the potential CP conserving. The explicit implementation of the  $\mathcal{Z}_2$  symmetry differentiates one doublet from the other and, therefore, is not scalar-basis invariant. In particular, if the  $\mathcal{Z}_2$  symmetry is imposed in the Higgs basis, all fermions are forced to couple to the field  $\Phi_1$  in order to get non-vanishing masses. This *inert* doublet model provides a natural frame for dark matter [42–45]; note however that although  $\Phi_2$  does not couple to fermions, it does have electroweak interactions.

The minimal supersymmetric extension of the SM corresponds at tree level with the type II 2HDM, which is the default version adopted in the majority of phenomenological analyses. The use of discrete symmetries guarantees the absence of FCNCs in the Yukawa sector, but eliminates at the same time the possibility to have additional CP-violating phases beyond the SM.

- Aligned 2HDM

A softer and more general way to avoid tree-level FCNC interactions is to require the alignment in flavour space of the Yukawa couplings of the two scalar doublets [74]. While this is also an ad-hoc constraint, lacking a proper dynamical explanation (probably coming from a more fundamental high-energy theory), it leads to a much more general framework which contains as particular cases all known 2HDMs based on  $\mathcal{Z}_2$  symmetries. All possible freedom in the Yukawa sector gets parametrized in terms of three complex couplings; their phases being possible new sources of CP violation.

In this thesis we will first present some features about the general 2HDM in Chapter 4, in particular, we will perform a general discussion about lepton flavour violation (LFV), which is allowed in this case. In Chapter 5 and Chapter 6, we will discuss further the general structure of this new *aligned* 2HDM (A2HDM) together with some relevant phenomenological implications. And finally, in Chapter 7, we will study also the 2HDM in the presence of an extra  $U(1)$  gauge boson, generating a framework similar to the inert model.



# Chapter 4

## The general two-Higgs-doublet model: LFV tests

### 4.1 Introduction

One of the most important features of the general 2HDM is the presence of flavour-changing neutral currents (FCNCs) at tree level. Contrary to the SM, which predicts diagonal neutral couplings in agreement with the experimental data (processes like  $\mu \rightarrow eee$  have never been observed), the 2HDM has to deal with these strongly constrained phenomena. However, under a different point of view, this “handicap” can also be interpreted as a positive feature of the model. FCNC interactions do not seem to violate any fundamental law of nature, they are only prohibited in the quark sector at tree level. Experimentally, the constraints are very tight, but on the other hand, in the leptonic sector they are easier to accommodate. Therefore, one can think that FCNCs make the model more versatile, providing more freedom. If FCNC signals are detected, the SM will not be able to fit them, while models like the general 2HDM would become a *natural* framework.

The up-to-date experimental bounds on these processes can be used to restrict the parameter space of the general 2HDM. Such analysis has not been performed systematically, but only taking the model to some limits (for an overview of the allowed parameter space in these limits see [75–79] and references therein). This is due to the large amount of degrees of freedom. In the quark sector it is rather difficult because there are two new Yukawa matrices,  $Y_u$  and  $Y_d$ , involved (see the Yukawa interactions in equation (3.34)) and the flavour structure is quite complicated. In the leptonic sector there is only one free Yukawa matrix,  $Y_l$ , due to the absence of right-handed neutrinos. Lepton flavour violation (LFV) is therefore the simplest flavour-changing neutral phenomenon that can be found in the model.

Motivated by that fact, we present in this chapter a general analysis [80] about LFV, focused on the study of different operators (scalar, vector and dipole) that could describe this kind of interactions. The analysis is of great interest for the general 2HDM, since it contributes with the scalar operator. We exploit the possibility of having some experi-

ments at low energies, whose results would allow us to discriminate among different models (operators). Those experiments are based in the  $\mu \rightarrow e$  conversion in some nuclei.

## 4.2 The model discriminating power of $\mu \rightarrow e$ conversion in nuclei

Lepton flavour violating decays of charged leptons provide a theoretically clean probe of physics beyond the Standard Model (SM), due to the un-observably small branching fractions ( $\sim 10^{-50}$ ) within the SM, minimally extended to include massive neutrinos. Searches for SM forbidden muon processes, such as  $\mu \rightarrow e\gamma$ ,  $\mu \rightarrow e\bar{e}e$ , and  $\mu \rightarrow e$  conversion in nuclei, have provided so far the strongest constraints on LFV dynamics, with 90% C.L. upper limits given by  $B_{\mu \rightarrow e\gamma} < 1.2 \times 10^{-11}$  [81],  $B_{\mu^+ \rightarrow e^+e^-e^+} < 1.0 \times 10^{-12}$  [82],  $B_{\mu \rightarrow e}(\text{Au}) < 8 \times 10^{-13}$  [83],  $B_{\mu \rightarrow e}(\text{Ti}) < 4.3 \times 10^{-12}$  [84],  $B_{\mu \rightarrow e}(\text{Pb}) < 4.6 \times 10^{-11}$  [85]<sup>1</sup>.

It is a well known fact that while the decay  $\mu \rightarrow e\gamma$  is only sensitive to a transition magnetic dipole operator, both  $\mu \rightarrow e\bar{e}e$  and  $\mu \rightarrow e$  conversion in nuclei are sensitive to transition charge radii operators as well as purely contact four-fermion interactions induced by physics beyond the SM. In other words, different LFV decays have different sensitivities to underlying LFV mechanisms (effective operators). This leads naturally to ask the question whether one could infer the relative strength of these different operators in a completely phenomenological and model-independent way. This would allow one to discriminate among different underlying models of LFV and thus would provide valuable input for model building.

In Ref. [86] it was pointed out that in principle, by combining the rates of  $\mu \rightarrow e\gamma$  and  $\mu \rightarrow e$  conversion on different target nuclei, one could obtain information on underlying models. There are three types of effective operators that contribute to the coherent  $\mu \rightarrow e$  conversion process: the dipole, the vector, and the scalar operators. In the non-relativistic approximation of the muon wave function, the three operators give the same form of overlapping integrals among the wave functions of the initial muon and the final electron and the nucleon density in the target nuclei. However, as the relativistic and finite nuclear size effects become important for heavy nuclei [86–88], the transition amplitudes for the three operators show different dependences on the atomic number  $Z$ . The relative numbers of neutrons and protons also change as  $Z$  increases. This fact helps to find out if the lepton-flavour-violating operators couples to up-type or down-type quarks again by looking at the target atom dependence. In this work [80] we go back to this issue with the aim to:

- quantify the theoretical uncertainty induced by the quark scalar density matrix elements in the nucleon;
- quantify the experimental precision required to realistically infer useful information on the underlying LFV mechanisms.

---

<sup>1</sup> $B_{\mu \rightarrow e}(Z, A)$  represents the ratio of  $\mu \rightarrow e$  conversion rate over muon capture rate, namely  $\frac{\Gamma_{conv}(Z, A)}{\Gamma_{capt}(Z, A)}$ .

We organize our discussion as follows: in Section 4.3 we review the derivation of the  $\mu \rightarrow e$  conversion rate starting from a general effective theory description of the LFV physics. In Section 4.4 we explore the phenomenological consequence of the simplest possible models, in which only one effective LFV operator dominates. We extend this analysis in Section 4.5 to the class of models in which two operators dominate. In Section 4.6 we specialize our discussion to a supersymmetric (SUSY) model and summarize the conclusions of our analysis in Section 4.7.

### 4.3 LFV effective interaction and the $\mu \rightarrow e$ conversion rate

In this section we review the procedure to calculate the rate of the  $\mu \rightarrow e$  conversion in nuclei, starting from a general parameterization of new physics effects via effective operators at a scale  $\Lambda$  larger than the electroweak scale  $v \simeq 174$  GeV.

#### 4.3.1 Effective Lagrangian

We start with the most general effective Lagrangian which describes LFV transitions between charged leptons of first and second families at the weak scale:

$$\begin{aligned} \mathcal{L}_{eff}^{(q)} = & -\frac{1}{\Lambda^2} \left[ (C_{DR} m_\mu \bar{e} \sigma^{\rho\nu} P_L \mu + C_{DL} m_\mu \bar{e} \sigma^{\rho\nu} P_R \mu) F_{\rho\nu} \right. \\ & + \sum_q \left( C_{VR}^{(q)} \bar{e} \gamma^\rho P_R \mu + C_{VL}^{(q)} \bar{e} \gamma^\rho P_L \mu \right) \bar{q} \gamma_\rho q \\ & + \sum_q \left( C_{SR}^{(q)} m_\mu m_q G_F \bar{e} P_L \mu + C_{SL}^{(q)} m_\mu m_q G_F \bar{e} P_R \mu \right) \bar{q} q \\ & \left. + (C_{GR} m_\mu G_F \bar{e} P_L \mu + C_{GL} m_\mu G_F \bar{e} P_R \mu) \frac{\beta_H}{2g_s^3} G_a^{\rho\nu} G_\rho^a + h.c. \right]. \quad (4.1) \end{aligned}$$

We have not included operators involving  $\bar{q} \gamma_\rho \gamma_5 q$ ,  $\bar{q} \gamma_5 q$ , or  $\bar{q} \sigma_{\rho\nu} q$  since they do not contribute to the coherent conversion processes. In the above expression  $\Lambda$  represents the scale where new physics effects appear. We take  $\Lambda \equiv 1$  TeV in this analysis. The  $C_{AB}$ 's are dimensionless constants containing information about the underlying theory; the subindexes  $R, L$  correspond to the chirality of the final electron which is determined by  $P_{R,L} = (1 \pm \gamma^5)/2$ ,  $q$  are light and heavy quarks. The field strength of the photon and the gluon are defined by  $F_{\rho\nu} = \partial_\rho A_\nu - \partial_\nu A_\rho$  and  $G_{\rho\nu}^a = \partial_\rho G_\nu^a - \partial_\nu G_\rho^a - f_{abc} G_\rho^b G_\nu^c$ , respectively. The normalization is chosen so that the kinetic terms are given by  $-(1/4)FF$  and  $-(1/4g_s^2)G^a G^a$ . The  $\sigma$  matrix is defined by  $\sigma^{\rho\nu} = \frac{i}{2}[\gamma^\rho, \gamma^\nu]$ .  $G_F = 1/(\sqrt{2}v^2)$  is the Fermi constant, while  $m_\mu$  and  $m_q$  represent the muon and running quark masses at  $\mu = \Lambda$ , respectively. We have introduced the running quark masses and the beta function of the QCD coupling constant,

$\beta = (g_s^3/16\pi^2)(11 - 2N_F/3)$ , so that the coefficients  $C$ 's do not depend on the renormalization scale under QCD running at 1-loop level. The notation  $\beta_{H,L}$  is used to distinguish the Lagrangian with all quarks contributions (H) from the one where heavy quarks are integrated out (L). The Lagrangian in Eq. (4.1) describes three kind of interactions that violate the lepton flavour: The effective interaction with a photon (Dipole term), the effective interaction with quarks (Scalar and Vector terms) and the effective interaction with gluons (Gluon term).

In order to evaluate the  $\mu \rightarrow e$  conversion rate, it is appropriate to use the effective Lagrangian at the nucleon level [89]. We first integrate out the heavy quarks before matching to the nucleon level Lagrangian. It can be straightforwardly done by using the matching of the trace anomaly [90]. The Lagrangian is given by

$$\begin{aligned} \mathcal{L}_{\text{eff}}^{(q')} &= -\frac{1}{\Lambda^2} \left[ (C_{DR} m_\mu \bar{e} \sigma^{\rho\nu} P_L \mu + C_{DL} m_\mu \bar{e} \sigma^{\rho\nu} P_R \mu) F_{\rho\nu} \right. \\ &+ \sum_{q=u,d,s} \left( C_{VR}^{(q)} \bar{e} \gamma^\rho P_R \mu + C_{VL}^{(q)} \bar{e} \gamma^\rho P_L \mu \right) \bar{q} \gamma_\rho q \\ &+ \sum_{q=u,d,s} \left( C_{SR}^{(q)} m_\mu m_q G_F \bar{e} P_L \mu + C_{SL}^{(q)} m_\mu m_q G_F \bar{e} P_R \mu \right) \bar{q} q \\ &\left. + (C_{GQR} m_\mu G_F \bar{e} P_L \mu + C_{GQL} m_\mu G_F \bar{e} P_R \mu) \frac{\beta_L}{2g_s^3} G_a^{\rho\nu} G_{\rho\nu}^a + h.c. \right], \quad (4.2) \end{aligned}$$

where  $\beta_L$  is the beta function of three-flavour QCD. The new coefficients of the gluon terms are expressed in terms of the original Lagrangian parameters as follows:

$$\begin{aligned} C_{GQR} &= \sum_{Q=c,b,t} C_{SR}^{(Q)} \kappa_Q + C_{GR} \kappa, \\ C_{GQL} &= \sum_{Q=c,b,t} C_{SL}^{(Q)} \kappa_Q + C_{GL} \kappa, \end{aligned} \quad (4.3)$$

where

$$\kappa_Q = \frac{\Delta(\beta/g_s^3)}{(\beta/g_s^3)_L} = \frac{27}{2}, \quad \kappa = \frac{(\beta/g_s^3)_H}{(\beta/g_s^3)_L} = \frac{7}{9}, \quad (4.4)$$

being  $\Delta(\beta/g_s^3) \equiv \frac{1}{3}[(\beta/g_s^3)_L - (\beta/g_s^3)_H]$ . The Lagrangian (4.2) can be evolved with the renormalization group down to energy scales of the order of  $\mu \sim 1$  GeV, by simply taking the quark masses and gauge coupling constants in the Lagrangian to be the running ones at  $\mu \sim 1$  GeV. At this low scale, we match to the effective Lagrangian written in terms of the relevant degrees of freedom, namely nucleons, leptons, and photons. That can be done by the following replacements of operators:

$$\begin{aligned} m_q \bar{q} q &\rightarrow f_{SN}^{(q)} m_N \bar{\psi}_N \psi_N, \\ \bar{q} \gamma_\rho q &\rightarrow f_{VN}^{(q)} \bar{\psi}_N \gamma_\rho \psi_N, \\ \frac{\beta_L}{2g_s^3} G G &\rightarrow f_{GN} m_N \bar{\psi}_N \psi_N. \end{aligned} \quad (4.5)$$

where  $N$  represents each nucleon ( $N = p, n$ ),  $\psi_N$  are the nucleon fields, and  $f$ 's are nucleon form factors. The form factors depend in principle on the momentum transfer, which we will neglect as it is smaller than the typical scale of the nucleon structure. The fact that  $\langle N | \theta_\alpha^\alpha | N \rangle = m_N \langle N | \bar{\psi}_N \psi_N | N \rangle$ , where  $\theta_\alpha^\alpha$  is the trace of the energy momentum tensor,

$$\theta_\alpha^\alpha = \sum_{q'=u,d,s} m_{q'} \bar{q}' q' + \sum_{Q=c,t,b} m_Q \bar{Q} Q + \frac{\beta_H}{2g_H^3} G_a^{\rho\nu} G_{\rho\nu}^a, \quad (4.6)$$

implies the simple sum-rule

$$1 = \sum_{q=u,d,s} f_{SN}^{(q)} + f_{GN}, \quad (4.7)$$

which we use to eliminate the form-factor  $f_{GN}$  in terms of the scalar nucleon form factors  $f_{SN}^{(q)}$ . The nucleon vector form factors are known from the vector current conservation,

$$\begin{aligned} f_{Vp}^{(u)} &= 2 & f_{Vn}^{(u)} &= 1, \\ f_{Vp}^{(d)} &= 1 & f_{Vn}^{(d)} &= 2, \\ f_{Vp}^{(s)} &= 0 & f_{Vn}^{(s)} &= 0, \end{aligned} \quad (4.8)$$

while the calculation of the scalar form factors  $f_{SN}^{(q)}$  is non-trivial. As discussed below, in our analysis we will use input from Chiral Perturbation Theory and the lattice QCD to asses the impact of current and future uncertainties on the conversion rate.

Collecting the above results, the Lagrangian at nucleon level can be written as

$$\begin{aligned} \mathcal{L}_{eff}^{(N)} &= -\frac{1}{\Lambda^2} \sum_{N=p,n} \left[ (C_{DR} m_\mu \bar{e} \sigma^{\rho\nu} P_{L\mu} + C_{DL} m_\mu \bar{e} \sigma^{\rho\nu} P_{R\mu}) F_{\rho\nu} \right. \\ &+ \left( \tilde{C}_{VR}^{(N)} \bar{e} \gamma^\rho P_{R\mu} + \tilde{C}_{VL}^{(N)} \bar{e} \gamma^\rho P_{L\mu} \right) \bar{\psi}_N \gamma_\rho \psi_N \\ &+ \left. G_F m_\mu m_N \left( \tilde{C}_{SR}^{(N)} \bar{e} P_{L\mu} + \tilde{C}_{SL}^{(N)} \bar{e} P_{R\mu} \right) \bar{\psi}_N \psi_N + h.c. \right]. \end{aligned} \quad (4.9)$$

The new effective couplings  $\tilde{C}$ 's contain the information about the underlying theory as well as the form factors. The vector couplings are:

$$\tilde{C}_{VR}^{(p)} = \sum_{q=u,d,s} C_{VR}^{(q)} f_{Vp}^{(q)}, \quad (4.10)$$

$$\tilde{C}_{VR}^{(n)} = \sum_{q=u,d,s} C_{VR}^{(q)} f_{Vn}^{(q)}, \quad (4.11)$$

$$\tilde{C}_{VL}^{(p)} = \sum_{q=u,d,s} C_{VL}^{(q)} f_{Vp}^{(q)}, \quad (4.12)$$

$$\tilde{C}_{VL}^{(n)} = \sum_{q=u,d,s} C_{VL}^{(q)} f_{Vn}^{(q)}, \quad (4.13)$$

while the scalar ones read:

$$\tilde{C}_{SR}^{(p)} = \sum_{q=u,d,s} C_{SR}^{(q)} f_{Sp}^{(q)} + C_{GQR} \left(1 - \sum_{q=u,d,s} f_{Sp}^{(q)}\right), \quad (4.14)$$

$$\tilde{C}_{SR}^{(n)} = \sum_{q=u,d,s} C_{SR}^{(q)} f_{Sn}^{(q)} + C_{GQR} \left(1 - \sum_{q=u,d,s} f_{Sn}^{(q)}\right), \quad (4.15)$$

$$\tilde{C}_{SL}^{(p)} = \sum_{q=u,d,s} C_{SL}^{(q)} f_{Sp}^{(q)} + C_{GQL} \left(1 - \sum_{q=u,d,s} f_{Sp}^{(q)}\right), \quad (4.16)$$

$$\tilde{C}_{SL}^{(n)} = \sum_{q=u,d,s} C_{SL}^{(q)} f_{Sn}^{(q)} + C_{GQL} \left(1 - \sum_{q=u,d,s} f_{Sn}^{(q)}\right). \quad (4.17)$$

### 4.3.2 Transition rates

The nucleon-level effective Lagrangian can be used to take matrix elements at the atomic and nuclear level. In the non-relativistic approximation, the relevant matrix elements are

$$\begin{aligned} \langle A, Z | \bar{\psi}_p \psi_p | A, Z \rangle &= Z \rho^{(p)}, \\ \langle A, Z | \bar{\psi}_n \psi_n | A, Z \rangle &= (A - Z) \rho^{(n)}, \\ \langle A, Z | \bar{\psi}_p \gamma^0 \psi_p | A, Z \rangle &= Z \rho^{(p)}, \\ \langle A, Z | \bar{\psi}_n \gamma^0 \psi_n | A, Z \rangle &= (A - Z) \rho^{(n)}, \\ \langle A, Z | \bar{\psi}_N \gamma^i \psi_N | A, Z \rangle &= 0. \end{aligned} \quad (4.18)$$

Here  $|A, Z\rangle$  represents the nuclear ground state, with  $A$  and  $Z$  the mass and atomic number of the isotope, while  $\rho^{(p)}$  and  $\rho^{(n)}$  are the proton and neutron densities respectively. The conversion rate of the process is written as

$$\begin{aligned} \Gamma_{conv} &= \frac{m_\mu^5}{4\Lambda^4} \left| C_{DR} D + 4G_F m_\mu \left( m_p \tilde{C}_{SR}^{(p)} S^{(p)} + m_n \tilde{C}_{SR}^{(n)} S^{(n)} \right) + \tilde{C}_{VR}^{(p)} 4V^{(p)} + \tilde{C}_{VR}^{(n)} 4V^{(n)} \right|^2 \\ &+ \frac{m_\mu^5}{4\Lambda^4} \left| C_{DL} D + 4G_F m_\mu \left( m_p \tilde{C}_{SL}^{(p)} S^{(p)} + m_n \tilde{C}_{SL}^{(n)} S^{(n)} \right) + \tilde{C}_{VL}^{(p)} 4V^{(p)} + \tilde{C}_{VL}^{(n)} 4V^{(n)} \right|^2 \end{aligned} \quad (4.19)$$

in terms of the dimensionless integrals  $D, V^{(N)}, S^{(N)}$ , representing the overlap of electron and muon wavefunctions weighted by appropriate combinations of protons and neutron densities [86]. For phenomenological applications, it is useful to normalize the conversion rate to the muon capture rate, introducing the quantity:

$$B_{\mu \rightarrow e}(Z) \equiv \frac{\Gamma_{conv}(Z, A)}{\Gamma_{capt}(Z, A)}. \quad (4.20)$$

Finally, we note here the branching ratio for the purely radiative process  $\mu \rightarrow e\gamma$  in terms of the effective couplings defined above:

$$B_{\mu \rightarrow e\gamma} \equiv \frac{\Gamma(\mu \rightarrow e\gamma)}{\Gamma(\mu \rightarrow e\nu_\mu \bar{\nu}_e)} = \frac{48\pi^2}{G_F^2 \Lambda^4} \left( |C_{DR}|^2 + |C_{DL}|^2 \right). \quad (4.21)$$

### 4.3.3 Sources of uncertainty

There are two sources of uncertainty in the calculation of the transition rate: (i) scalar form factors and (ii) neutron density (for high  $Z$  nuclei). The latter uncertainty has been carefully discussed in Ref. [86], where several approaches to determine the neutron density have been reviewed and used in the calculation of the overlap integrals. Whenever data from polarized proton scattering exists, the uncertainty on the overlap integrals  $S^{(n)}$  and  $V^{(n)}$  can be reduced to a few percent even for heavy nuclei such as Pb. Otherwise, it should be considered to be of the order of 10%. In this work we focus on the uncertainty induced by the scalar density matrix elements in the nucleon.

The scalar form factors defined in Eq. (4.5) can be re-expressed in terms of ratio of quark masses and ratios of nucleon matrix elements as follows [91]:

$$f_{Sp}^{(u)} = \frac{m_u}{m_u + m_d} (1 + \xi) \frac{\sigma_{\pi N}}{m_p}, \quad (4.22)$$

$$f_{Sp}^{(d)} = \frac{m_d}{m_u + m_d} (1 - \xi) \frac{\sigma_{\pi N}}{m_p}, \quad (4.23)$$

$$f_{Sp}^{(s)} = \frac{m_s}{m_u + m_d} y \frac{\sigma_{\pi N}}{m_p}, \quad (4.24)$$

$$f_{Sn}^{(u)} = \frac{m_u}{m_u + m_d} (1 - \xi) \frac{\sigma_{\pi N}}{m_p}, \quad (4.25)$$

$$f_{Sn}^{(d)} = \frac{m_d}{m_u + m_d} (1 + \xi) \frac{\sigma_{\pi N}}{m_p}, \quad (4.26)$$

$$f_{Sn}^{(s)} = \frac{m_s}{m_u + m_d} y \frac{\sigma_{\pi N}}{m_p}, \quad (4.27)$$

where

$$\sigma_{\pi N} = \frac{m_u + m_d}{2} \langle p | \bar{u}u + \bar{d}d | p \rangle, \quad (4.28)$$

$$\xi = \frac{\langle p | \bar{u}u - \bar{d}d | p \rangle}{\langle p | \bar{u}u + \bar{d}d | p \rangle}, \quad (4.29)$$

$$y = \frac{2 \langle p | \bar{s}s | p \rangle}{\langle p | \bar{u}u + \bar{d}d | p \rangle}. \quad (4.30)$$

Information on the above matrix elements can be obtained from  $\pi N$  scattering data, from an analysis of the octet baryon masses within Heavy Baryon Chiral Perturbation Theory, or from Lattice QCD.

For the  $\sigma$ -term, we will use the lattice result [92]

$$\sigma_{\pi N} = (53 \pm 2(\text{stat})_{-7}^{+21}(\text{sys})) \text{ MeV}, \quad (4.31)$$

whose uncertainty covers determinations from  $\pi N$  scattering [93–95], from ChPT analysis of baryon masses [96], as well as from previous lattice analyses [97, 98]. For the ratio measuring isospin-breaking, we will use [91, 99]:

$$\xi = 0.132 \pm 0.035. \quad (4.32)$$

For the ratio  $y$  quantifying the strange quark content of the nucleon, the situation is less clear. A Chiral Perturbation Theory analysis gives the range  $y = 0.21 \pm 0.2$  [96]. The large uncertainty reflects the poor knowledge of the relevant low-energy constants, even within resonance saturation (the matching renormalization scale is arbitrary). A recent lattice QCD analysis [92] of the matrix element  $\langle N | \bar{s}s | N \rangle$  within the overlap fermion formulation with two dynamical flavours leads to

$$y = 0.030 \pm 0.016(\text{stat})_{-0.008}^{+0.006}(\text{extrap})_{-0.002}^{+0.001}(m_s) . \quad (4.33)$$

This result is obtained from the lattice matrix element  $\langle N | \bar{s}s | N \rangle$  by dividing out the sigma-term as calculated in the same lattice simulation. Therefore, the uncertainty in  $f_{SN}^{(s)} \propto y \times \sigma_{\pi N}$  is controlled by Eq. (4.33), with  $\sigma_{\pi N} = 53$  MeV simply providing the normalization. The lattice result is consistent with the Chiral Perturbation Theory range, although suggesting a much smaller strange content of the nucleon. The difference with respect to previous lattice results has been attributed to a lattice artifact (mixing with wrong chirality operator) in the Wilson fermion approach. The uncertainty on this value is at the moment dominated by statistics.

For the purpose of this work, we will vary the parameter  $y$  within both a “conservative” range and an “optimistic” range. For the conservative range we take  $y \in [0, 0.4]$ , which coincides with the ChPT range of Ref [96]. For the optimistic range we take  $y \in [0, 0.05]$  which reflects more closely the recent JLQCD result [92] and seems a realistic guess of the uncertainty that will be reached by lattice calculations in the next decade.

Finally, for the ratios of quark masses, we use the the input [100]

$$\frac{m_u}{m_d} = 0.553 \pm 0.043 , \quad (4.34)$$

$$\frac{m_s}{m_d} = 18.9 \pm 0.8 . \quad (4.35)$$

## 4.4 Testing the single operator dominance hypothesis

We now turn to illustrate the model discriminating power of a combined phenomenological analysis of  $\mu \rightarrow e\gamma$  and  $\mu \rightarrow e$  conversion on different target nuclei. In order to organize the discussion, we define here four classes of models, in which only one underlying short distance operator dominates over all the others. We call these four classes of models the “single-operator” dominance models. We will first analyze this simplest class of models and then consider the more involved case in which two operators have comparable strengths and interference effects cannot be neglected.

### 4.4.1 Dipole, Vector and Scalar models

- **Dipole model**

The Dipole model is defined by the assumption that, among all LFV short-distance operators, the dipole operator is the dominant one. For simplicity, we focus on the

case in which the outgoing lepton has definite chirality<sup>2</sup>. Explicitly, in terms of the effective couplings defined in Eq. (4.1), this class of models is defined by:

$$C_D \equiv C_{DR} \neq 0, \quad C_{\text{else}} = 0. \quad (4.36)$$

Most supersymmetric scenarios, including SUSY-GUT models [101–103] and SUSY see-saw models [104, 105] fall in this class of models.

- **Vector model 1:**  $V^{(\gamma)}$

This model is defined by the assumption that the transition charge radius operator gives the dominant contribution to the LFV lagrangian. The model is defined by

$$C_V \equiv C_{VR}^{(u)} = -2C_{VR}^{(d)} \neq 0, \quad C_{\text{else}} = 0, \quad (4.37)$$

and is explicitly realized in large regions of the Left-Right symmetric model parameter space [106]. In this model  $\tilde{C}_{VR}^{(p)} \neq 0$ , while  $\tilde{C}_{VR}^{(n)} = 0$ .

- **Vector model 2:**  $V^{(Z)}$

The Vector model 2 is defined by the assumption that the underlying dominant operator is an effective  $Z$ -penguin. The ratios of couplings of different quarks is governed by the couplings of the  $Z^0$  coupling to quarks. The model is defined by:

$$C_V \equiv C_{VR}^{(u)} = \frac{C_{VR}^{(d)}}{a} \neq 0, \quad C_{\text{else}} = 0, \quad (4.38)$$

where  $a$  is the ratio of the *down* and *up* quarks coupling to the  $Z$ -boson:

$$a = \frac{T_{dL}^3 + T_{dR}^3 - (Q_{dL} + Q_{dR}) \sin^2 \theta_W}{T_{uL}^3 + T_{uR}^3 - (Q_{uL} + Q_{uR}) \sin^2 \theta_W} = -1.73. \quad (4.39)$$

With this value of  $a$  (corresponding to  $\sin^2 \theta_W = 0.223$ ) we obtain  $\tilde{C}_{VR}^{(n)}/\tilde{C}_{VR}^{(p)} = -9.26$ , in contrast to the  $V^{(\gamma)}$  model.

- **Scalar model**

This model is the general case of the 2HDM, in which scalar operators mediate the interactions. It is defined by:

$$C_S \equiv C_{SR}^{(d)} = C_{SR}^{(s)} = C_{SR}^{(b)} \neq 0, \quad C_{\text{else}} = 0. \quad (4.40)$$

This model may be explicitly realized in some regions of the usual R-parity conserving SUSY see-saw parameter space [107] (large  $\tan \beta$  and relatively low "heavy" Higgs sector) and within R-parity violating SUSY [108–111].

---

<sup>2</sup>Allowing for the presence of outgoing leptons with both chiralities (e.g. both  $C_{DR} \neq 0$  and  $C_{DL} \neq 0$ ) would not change the conclusions of the single-operator analysis of this section.

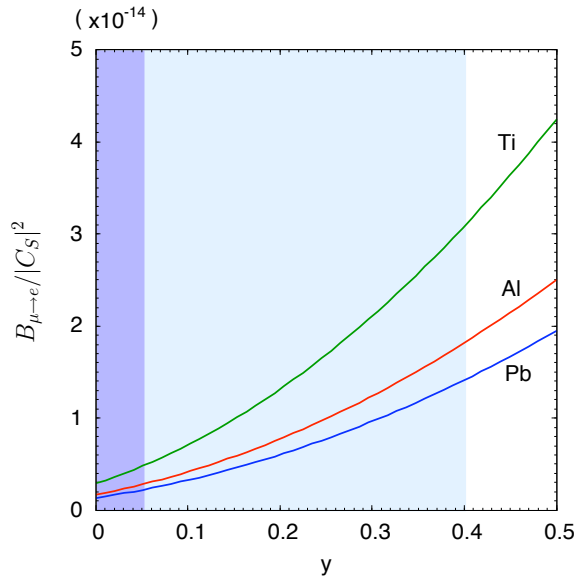


Figure 4.1: The  $y$ -parameter dependence of the conversion branching ratio in the scalar model.

Among the above models, the scalar model suffers from the uncertainty in the  $y$  parameter. We show in Fig. 4.1 the  $y$ -parameter dependence of the conversion branching ratio. The uncertainty is quite large if we take the conservative range,  $y \in [0, 0.4]$ .

Each of the above classes of models has only one free parameter – the ratio  $C_i/\Lambda^2$  of the dominant effective coupling over the square of the new physics scale. It is clear, then, that the single-operator dominance hypothesis makes parameter-free predictions for ratios of LFV branching fractions and therefore it can be tested so long as two LFV rates are measured. We will discuss how well one can distinguish models in the presence of the theoretical uncertainties.

#### 4.4.2 $\mu \rightarrow e\gamma$ vs $\mu \rightarrow e$ conversion

If  $\mu \rightarrow e\gamma$  and  $\mu \rightarrow e$  conversion in at least one target nucleus are observed, this immediately opens up the possibility to test the Dipole dominance model. In fact, in this model the ratio

$$R(Z) = \frac{B_{\mu \rightarrow e}(Z)}{B_{\mu \rightarrow e\gamma}} \quad (4.41)$$

is entirely fixed by the overlap integrals  $D$  [86], which are essentially free of theoretical uncertainty.  $R(Z)$  is predicted to scale as  $\mathcal{O}(\alpha/\pi)$  and we plot it in Fig. 4.2. We omit from the plot the points corresponding to  $^{166}_{68}\text{Er}$ ,  $^{181}_{73}\text{Ta}$ , and  $^{197}_{79}\text{Au}$ , as data on the nucleon densities are either obtained from quite old experiments or not well established [112, 113]. Any deviation from the pattern shown in Fig. 4.2 would imply the presence of scalar or/and vector contributions. In order to disentangle these possibilities, one needs to study the target dependence of the conversion rate.

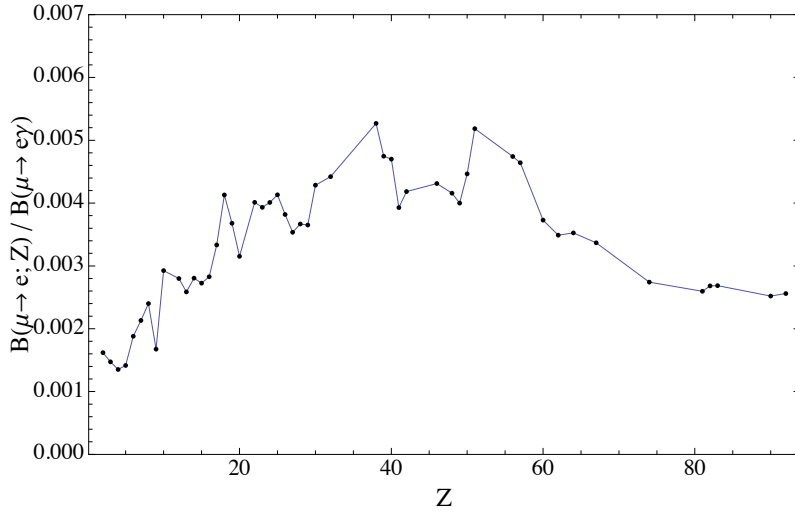


Figure 4.2: Ratio  $R(Z)$  of  $\mu \rightarrow e$  conversion over  $B(\mu \rightarrow e\gamma)$  versus  $Z$  in the case of Dipole dominance model.

#### 4.4.3 Target dependence of $\mu \rightarrow e$ conversion

In principle, any single-operator model can be tested with two conversion rates, even if  $\mu \rightarrow e\gamma$  is not observed. To illustrate this point, we update the analysis of Ref. [86] and plot in Fig. 4.3 the conversion rate (normalized to the rate in Aluminum) as a function of the  $Z$  of the target nucleus, for the four classes of single-operator models defined above. Compared to Ref. [86], the novelty here is the inclusion of a second vector model ( $V^{(Z)}$ ).

The results of Fig. 4.3 show some noteworthy features. First, we note the quite different target dependence of the conversion rate in the two vector models considered. This can be understood as follows: in the case of the  $V^{(\gamma)}$  model, the behavior in Fig. 4.3 simply traces the  $Z$ -dependence of  $V^{(p)}$  (the photon only couples to the protons in the nucleus). On the other hand, in the case of the  $V^{(Z)}$  model, the  $Z$  boson couples predominantly to the neutrons in the nucleus and the target dependence of the ratio  $V^{(n)}/V^{(p)} \sim (A - Z)/Z$  generates the behavior observed in Fig. 4.3.

Next, let us focus on the actual discriminating power of the  $Z$ -dependence. Clearly, the plot shows that the model-discriminating power tends to increase with  $Z$ . This is a simple reflection of the fact that the whole effect is of relativistic origin and increases in heavy nuclei. So in an ideal world, in order to maximize the chance to discriminate among underlying models, one would like to measure the conversion rate in a light nucleus, say Aluminum or Titanium, as well as in a large- $Z$  nucleus, like Lead or Gold. This simplified view, however, has to be confronted both with theoretical uncertainties and the actual experimental feasibility. Concerning the uncertainties, a simple analysis shows that the dominant uncertainty coming from the scalar matrix elements almost entirely cancels when taking ratios of conversion rates (even using the conservative range  $y \in [0, 0.4]$  for the strange scalar density matrix element). Moreover, in the large- $Z$  tail of the plot, some residual uncertainty arises from the input on the neutron density profile. When

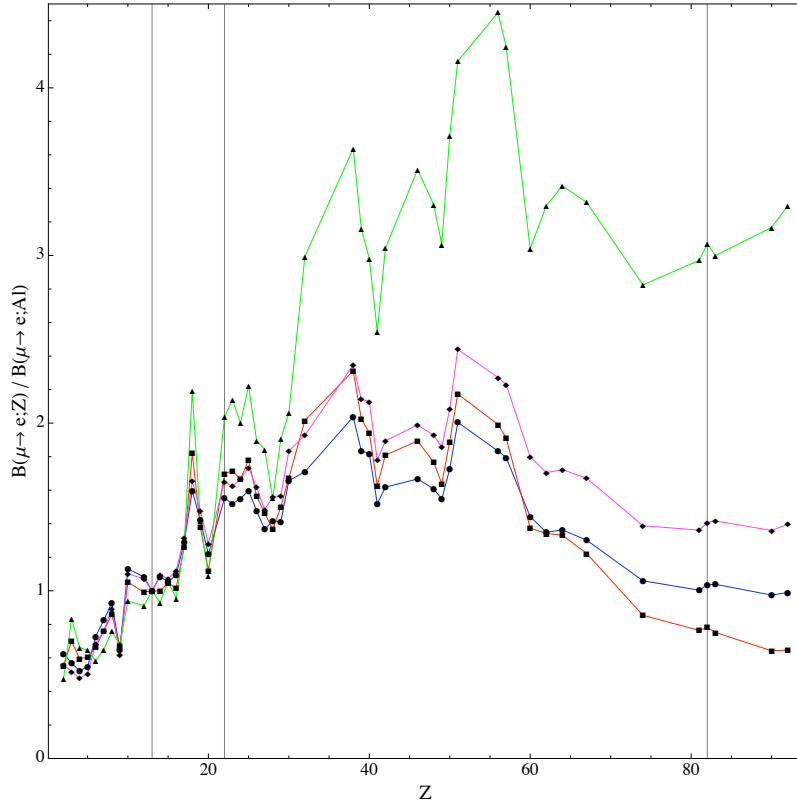


Figure 4.3: Target dependence of the  $\mu \rightarrow e$  conversion rate in different single-operator dominance models. We plot the conversion rates normalized to the rate in Aluminum ( $Z = 13$ ) versus the atomic number  $Z$  for the four theoretical models described in the text:  $D$  (blue),  $S$  (red),  $V^{(\gamma)}$  (magenta),  $V^{(Z)}$  (green). The vertical lines correspond to  $Z = 13$  (Al),  $Z = 22$  (Ti), and  $Z = 83$  (Pb).

polarized proton scattering data exists, the uncertainty on the ratios of conversion rates becomes negligible. This point is illustrated by Table 4.1, where we report the detailed breakdown of uncertainties in the ratios  $B_{\mu \rightarrow e}(\text{Ti})/B_{\mu \rightarrow e}(\text{Al})$  and  $B_{\mu \rightarrow e}(\text{Pb})/B_{\mu \rightarrow e}(\text{Al})$ . For other targets, the uncertainty induced by neutron densities never exceeds 5% [86]. The conclusions of this exercise are that:

- The theoretical uncertainties (scalar matrix elements and neutron densities) largely cancel when we take a ratio.
- As evident from Fig. 4.3, a realistic discrimination among models requires a measure of  $B_{\mu \rightarrow e}(\text{Ti})/B_{\mu \rightarrow e}(\text{Al})$  at the level of 5% or better, or alternatively a measure of  $B_{\mu \rightarrow e}(\text{Pb})/B_{\mu \rightarrow e}(\text{Al})$  at the 20% level. These are two cases that well represent the trend in light and heavy target nuclei.

	$S$	$D$	$V^{(\gamma)}$	$V^{(Z)}$
$\frac{B(\mu \rightarrow e, \text{Ti})}{B(\mu \rightarrow e, \text{Al})}$	$1.70 \pm 0.005_y$	1.55	1.65	2.0
$\frac{B(\mu \rightarrow e, \text{Pb})}{B(\mu \rightarrow e, \text{Al})}$	$0.69 \pm 0.02_{\rho_n}$	1.04	1.41	$2.67 \pm 0.06_{\rho_n}$

Table 4.1: Ratios of conversion rates in Titanium and Lead over Aluminum, in each of the four single-operator models: scalar (S), dipole (D), vector 1 (photon coupling to the quarks) and vector 2 ( $Z$  boson coupling to the quarks). In the scalar model, the scalar form factor induces a negligible uncertainty in the ratios involving two targets (denoted by the subscript  $y$ ). In the case of Lead over Aluminum, the small uncertainty is dominated by the neutron density input (denoted by the subscript  $\rho_n$ ).

## 4.5 Testing the two-operator dominance hypothesis

In the last section we have discussed how to test the hypothesis of a single operator dominance, and how to discriminate among different single-operator dominance models. If the single operator dominance hypothesis fails, one is lead to consider the next simplest case, namely the two-operator dominance models, defined by the assumption that only two underlying operators have appreciable coefficients. Each model is characterized by two parameters, the effective strength  $C_1/\Lambda^2$  of one of the two operators and the ratio  $C_2/C_1$  of the effective couplings of the two dominant operators. This class of models can be tested so long as two double ratios of LFV rates are available (three LFV measurements!).

For the sake of illustration, we will consider the following three two-operator models: Dipole-Scalar, Dipole-Vector( $Z$ ) and Scalar-Vector( $Z$ ). We consider both the case of constructive and destructive interference among the two dominant operators, assuming that the ratio of Wilson coefficients  $r \equiv C_2/C_1$  is real (a relative phase can be included but it would unnecessarily complicate the analysis at this early stage). In order to test this class of models, one has to assume that at least three LFV processes have been observed, so one can construct two independent double ratios that are entirely determined by the single parameter  $r$ . In models involving the Dipole operator among the dominant terms (such as Dipole-Scalar and Dipole-Vector) the three observables could be (i)  $\mu \rightarrow e\gamma$  and  $\mu \rightarrow e$  conversion in two different targets; or (ii)  $\mu \rightarrow e$  conversion in three different targets. In models that do not involve a Dipole term (such as Scalar-Vector), only the possibility (ii) above is available. As representative target nuclei, we have chosen aluminum (Al), titanium (Ti), and lead (Pb).

### 4.5.1 Dipole-Scalar

In terms of the parameters introduced in Section 4.4.1, this model is defined by  $C_S \neq 0$  and  $C_D \equiv \pm \frac{r}{8e} C_S$ . The single-operator models are recovered in the limiting cases  $r \rightarrow 0$

(scalar) and  $r \rightarrow \infty$  (dipole)<sup>3</sup>. Note that in this particular case the asymptotic dipole regime is reached already for  $r \ll 1$  because of the peculiar normalization of the scalar operators (suppressed by the factor  $G_F m_q m_\mu$ ).

We illustrate the features of this model in Figs. 4.4 and 4.5, which correspond to positive and negative sign of the ratio  $C_D/C_S$ , respectively. Panel (a) shows the behavior of  $B_{\mu \rightarrow e}(\text{Al})/B_{\mu \rightarrow e\gamma}$  versus the parameter  $r$ , while panels (b) and (c) show the ratios  $B_{\mu \rightarrow e}(\text{Pb})/B_{\mu \rightarrow e}(\text{Al})$  and  $B_{\mu \rightarrow e}(\text{Ti})/B_{\mu \rightarrow e}(\text{Al})$ , respectively. In panels (a) and (c) the curve is widened in the interference region by the uncertainty in the scalar form factors. The dominant uncertainty comes from the input parameter  $y$ , characterizing the strangeness content of the nucleon. On the other hand, the ratio  $B_{\mu \rightarrow e}(\text{Pb})/B_{\mu \rightarrow e}(\text{Al})$  is affected not only by the uncertainty in the scalar form factors, but also by the uncertainty induced in the overlap integral by the neutron density in Pb. The width of the bands in panel (b) is determined by the most conservative combination of two kinds of uncertainties.

In all panels the wide band corresponds to the range  $y \in [0, 0.4]$ , while the narrow band corresponds to the range  $y \in [0, 0.05]$ . This illustrates the effect of current and future hadronic uncertainties on the process of extracting information on short distance LFV couplings. The prominent feature in Fig. 4.5 is induced by the destructive interference dipole and scalar amplitudes.

## 4.5.2 Dipole-Vector

In terms of the parameters defined in Section 4.4.1, this model is defined by  $C_V \neq 0$  and  $C_D \equiv \pm \frac{r}{g_e} C_V$ . The single-operator models are recovered in the limiting cases  $r \rightarrow 0$  (vector) and  $r \rightarrow \infty$  (dipole). In figures 4.6 and 4.7 we plot the ratios  $B_{\mu \rightarrow e}(\text{Al})/B_{\mu \rightarrow e\gamma}$  (panel (a)),  $B_{\mu \rightarrow e}(\text{Pb})/B_{\mu \rightarrow e}(\text{Al})$  (panel (b)), and  $B_{\mu \rightarrow e}(\text{Ti})/B_{\mu \rightarrow e}(\text{Al})$  (panel (c)) versus the parameter  $r$ . Figures 4.6 and 4.7 correspond to positive and negative sign of the ratio  $C_D/C_V$ , respectively. Within this model, the only source of uncertainty arises from the vector overlap integral  $V^{(n)}(\text{Pb})$ , sensitive to the neutron density in Pb. This uncertainty is quantified by the thickness of the band in panel (b).

## 4.5.3 Scalar-Vector

In terms of the parameters defined in Section 4.4.1, this model is defined by  $C_V \neq 0$  and  $C_S \equiv \pm r C_V$ . The single-operator models are recovered in the limiting cases  $r \rightarrow 0$  (vector) and  $r \rightarrow \infty$  (scalar). Since the Dipole term is assumed to be subdominant, in this case we include in the analysis only the ratios  $B_{\mu \rightarrow e}(\text{Pb})/B_{\mu \rightarrow e}(\text{Al})$  and  $B_{\mu \rightarrow e}(\text{Ti})/B_{\mu \rightarrow e}(\text{Al})$ , shown in panels (b) and (c) of Figures 4.8 and 4.9 (for positive and negative values of  $C_S/C_V$ , respectively). While the ratio  $B_{\mu \rightarrow e}(\text{Ti})/B_{\mu \rightarrow e}(\text{Al})$  is affected only by the uncertainty in  $y$ , the ratio  $B_{\mu \rightarrow e}(\text{Pb})/B_{\mu \rightarrow e}(\text{Al})$  is affected also by the uncertainty in the Pb neutron density

---

<sup>3</sup>We consider here the case in which dipole and scalar operators produce outgoing lepton with definite chirality (L or R). If both chiralities are allowed, then in principle  $C_{DR}/C_{SR} \neq C_{DL}/C_{SL}$  and one more parameter has to be introduced in the analysis.

(through the overlap integrals). The width of the bands in the plots is determined by the most conservative combination of two kinds of uncertainties.

In all panels the wide band corresponds to the range  $y \in [0, 0.4]$ , while the narrow band corresponds to the range  $y \in [0, 0.05]$ . As in the case of the Dipole-Scalar model, the bands illustrate the effect of current and future hadronic uncertainties on extracting short distance LFV couplings.

We conclude this section by summarizing what one could learn about the two-operator dominance models in the case that two double ratios of LFV rates could be measured experimentally. Our exercise shows that:

- The current theoretical uncertainty on the strange content of the nucleon prevents a realistic test of the two-operator models involving the Scalar amplitude. The range  $y \in [0, 0.4]$  induces uncertainties of up to one order of magnitude in the relevant double ratios in the interference region (thick bands in all plots above). However, the uncertainty within reach of lattice QCD calculations will remove this obstacle in the coming years (this is illustrated by the thin bands in all plots above).
- Testing and discriminating among two-operator dominance models requires an experimental precision on the LFV rates that is comparable to the one needed to test the single operator models.

## 4.6 Application to a SUSY model

An example of the two-operator dominance model is given by a SUSY scenario with flavour mixing in the left-handed sleptons. Such a mixing, for example, can be induced from the Yukawa interaction in the see-saw model. As it is shown in Ref. [107], the scalar operator originated from the Higgs-boson-exchange diagrams can be sizable in this model if  $\tan\beta$  is large and the heavy Higgs boson is relatively lighter than the other SUSY particles. The ratio  $B_{\mu \rightarrow e}(\text{Al})/B_{\mu \rightarrow e\gamma}$  can therefore be enhanced in such a parameter region, while the ratio  $B_{\mu \rightarrow e}(\text{Pb})/B_{\mu \rightarrow e}(\text{Al})$  can show substantial deviations from the dipole-dominance value.

In Fig. 4.10 we show the pseudoscalar-Higgs mass ( $m_A$ ) dependence of the ratio for  $\mu > 0$  (left) and  $\mu < 0$  (right). We have taken the common mass ( $m_{\text{SUSY}} = 1$  TeV) for the slepton masses, the universal gaugino mass at the GUT scale, and the Higgsino mass parameter, and we fixed  $\tan\beta = 60$ . Since the scalar operator does not decouple in the  $m_{\text{SUSY}} \rightarrow \infty$  limit, we see the enhancement in the small  $m_A$  region. The light (dark) shaded regions correspond to the conservative (optimistic) range of the  $y$  parameter,  $y \in [0, 0.4]$  ( $y \in [0, 0.05]$ ). Within the same framework, the ratio  $B_{\mu \rightarrow e}(\text{Pb})/B_{\mu \rightarrow e}(\text{Al})$  is shown in Fig. 4.11.

In both cases, the theoretical uncertainty becomes significant as the scalar operator gets important. In the context of this explicit supersymmetric model, a precise determination of the  $y$  parameter is quite important in order to extract information on the underlying model parameters. To illustrate this even more explicitly, in Fig. 4.12 we show for  $\mu > 0$

the  $m_A$  dependence of  $B_{\mu \rightarrow e}(\text{Al})/B_{\mu \rightarrow e\gamma}$  (left) and  $B_{\mu \rightarrow e}(\text{Pb})/B_{\mu \rightarrow e}(\text{Al})$  (right) for different values of  $\tan\beta = 40, 50, 60$ . In these plots, only the small uncertainty window is reported ( $y \in [0, 0.05]$ ), to illustrate the enhanced discriminating power.

## 4.7 Conclusions

In this Chapter we have investigated whether the target-dependence of  $\mu$ -to- $e$  conversion rate can be exploited to discriminate among underlying dynamical mechanisms of lepton flavour violation, once one takes into account realistic hadronic and nuclear uncertainties. The major source of theoretical uncertainty arises from the nucleon matrix element of the strange quark scalar density. This is expressed in terms of the parameter  $y$  (see Eq. (4.30)), which we have varied within two ranges reflecting the current uncertainty ( $y \in [0, 0.4]$ ) and the projected uncertainty within reach of lattice QCD calculations ( $y \in [0, 0.05]$ ).

In order to assess the model discriminating power of a combined phenomenological analysis of  $\mu \rightarrow e\gamma$  and  $\mu \rightarrow e$  conversion on different target nuclei, we have defined four classes of models, in which only one underlying short distance operator dominates over all the others (Dipole, Scalar, Vector ( $\gamma$ ) and Vector ( $Z$ )). Ratios of LFV branching fractions can be used to test the various models. The single-operator hypothesis can be tested with at least one ratio (two LFV measurements), while the two-operator models, where two operators have comparable strength and interfere, can be tested with at least two ratios (three LFV measurements).

Our conclusions are encouraging: the theoretical uncertainties (even at the current level) are not an issue in testing the single-operator dominance model, as they largely cancel when we take ratios of different conversion rates. On the other hand, the current uncertainty prevents meaningful tests of two-operator models involving the Scalar operator, as it produces errors of up to one order of magnitude in the double ratios in the interference region. However, with the anticipated reduced lattice error on the strange content of the nucleon, this will not be an issue in the future. We have illustrated these main conclusions also in the context of a supersymmetric model.

Having established that the hadronic uncertainties will not be a limiting factor, we can ask how well one should measure the LFV rates in order to discriminate the underlying models. Fig. 4.3 shows that a realistic discrimination among single-operator models requires a measure of the ratio of conversion rates in light nuclei (such as  $B_{\mu \rightarrow e}(\text{Ti})/B_{\mu \rightarrow e}(\text{Al})$ ) at the level of 5% or better. Alternatively, one would need to measure the ratio of conversion rates in a heavy and light element (such as  $B_{\mu \rightarrow e}(\text{Pb})/B_{\mu \rightarrow e}(\text{Al})$ ) at the 20% level. Similar accuracy is required on the experimental side to be sensitive to interference effects when more than one operator is at work. Whether these challenging benchmark numbers can be reached in the future round of experiments [114, 115] depends on many issues, including the value of the branching fraction themselves (we are concerned here with ratios). Nonetheless, we hope that our results will stimulate further experimental efforts towards measurements of  $\mu \rightarrow e\gamma$  and  $\mu$ -to- $e$  conversion and consideration of various options for target nuclei.

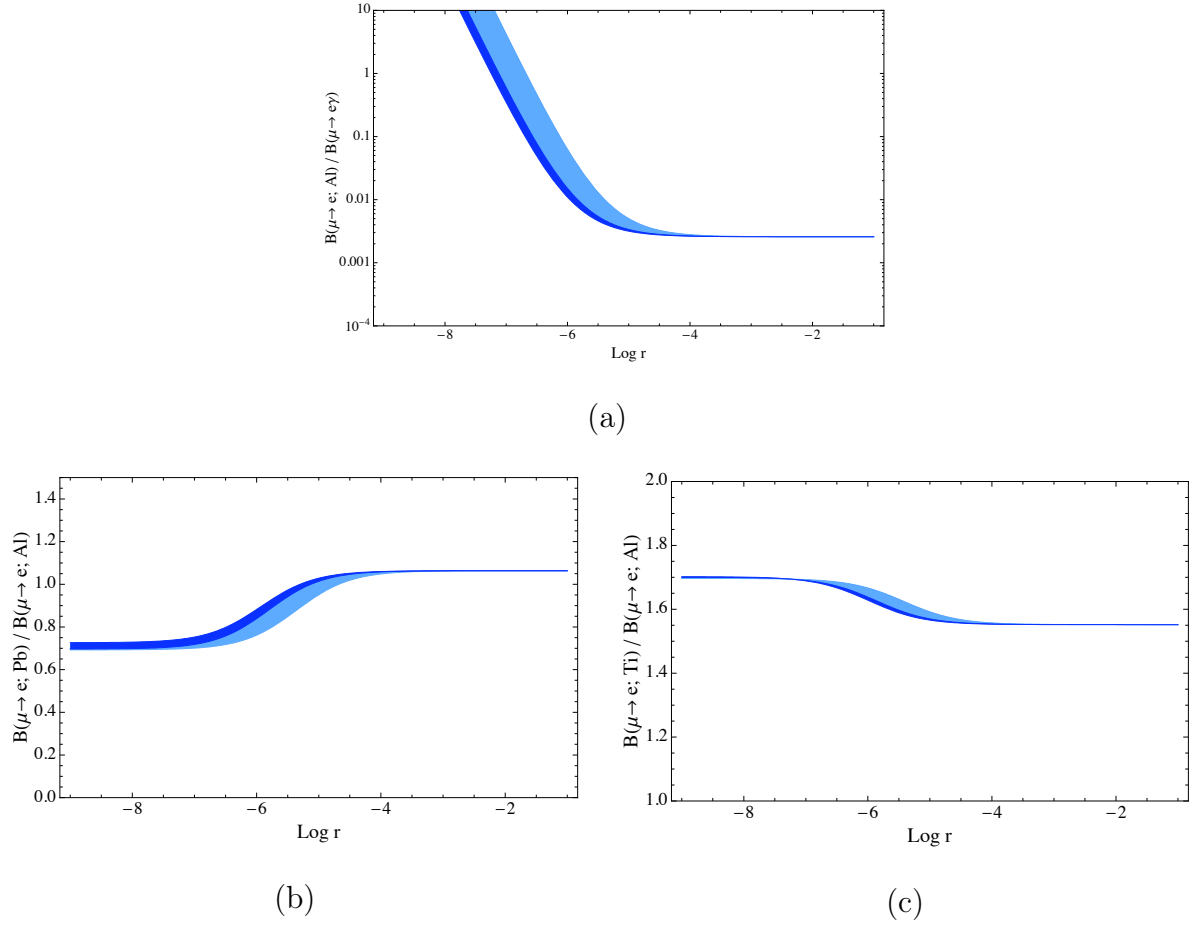


Figure 4.4: *Dipole-Scalar model*: Ratios  $B_{\mu \rightarrow e}(\text{Al})/B_{\mu \rightarrow e\gamma}$  (panel (a)),  $B_{\mu \rightarrow e}(\text{Pb})/B_{\mu \rightarrow e}(\text{Al})$  (panel (b)), and  $B_{\mu \rightarrow e}(\text{Ti})/B_{\mu \rightarrow e}(\text{Al})$  (panel (c)) as a function of  $\text{Log}_{10}(r)$  for positive  $C_D/C_S$ . See text for details.

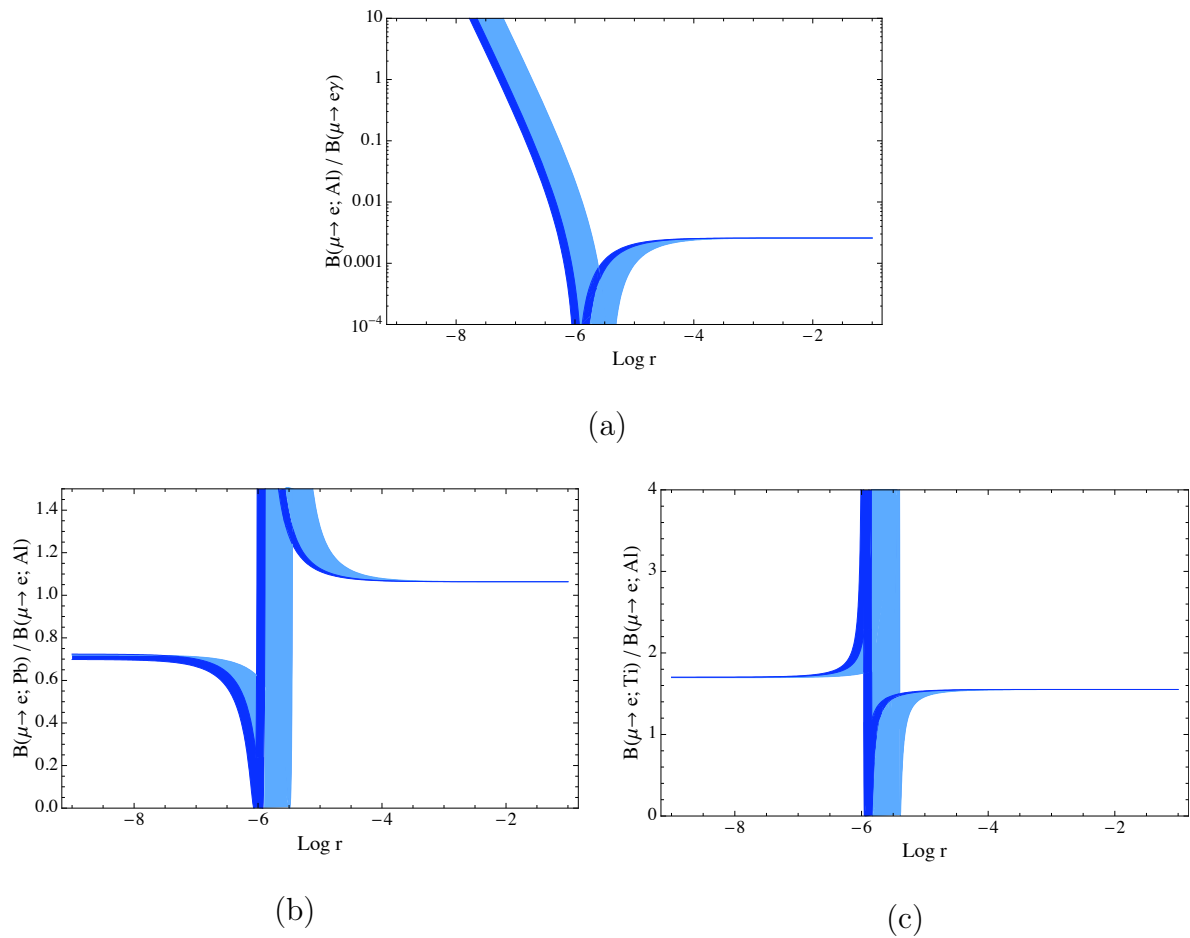


Figure 4.5: *Dipole-Scalar model*: Ratios  $B_{\mu \rightarrow e}(\text{Al})/B_{\mu \rightarrow e\gamma}$  (panel (a)),  $B_{\mu \rightarrow e}(\text{Pb})/B_{\mu \rightarrow e}(\text{Al})$  (panel (b)), and  $B_{\mu \rightarrow e}(\text{Ti})/B_{\mu \rightarrow e}(\text{Al})$  (panel (c)) as a function of  $\text{Log}_{10}(r)$  for negative  $C_D/C_S$ . See text for details.

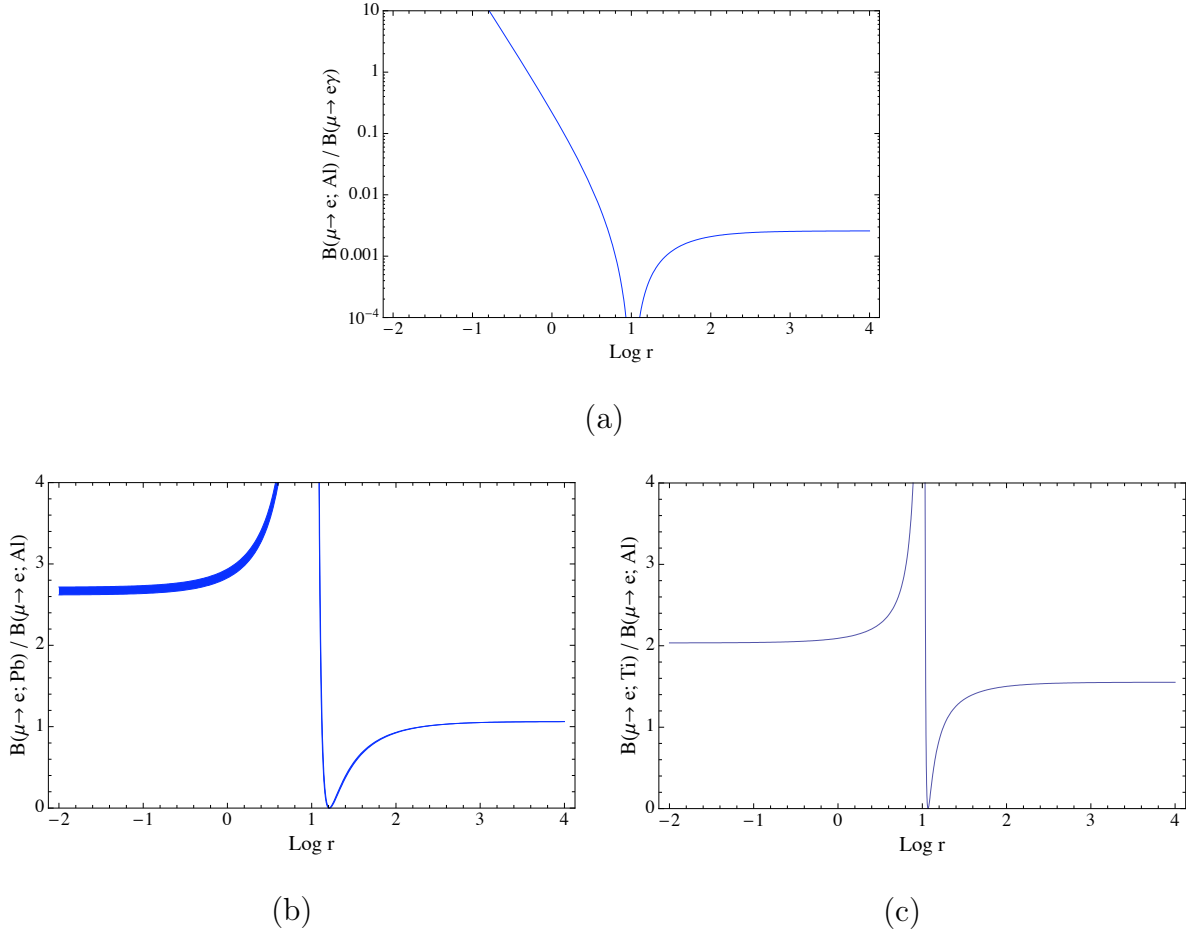
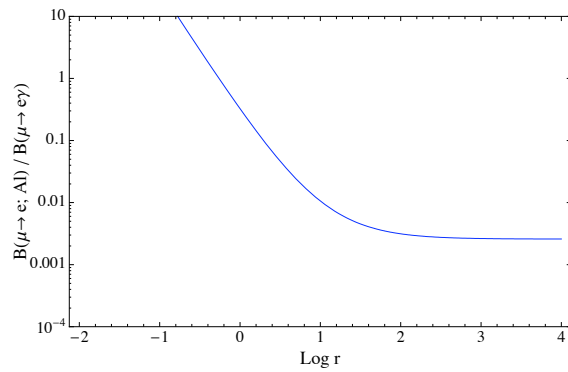
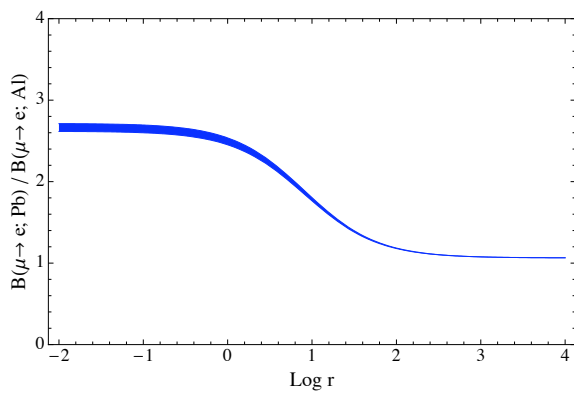


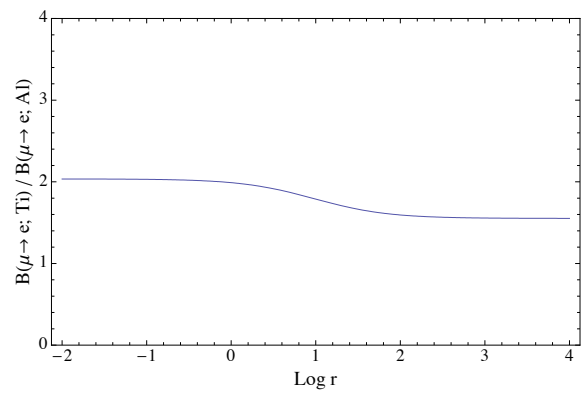
Figure 4.6: *Dipole-Vector model*: Ratios  $B_{\mu \rightarrow e}(\text{Al})/B_{\mu \rightarrow e\gamma}$  (panel (a)),  $B_{\mu \rightarrow e}(\text{Pb})/B_{\mu \rightarrow e}(\text{Al})$  (panel (b)), and  $B_{\mu \rightarrow e}(\text{Ti})/B_{\mu \rightarrow e}(\text{Al})$  (panel (c)) as a function of  $\text{Log}_{10}(r)$  for positive  $C_D/C_V$ . See text for details.



(a)



(b)



(c)

Figure 4.7: *Dipole-Vector model*: Ratios  $B_{\mu \rightarrow e}(\text{Al})/B_{\mu \rightarrow e\gamma}$  (panel (a)),  $B_{\mu \rightarrow e}(\text{Pb})/B_{\mu \rightarrow e}(\text{Al})$  (panel (b)), and  $B_{\mu \rightarrow e}(\text{Ti})/B_{\mu \rightarrow e}(\text{Al})$  (panel (c)) as a function of  $\text{Log}_{10}(r)$  for negative  $C_D/C_V$ . See text for details.

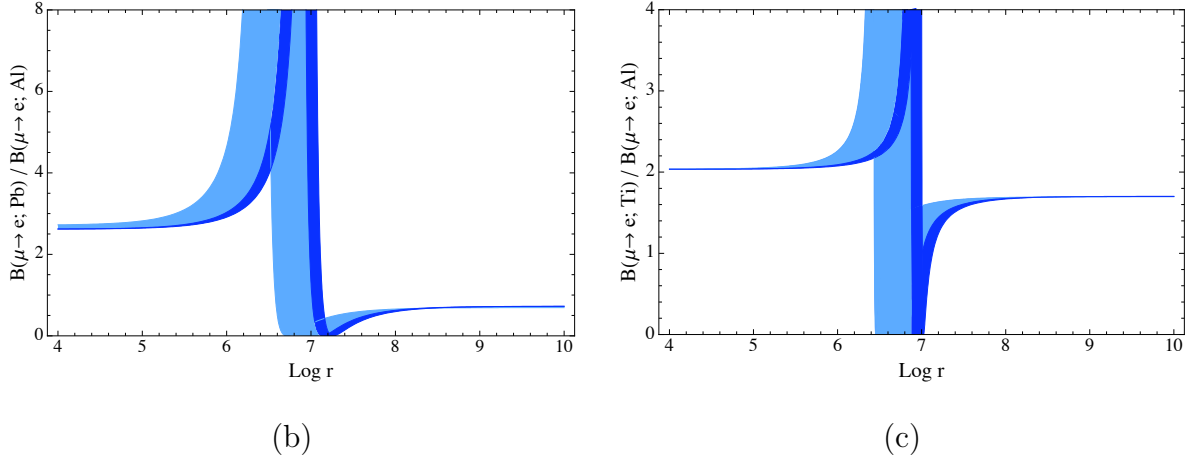


Figure 4.8: *Scalar-Vector model*: Ratios  $B_{\mu \rightarrow e}(\text{Pb})/B_{\mu \rightarrow e}(\text{Al})$  (panel (b)) and  $B_{\mu \rightarrow e}(\text{Ti})/B_{\mu \rightarrow e}(\text{Al})$  (panel (c)) as a function of  $\text{Log}_{10}(r)$  for positive  $C_S/C_V$ . See text for details.

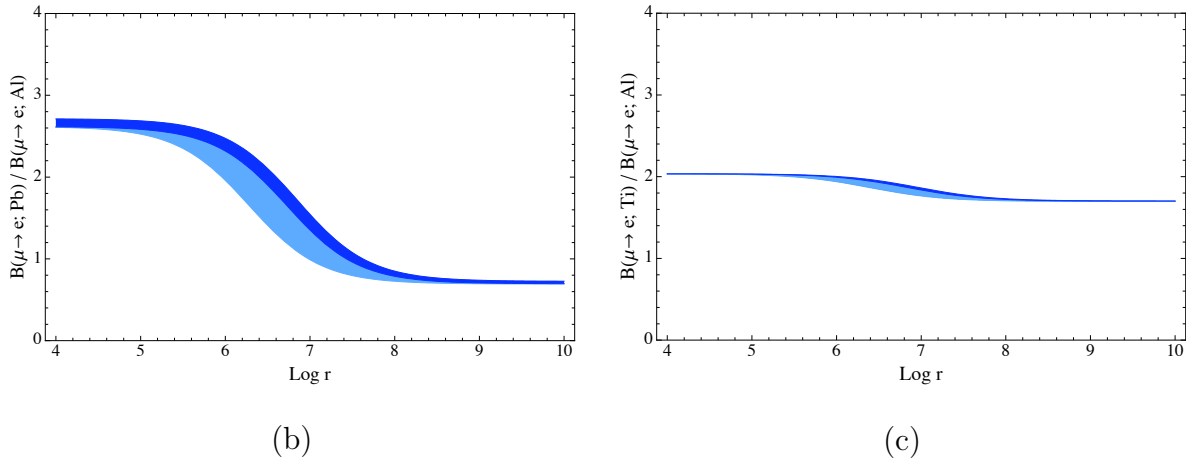


Figure 4.9: *Scalar-Vector model*: Ratios  $B_{\mu \rightarrow e}(\text{Pb})/B_{\mu \rightarrow e}(\text{Al})$  (panel (b)) and  $B_{\mu \rightarrow e}(\text{Ti})/B_{\mu \rightarrow e}(\text{Al})$  (panel (c)) as a function of  $\text{Log}_{10}(r)$  for negative  $C_S/C_V$ . See text for details.

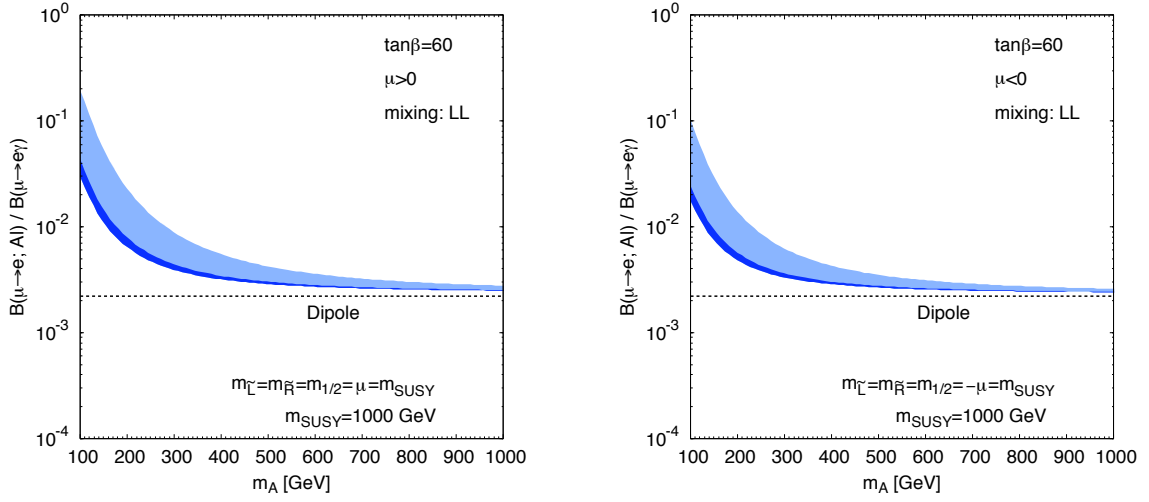


Figure 4.10: The pseudoscalar-Higgs mass dependence of  $B_{\mu \rightarrow e}(Al)/B_{\mu \rightarrow e\gamma}$  in a SUSY model with a left-handed slepton mixing. The slepton masses, the gaugino masses at the GUT scale, and the Higgsino mass parameter are all fixed to be 1 TeV. The light and dark shaded regions respectively correspond to the conservative and optimistic ranges of the  $y$  parameter.

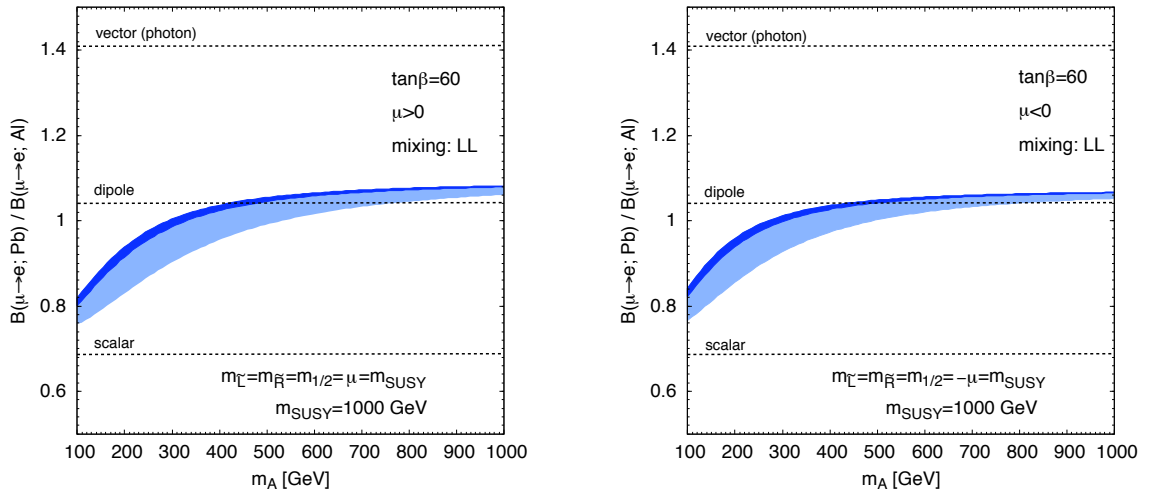


Figure 4.11: The pseudoscalar-Higgs mass dependence of  $B_{\mu \rightarrow e}(Pb)/B_{\mu \rightarrow e}(Al)$  in a SUSY model with a left-handed slepton mixing. The slepton masses, the gaugino masses at the GUT scale, and the Higgsino mass parameter are all fixed to be 1 TeV. The light and dark shaded regions respectively correspond to the conservative and optimistic ranges of the  $y$  parameter.

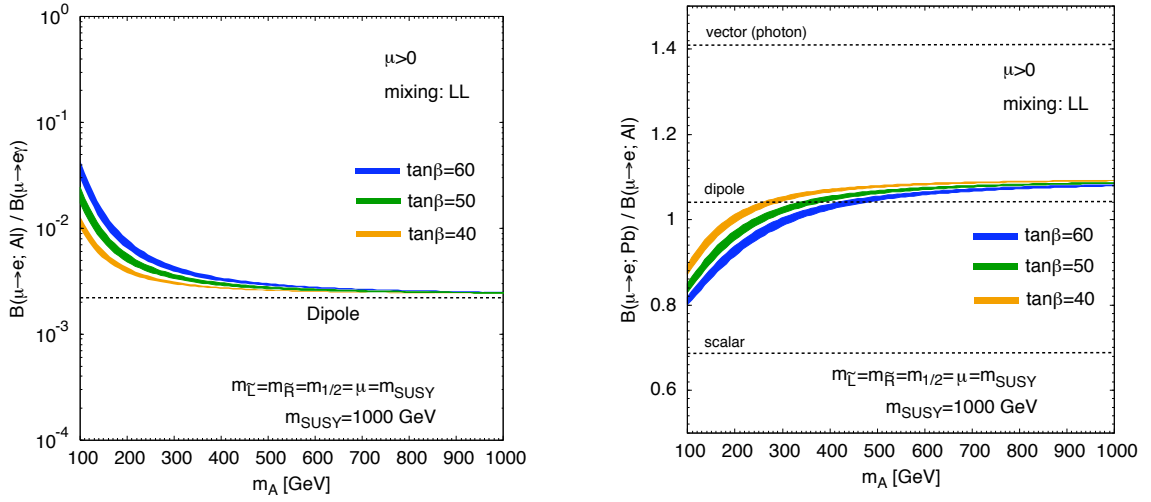


Figure 4.12: The pseudoscalar-Higgs mass dependence of  $B_{\mu \rightarrow e}(\text{Al})/B_{\mu \rightarrow e\gamma}$  (left) and  $B_{\mu \rightarrow e}(\text{Pb})/B_{\mu \rightarrow e}(\text{Al})$  (right) for different values of  $\tan\beta$ . The thickness of the bands corresponding to varying  $y$  in the optimistic range  $[0, 0.05]$ .



# Chapter 5

## The Aligned two-Higgs-doublet model

### 5.1 Introduction

Within the context of flavour physics in models with two Higgs doublets, there was the prejudice that sources of CP violation different from the SM CKM phase could only be generated by breaking flavour conservation in neutral interactions. In this sense, the Aligned two-Higgs-doublet model (A2HDM) [74] represents a counter-example, capable to maintain a flavour structure consistent with the experiments with non-standard phases, opening for this framework a new window in flavour physics.

The Aligned two-Higgs-doublet model describes a particular way of enlarging the scalar sector of the SM, with a second Higgs doublet which is aligned to the first one in flavour space, i.e. the Yukawa matrices of both doublets coupled to a given right-handed fermion sector are assumed to be proportional. This is what immediately guarantees the absence of FCNCs at tree level, while introducing new sources of CP violation in the Yukawa sector through the proportionality parameters, which are in general complex numbers and have full control of the new dynamics. Moreover, this Yukawa structure results in a generic way to describe all the 2HDMs defined by the implementation of a discrete symmetry,  $\mathcal{Z}_2$ , that are nothing but particular cases of the proportionality relation. Another important advantage of the model is that those parameters are all observables (none of them depends on the scalars basis). On the other hand, the structure of the potential is allowed to be as general as in the 2HDM (3.9), then, if it is not assumed to be CP conserving, there will be more phases coming from the neutral Higgs spectrum, which could generate interesting effects in processes with neutral Higgs exchanges. Another important feature of the A2HDM Lagrangian that will be analyzed in this chapter is the presence of radiative FCNCs. The alignment condition is broken by quantum corrections, since it is not protected by any symmetry. This generates minimal-flavour-violation structures with flavour blind phases suppressed by the corresponding loop factors, potentially relevant in heavy quark systems, which finally leads the A2HDM to a rich and viable phenomenology with an interesting hierarchy of FCNC effects.

The structure of the A2HDM is analyzed at tree level in section 5.2 and at one-loop

level in section 5.3.

## 5.2 The model

The alignment conditions read from (3.32) are [74]

$$\Gamma_2 = \xi_d e^{-i\theta} \Gamma_1, \quad \Delta_2 = \xi_u^* e^{i\theta} \Delta_1, \quad \Pi_2 = \xi_l e^{-i\theta} \Pi_1, \quad (5.1)$$

where the proportionality parameters  $\xi_f$  are arbitrary complex numbers. To simplify later equations, we have redefined these parameters introducing the explicit phases  $e^{\mp i\theta}$  which cancel the relative global phases between the two scalar doublets. The Yukawa alignment guarantees that the  $Y'_f$  and  $M'_f$  matrices are proportional and, therefore, can be simultaneously diagonalized with the result:

$$Y_{d,l} = \varsigma_{d,l} M_{d,l}, \quad Y_u = \varsigma_u^* M_u, \quad \varsigma_f \equiv \frac{\xi_f - \tan \beta}{1 + \xi_f \tan \beta}. \quad (5.2)$$

In terms of the mass-eigenstate fields, the Yukawa interactions take then the form:

$$\begin{aligned} \mathcal{L}_Y = & -\frac{\sqrt{2}}{v} H^+(x) \bar{u}(x) [\varsigma_d V M_d \mathcal{P}_R - \varsigma_u M_u V \mathcal{P}_L] d(x) \\ & -\frac{\sqrt{2}}{v} H^+(x) \varsigma_l \bar{\nu}(x) M_l \mathcal{P}_R l(x) \\ & -\frac{1}{v} \sum_{\varphi_i^0, f} \varphi_i^0(x) y_f^{\varphi_i^0} \bar{f}(x) M_f \mathcal{P}_R f(x) + \text{h.c.} \end{aligned} \quad (5.3)$$

where  $V$  is the Cabibbo-Kobayashi-Maskawa quark mixing matrix and  $\mathcal{P}_{R,L} \equiv \frac{1}{2}(1 \pm \gamma_5)$  the chirality projectors.

The flavour alignment of the Yukawa couplings results in a very specific structure for the scalar-fermion interactions:

- i) All fermionic couplings of the physical scalar fields are proportional to the corresponding fermion mass matrices.
- ii) The neutral Yukawas are diagonal in flavour. The couplings of the physical scalar fields  $H$ ,  $h$  and  $A$  are obviously proportional to the corresponding elements of the orthogonal matrix  $\mathcal{R}$ ,

$$\begin{aligned} y_{d,l}^{\varphi_i^0} &= \mathcal{R}_{i1} + (\mathcal{R}_{i2} + i \mathcal{R}_{i3}) \varsigma_{d,l}, \\ y_u^{\varphi_i^0} &= \mathcal{R}_{i1} + (\mathcal{R}_{i2} - i \mathcal{R}_{i3}) \varsigma_u^*. \end{aligned} \quad (5.4)$$

- iii) The only source of flavour-changing phenomena is the quark-mixing matrix  $V$ , which regulates the quark couplings of the  $W^\pm$  gauge bosons and the charged scalars  $H^\pm$ .

Model	$(\xi_d, \xi_u, \xi_l)$	$\varsigma_d$	$\varsigma_u$	$\varsigma_l$
Type I	$(\infty, \infty, \infty)$	$\cot \beta$	$\cot \beta$	$\cot \beta$
Type II	$(0, \infty, 0)$	$-\tan \beta$	$\cot \beta$	$-\tan \beta$
Type X	$(\infty, \infty, 0)$	$\cot \beta$	$\cot \beta$	$-\tan \beta$
Type Y	$(0, \infty, \infty)$	$-\tan \beta$	$\cot \beta$	$\cot \beta$
Inert	$(\tan \beta, \tan \beta, \tan \beta)$	0	0	0

Table 5.1: Limits on  $\xi_f$  that recover the different  $\mathcal{Z}_2$ -type models and the corresponding  $\varsigma_f$  values.

- iv) All leptonic couplings are diagonal in flavour. This is obviously related to the absence of right-handed neutrino fields in our low-energy Lagrangian. As it is mentioned in previous chapters, since neutrinos are massless, the leptonic mixing matrix  $V_L$  can be reabsorbed through a redefinition of the neutrino fields.
- v) The only new couplings introduced by the Yukawa Lagrangian are the three parameters  $\varsigma_f$ , which encode all possible freedom allowed by the alignment conditions. These couplings satisfy universality among the different generations: all fermions of a given electric charge have the same universal coupling  $\varsigma_f$ , they are “flavour-blind”. Moreover, the parameters  $\varsigma_f$  are invariant under global  $U(2)$  transformations of the scalar fields,  $\phi_a \rightarrow \phi'_a = \mathcal{U}_{ab}\phi_b$  [7,17–23]; i.e., they are independent of the basis choice adopted in the scalar space.
- vi) The usual models with a single scalar doublet coupling to each type of right-handed fermions are recovered taking the appropriate limits  $\xi_f \rightarrow 0$  or  $\xi_f \rightarrow \infty$  ( $1/\xi_f \rightarrow 0$ ); i.e.,  $\varsigma_f \rightarrow -\tan \beta$  or  $\varsigma_f \rightarrow \cot \beta$ . The type-I model corresponds to  $(\xi_d, \xi_u, \xi_l) = (\infty, \infty, \infty)$ , type II to  $(0, \infty, 0)$ , type X to  $(\infty, \infty, 0)$  and type Y to  $(0, \infty, \infty)$ . The *inert* doublet model corresponds to  $\varsigma_f = 0$  ( $\xi_f = \tan \beta$ ). The  $\varsigma_f$  values for all these particular models based on  $\mathcal{Z}_2$  symmetries are given in Table 5.1.
- vii) The  $\varsigma_f$  can be arbitrary complex numbers, opening the possibility to have new sources of CP violation without tree-level FCNCs.

The Yukawa alignment provides a general setting to discuss the phenomenology of 2HDMs without tree-level FCNCs, parameterizing the different possibilities through the three complex couplings  $\varsigma_f$ .

### 5.3 Quantum corrections

Quantum corrections induce some misalignment of the Yukawa coupling matrices, generating small FCNC effects suppressed by the corresponding loop factors. However, the special

structure of the A2HDM strongly constrains the possible FCNC interactions [74,116]. Obviously, the alignment condition remains stable under renormalization when it is protected by a  $\mathcal{Z}_2$  symmetry [117], i.e. for the particular cases indicated in table 5.1. In the most general case loop corrections do generate some FCNC effects, but the resulting structures are enforced to satisfy the flavour symmetries of the model. The Lagrangian of the A2HDM is invariant under flavour-dependent phase transformations of the fermion mass eigenstates ( $f = d, u, l, \nu, X = L, R, \alpha_i^{\nu,L} = \alpha_i^{l,L}$ ):

$$f_X^i(x) \rightarrow e^{i\alpha_i^{f,X}} f_X^i(x), \quad V_{ij} \rightarrow e^{i\alpha_i^{u,L}} V_{ij} e^{-i\alpha_j^{d,L}}, \quad M_{f,ij} \rightarrow e^{i\alpha_i^{f,L}} M_{f,ij} e^{-i\alpha_j^{f,R}}. \quad (5.5)$$

Owing to this symmetry, lepton-flavour-violating neutral couplings are identically zero to all orders in perturbation theory, while in the quark sector the CKM mixing matrix remains the only possible source of flavour-changing transitions. The only allowed local FCNC structures are of the type  $\bar{u}_L V (M_d M_d^\dagger)^n V^\dagger (M_u M_u^\dagger)^m M_u u_R, \bar{d}_L V^\dagger (M_u M_u^\dagger)^n V (M_d M_d^\dagger)^m M_d d_R$ , or similar structures with additional factors of  $V, V^\dagger$  and quark mass matrices [74]. Therefore, at the quantum level the A2HDM provides an explicit implementation of the popular Minimal Flavour Violation scenarios [118–123], but allowing at the same time for new CP-violating phases<sup>1</sup>. Structures of this type have been recently discussed in [63].

Using the renormalization-group equations [117,126], one can easily check that the one-loop gauge corrections preserve the alignment while the only FCNC structures induced by the scalar contributions take the form [116]:

$$\begin{aligned} \mathcal{L}_{\text{FCNC}} = & \frac{C(\mu)}{4\pi^2 v^3} (1 + \varsigma_u^* \varsigma_d) \sum_i \varphi_i^0(x) \left\{ (\mathcal{R}_{i2} + i \mathcal{R}_{i3}) (\varsigma_d - \varsigma_u) \left[ \bar{d}_L V^\dagger M_u M_u^\dagger V M_d d_R \right] \right. \\ & \left. - (\mathcal{R}_{i2} - i \mathcal{R}_{i3}) (\varsigma_d^* - \varsigma_u^*) \left[ \bar{u}_L V M_d M_d^\dagger V^\dagger M_u u_R \right] \right\} + \text{h.c.} \quad (5.6) \end{aligned}$$

As they should, these FCNC effects vanish identically when  $\varsigma_d = \varsigma_u$  ( $\mathcal{Z}_2$  models of type I, X and Inert) or  $\varsigma_d = -1/\varsigma_u^*$  (types II and Y). The leptonic coupling  $\varsigma_l$  does not induce any FCNC interaction, independently of its value; the usually adopted  $\mathcal{Z}_2$  symmetries are unnecessary in the lepton sector. Assuming the alignment to be exact at some scale  $\mu_0$ , i.e.  $C(\mu_0) = 0$ , a non-zero value for the FCNC coupling,  $C(\mu) = -\log(\mu/\mu_0)$ , is generated when running to a different scale.

The numerical effect of these contributions is, in any case, suppressed by  $m_q m_q^2/v^3$  and quark-mixing factors. This implies an interesting hierarchy of FCNC effects, avoiding the stringent experimental constraints for light-quark systems, while allowing at the same time for potential interesting signals in heavy-quark transitions. Obviously, the most relevant terms in (5.6) are the  $\bar{s}_L b_R$  and  $\bar{c}_L t_R$  operators. The  $\bar{s}_L b_R$  term induces a calculable contribution to  $B_s^0 - \bar{B}_s^0$  mixing through  $\varphi_i^0$  exchanges, which modifies the mixing phase and could explain the like-sign dimuon charge asymmetry recently observed by D0 [14]. Tree-level scalar exchanges from FCNC vertices have been already suggested as a possible explanation of the D0 measurement [127]. In ref. [128] an approximate solution to the

<sup>1</sup>Minimal flavour violation within the context of the Type II 2HDM has been discussed in [118,124,125].

renormalization-group equations of the A2HDM is analyzed and the generated FCNC terms are studied numerically, parametrizing the off-diagonal Yukawa couplings with the Sher-Cheng approximation. They also perform the analytical calculation by using the “leading log approximation” for the couplings at the electroweak scale. The results presented there agree with our FCNC operator (5.6) and it is concluded that the induced FCNC effects are well below the present experimental bounds. Ref. [124] analyzes the strength of FCNC effects mediated by neutral scalars in minimal-flavour-violation models containing two Higgs doublets. The tree-level alignment conditions presented here are reproduced, the one-loop FCNC structures in (5.6) are discussed and their coefficients are estimated at large  $\tan\beta$  in the decoupling limit.

A very interesting work providing alignment as an effective effect of theory with Natural Flavour Conservation at the UV scale has been presented recently in [129]. The most important feature of that model is the possibility of having alignment to all orders. The model starts with  $2 + N$  scalar doublets with a discrete symmetry that preserves natural flavour conservation; only two of these scalars are coupled to fermions while the other are “hidden”. Then, the two interacting Higgs are assumed to be very heavy so their decoupling leads to an effective Yukawa interaction, which connects a given fermion sector with the  $N$  hidden Higgs with the same Yukawa matrix for all them (alignment). What this model presents is, therefore, a way of having an *exact* alignment when all orders are resummed.

Still, it is very interesting to study the size of the one-loop FCNC effects provided by the misalignment, as it is mentioned here and analyzed in the works cited above, not only to understand the structure of the model at that level but also under a phenomenological point of view.



# Chapter 6

## Charged Higgs phenomenology in the Aligned two-Higgs-doublet model

### 6.1 Introduction

This Chapter focuses on a phenomenological analysis of the aligned two-Higgs-doublet model (A2HDM) [74] introduced in Chapter 5, which enforces the alignment in flavour space of the Yukawa couplings of the two scalar doublets, guaranteeing the absence of tree-level FCNC interactions. The Yukawa structure of the resulting A2HDM is fully characterized by the fermion masses, the CKM quark mixing matrix and three complex parameters  $\zeta_f$  ( $f = u, d, l$ ), whose phases are potential new sources of CP violation [74].

The presence of a charged scalar  $H^\pm$  is one of the most distinctive features of an extended scalar sector. In the following we analyze its phenomenological impact in low-energy flavour-changing processes within the A2HDM, and constrain the three complex parameters  $\zeta_f$  with present data on different leptonic, semileptonic and hadronic decays [116]. We proceed as follows: Section 6.2 explains our statistical treatment of theoretical uncertainties and compiles the inputs used in our analysis. The phenomenological consequences of having a charged Higgs field are analyzed next, process by process, extracting the corresponding constraints on the new-physics parameters  $\zeta_f$ . In section 6.3 we discuss the constraints derived from tree-level leptonic and semileptonic decays, while section 6.4 describes the information obtained from loop-induced processes. Finally, in section 6.5 we analyze the CP asymmetries in B-systems, with emphasis on its scale dependence, and discuss its potential impact on the parameter space of the A2HDM. We analyze their impact regarding the possible influence of charged-scalar effects on the like-sign dimuon charge asymmetry (LDCA) in our framework. Then, we give our conclusions in section 6.6. Some technical aspects related to  $\Delta F = 2$  transitions have been relegated to the Appendix B.

## 6.2 Inputs and statistical treatment

In the following sections we will analyze the most important flavour-changing processes that are sensitive to charged-scalar exchange and will try to constrain from them the new-physics parameters  $\zeta_f$ . Most of these observables have been discussed in recent phenomenological analyses, usually in the framework of the type II 2HDM [130–132], but also in the type III 2HDM [133].

For that purpose, a good control of the hadronic decay parameters is necessary. These usually involve large theoretical uncertainties whose treatment is not well defined. In our work we use the statistical approach RFit [9], which has been implemented in the CKMfitter package [134]. The new-physics parameter space is explored, assigning to each point the maximal relative likelihood under variation of the theoretical parameters which are not shown. Theoretical uncertainties are treated by defining allowed ranges within which the contribution of the corresponding theoretical quantity to the  $\Delta\chi^2$  is set to zero, while it is set to infinity outside. This treatment implies that uncertainties of this kind should be chosen conservatively and added linearly.

Another related problem is the combination of different theoretical determinations of a hadronic quantity, which is even less well defined. We follow the prescription given in [134]. However, lattice results with 2 and 2 + 1 flavours are not averaged because they are determined in different theoretical frameworks. Unless commented explicitly, we only take results coming from 2 + 1 flavours. For quantities concerning the light hadrons, we consider the determinations recommended by the Flavour Lattice Averaging Group (FLAG) [135, 136]. The obtained values are collected in table 6.1.

For  $f_+^{K\pi}(0)$  the only published value with 2+1 dynamical quarks is the one from RBC/UKQCD [137, 138], which however fails to fulfill the FLAG standards. On the other hand, there is one 2-flavour result, which fulfills the FLAG criteria [139]. Although consistent with the old Leutwyler-Roos estimate [140], based on  $O(p^4)$  Chiral Perturbation Theory ( $\chi$ PT), these lattice determinations are somewhat smaller than the  $O(p^6)$  analytical calculations [141–144]. We take this into account and adopt the conservative range  $f_+^{K\pi}(0) = 0.965 \pm 0.010$ .

To fix the values of the relevant CKM entries we only use determinations which are not sensitive to the new-physics contributions. Thus, we use the  $V_{ud}$  value extracted from superallowed ( $0^+ \rightarrow 0^+$ ) nuclear  $\beta$  decays and CKM unitarity to determine  $V_{us} \equiv \lambda$ . The values of  $V_{ub}$  and  $V_{cb} = A\lambda^2$  are determined from exclusive and inclusive  $b \rightarrow ul\bar{\nu}_l$  and  $b \rightarrow cl\bar{\nu}_l$  transitions, respectively, with  $l = e, \mu$ . The apex  $(\bar{\rho}, \bar{\eta})$  of the unitarity triangle has been determined from  $|V_{ub}/V_{cb}|$ ,  $\lambda$  and the ratio  $\Delta m_{B_s^0}/\Delta m_{B_d^0}$  (see section 6.4.2). For the top quark mass we have adopted the usual assumption that the Tevatron value [157] corresponds to the pole mass, but increasing its systematic error by 1 GeV to account for the intrinsic ambiguity in the  $m_t$  definition; i.e. we have taken  $m_t^{\text{pole}} = (173.1 \pm 0.6 \pm 2.1)$  GeV and have converted this value into the running  $\overline{\text{MS}}$  mass. The measurements used in our analysis are listed in table 6.2.

Concerning the charged-scalar mass, we will use the LEP lower bound  $M_{H^\pm} > 78.6$  GeV (95% CL), which does not refer to any specific Yukawa structure [41, 74]. This limit

Parameter	Value	Comment
$f_{B_s}$	$(0.242 \pm 0.003 \pm 0.022)$ GeV	Our average [145–147]
$f_{B_s}/f_{B_d}$	$1.232 \pm 0.016 \pm 0.033$	Our average [146, 147]
$f_{D_s}$	$(0.2417 \pm 0.0012 \pm 0.0053)$ GeV	Our average [145, 147, 148]
$f_{D_s}/f_{D_d}$	$1.171 \pm 0.005 \pm 0.02$	Our average [147, 148]
$f_K/f_\pi$	$1.192 \pm 0.002 \pm 0.013$	Our average [148–150]
$f_{B_s}\sqrt{\hat{B}_{B_s^0}}$	$(0.266 \pm 0.007 \pm 0.032)$ GeV	[146]
$f_{B_d}\sqrt{\hat{B}_{B_d^0}}/(f_{B_s}\sqrt{\hat{B}_{B_s^0}})$	$1.258 \pm 0.025 \pm 0.043$	[146]
$\hat{B}_K$	$0.732 \pm 0.006 \pm 0.043$	[151, 152]
$ V_{ud} $	$0.97425 \pm 0.00022$	[153]
$\lambda$	$0.2255 \pm 0.0010$	$(1 -  V_{ud} ^2)^{1/2}$
$ V_{ub} $	$(3.8 \pm 0.1 \pm 0.4) \cdot 10^{-3}$	$b \rightarrow ul\nu$ (excl. + incl.) [154, 155]
$A$	$0.80 \pm 0.01 \pm 0.01$	$b \rightarrow cl\nu$ (excl. + incl.) [154, 155]
$\bar{\rho}$	$0.15 \pm 0.02 \pm 0.05$	Our fit
$\bar{\eta}$	$0.38 \pm 0.01 \pm 0.06$	Our fit
$\bar{m}_u(2 \text{ GeV})$	$(0.00255^{+0.00075}_{-0.00105})$ GeV	[156]
$\bar{m}_d(2 \text{ GeV})$	$(0.00504^{+0.00096}_{-0.00154})$ GeV	[156]
$\bar{m}_s(2 \text{ GeV})$	$(0.105^{+0.025}_{-0.035})$ GeV	[156]
$\bar{m}_c(2 \text{ GeV})$	$(1.27^{+0.07}_{-0.11})$ GeV	[156]
$\bar{m}_b(m_b)$	$(4.20^{+0.17}_{-0.07})$ GeV	[156]
$\bar{m}_t(m_t)$	$(165.1 \pm 0.6 \pm 2.1)$ GeV	[157]
$\delta_{\text{em}}^{K\ell 2/\pi\ell 2}$	$-0.0070 \pm 0.0018$	[158–161]
$\delta_{\text{em}}^{\tau K 2/K\ell 2}$	$0.0090 \pm 0.0022$	[162–164]
$\delta_{\text{em}}^{\tau\pi 2/\pi\ell 2}$	$0.0016 \pm 0.0014$	[162–164]
$\rho^2 _{B \rightarrow Dl\nu}$	$1.18 \pm 0.04 \pm 0.04$	[155]
$\Delta _{B \rightarrow Dl\nu}$	$0.46 \pm 0.02$	[165]
$f_+^{K\pi}(0)$	$0.965 \pm 0.010$	[137–139, 141–144]
$\bar{g}_{b,SM}^L$	$-0.42112^{+0.00035}_{-0.00018}$	[166, 167]
$\kappa_\epsilon$	$0.94 \pm 0.02$	[168]
$\bar{g}_{b,SM}^R$	$0.07744^{+0.00006}_{-0.00008}$	[166, 167]

Table 6.1: *Input values for the hadronic parameters, obtained as described in the text. The first error denotes statistical uncertainty, the second systematic/theoretical.*

assumes only that  $H^+$  decays dominantly into  $u_i\bar{d}_j$  and  $l^+\nu_l$ . Obviously, the bound is avoided by a fermiophobic (inert) A2HDM with  $\zeta_f \ll 1$ , but all our constraints would also disappear in this case. The charged scalar could still be detected through the decay mode  $H^\pm \rightarrow W^\pm A$ , provided it is kinematically allowed. Assuming a CP-conserving scalar potential, OPAL finds the 95% CL constraints  $M_{H^\pm} > 56.5$  (64.8) GeV, for  $12$  (15) GeV  $< M_A < M_{H^\pm} - M_{W^\pm}$  [46].

Observable	Value	Comment
$ g_{RR}^S _{\tau \rightarrow \mu}$	$< 0.72$ (95% CL)	[156]
$\text{Br}(\tau \rightarrow \mu \nu_\tau \bar{\nu}_\mu)$	$(17.36 \pm 0.05) \times 10^{-2}$	[156]
$\text{Br}(\tau \rightarrow e \nu_\tau \bar{\nu}_e)$	$(17.85 \pm 0.05) \times 10^{-2}$	[156]
$\text{Br}(\tau \rightarrow \mu \nu_\tau \bar{\nu}_\mu) / \text{Br}(\tau \rightarrow e \nu_\tau \bar{\nu}_e)$	$0.9796 \pm 0.0039$	[169]
$\text{Br}(B \rightarrow \tau \nu)$	$(1.73 \pm 0.35) \times 10^{-4}$	[8]
$\text{Br}(D \rightarrow \mu \nu)$	$(3.82 \pm 0.33) \times 10^{-4}$	[170]
$\text{Br}(D \rightarrow \tau \nu)$	$\leq 1.3 \times 10^{-3}$ (95% CL)	[170]
$\text{Br}(D_s \rightarrow \tau \nu)$	$(5.58 \pm 0.35) \times 10^{-2}$	[171–175]
$\text{Br}(D_s \rightarrow \mu \nu)$	$(5.80 \pm 0.43) \times 10^{-3}$	[171, 175, 176]
$\Gamma(K \rightarrow \mu \nu) / \Gamma(\pi \rightarrow \mu \nu)$	$1.334 \pm 0.004$	[161]
$\Gamma(\tau \rightarrow K \nu) / \Gamma(\tau \rightarrow \pi \nu)$	$(6.50 \pm 0.10) \times 10^{-2}$	[156, 169]
$\log C$	$0.194 \pm 0.011$	[177, 178]
$\text{Br}(B \rightarrow D \tau \nu) / \text{Br}(B \rightarrow D \ell \nu)$	$0.392 \pm 0.079$	[179–181]
$\Gamma(Z \rightarrow b \bar{b}) / \Gamma(Z \rightarrow \text{hadrons})$	$0.21629 \pm 0.00066$	[182]
$\text{Br}(\bar{B} \rightarrow X_s \gamma)_{E_\gamma > 1.6 \text{ GeV}}$	$(3.55 \pm 0.26) \times 10^{-4}$	[155]
$\text{Br}(\bar{B} \rightarrow X_c e \bar{\nu}_e)$	$(10.74 \pm 0.16) \times 10^{-2}$	[155]
$\Delta m_{B_d^0}$	$(0.507 \pm 0.005) \text{ ps}^{-1}$	[155]
$\Delta m_{B_s^0}$	$(17.77 \pm 0.12) \text{ ps}^{-1}$	[155]
$ \epsilon_K $	$(2.228 \pm 0.011) \times 10^{-3}$	[156]

Table 6.2: *Measurements used in the analysis. Masses and lifetimes are taken from the PDG [156].*

## 6.3 Tree-level decays

### 6.3.1 Lepton decays

The pure leptonic decays  $l \rightarrow l' \bar{\nu}_{l'} \nu_l$  provide accurate tests of the universality of the leptonic  $W$  couplings and of their left-handed current structure [156, 183, 184]. The exchange of a charged scalar induces an additional amplitude mediating the decay of a right-handed initial lepton into a right-handed final charged lepton; in standard notation [184, 185], this scalar contribution gets parametrized through the effective low-energy coupling  $g_{RR}^S = -\frac{m_l m_{l'}}{M_{H^\pm}^2} |\zeta_l|^2$ . Its phenomenological effects can be isolated through the Michel parameters governing the decay distribution,

$$\rho - \frac{3}{4} = 0, \quad \eta = \frac{1}{2N} \text{Re}(g_{RR}^S), \quad \xi - 1 = -\frac{1}{2N} |g_{RR}^S|^2, \quad \xi\delta - \frac{3}{4} = -\frac{3}{8N} |g_{RR}^S|^2, \quad (6.1)$$

and in the total decay width

$$\Gamma(l \rightarrow l' \bar{\nu}_{l'} \nu_l) = \frac{G_F^2}{192\pi^3} m_l^5 N \left[ f \left( \frac{m_{l'}^2}{m_l^2} \right) + 4 \eta \frac{m_{l'}}{m_l} g \left( \frac{m_{l'}^2}{m_l^2} \right) \right] r_{\text{RC}}, \quad (6.2)$$

where  $f(x) = 1 - 8x + 8x^3 - x^4 - 12x^2 \log x$ ,  $g(x) = 1 + 9x - 9x^2 - x^3 + 6x(1+x) \log x$ ,  $N = 1 + \frac{1}{4}|g_{RR}^S|^2$  and [186]

$$r_{\text{RC}} = \left[ 1 + \frac{\alpha(m_l)}{2\pi} \left( \frac{25}{4} - \pi^2 \right) \right] \left[ 1 + \frac{3}{5} \frac{m_l^2}{M_W^2} - 2 \frac{m_{l'}^2}{M_W^2} \right]. \quad (6.3)$$

Since the scalar couplings are proportional to lepton masses, the decay  $\tau \rightarrow \mu \bar{\nu}_\mu \nu_\tau$  is the most sensitive one to the scalar-exchange contribution. The present bound  $|g_{RR}^S|_{\tau \rightarrow \mu} < 0.72$  (95% CL) [156] translates into  $|\zeta_l|/M_{H^\pm} \leq 1.96 \text{ GeV}^{-1}$  (95% CL). A better limit can be obtained from the ratio of the total  $\tau$  decay widths into the muon and electron modes. The universality test  $|g_\mu/g_e|^2 \equiv |\text{Br}(\tau \rightarrow \mu)/\text{Br}(\tau \rightarrow e)| |f(m_e^2/m_\tau^2)/f(m_\mu^2/m_\tau^2)| = 1.0036 \pm 0.0029$  [156, 169] implies:

$$\frac{|\zeta_l|}{M_{H^\pm}} \leq 0.40 \text{ GeV}^{-1} \quad (95\% \text{ CL}). \quad (6.4)$$

### 6.3.2 Leptonic decays of pseudoscalar mesons

Information about new-physics parameters can be also extracted from leptonic decays of pseudoscalar mesons,  $P^+ \rightarrow l^+ \nu_l$ , which are very sensitive to  $H^+$  exchange due to the helicity suppression of the SM amplitude. The total decay width is given by <sup>1</sup>

$$\Gamma(P_{ij}^+ \rightarrow l^+ \nu_l) = G_F^2 m_l^2 f_P^2 |V_{ij}|^2 \frac{m_{P_{ij}^+}}{8\pi} \left( 1 - \frac{m_l^2}{m_{P_{ij}^+}^2} \right)^2 (1 + \delta_{\text{em}}^{M\ell 2}) |1 - \Delta_{ij}|^2, \quad (6.5)$$

where  $i, j$  represent the valence quarks of the meson under consideration. The correction

$$\Delta_{ij} = \left( \frac{m_{P_{ij}^\pm}}{M_{H^\pm}} \right)^2 \zeta_l^* \frac{\zeta_u m_{u_i} + \zeta_d m_{d_j}}{m_{u_i} + m_{d_j}} \quad (6.6)$$

encodes the new-physics information and  $\delta_{\text{em}}^{M\ell 2}$  denotes the electromagnetic radiative contributions. These corrections are relevant because the additional photon lifts the helicity suppression of the two-body decay, thereby compensating in part for the additional electromagnetic coupling, and the two processes are not distinguishable experimentally for low photon energies. Their relative importance therefore increases for decreasing lepton masses.

The correction  $\Delta_{ij}$  is predicted to be positive in model I, negative in model X and can have either sign in the models II and Y, depending on the decaying meson, while it is of course absent in the *inert* scenario. In the more general A2HDM it is a complex number with a real part of either sign. To determine its size one needs to know  $|V_{ij}|$  and a theoretical determination of the meson decay constant.

<sup>1</sup>The normalization of the meson decay constant corresponds to  $f_\pi = \sqrt{2}F_\pi = 131 \text{ MeV}$ .

The SM as well as the 2HDM contribution to this class of decays start at tree level. Therefore they can be assumed to remain the dominant contributions, relatively independent of a possible high-energy completion of the theory. Electroweak loop corrections are of course expected and they could be sizeable in some cases, for example in supersymmetry at large values of  $\tan\beta$  [187, 188].

### Heavy pseudoscalar mesons

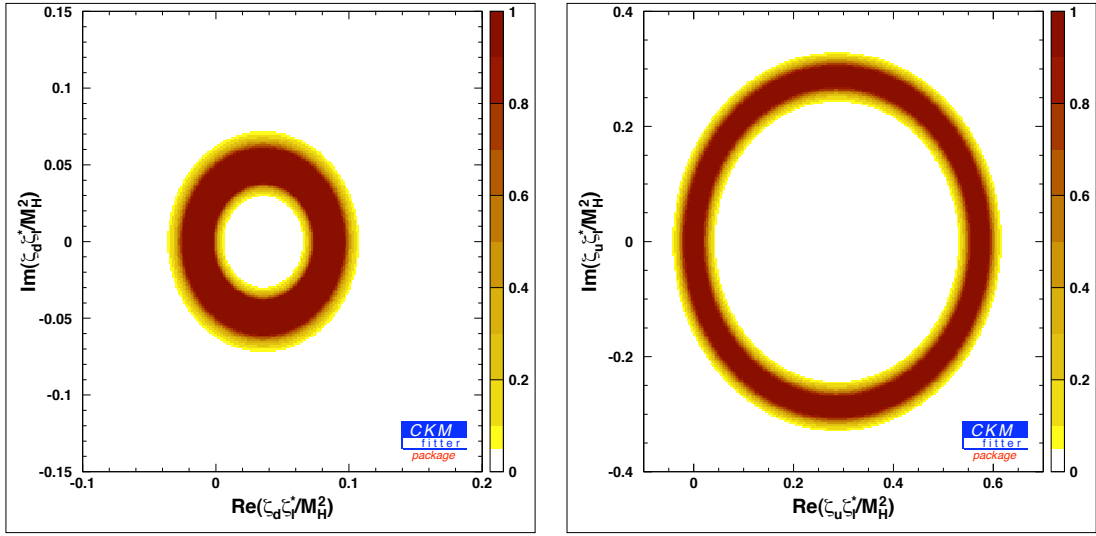


Figure 6.1: Constraints in the complex  $\zeta_l^* \zeta_{u,d}/M_{H^\pm}^2$  planes from  $B \rightarrow \tau\nu$  (left) and  $D \rightarrow \mu\nu$  (right), in units of  $\text{GeV}^{-2}$ . The colour code indicates confidence levels ( $1 - CL$ ).

The leptonic decays of heavy pseudoscalar mesons that have been measured up to now are  $B \rightarrow \tau\nu$ ,  $D_s \rightarrow \mu\nu$ ,  $D_s \rightarrow \tau\nu$  and  $D \rightarrow \mu\nu$ . The radiative corrections for the leptonic decays of heavy mesons have been estimated in [189], and are already taken into account in the experimental values given in table 6.2; therefore the electromagnetic correction is set to zero in Eq. (6.5).

In B and D decays the function  $\Delta_{ij}$  can be approximated by neglecting the contribution proportional to the light quark mass, because  $m_u/m_b \lesssim m_d/m_c \sim \mathcal{O}(10^{-3})$ . Therefore the relations

$$\Delta_{ub} \approx \frac{m_B^2}{M_{H^\pm}^2} \zeta_l^* \zeta_d, \quad \Delta_{cd} \approx \frac{m_D^2}{M_{H^\pm}^2} \zeta_l^* \zeta_u \quad (6.7)$$

hold, leading to a direct constraint on these combinations. While for  $D_{(s)} \rightarrow \tau\nu$  the helicity suppression is absent, the corresponding phase space is small and there are two neutrinos in the final state, which is why  $D \rightarrow \tau\nu$  has not been measured up to now. Nevertheless, the upper limit set by CLEO [170] starts to become relevant in constraining

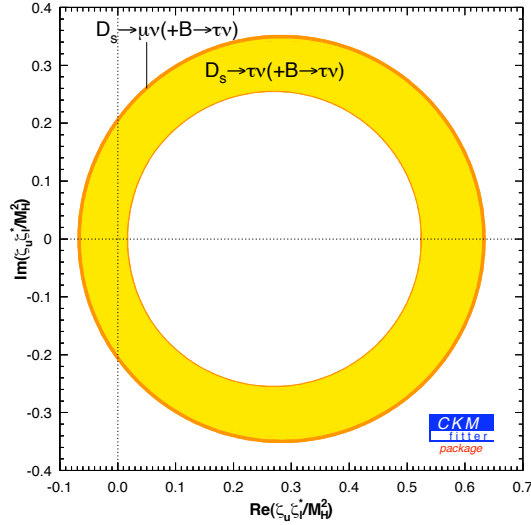


Figure 6.2: 95% CL constraints in the complex  $\zeta_l^* \zeta_u / M_{H^\pm}^2$  plane from  $D_s \rightarrow (\tau, \mu)\nu$ , in units of  $\text{GeV}^{-2}$ , using  $B \rightarrow \tau\nu$  to constrain  $\zeta_l^* \zeta_d / M_{H^\pm}^2$ .

our parameters:  $|1 - \Delta_{cd}| < 1.19$  (95% CL). The present experimental limit on  $B \rightarrow \mu\nu$  gives  $|1 - \Delta_{ub}| < 2.04$  (95% CL). The information obtained from the decays  $B \rightarrow \tau\nu$  and  $D \rightarrow \mu\nu$  is shown in figure 6.1. The broad dark red (black) ring in the middle reflects the fact, that the systematic error is dominant in these constraints, leading to a large amount of degeneracy for the ‘best fit value’. To infer a limit at a certain confidence level, the corresponding number of rings has to be included, for example for 95% up to the light grey corresponding to  $1 - CL = 0.05$ . The resulting 95% CL constraints,  $|1 - \Delta_{ub}| \in [0.8, 2.0]$  and  $|1 - \Delta_{cd}| \in [0.87, 1.12]$ , translate into corresponding allowed circular bands in the  $\zeta_l^* \zeta_{u,d} / M_{H^\pm}^2$  complex planes. For real Yukawa couplings there is a two-fold sign ambiguity generating two possible solutions, the expected one around  $\Delta_{ij} = 0$  (the SM amplitude dominates) and its mirror around  $\Delta_{ij} = 2$ , corresponding to a new-physics contribution twice as large as the SM one and of opposite sign. The real solutions are  $\zeta_l^* \zeta_d / M_{H^\pm}^2 \in [-0.036, 0.008] \text{ GeV}^{-2}$  or  $[0.064, 0.108] \text{ GeV}^{-2}$ , and  $\zeta_l^* \zeta_u / M_{H^\pm}^2 \in [-0.037, 0.037] \text{ GeV}^{-2}$  or  $[0.535, 0.609] \text{ GeV}^{-2}$ .

In  $D_s$  decays we get  $|1 - \Delta_{cs}| \in [0.97, 1.18]$  from  $D_s \rightarrow \mu\nu$  and  $|1 - \Delta_{cs}| \in [0.98, 1.16]$  from  $D_s \rightarrow \tau\nu$ . Here the situation is a bit more complex, because  $m_s/m_c \approx 10\%$  and the light-quark term in the  $\Delta_{cs}$  function cannot be neglected since this suppression could be compensated by the different  $\zeta_f$ . Therefore there is no direct constraint, neither on  $\zeta_l^* \zeta_u / M_{H^\pm}^2$  nor on  $\zeta_l^* \zeta_d / M_{H^\pm}^2$ , only a correlation among them. For that reason, we use the additional information from  $B \rightarrow \tau\nu$  to constrain the parameters which are not shown. This suffices to render the influence of the mass-suppressed term subdominant.

If CP symmetry were only broken by the CKM phase, the parameters  $\zeta_f$  would be real. In this case, the constraints from  $D_s \rightarrow \tau\nu_\tau$  and  $D_s \rightarrow \mu\nu_\mu$  can be visualized as shown in figure 6.3, plotting the correlation between the two real parameters. The two grey bands

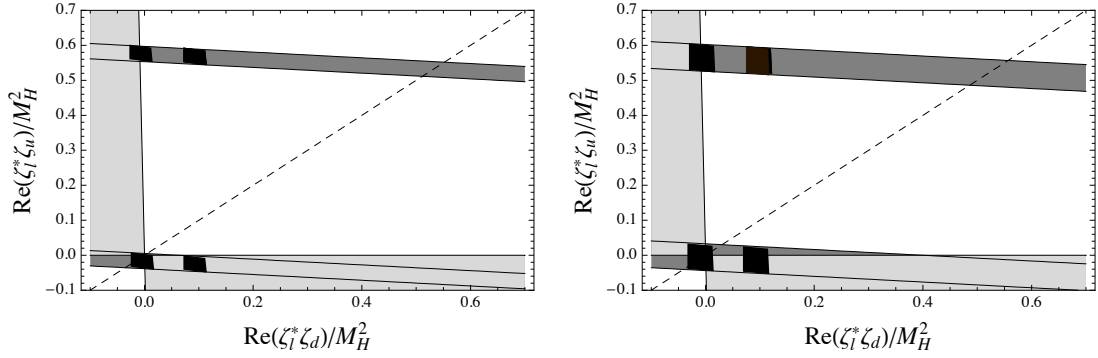


Figure 6.3: Constraints from  $D_s \rightarrow \tau\nu_\tau$  (left) and  $D_s \rightarrow \mu\nu_\mu$  (right), in units of  $\text{GeV}^{-2}$ , under the assumption of real parameters  $\varsigma_f$ . The grey bands correspond to 95% CL. Also shown are the cuts for the 2HDM of type I/X (dashed line) and II (lighter grey area,  $\tan\beta \in [0.1, 60]$ ). Finally, the four black regions are the possible allowed areas considering the information coming from  $B \rightarrow \tau\nu_\tau$ .

are associated with the two possible solutions around  $\Delta_{cs} = 0$  and  $\Delta_{cs} = 2$ . The different models with  $\mathcal{Z}_2$ -symmetry correspond to cuts in these plots. The plots show the small influence of the term proportional to the strange quark mass, as long as the couplings are of the same order. Using the constraints on  $\varsigma_l^* \varsigma_d/M_{H^\pm}^2$  from  $B \rightarrow \tau\nu$ , one finds for the other coupling combination the two real solutions  $\varsigma_l^* \varsigma_u/M_{H^\pm}^2 \in [-0.005, 0.041] \text{ GeV}^{-2}$  or  $[0.511, 0.557] \text{ GeV}^{-2}$ , at 95% CL, which agree with the corresponding constraints from  $D \rightarrow \mu\nu$ . Putting together all the information from leptonic B, D and  $D_s$  decays, the real solutions are:

$$\frac{\varsigma_l^* \varsigma_d}{M_{H^\pm}^2} \in \begin{cases} [-0.036, 0.008] \text{ GeV}^{-2}, \\ [0.064, 0.108] \text{ GeV}^{-2}, \end{cases} \quad \frac{\varsigma_l^* \varsigma_u}{M_{H^\pm}^2} \in \begin{cases} [-0.006, 0.037] \text{ GeV}^{-2}, \\ [0.511, 0.535] \text{ GeV}^{-2}. \end{cases} \quad (6.8)$$

### Light pseudoscalar mesons

Due to the cancellation of common uncertainties, lattice calculations of the ratio  $f_K/f_\pi$  are more precise than the determinations of the individual decay constants. This ratio can be extracted experimentally from two different ratios of decay widths:

$$\frac{\Gamma(K \rightarrow \mu\nu)}{\Gamma(\pi \rightarrow \mu\nu)} = \frac{m_K}{m_\pi} \left( \frac{1 - m_\mu^2/m_K^2}{1 - m_\mu^2/m_\pi^2} \right)^2 \left| \frac{V_{us}}{V_{ud}} \right|^2 \left( \frac{f_K}{f_\pi} \right)^2 (1 + \delta_{\text{em}}^{K\ell 2/\pi\ell 2}) \left| \frac{1 - \Delta_{us}}{1 - \Delta_{ud}} \right|^2, \quad (6.9)$$

$$\frac{\Gamma(\tau \rightarrow K\nu)}{\Gamma(\tau \rightarrow \pi\nu)} = \left( \frac{1 - m_K^2/m_\tau^2}{1 - m_\pi^2/m_\tau^2} \right)^2 \left| \frac{V_{us}}{V_{ud}} \right|^2 \left( \frac{f_K}{f_\pi} \right)^2 (1 + \delta_{\text{em}}^{\tau K 2/\tau\pi 2}) \left| \frac{1 - \Delta_{us}}{1 - \Delta_{ud}} \right|^2, \quad (6.10)$$

where  $\delta_{\text{em}}^{K\ell 2/\pi\ell 2}$  is given in table 6.1 and  $\delta_{\text{em}}^{\tau K 2/\tau\pi 2} = \delta_{\text{em}}^{(\tau K 2/K\ell 2)} + \delta_{\text{em}}^{K\ell 2/\pi\ell 2} - \delta_{\text{em}}^{\tau\pi 2/\pi\ell 2} = 0.0004 \pm 0.0054$ .

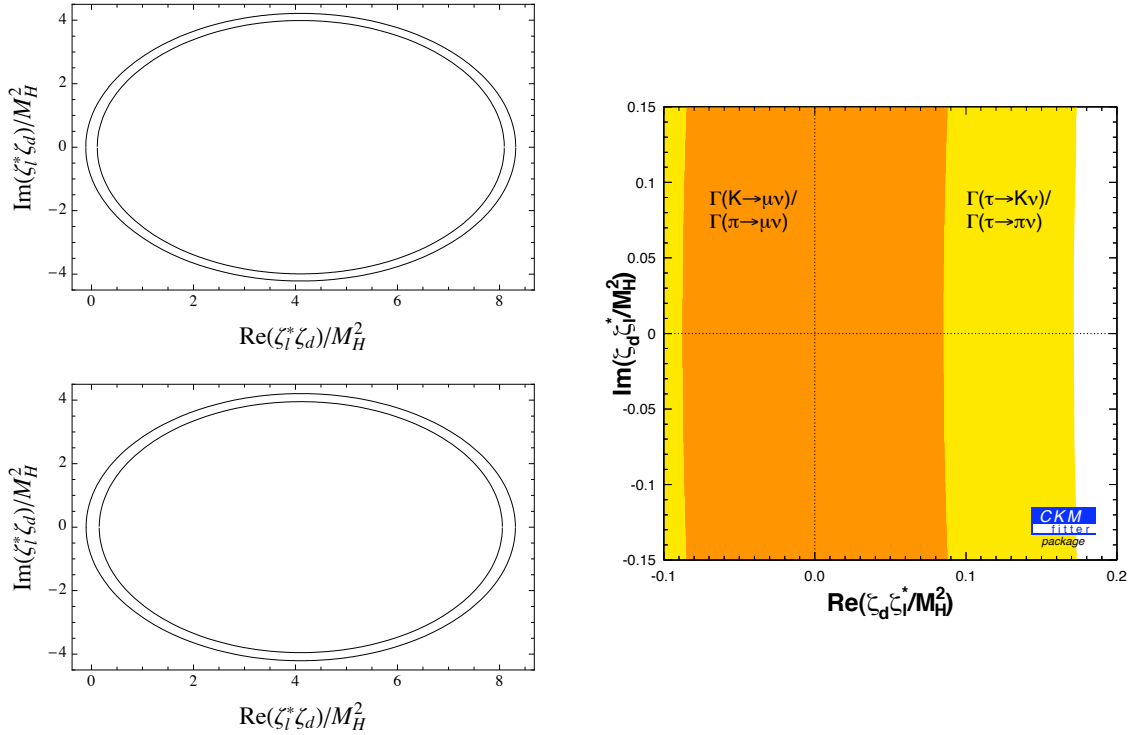


Figure 6.4: Constraints in the complex plane  $(\zeta_l^* \zeta_d)/M_{H^\pm}^2$ , in units of  $\text{GeV}^{-2}$ . Left: Full regions allowed at 95% CL for  $K/\pi \rightarrow \mu\nu$  (upper plot) and  $\tau \rightarrow K/\pi\nu$  (lower plot). Right: 95% CL constraints in the interesting region (from the global fit) for both constraints, using  $D \rightarrow \mu\nu$  to constrain  $\zeta_l^* \zeta_u/M_{H^\pm}^2$ .

The new-physics corrections are dominated by  $\Delta_{us} \simeq \zeta_l^* \zeta_d m_K^2/M_{H^\pm}^2$ . As  $m_K^2/m_B^2 \sim 1\%$ , the scalar contributions to these decays are much smaller than for the heavy mesons. However, the good experimental precision achieved provides interesting constraints, as shown in figure 6.4, which are dominated by the  $K_{\mu 2}/\pi_{\mu 2}$  ratio. At 95% CL, one finds  $|1 - \Delta_{us}| \in [0.984, 1.017]$  from  $K_{\mu 2}/\pi_{\mu 2}$  and  $|1 - \Delta_{us}| \in [0.965, 1.025]$  from the ratio  $\tau \rightarrow \nu K/\pi$ . The real solutions are then,  $\zeta_l^* \zeta_d/M_{H^\pm}^2 \in [-0.07, 0.07] \text{ GeV}^{-2}$  or  $[8.14, 8.28] \text{ GeV}^{-2}$ . The larger real solution is already excluded by the  $B \rightarrow \tau\nu$  data.

### 6.3.3 Semileptonic decays of pseudoscalar mesons

Semileptonic decays receive contributions from a charged scalar as well, but in this case the leading SM amplitude is not helicity suppressed, therefore the relative influence is smaller. In addition, there are momentum-dependent form factors involved. The decay amplitude  $M \rightarrow M' l \bar{\nu}_l$  is characterized by two form factors,  $f_+(t)$  and  $f_0(t)$  associated with the P-wave and S-wave projections of the crossed-channel matrix element  $\langle 0 | \bar{u}_i \gamma^\mu d_j | M \bar{M}' \rangle$ . The scalar-exchange amplitude only contributes to the scalar form factor; it amounts to a

multiplicative correction

$$\tilde{f}_0(t) = f_0(t) (1 + \delta_{ij} t) , \quad (6.11)$$

where

$$\delta_{ij} \equiv -\frac{\zeta_l^*}{M_{H^\pm}^2} \frac{m_i \zeta_u - m_j \zeta_d}{m_i - m_j} . \quad (6.12)$$

The determination of the CKM matrix element  $|V_{ij}|$  is not contaminated by the new-physics contribution, because it is governed by the vector form factor. One measures the electron mode  $M \rightarrow M' e \bar{\nu}_e$ , where the scalar contribution is heavily suppressed by the electron mass, determining the product  $|V_{ij}| |f_+(t_0)|$ , with  $t_0 = 0$  for light-quark transitions and  $t_0 = (m_M - m_{M'})^2$  for heavy quarks. A theoretical calculation of  $|f_+(t_0)|$  is then needed to extract  $|V_{ij}|$ . The sensitivity to the scalar contribution can only be achieved in semileptonic decays into heavier leptons. Whenever available, one can make use of the differential decay distribution to separate the scalar and vector amplitudes. In any case, theoretical determinations of the scalar and vector form factors are needed to extract information on  $\delta_{ij}$ .

$B \rightarrow D \tau \nu_\tau$

To reduce the uncertainty from the vector form factor, let us consider the ratio

$$\frac{\text{Br}(B \rightarrow D \tau \nu_\tau)}{\text{Br}(B \rightarrow D e \nu_e)} = a_0 + a_1 (m_B^2 - m_D^2) \text{Re}(\delta_{cb}) + a_2 (m_B^2 - m_D^2)^2 |\delta_{cb}|^2 . \quad (6.13)$$

The coefficients  $a_i$ , which contain the dependence on the strong-interaction dynamics, have been studied recently and parametrized in terms of the vector form-factor slope  $\rho^2$  and the scalar density  $\Delta(v_B \cdot v_D) \equiv \Delta$ , assumed to be constant [131, 190]. We make use of these parametrizations, taking for the two parameters the values indicated in table 6.1. The function  $\Delta(v_B \cdot v_D) \propto f_0(t)/f_+(t)$  has been studied in the lattice, in the range  $v_B \cdot v_D = 1-1.2$ , and found to be consistent with a constant value  $\Delta = 0.46 \pm 0.02$ , very close to its static-limit approximation  $(m_B - m_D)/(m_B + m_D)$  [165].

We obtain once more a correlation between  $\zeta_l^* \zeta_u / M_{H^\pm}^2$  and  $\zeta_l^* \zeta_d / M_{H^\pm}^2$ , where the term proportional to the charm quark mass is in general potentially more important than in the type II model. The results are shown in figure 6.5 for both parameter combinations. As can be seen there, the constraint on  $\zeta_d \zeta_l^* / M_{H^\pm}^2$  is consistent with the information coming from  $B \rightarrow \tau \nu$  and the leptonic decays of light mesons, but does not constrain this combination further as long as only the information of  $B \rightarrow D \tau \nu_\tau$  is used. The red lines indicating the constraint for  $\zeta_l^* \zeta_u \rightarrow 0$ , however, show that the semileptonic decay can exclude a small region around  $(0.08, 0)$ , once that combination is bound to be small. We will use this to exclude the second real solution for  $\zeta_l^* \zeta_d / M_{H^\pm}^2$  with aid of the processes  $\epsilon_K, Z \rightarrow bb$  and  $\tau \rightarrow \mu \nu \nu$  (see figure 6.8). Also, when plotted in the complex  $\zeta_l^* \zeta_u / M_{H^\pm}^2$  plane, it becomes apparent that this constraint is important to exclude the second real solution allowed by  $D_{(s)} \rightarrow \ell \nu$  decays, already using only the information from leptonic decays in addition (see again figure 6.8).

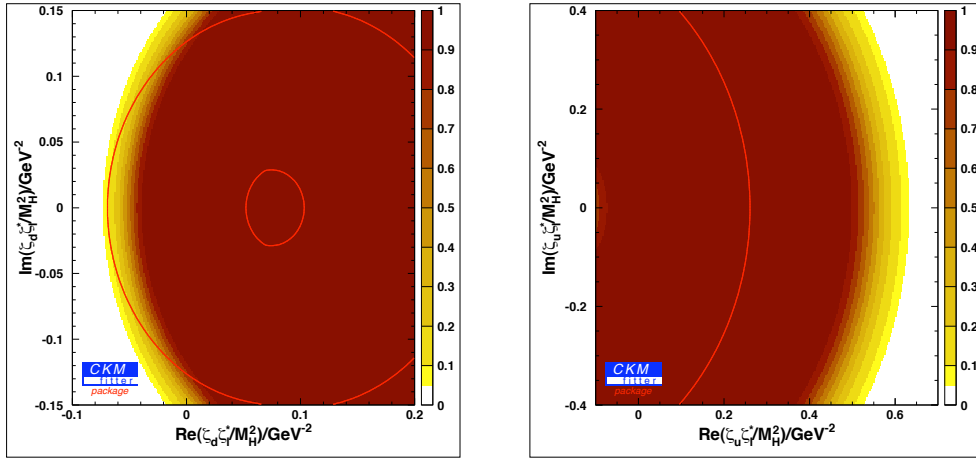


Figure 6.5: Constraints from  $B \rightarrow D\tau\nu_\tau$ , in units of  $\text{GeV}^{-2}$ , plotted in the complex plane for  $\zeta_d^* \zeta_u / M_H^2$  (left) and  $\zeta_u^* \zeta_d / M_H^2$  (right), using  $D \rightarrow \mu\nu$  and  $B \rightarrow \tau\nu$  to constrain the combination not shown, respectively. The colours indicate  $1 - \text{CL}$ , the red lines the constraint (95% CL) for  $\zeta_l^* \zeta_{u,d} / M_H^2 \rightarrow 0$ .

Considering the limit of real  $\zeta_f$ 's, the correlation between the real parts is visualized in figure 6.6, together with the cuts corresponding to the different models with  $\mathcal{Z}_2$  symmetries. The plot shows that the  $m_b$  and  $m_c$  terms have potentially similar influence in this case.

It has been pointed out in [191] that measuring the spectrum instead of just the branching ratio will increase the sensitivity of the channel. This, however, has not been done up to now, due to lack of statistics.

### $K \rightarrow \pi\ell\nu$

In semileptonic kaon decays the Callan-Treiman theorem [192, 193] allows to relate the scalar form factor at the kinematic point  $t_{\text{CT}} = m_K^2 - m_\pi^2$  to the ratio of kaon and pion decay constants:  $C \equiv f_0(t_{\text{CT}})/f_+(0) = \frac{f_K}{f_\pi} \frac{1}{f_+(0)} + \Delta_{\text{CT}}$ , where  $\Delta_{\text{CT}} = (-3.5 \pm 8) \cdot 10^{-3}$  is a small  $\chi\text{PT}$  correction of  $O[m_\pi^2/(4\pi f_\pi)^2]$  [144, 194, 195]. Using a twice-subtracted dispersion relation for  $f_0(t)$  [196], the constant  $C$  has been determined from the  $K_{\mu 3}$  data by KLOE [177], KTeV [178] and NA48 [197]. In the average quoted in table 6.2 the NA48 result has been excluded because it disagrees with the other two measurements by more than  $2\sigma$ .

In the presence of charged-scalar contributions, the scalar form factor gets modified as indicated in Eq. (6.11), inducing a corresponding change in  $C$ . Taking into account that the analyzed experimental distribution is only sensitive to  $|\tilde{f}_0(t)|^2$ , to first order in the new-physics correction  $\delta_{us}$ , the measured value of  $C$  corresponds to

$$\log C = \log \left( \frac{f_K}{f_\pi} \frac{1}{f_+(0)} + \Delta_{\text{CT}} \right) + \text{Re} [\delta_{us}(m_K^2 - m_\pi^2)] . \quad (6.14)$$

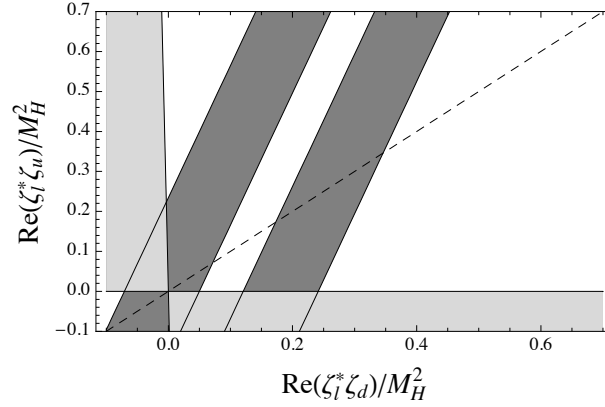


Figure 6.6: Allowed regions for  $\text{Re}(\zeta_l^* \zeta_d)/M_{H^\pm}^2$  and  $\text{Re}(\zeta_l^* \zeta_u)/M_{H^\pm}^2$  from the process  $B \rightarrow D\tau\nu$  at 95% CL (grey), in units of  $\text{GeV}^{-2}$ , assuming that their imaginary parts are zero. The projections for the 2HDMs of types I/X (dashed line) and II (lighter grey area,  $\tan\beta \in [0.1, 60]$ ) are also shown.

The resulting constraint on the real part of  $\zeta_d \zeta_l^*/M_{H^\pm}^2$  is shown in figure 6.7, leading to

$$\text{Re}\left(\frac{\zeta_l^* \zeta_d}{M_{H^\pm}^2}\right) \in [-0.16, 0.30] \text{ GeV}^{-2} \quad (95\% \text{ CL}), \quad (6.15)$$

which is in agreement with the previous constraints, but with larger uncertainties. This might change in the near future, due to improved lattice determinations of  $f_+(0)$  and  $f_K/f_\pi$ , as well as improved experimental precision, e.g. from NA62 or KLOE-2.

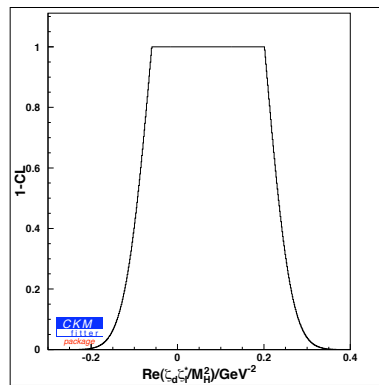


Figure 6.7: Constraint from the direct measurement of  $\log C$ , in units of  $\text{GeV}^{-2}$ .

### 6.3.4 Global fit to leptonic and semileptonic decays

Combining the information from all leptonic and semileptonic decays discussed before, one gets the constraints shown in figure 6.8.  $|\zeta_d \zeta_l^*/M_{H^\pm}^2|$  is bounded to be smaller than  $\sim 0.1 \text{ GeV}^{-2}$  (95% CL) from these decays alone, while for  $\zeta_u \zeta_l^*/M_{H^\pm}^2$  the constraints are relatively weak, due to the similar masses of the mesons in the leptonic decays. Note that in both cases there are two real solutions. For the combination  $\zeta_u \zeta_l^*/M_{H^\pm}^2$ , one real solution is excluded in the global fit at 95% CL, while the other, including the SM point of vanishing couplings remains allowed. As mentioned before, this exclusion is due to  $B \rightarrow D\tau\nu$  in combination with the constraint on  $\zeta_d \zeta_l^*/M_{H^\pm}^2$ . For the latter, the situation is more complicated. The second solution remains allowed, due to the overlapping of the two main constraints in both regions and the weak constraint on  $\zeta_u \zeta_l^*/M_{H^\pm}^2$  derived from semileptonic decays. However, using in addition the information coming from leptonic  $\tau$  decays in (6.4), the lower Higgs mass bound from LEP and the constraint from  $\epsilon_K, Z \rightarrow \bar{b}b$  (see section 6.4.1) in a conservative way,  $|\zeta_u \zeta_l^*|/M_H^2 \lesssim 0.01$ , the second real solution for  $\zeta_d \zeta_l^*/M_{H^\pm}^2$  is excluded as well by  $B \rightarrow D\tau\nu$ .

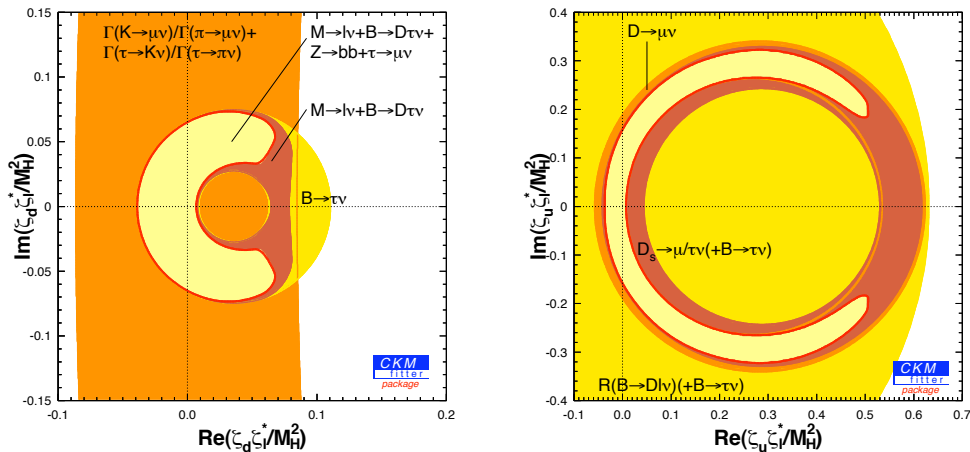


Figure 6.8:  $\zeta_d \zeta_l^*/M_{H^\pm}^2$  (left) and  $\zeta_u \zeta_l^*/M_{H^\pm}^2$  (right) in the complex plane, in units of  $\text{GeV}^{-2}$ , constrained by leptonic decays and  $B \rightarrow D\ell\nu$ . The inner yellow area shows the allowed region at 95% CL, in the case of  $\zeta_d \zeta_l^*/M_{H^\pm}^2$  using additional information (see text).

## 6.4 Loop-induced processes

For processes where new-physics contributions appear only through quantum loop effects, the situation becomes obviously more difficult, regarding not only the calculation but also the interpretation of the results. If the SM amplitude is also mediated only by loops, the relative importance of the charged-scalar contributions is expected to be higher, but this implies also a higher sensitivity to the framework in which the A2HDM is eventually to be embedded in. In the following we make the assumption that for the observables under

discussion the dominant new-physics corrections are those generated by the charged scalar. Moreover, since no significant signal for new physics has been found up to now in flavour observables, we assume these effects to be subleading with respect to the SM contribution.

### 6.4.1 $Z \rightarrow b\bar{b}$

The high-precision data collected at LEP and SLD has made possible to accurately test the SM electroweak loop corrections at the  $Z$  scale, providing information on the Higgs mass and useful constraints on many new-physics scenarios. While most  $Z$ -peak observables are only sensitive to the gauge-boson selfenergies, the decay  $Z \rightarrow b\bar{b}$  provides valuable information on fermionic vertex corrections induced by charged-current exchanges. Since  $V_{tb} \approx 1$ , those loop diagrams involving virtual top quarks generate quantum corrections to the  $Zb\bar{b}$  vertex, which are absent in the  $Zd\bar{d}$  and  $Zs\bar{s}$  vertices. These corrections are enhanced by a factor  $m_t^2$ , allowing for a quite accurate determination of the top quark mass [198, 199]. The same arguments apply to the charged-scalar contributions present in the A2HDM, providing a sensitive probe of the corresponding  $H^+\bar{t}b$  coupling. For very large values of  $|\zeta_d|$  this decay would also be sensitive to contributions from neutral scalars [200], but this possibility is excluded by the constraints obtained through other processes. Therefore, we assume the dominance of charged-scalar effects in the following, allowing only for  $|\zeta_d| \leq 50$ . We disregard the information coming from the forward-backward polarization asymmetry  $A_b$ , because the scalar-exchange contributions to  $A_b$  are small compared to the present uncertainties.

It is convenient to normalize the  $Z \rightarrow b\bar{b}$  decay width to the total hadronic width of the  $Z$ , because many QCD and electroweak corrections cancel in the ratio, amplifying the sensitivity to the wanted vertex contribution [199]. Within the A2HDM, this ratio can be written as [167, 200, 201]

$$R_b \equiv \frac{\Gamma(Z \rightarrow b\bar{b})}{\Gamma(Z \rightarrow \text{hadrons})} = \left[ 1 + \frac{S_b}{s_b} C_b^{\text{QCD}} \right]^{-1}, \quad (6.16)$$

where

$$s_q = [(\bar{g}_b^L - \bar{g}_b^R)^2 + (\bar{g}_b^L + \bar{g}_b^R)^2] \left( 1 + \frac{3\alpha}{4\pi} Q_q^2 \right), \quad S_b \equiv \sum_{q \neq b, t} s_q, \quad (6.17)$$

with  $\mu_q \equiv m_q^2/M_Z^2$  and  $C_b^{\text{QCD}} = 1.0086$  a factor including QCD and quark-mass corrections [202]. The A2HDM contributions are encoded through the effective left- and right-handed  $Zb\bar{b}$ -couplings:

$$\bar{g}_b^L = \bar{g}_{b,SM}^L + \frac{\sqrt{2} G_F M_W^2}{16\pi^2} \frac{m_t^2}{M_W^2} |\zeta_u|^2 \left[ f_1(t_h) + \frac{\alpha_s}{3\pi} f_2(t_h) \right], \quad (6.18)$$

$$\bar{g}_b^R = \bar{g}_{b,SM}^R - \frac{\sqrt{2} G_F M_W^2}{16\pi^2} \frac{m_b^2}{M_W^2} |\zeta_d|^2 \left[ f_1(t_h) + \frac{\alpha_s}{3\pi} f_2(t_h) \right], \quad (6.19)$$

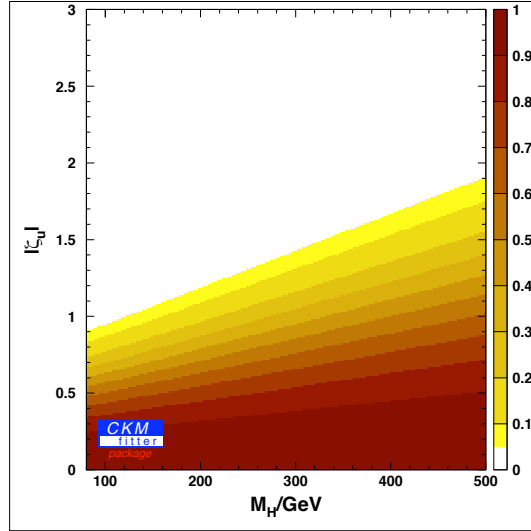


Figure 6.9: Constraint from  $R_b$  in the  $|\varsigma_u| - M_{H^\pm}$  plane ( $M_{H^\pm}$  in GeV units), allowing for  $|\varsigma_d| \leq 50$ .

where  $t_h \equiv m_t^2/M_{H^\pm}^2$ ,  $f_1(t_h) = [t_h^2 - t_h - t_h \log t_h]/(1 - t_h)^2$  and the function  $f_2(t_h)$  governing the NLO correction is given in [167]. If running quark masses  $\bar{m}_t(M_Z)$  and  $\bar{m}_b(M_Z)$  are used, this NLO QCD correction is small. The light-quark coupling contribution  $S_b = 1.3214$  [167] is not sensitive to the new-physics effects. The SM values of the couplings  $\bar{g}_{b,SM}^{L,R}$ , given in table 6.1, have been computed removing the  $Z \rightarrow b\bar{b}$  information from the standard electroweak fit [167].

In contrast to the leptonic and semileptonic constraints discussed before, here the parameters  $|\varsigma_{u,d}|$  enter directly, allowing to bound them without information on  $|\varsigma_l|$ . The constraint resulting from the input values in tables 6.1 and 6.2 is shown in figure 6.9. The constraint is plotted in the  $|\varsigma_u| - M_{H^\pm}$  plane, as obviously it is much weaker for  $|\varsigma_d|$ , once again due to the relative factor  $m_b/m_t$ . For large scalar masses, the constraint weakens as the effects start to decouple, reflected in  $\lim_{t_h \rightarrow 0} f_{1,2}(t_h) = 0$ . In the range of scalar masses considered, it leads to a 95% CL upper bound  $|\varsigma_u| \leq 0.91$  (1.91), for  $M_{H^\pm} = 80$  (500) GeV. The upper bound increases linearly with  $M_{H^\pm}$ , implying

$$\frac{|\varsigma_u|}{M_{H^\pm}} < 0.0024 \text{ GeV}^{-1} + \frac{0.72}{M_{H^\pm}} < 0.011 \text{ GeV}^{-1}, \quad (6.20)$$

where we have used the lower bound on the charged-scalar mass from LEP searches,  $M_{H^\pm} > 78.6$  GeV (95% CL) [41, 74]. Combined with the limit on  $|\varsigma_l/M_{H^\pm}|$  from leptonic  $\tau$  decays, this already constrains the combination  $|\varsigma_u \varsigma_l^*|/M_{H^\pm}^2$  much stronger than the global fit to (semi)leptonic decays, leading to

$$\frac{|\varsigma_u \varsigma_l^*|}{M_{H^\pm}^2} < 0.005 \text{ GeV}^{-2}; \quad (6.21)$$

given the additional assumptions of  $|\varsigma_d| \leq 50$  and charged-scalar effects dominating the new-physics contributions to  $R_b$ . The range allowed for  $|\varsigma_d|$  in the fit does not influence the upper bound on  $|\varsigma_u|$ , apart from the exclusion of neutral-scalar effects, since both contributions can only lower the value for  $R_b$  and both are allowed to vanish in the fit. Therefore the upper limit stems from points with  $|\varsigma_d| = 0$ .

### 6.4.2 $B^0$ - $\bar{B}^0$ mixing

The mixing of neutral  $B$  mesons is very sensitive to charged-scalar effects, as the leading contribution stems from top-quark loops, rendering the new-physics and SM contributions comparable. Besides the high precision of the measurement for the mass difference  $\Delta m_{B^0}$ , the  $B_s^0$  mixing is especially interesting due to the observed tension in its phase [14, 155]. In the usual 2HDMs with a  $\mathcal{Z}_2$  symmetry the scalar couplings are necessarily real, leading to a vanishing contribution to this phase. However, the complex Yukawa couplings  $\varsigma_{u,d}$  of the A2HDM provide a potential new-physics contribution, which could account for the experimentally observed phase.

In the SM, the calculation is simplified by the fact that only one operator contributes, denoted  $\mathcal{O}^{\text{VLL}}$  below. In the presence of a charged scalar, an enlarged effective Hamiltonian

$$\mathcal{H}_{\text{eff}}^{\Delta B=2} = \frac{G_F^2 M_W^2}{16\pi^2} (V_{td}^* V_{tb})^2 \sum_i C_i(\mu) \mathcal{O}_i \quad (6.22)$$

has to be considered, involving a basis of eight operators [203–206]:

$$\begin{aligned} \mathcal{O}^{\text{VLL,VRR}} &= (\bar{d}^\alpha \gamma_\mu \mathcal{P}_{L,R} b^\alpha) (\bar{d}^\beta \gamma^\mu \mathcal{P}_{L,R} b^\beta) , \\ \mathcal{O}_1^{\text{LR}} &= (\bar{d}^\alpha \gamma_\mu \mathcal{P}_L b^\alpha) (\bar{d}^\beta \gamma^\mu \mathcal{P}_R b^\beta) , \\ \mathcal{O}_2^{\text{LR}} &= (\bar{d}^\alpha \mathcal{P}_L b^\alpha) (\bar{d}^\beta \mathcal{P}_R b^\beta) , \\ \mathcal{O}_1^{\text{SLL,SRR}} &= (\bar{d}^\alpha \mathcal{P}_{L,R} b^\alpha) (\bar{d}^\beta \mathcal{P}_{L,R} b^\beta) , \\ \mathcal{O}_2^{\text{SLL,SRR}} &= (\bar{d}^\alpha \sigma_{\mu\nu} \mathcal{P}_{L,R} b^\alpha) (\bar{d}^\beta \sigma^{\mu\nu} \mathcal{P}_{L,R} b^\beta) , \end{aligned} \quad (6.23)$$

with  $\alpha, \beta$  being colour indices and  $\sigma^{\mu\nu} = \frac{1}{2}[\gamma^\mu, \gamma^\nu]$ . We have written the effective Hamiltonian relevant for  $B_d^0$ - $\bar{B}_d^0$  mixing; the mixing of  $B_s^0$  mesons is described by the analogous expression, changing the label  $d$  to  $s$  everywhere.

We have performed the matching of the underlying A2HDM and the low-energy effective Hamiltonian at the scale  $\mu_{tW} \sim M_W, m_t$ . The resulting Wilson coefficients, given in the Appendix B, reproduce the SM result as well as the matching for the 2HDM in the limit  $m_d \rightarrow 0$ , given in [207]. As noted above, the contribution of the A2HDM to  $C_{\text{VLL}}(\mu_{tW})$  is an  $\mathcal{O}(1)$  effect. For that reason, we calculate this contribution at NLO, implementing the results of [207] within the A2HDM.<sup>2</sup> Owing to their chirality structure, the remaining Wilson coefficients are all suppressed by powers of the light-quark mass  $m_d$  ( $m_s$  in the  $B_s^0$  case), except  $C_{\text{SRR}}^1$  which is proportional to  $m_b^2$ . Restricting the parameter ranges to

<sup>2</sup>Note, that there are several smaller errors in that paper, most of which have been pointed out in [130].

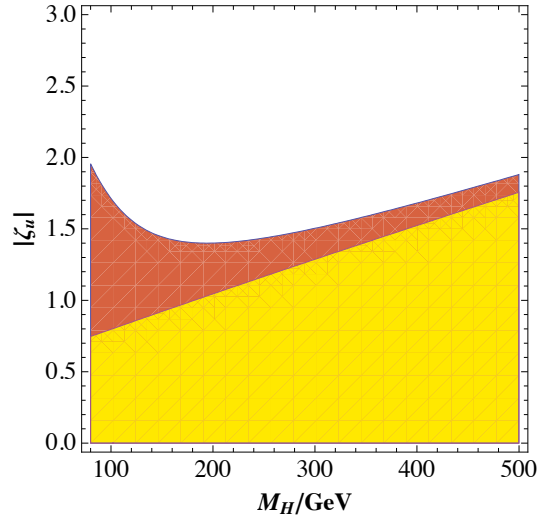


Figure 6.10: The 95% CL constraint coming from  $\Delta m_{B_s^0}$  in the  $M_{H^\pm} - |\zeta_u|$  plane for  $|\zeta_d| \in [0, 50]$ , varying in addition the relative phase  $\varphi$  in  $[0, 2\pi]$ . The excluded area lies above the dark (red) region only. In yellow the allowed area for  $\zeta_d = 0$  is shown.

$|\zeta_u| \in [0, 5]$  and  $|\zeta_d| \in [0, 50]$ , the ratio  $|C_i(\mu_{tW})/C_{\text{VLL}}(\mu_{tW})|$  is then below two percent for all operators apart from  $\mathcal{O}_1^{\text{SRR}}$ . Since the matrix elements for the  $B^0$  mixing do not contain the large (chiral) enhancement factors present in the kaon system, this allows us to restrict ourselves to two operators only. Moreover, the ratio  $C_{\text{SRR}}^1/C_{\text{VLL}}$  is a small quantity (10% at most for  $|\zeta_d| \leq 25$ , still below 40% for  $|\zeta_d| = 50$ ) and therefore a leading-order estimate of the  $\mathcal{O}_1^{\text{SRR}}$  contribution is enough for our purposes, while the dominant  $\mathcal{O}^{\text{VLL}}$  contribution is included at NLO.

The strong  $(m_s - m_d)/M_W$  suppression of SU(3)-breaking effects implies that, for the parameter ranges considered, the ratio  $\Delta m_{B_s^0}/\Delta m_{B_d^0}$  is unaffected by charged-scalar contributions and can be used in the CKM fit. Note, however, that in the limit  $|\zeta_d| \gg 50$ ,  $|\zeta_u| \ll 1$ , which corresponds to the large- $\tan\beta$  scenario in the type II model, the contribution from  $\mathcal{O}^{\text{VRR}}$  might become the dominant new-physics correction to  $B_s^0$  mixing, but remains small compared to the SM one.

We use the ratio  $\Delta m_{B_s^0}/\Delta m_{B_d^0}$  to determine the apex  $(\bar{\rho}, \bar{\eta})$  of the unitarity triangle, and bound the charged-scalar parameters with the  $B_s^0$  mixing information. The resulting constraint from  $\Delta m_{B_s^0}$  in the  $M_{H^\pm} - |\zeta_u|$  plane is shown in figure 6.10, using the scales  $\mu_{tW} = m_t$  and  $\mu_b = 4.2$  GeV. The error includes the variations in the CKM parameters,  $f_{B_s^0}$ ,  $\hat{B}_{B_s^0}$  and the experimental uncertainty. The leading  $\mathcal{O}^{\text{VLL}}$  contribution depends on  $|\zeta_u|^2$  only, while  $C_{\text{SRR}}^1$  is proportional to  $\zeta_u^* \zeta_d = |\zeta_u| |\zeta_d| e^{i\varphi}$ , being  $\varphi$  the relative phase between the two Yukawa couplings. To determine the allowed region shown in figure 6.10, we have varied  $\zeta_d$  in the range  $|\zeta_d| < 50$  and  $\varphi \in [0, 2\pi]$ .

Interestingly, the dominant contribution to a possible phase shift in the mixing is also the one from  $\mathcal{O}_1^{\text{SRR}}$ . The factor  $M_W^4 D_0(m_t, M_H)$  (see Appendix B) varies between zero and  $\sim -3\%$  for scalar masses between 50 and 500 GeV, while  $4m_b^2 m_t^4/M_W^6 \sim 10\%$ . For

relatively large values of the product  $|\varsigma_u^* \varsigma_d|$  ( $\gtrsim 20$ ) this factor can contribute sizeably to the  $B^0$  mixing phase, as long as  $M_{H^\pm}$  is relatively small. The sign of the shift is obviously not fixed, but depends on the sign of the relative Yukawa phase  $\varphi$ . As long as  $|\varsigma_d|$  is not too large, the effect is the same in  $B_d^0$  and  $B_s^0$ .

### 6.4.3 $K^0$ - $\bar{K}^0$ mixing: $\epsilon_K$

The  $\Delta S = 2$  effective Hamiltonian is described by the same basis of four-quark operators given in (6.23), changing the flavour  $b$  to  $s$  everywhere. However, the small light-quark masses  $m_d$  and  $m_s$  suppress now the contributions from all operators except  $\mathcal{O}^{\text{VLL}}$ . Another difference with respect to  $B^0$  mixing is that, owing to the different CKM factors, one needs to consider the virtual contributions from top and charm quark exchanges within the box diagrams:

$$\mathcal{H}_{\text{eff}}^{\Delta S=2} = \frac{G_F^2 M_W^2}{16\pi^2} \{ \lambda_t^2 C_{\text{VLL}}^{tt}(\mu) + \lambda_c^2 C_{\text{VLL}}^{cc}(\mu) + 2\lambda_t \lambda_c C_{\text{VLL}}^{ct}(\mu) \} (\bar{d}\gamma_\mu \mathcal{P}_L s) (\bar{d}\gamma^\mu \mathcal{P}_L s) . \quad (6.24)$$

Since  $\lambda_t \equiv V_{td}^* V_{ts} \sim A^2 \lambda^5$  while  $\lambda_c \equiv V_{cd}^* V_{cs} \sim \lambda$ , in spite of the  $m_c^2/m_t^2$  relative suppression, the charm loop gives the dominant short-distance contribution to  $\Delta m_K$ . There are in addition large corrections from long-distance physics, which make difficult to extract from  $\Delta m_K$  useful constraints on the new-physics amplitude.

More interesting is the CP-violating parameter  $\epsilon_K$ , which can be written in the form [168, 208]

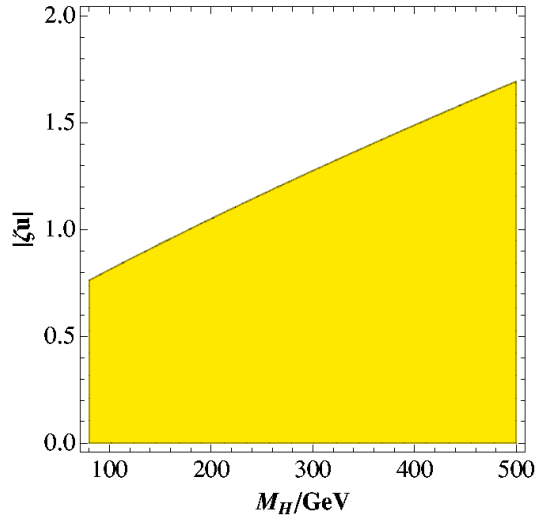
$$\epsilon_K = \frac{\kappa_\epsilon}{\sqrt{2}} \frac{e^{i\phi_\epsilon}}{\Delta m_K} \text{Im}(\mathcal{H}_{\text{eff}}^{\Delta S=2}), \quad (6.25)$$

where  $\kappa_\epsilon = 0.94 \pm 0.02$  takes into account small long-distance corrections [168, 208]. The top and charm contributions are now weighted by less hierarchical CKM factors  $\text{Im}(\lambda_t^2) \sim \lambda^4 \text{Im}(\lambda_c \lambda_t) \sim \lambda^4 \text{Im}(\lambda_c^2)$ ; the mass hierarchy compensates for this, implying that the top quark gives the most important contribution to  $\epsilon_K$ .

The relevant Wilson coefficients  $C_{\text{VLL}}^{qq'}$ , containing the SM and new-physics contributions, are given in the Appendix B. The corrections induced by the charged scalar are proportional to  $|\varsigma_u|^2$  and  $|\varsigma_u|^4$ . All contributions from the coupling  $\varsigma_d$  are absent in the limit  $m_{d,s} = 0$ . The matrix element  $\langle K^0 | \mathcal{H}_{\text{eff}}^{\Delta S=2} | \bar{K}^0 \rangle$  is parametrized through the hadronic quantity  $f_K^2 \hat{B}_K$ . We use the numerical values of  $f_K/f_\pi$  and  $\hat{B}_K$ , given in table 6.1, together with the phenomenological determination of the pion decay constant from  $\Gamma(\pi^+ \rightarrow \mu^+ \nu_\mu)$ ,  $f_\pi = 130.4 \pm 0.04 \pm 0.2$  MeV [156]. Figure 6.11 shows the constraint obtained from  $\epsilon_K$  in the plane  $M_{H^\pm} - |\varsigma_u|$ . It is very similar to the one extracted from  $Z \rightarrow b\bar{b}$ , and even slightly stronger.

### 6.4.4 $\bar{B} \rightarrow X_s \gamma$

The radiative decay  $\bar{B} \rightarrow X_s \gamma$  has been calculated at NNLO in the SM whereas in the 2HDM the decay amplitude is known at NLO [167, 209–211]. While the problem of a sizable

Figure 6.11: 95% CL constraints from  $\epsilon_K$ .

scale dependence has been basically resolved with the calculation of the NLO corrections, the issue of charm-mass scheme dependence can only be addressed at NNLO [212]. To achieve this, a huge effort is being made, and by now the branching ratio is essentially<sup>3</sup> calculated up to that order. We follow here the calculation by [216], giving  $\text{Br}(\bar{B} \rightarrow X_s \gamma)_{E_\gamma > 1.6 \text{ GeV}}^{\text{SM, theo}} = (3.15 \pm 0.23) \times 10^{-4}$ , in agreement with the present world average [217]

$$\text{Br}(\bar{B} \rightarrow X_s \gamma)_{E_\gamma \geq 1.6 \text{ GeV}}^{\text{exp}} = (3.55 \pm 0.26) \times 10^{-4}. \quad (6.26)$$

Note however, that different treatments of photon-energy-cut related effects lead to slightly different results [218–220] (see also [221]). The related shifts are of the order of the uncertainty assigned in [216]. Regarding the non-perturbative part of this calculation, contributions with the photon coupling to light partons (“resolved” photon contributions) lead to the appearance of non-local matrix elements, implying an unreducible error of  $\sim 5\%$  [222]. Following the steps given in [223], one can express the branching ratio as

$$\text{Br}(\bar{B} \rightarrow X_s \gamma)_{E_\gamma > E_0} = \text{Br}(\bar{B} \rightarrow X_c e \bar{\nu})_{\text{exp}} \left| \frac{V_{ts}^* V_{tb}}{V_{cb}} \right|^2 \frac{6\alpha}{\pi C_B} [P(E_0) + N(E_0)], \quad (6.27)$$

where the phase-space factor  $C_B = |V_{ub}/V_{cb}|^2 \Gamma(\bar{B} \rightarrow X_c e \bar{\nu}) / \Gamma(\bar{B} \rightarrow X_u e \bar{\nu}) = 0.580 \pm 0.016$  [224] accounts for the  $m_c$  dependence of  $\text{Br}(\bar{B} \rightarrow X_c e \bar{\nu})$ . Normalizing the result with the  $\bar{B} \rightarrow X_c e \bar{\nu}$  transition, one cancels the leading non-perturbative corrections of order  $\Lambda^2/m_b^2$  and minimizes many sources of uncertainties, such as those generated by the CKM quark-mixing factors, the dependence on  $m_b^5$  and the sensitivity to  $m_c$ . The sub-leading non-perturbative contributions are contained in  $N(E_0)$ , which includes corrections of  $\mathcal{O}(\Lambda^2/m_c^2)$  [225],  $\mathcal{O}(\Lambda^3/m_b^3)$ ,  $\mathcal{O}(\Lambda^3/m_b m_c^2)$  [226] and  $\mathcal{O}(\alpha_s \Lambda^2/(m_b - 2E_0)^2)$  [227]. The

<sup>3</sup>For the present status and recent developments, see e.g. [213–215].

relevant combination of CKM factors is given by

$$\left| \frac{V_{ts}^* V_{tb}}{V_{cb}} \right|^2 = 1 + \lambda^2(2\bar{\rho} - 1) + \lambda^4(\bar{\rho}^2 + \bar{\eta}^2 - A^2) + \mathcal{O}(\lambda^6) = 0.963 \pm 0.002 \pm 0.005, \quad (6.28)$$

where the sensitivity to the apex  $(\bar{\rho}, \bar{\eta})$  of the unitarity triangle is suppressed by two powers of  $\lambda$ .

For  $m_s = 0$  the effective low-energy operator basis remains the same as in the SM. The modifications induced by new-physics contributions appear only in the Wilson coefficients, which are included in the perturbative part  $P(E_0)$ :

$$C_i^{\text{eff}}(\mu_W) = C_{i,SM} + |\varsigma_u|^2 C_{i,uu} - (\varsigma_u^* \varsigma_d) C_{i,ud}, \quad (6.29)$$

where  $\varsigma_u^* \varsigma_d = |\varsigma_u| |\varsigma_d| e^{i\varphi}$ ,  $\varphi$  being the relative phase. The virtual top-quark contributions dominate the coefficients  $C_{i,uu}$  and  $C_{i,ud}$ ; their explicit expressions as a function of  $m_t$  can be found in [167]. Depending on the value of the phase  $\varphi$ , the combined effect of the two terms  $C_{i,uu}$  and  $C_{i,ud}$  can be rather different. For instance, these two terms tend to cancel each other in the type I model where  $\varphi = 0$ , while in the type II version with  $\varphi = \pi$  they add constructively.

Since the new-physics contribution is only calculated up to NLO, terms in the branching ratio of  $\mathcal{O}(\alpha_s^2)$  coming from the square of the 2HDM amplitude are neglected consistently. In some regions of the parameter space, leading to large new-physics effects of opposite sign to the SM amplitude, the cancellations between the two contributions enhance the sensitivity to higher-order QCD corrections, generating in some cases unphysical results (for instance in the type I model at small values of  $\tan\beta$ ) [210]. Fortunately, the most problematic region (large values of  $|\varsigma_u|$ ) is already excluded by the constraints from  $Z \rightarrow \bar{b}b$ ,  $\epsilon_K$  and  $\Delta m_{B_s^0}$ , allowing us to perform a consistent theoretical study of  $\text{Br}(\bar{B} \rightarrow X_s \gamma)$  in the whole remaining parameter space. The inclusion of the SM NNLO contributions substantially improves the reliability of the theoretical predictions.

To extract the information on the A2HDM couplings, we take into account the latest experimental values, given in table 6.2, and use the same renormalization scales as in [223] ( $\mu_0 = 160$  GeV,  $\mu_b = 2.5$  GeV and  $\mu_c = 1.5$  GeV as central values and the same ranges of variation). We follow again the RFit approach, adding the theoretical uncertainty linearly to the systematic error. The resulting constraints on  $|\varsigma_u|$  and  $|\varsigma_d|$  are shown in figure 6.12, varying the charged-scalar mass in the range  $M_{H^\pm} \in [80, 500]$  GeV. The white areas are excluded at 95% CL. In the left plot, the phase  $\varphi$  has been scanned in the whole range from 0 to  $2\pi$ ; the resulting constraints are not very strong because a destructive interference between the two terms in (6.29) can be adjusted through the relative phase. In the range  $|\varsigma_u| < 2$ , one finds roughly  $|\varsigma_d| |\varsigma_u| < 20$  (95% CL). More stringent bounds are obtained at fixed values of the relative phase. This is shown in the right plot, where  $\varsigma_u$  and  $\varsigma_d$  have been assumed to be real (i.e.  $\varphi = 0$  or  $\pi$ ). In that case, couplings of different sign are excluded, except at very small values, while a broad region of equal-sign couplings is allowed, reflecting again the possibility of a destructive interference.

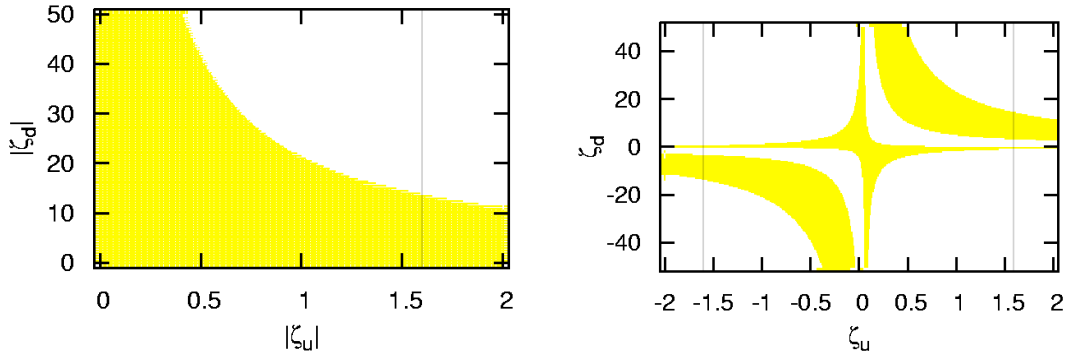


Figure 6.12: Constraints on  $\varsigma_u$  and  $\varsigma_d$  from  $\bar{B} \rightarrow X_s \gamma$ , taking  $M_{H^\pm} \in [80, 500]$  GeV. The white areas are excluded at 95% CL. The black line corresponds to the upper limit from  $\epsilon_K, Z \rightarrow \bar{b}b$  on  $|\varsigma_u|$ . In the left panel, the relative phase has been varied in the range  $\varphi \in [0, 2\pi]$ . The right panel assumes real couplings.

The sensitivity to the charged-scalar mass is illustrated in figure 6.13, which shows the constraints on  $|\varsigma_d|$  versus  $M_{H^\pm}$  for fixed values of  $\varsigma_u = 0.5$  (left) and  $\varsigma_u = 1.5$  (right). Again, in the upper plots the relative phase has been varied in the whole range  $\varphi \in [0, 2\pi]$ , while the lower plots assume real couplings. Figure 6.14 shows the constraints on the  $|\varsigma_u| - M_{H^\pm}$  plane, for  $\varsigma_d = 0$ . Finally, in figure 6.15 we show the constraints obtained for fixed values of the charged-scalar mass, assuming  $\varsigma_u$  and  $\varsigma_d$  to be real. We reproduce in this case the qualitative behaviour obtained in [133].

We observe that for small values of  $|\varsigma_u|$  no constraint on  $\varsigma_d$  is obtained, because in the limit  $|\varsigma_u| \rightarrow 0$  the SM is recovered, which is compatible with the data. With growing  $|\varsigma_u|$  a bound on  $|\varsigma_d|$  emerges, corresponding to  $|\varsigma_u \varsigma_d| \lesssim 25$ . For  $\varsigma_d = 0$  on the other hand, a limit of  $|\varsigma_u| \lesssim 3$  can be observed for large scalar masses around 500 GeV, strengthening to  $|\varsigma_u| \lesssim 1.3$  for smaller values of  $M_{H^\pm}$ . The overall constraint is relatively weak compared to the strong bound on  $M_{H^\pm}$  obtained in the type II 2HDM, due to the correlation  $\varsigma_u \varsigma_d = -1$ . However, it can be seen from the plots with vanishing phase and/or a fixed value for  $|\varsigma_{d,u}|$  that this strength is recovered, once some parameters are constrained independently. Comparing the plots with complex input parameters to their real counterparts, we observe that the effect of the relative phase is mainly to extend the allowed bands in a way that the excluded space between them is rendered allowed, too.

As we have shown up to this point, due to the additional degrees of freedom, the resulting constraint is relatively weak; especially, no direct bound can be found with respect to the charged-scalar mass, in striking contrast to the 2HDM type II. However, this changes as soon as the phase is kept fixed to a certain value. Numerically, the decay amplitude has roughly the following structure for large scalar masses (using numerical estimates for the

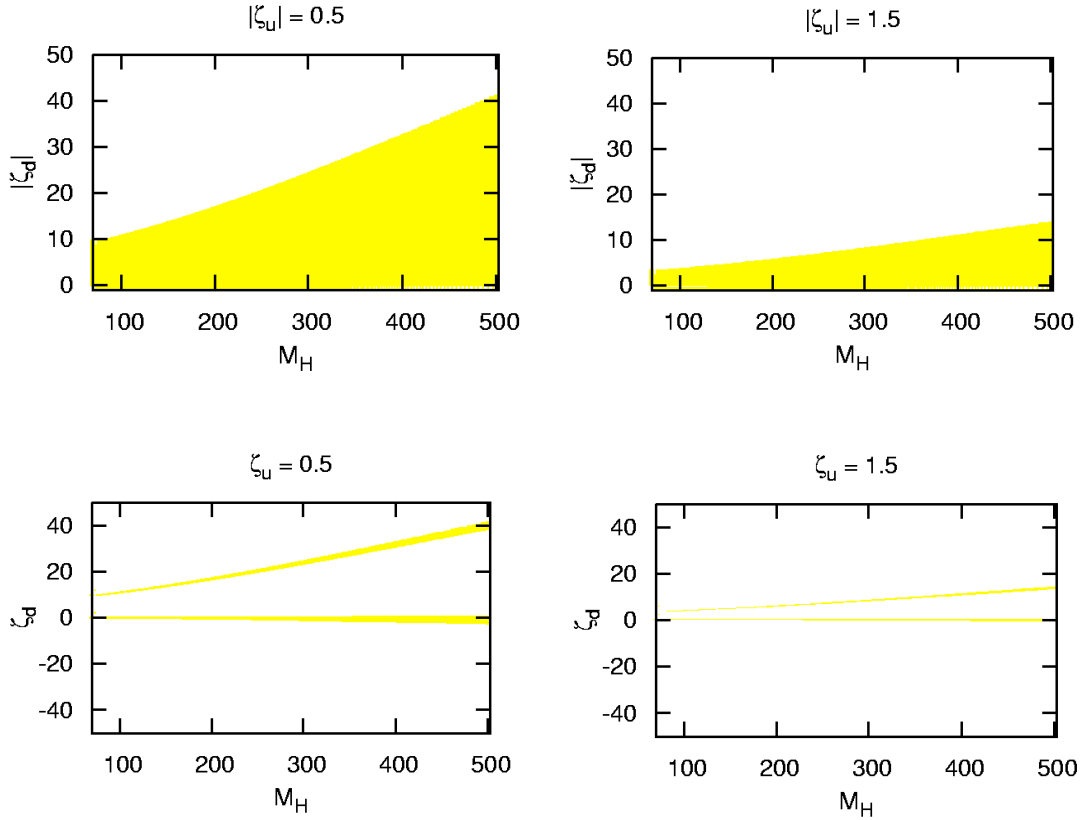


Figure 6.13: Constraints on  $|\zeta_d|$  versus  $M_{H^\pm}$  (in GeV) from  $\bar{B} \rightarrow X_s \gamma$ , for  $\zeta_u = 0.5$  (left) and  $\zeta_u = 1.5$  (right). The white areas are excluded at 95% CL. In the upper panels, the phase has been varied in the range  $\varphi \in [0, 2\pi]$ . The lower panels assume real couplings.

different contributions from [210]):

$$A \sim A_{SM} \left\{ 1 - 0.1 \zeta_u^* \zeta_d \left( \frac{500 \text{ GeV}}{M_{H^\pm}} \right)^2 + 0.01 |\zeta_u|^2 \left( \frac{500 \text{ GeV}}{M_{H^\pm}} \right)^2 \right\}. \quad (6.30)$$

From this it is obvious that we can expect in that case constraints on the parameter combinations  $|\zeta_u|^2/M_{H^\pm}^2$  and  $\zeta_u^* \zeta_d/M_{H^\pm}^2$ , the latter being complex. For sizable  $|\zeta_d|$ , the last term is negligible, as  $|\zeta_u|$  is constrained to be  $\mathcal{O}(1)$  at most, leaving only the dependence on the combination  $\zeta_u^* \zeta_d/M_{H^\pm}^2$ . The resulting limits on the single parameters in this ratio are relatively weak, as seen above. The strength of the constraint lies however in creating strong correlations between different parameter combinations [228]. This is illustrated in Fig. 6.16, where the product  $|\zeta_u^* \zeta_d|$  is plotted against the charged-scalar mass  $M_{H^\pm}$  and the relative phase  $\varphi$ , respectively. The hole in the left plot can be understood as separating two regions where the NP influence is relatively small (lower part) and where it is approximately twice the size of the SM contribution (upper part), the latter corresponding to a fine-tuned solution. For larger phases it is not possible anymore to cancel the SM amplitude

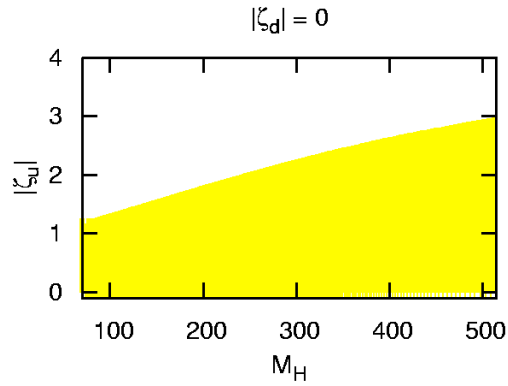


Figure 6.14: Constraints on  $|\zeta_u|$  versus  $M_{H^\pm}$  (in GeV) from  $\bar{B} \rightarrow X_s \gamma$ , for  $\zeta_d = 0$ . The white area is excluded at 95% CL.

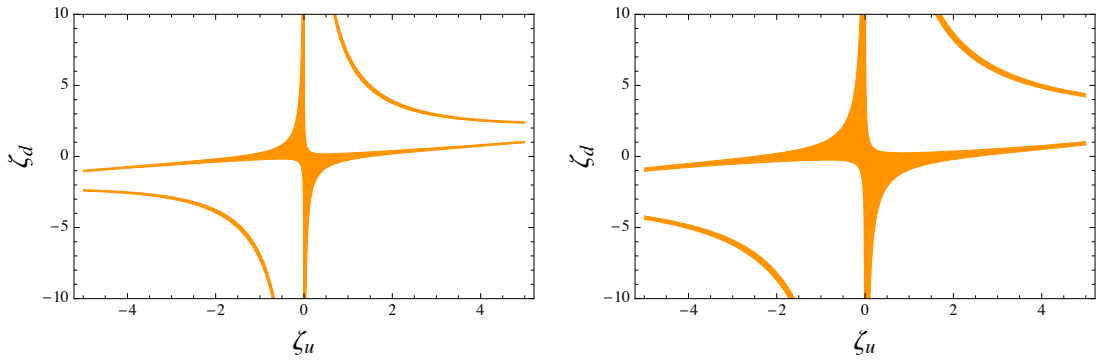


Figure 6.15: Constraints on  $\zeta_d$  versus  $\zeta_u$  (95% CL) from  $\bar{B} \rightarrow X_s \gamma$ , assuming real couplings and taking  $M_{H^\pm} = 150$  GeV (left) and  $M_{H^\pm} = 400$  GeV (right).

completely, so only one constraint is remaining, making the gap disappear. From the right plot it becomes obvious that high values for the product  $|\zeta_u^* \zeta_d|$  are only allowed for large values of the charged-scalar mass, due to the restriction on the ratio. The effect of these correlations can obviously be large in observables where the phase plays an important role, as it is shown in the next section with the CP asymmetries generated in some of these processes.

## 6.5 CP Asymmetries in B-systems

The presence of new weak phases immediately poses the question of compatibility with existing measurements of CP violating observables. One decay where a high sensitivity is expected is  $b \rightarrow s \gamma$ , for three reasons: the SM asymmetry is known to be tiny [229–231], its measurement is rather precise and compatible with zero, and the potential influence of new

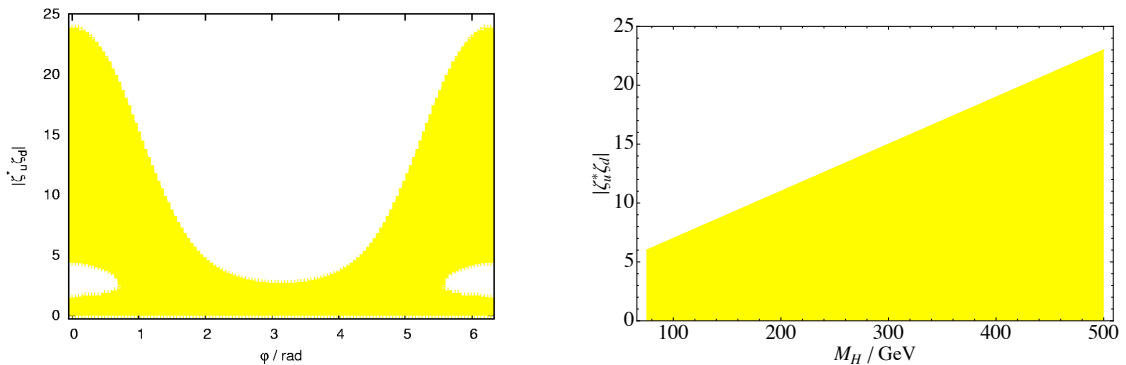


Figure 6.16: The constraint from  $\text{Br}(b \rightarrow s\gamma)$  plotted in the planes  $|\zeta_u^* \zeta_d| - \varphi$  (left) and  $|\zeta_u^* \zeta_d| - M_{H^\pm}$  (right).

physics in this decay is large. In addition, being an inclusive process, non-perturbative uncertainties are expected to be under better control than for exclusive modes. The branching ratio and the CP rate asymmetry have both been analyzed within the context of a general 2HDM [210], and it has been pointed out that in large regions of the parameter space the NLO predictions are not reliable, because they suffer from a very large renormalization-scale dependence. For the part of the parameter space not affected by these problems the asymmetry was found to be small.

In this section, we update the calculation for the asymmetry within the framework of the A2HDM, extending the phenomenological analysis and discussing its implications for the model parameters [228]. The predicted range for the CP asymmetry turns out to be within the present experimental limits for all allowed ranges of the A2HDM couplings, although for some particular values of the parameters it is not far from the achieved sensitivity. This makes future high-precision measurements of this quantity very desirable and calls for a better control of theoretical uncertainties.

To that end, the detailed discussion on the branching ratio performed in the previous section is essential, due to its relevance for the rate asymmetry, but also due to its own high sensitivity and its intimate relation to the like-sign dimuon charge asymmetry (LDCA) in  $B^0$ -decays.

### 6.5.1 $\bar{B} \rightarrow X_s \gamma$

The CP rate asymmetry for the process  $b \rightarrow s\gamma$  is defined as

$$a_{CP} = \frac{\text{Br}(\bar{B} \rightarrow X_s \gamma) - \text{Br}(B \rightarrow X_{\bar{s}} \gamma)}{\text{Br}(\bar{B} \rightarrow X_s \gamma) + \text{Br}(B \rightarrow X_{\bar{s}} \gamma)}. \quad (6.31)$$

Being doubly Cabibbo suppressed, it is known to be tiny in the SM, below 1% [229–231], making it a sensitive probe of new-physics effects. The relative scale uncertainty is large, as it is to be expected from a NLO calculation for a CP asymmetry, because it is the

first contributing order. However, it is small in absolute terms. The same is true for the charm-mass dependence. Note that the enhanced power-corrections at order  $\mathcal{O}(\alpha_s \frac{\Lambda}{m_b})$  [222], mentioned above in the discussion of the rate, are not yet included in the calculation for the asymmetry. Being of relative order  $\Lambda/m_b$ , they are likely to increase the uncertainty significantly. However, the experimental uncertainty of the present world average [217],

$$a_{CP}^{\text{exp}}(\bar{B} \rightarrow X_s \gamma) = -0.012 \pm 0.028, \quad (6.32)$$

is much larger than the expected value, so the calculation at NNLO has been considered less interesting up to now.

Within the context of the general 2HDM the analysis has been performed at LO [232, 233] and then at NLO [210], working in the limit  $V_{ub}V_{us}^* = 0$ , which implies by unitarity that  $V_{cb}V_{cs}^* = -V_{tb}V_{ts}^*$ . It was pointed out in [210] that, given the cancellation problems in the branching ratio described before, the prediction was not reliable in part of the parameter space where it exhibited a large scale dependence, but that for parameter choices where the branching ratio was well behaved the predicted  $a_{CP}$  was very small,  $\mathcal{O}(1\%)$ .

We now turn to reanalyze the asymmetry in the context of the A2HDM. In our previous study we have used the SM NNLO calculation of the branching ratio; however, we will not include NNLO information in the predicted asymmetry, for two reasons: First, the necessary calculation does not exist completely, and the interpolation for the charm-mass dependence has been done specifically for the branching ratio, ignoring some imaginary parts which can be relevant for the asymmetry. Second, and more importantly, in our approximation the asymmetry is a pure new-physics effect. Therefore, QCD corrections should enter at the same level for the SM and new-physics amplitudes. Moreover, as the scale dependence at NLO is in general more severe for the A2HDM than for the SM, inclusion of the NNLO SM corrections only would not stabilize the full result.

We confirmed these expectations explicitly by calculating the asymmetry with the NNLO SM contributions to the branching ratio included. The result showed a relatively large shift in the central value, which we attribute to the different charm-mass dependence, and no stabilization of the scale dependence at all. This behaviour is uniform for different values of  $\varsigma_{u,d}$  and  $M_{H^\pm}$ . We conclude that for the inclusion of NNLO corrections important parts are missing, the calculation of which is beyond the scope of this work. This lack of NNLO corrections will make the problems described in the branching-ratio analysis reappear. Nevertheless, we start by analyzing the asymmetry for the same range of parameters considered in our previous study of the branching ratio,  $|\varsigma_u| \in [0, 2]$ ,  $|\varsigma_d| \in [0, 50]$ ,  $\varphi \in [0, 2\pi]$ , and  $M_{H^\pm} \in [80, 500]$  GeV, to examine the strength of this observable by itself.

Figure 6.17 shows the  $\mu_b$  renormalization-scale dependence of the predicted CP asymmetry at NLO, as a function of the phase  $\varphi$ , taking  $M_{H^\pm} = 200$  GeV,  $|\varsigma_u| = 0.1$  and  $|\varsigma_d| = 5$  (left) and 50 (right). The black central curve represents  $a_{CP}$  for  $\mu_b = 2.5$  GeV, while the outer (larger absolute values) and inner (smaller absolute values) lines correspond to  $\mu_b = 2$  and 5 GeV, respectively, using the same range of variation considered in the branching ratio analysis. We observe that the  $\mu_b$  dependence is proportional to  $|a_{CP}|$ ; therefore in the regions where the asymmetry is relevant the theoretical error from the scale dependence

is as well. As noted before, the overall scale dependence is strong, approximately 25% in most of the parameter space. If not noted otherwise, in the following the scale is fixed to  $\mu_b = 2.5$  GeV.

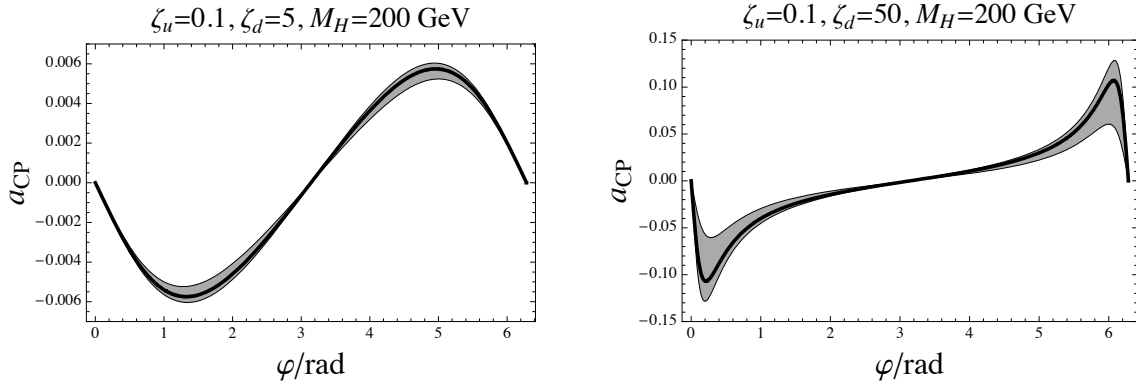


Figure 6.17:  $CP$  asymmetry at  $NLO$ , as function of the relative phase  $\varphi$ , for  $\zeta_u = 0.1$ ,  $\zeta_d = 5$  (left) and 50 (right) and  $M_{H^\pm} = 200$  GeV. The band shows the variation with the scale, taking  $\mu_b = 2.5$  GeV (central black line), 2 GeV (outer line) and 5 GeV (inner line).

The asymmetry is small for most values of the phase  $\varphi$ , apart from values around zero, where for some parameter choices one observes an unphysical enhancement of  $|a_{CP}|$ . This is apparent in Fig. 6.17 (right panel), corresponding to  $\zeta_d = 50$ , which shows a large predicted asymmetry around  $\varphi = \pm 0.2$  rad (modulo  $2\pi$ ), with a very large scale dependence. This enhancement does not correspond to any large CP-odd contribution, but rather to a destructive interference in the decay amplitude leading to a nearly vanishing rate, which is only possible for small imaginary parts. This resonant behaviour can again be easily understood from Eq. (6.30); a zero of the amplitude occurs around  $\zeta_u^* \zeta_d / M_{H^\pm}^2 \sim 4 \times 10^{-5} \text{ GeV}^{-2}$  with  $e^{i\varphi} \sim 1$ . For lower scalar masses the  $|\zeta_u|^2$  term can give a more sizable contribution, modifying this simplified behaviour, but again the amplitude can become small through the cancellation of the SM and new-physics contributions. We illustrate this fact in Fig. 6.18, which shows the parameter region in the  $|\zeta_u||\zeta_d|/M_{H^\pm}^2 - M_{H^\pm}$  plane leading to values of  $a_{CP}$  outside the (95% CL) allowed experimental range, taking  $\varphi = 6.15$  rad and fixing the renormalization scale at  $\mu_b = 2.5$  GeV.

The regions of small amplitudes around values of  $\varphi \sim 0, 2\pi$  are of course very sensitive to the adopted truncation of the perturbative expansion in powers of the strong coupling and introduce a correspondingly large theoretical uncertainty. Their appearance signals the need to incorporate higher-order corrections into the calculation. Fortunately, since the measured branching ratio is definitely non zero (by many standard deviations) and compatible with the SM prediction, these problematic regions of the parameter space, where cancellations occur, are already excluded. Imposing the constraint that the experimental branching ratio should be reproduced, the surviving allowed parameter ranges lead to well-behaved amplitudes and small asymmetries below the present limits.

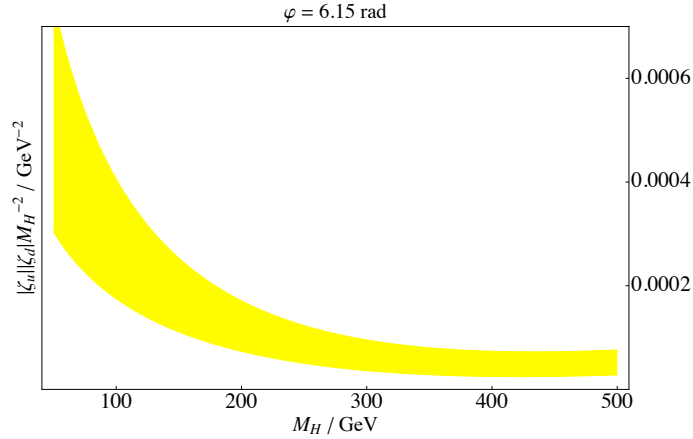


Figure 6.18: Region in the  $|\kappa_u||\kappa_d|/M_{H^\pm}^2 - M_{H^\pm}$  plane leading to values of  $a_{CP}$  outside the (95% CL) allowed experimental range, for fixed phase  $\varphi = 6.15$  rad and scale  $\mu_b = 2.5$  GeV ( $M_{H^\pm}$  in GeV units).

In Fig. 6.19 we plot the predicted maximal value for the CP rate asymmetry, as a function of the Yukawa phase  $\varphi = \arg(\varsigma_u^*\varsigma_d)$ , including the  $\text{Br}(\bar{B} \rightarrow X_s\gamma)$  constraint by showing only points that lie within its 95% CL experimental range. We have scanned the predictions over the parameter ranges  $M_{H^\pm} \in [80, 500]$  GeV,  $|\kappa_u| \in [0, 2]$  and  $|\kappa_d| \in [0, 50]$ , and have treated the error for the branching ratio as explained in [116]. We find as expected that the problematic regions have been excluded, and that the maximal achievable asymmetry is compatible with the present experimental limits at 95% CL, given the scale dependence of the prediction. Sizable asymmetries at the 1-5% level seem possible for  $\varphi \sim \pm 0.7$  rad, but the corresponding theoretical uncertainty is unfortunately quite large, as shown by the large scale-dependence of the theoretical results.

### 6.5.2 $B^0$ - $\bar{B}^0$

The D0 experiment measured [14] a like-sign dimuon charge asymmetry leading to  $A_{sl}^b = -0.00957 \pm 0.00251 \pm 0.00146$ , which differs by over three standard deviations from the SM prediction [234]. The measurement includes contributions from  $B_d^0$  and  $B_s^0$  mesons, corresponding to  $A_{sl}^b = (0.506 \pm 0.043) a_{sl}^d + (0.494 \pm 0.043) a_{sl}^s$ , with ( $q = d, s$ )

$$a_{sl}^q = \text{Im} \left( \frac{\Gamma_{12}^q}{M_{12}^q} \right) = \frac{|\Gamma_{12}^q|}{|M_{12}^q|} \sin \phi_q = \frac{\Delta\Gamma_{B_q^0}}{\Delta M_{B_q^0}} \tan \phi_q, \quad (6.33)$$

where  $M_{12}^q - \frac{i}{2}\Gamma_{12}^q \equiv \langle B_q^0 | \mathcal{H}_{\text{eff}}^{\Delta B=2} | \bar{B}_q^0 \rangle$ . Using the current  $B_d^0$  experimental asymmetry,  $a_{sl}^d = -0.0047 \pm 0.0046$  [155], the measured value of  $\Delta M_{B_s^0}$  and the SM prediction for  $\Delta\Gamma_{B_s^0}$ , the D0 asymmetry implies  $\sin \phi_s = -2.7 \pm 1.4 \pm 1.6$ , showing that the central value of this measurement is incompatible with the assumption of negligible influence of new physics on  $\Gamma_s^{12}$ , while the uncertainties are large enough to allow every value for the mixing

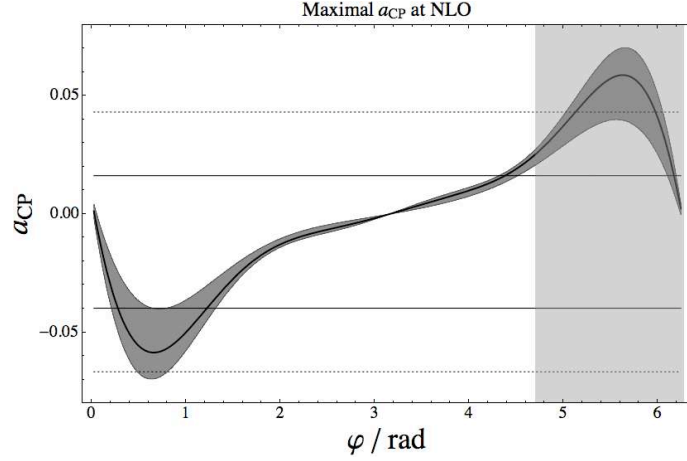


Figure 6.19: Maximal value of  $a_{CP}$  versus the phase  $\varphi$  at NLO, for  $M_{H^\pm} \in [80, 500]$  GeV,  $|\zeta_u| \in [0, 2]$  and  $|\zeta_d| \in [0, 50]$ , taking into account the experimental  $Br(\bar{B} \rightarrow X_s \gamma)$  constraint at 95% CL. The three curves correspond to  $\mu_b = 2$  (outer), 2.5 (center) and 5 GeV (inner). The dotted (continuous) horizontal lines denote the allowed experimental range at 95% CL (68% CL). The vertical shadowed band indicates the region in which an enhancement of the LDCA induced by charged-scalar effects in the direction of the measured value may occur (see section 6.5.2 for further details).

phase at  $2\sigma$ . Using in addition the direct measurement of  $a_{sl}^s$  through  $B_s^0 \rightarrow \mu^+ D_s^- X$  decays by D0 [235],  $a_{sl}^s = -0.0017 \pm 0.0091$ , results in  $\sin \phi_s = -1.7 \pm 1.1 \pm 1.0$ . Hints of a large  $\phi_s$  value have been also obtained previously from  $B_s^0 \rightarrow J/\psi \phi$  decays [236–238], where the extraction of the phase might however be influenced by contributions to the decay amplitude. The SM predicts a very small positive value for  $\phi_s$  and a much larger and negative result for  $\phi_d$ . The theoretical values quoted in [234] are  $\phi_s = 0.24^\circ \pm 0.08^\circ$  and  $\phi_d = -5.2^\circ \pm_{-2.1}^{+1.5}$ .

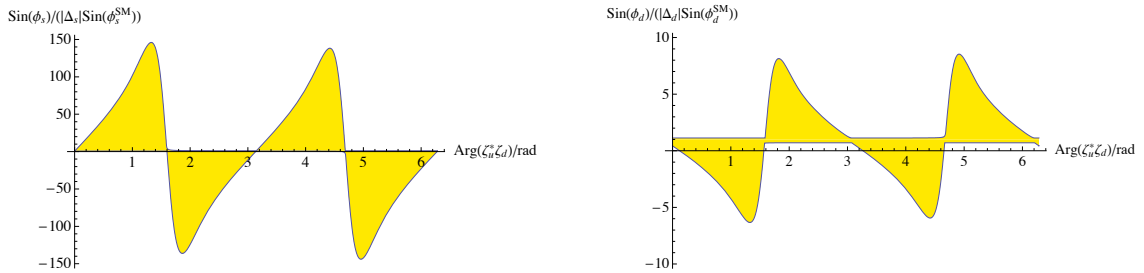


Figure 6.20: Dependence of  $\sin \phi_q / (|\Delta_q| \sin \phi_q^{\text{SM}})$  on  $\varphi \equiv \arg(\zeta_u^* \zeta_d)$ .

Assuming that the charged-scalar contributions are the only relevant new-physics effects, we can analyze the possibility to accommodate a large  $\phi_s$  phase within the A2HDM.

In figure 6.20 we plot the allowed range for  $\sin \phi_q / (|\Delta_q| \sin \phi_q^{\text{SM}})$ , where  $\Delta_q \equiv M_{12}^q / M_{12}^{q,\text{SM}}$ , as a function of the relative Yukawa phase  $\varphi \equiv \arg(\zeta_u^* \zeta_d)$ . The other scalar parameters have been varied in the ranges  $|\zeta_d| \in [0, 50]$ ,  $M_{H^\pm} \in [80, 500]$  GeV, and  $|\zeta_u|$  according to the allowed range from  $\epsilon_K, Z \rightarrow \bar{b}b$ , which includes only values for  $(|\zeta_u|, M_H)$  which lead to acceptable values for  $\Delta m_{s,d}$ . While it is indeed possible to obtain a large value of  $\phi_s$ , the predicted equality of  $\Delta_s$  and  $\Delta_d$  implies a strong anti-correlation of  $\sin \phi_d / (|\Delta_d| \sin \phi_d^{\text{SM}})$  and  $\sin \phi_s / (|\Delta_s| \sin \phi_s^{\text{SM}})$ , due to the different sign (and size) of  $\phi_d^{\text{SM}}$  and  $\phi_s^{\text{SM}}$ . This leads to a prediction for the sign of  $a_{sl}^d$ , which could be verified/falsified, once higher experimental precision is achieved. As can be seen, the preferred negative sign for the  $a_{sl}^s$  asymmetry implies  $\arg(\zeta_u^* \zeta_d) \in [\pi/2, \pi], [3\pi/2, 2\pi]$ , and for possible large values the Yukawa phase should not be close to  $0, \pi$  (obviously).

Figure 6.21 shows the dependence of  $\sin \phi_s / (|\Delta_s| \sin \phi_s^{\text{SM}})$  with  $|\zeta_d|$  (left) and  $M_{H^\pm}$  (right), varying the remaining parameters within their allowed ranges. If large values for the  $a_{sl}^s$  asymmetry are confirmed (within the physical range  $|\sin \phi_s| \leq 1$ ), this would point towards large values of  $|\zeta_d|$  and small charged Higgs masses.

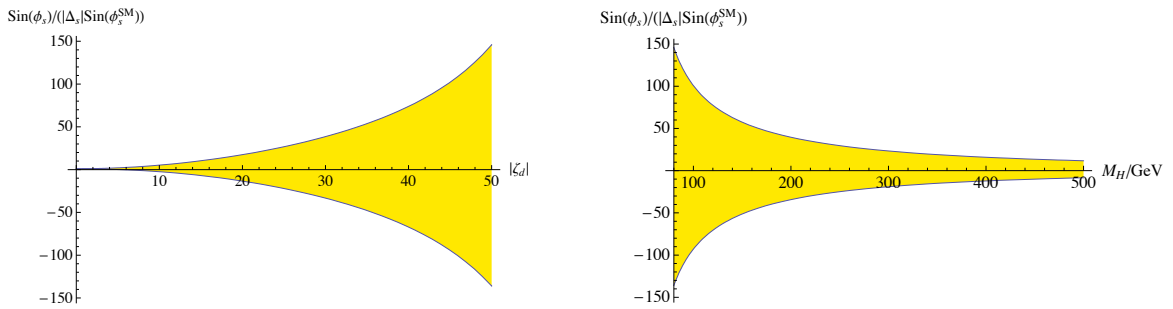


Figure 6.21: *Dependence of  $\sin \phi_s / (|\Delta_s| \sin \phi_s^{\text{SM}})$  on  $|\zeta_d|$  (left) and  $M_{H^\pm}$  (right).*

We show in figure 6.22 the plots from figure 6.20 again, restricting the product  $|\zeta_u \zeta_d^*| \leq 20$ . The corresponding maximal asymmetry is correspondingly smaller, but still relative factors up to  $\sim 60$  are allowed for  $B_s$  with respect to the SM.

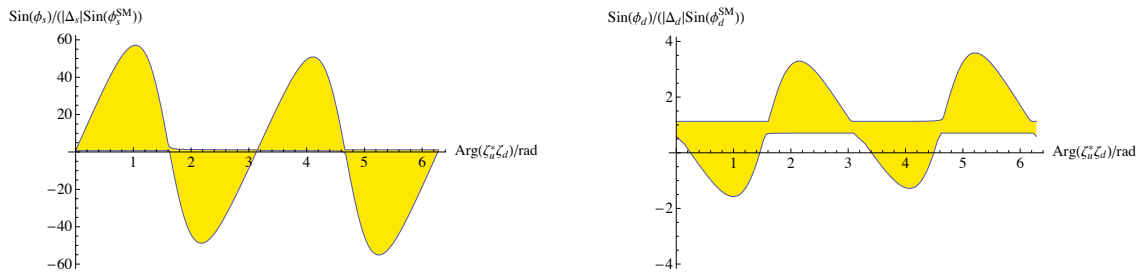


Figure 6.22: *Dependence of  $\sin \phi_q / (|\Delta_q| \sin \phi_q^{\text{SM}})$  on  $\varphi \equiv \arg(\zeta_u^* \zeta_d)$ , constraining  $|\zeta_u \zeta_d^*| \leq 20$ .*

However, taking all the correlations into account by using a parametrization  $|\zeta_u^* \zeta_d|_{\max}(\varphi, M_{H^\pm})$  for the constraints shown in Fig. 6.16, the potential influence of charged-scalar effects on this observable is reduced by roughly a factor of 10 compared to the result without correlations. While an enhancement by a factor of  $\sim 5$  is still possible, larger effects from charged-scalar contributions are excluded. This large impact can be understood as due to

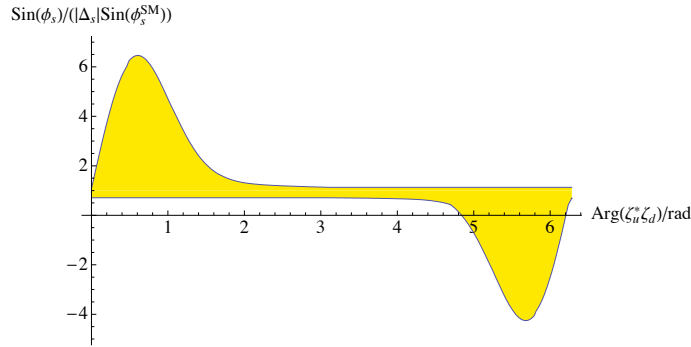


Figure 6.23: Possible influence of charged-scalar-effects on the LDCA, taking the constraint from  $\text{Br}(b \rightarrow s\gamma)$  shown in Figs 6.16 into account. The figure plots the allowed range for the relative factor with respect to the SM result as a function of the phase  $\varphi$ .

a combination of the two correlations shown above: as discussed in [116], sizable values of the LDCA require relatively low charged-scalar masses, a sizable phase and large values for the product  $|\zeta_u^* \zeta_d|$ . The correlations in the constraint from  $b \rightarrow s\gamma$  imply that the latter can only be achieved for relatively high masses and small values of the phase. Therefore the full suppression shows up only in the correlated analysis performed here. A possible enhancement from additional neutral scalars remains untouched by this. The present data suggest a preferred negative sign for the  $B_s^0$  semileptonic asymmetry  $a_{sl}^s$ , which for charged-scalar effects to be in the right direction requires  $\arg(\zeta_u^* \zeta_d) \in [3\pi/2, 2\pi]$ . Due to the different structure of its amplitude, the  $b \rightarrow s\gamma$  rate asymmetry could provide complementary information on the Yukawa phase.

## 6.6 Discussion

Imposing natural flavour conservation through discrete  $\mathcal{Z}_2$  symmetries, one finds that the CKM phase is the only source of CP violation in the resulting 2HDMs. During the last thirty years, it has been common lore to assume that this is a more general fact, i.e. that the absence of tree-level FCNCs implies the absence of additional phases beyond the CKM one. The A2HDM provides an explicit counter-example, where FCNC couplings are absent at the Lagrangian level, while additional unconstrained complex phases generate new sources of CP violation. Since all Yukawa couplings are proportional to fermion masses, the A2HDM gives rise to an interesting hierarchy of FCNC effects, avoiding the stringent experimental constraints for light-quark systems and predicting at the same time

interesting signals in heavy-quark transitions. The flavour-blind phases present in the model open a very interesting phenomenology which is worth to be investigated. The built-in flavour symmetries protect very efficiently the A2HDM from unwanted FCNC effects generated through quantum corrections. At the one-loop level the only allowed FCNC local structures are the two operators in (5.6), which could have very interesting (and computable) implications for  $B_s^0$  mixing.

Besides the fermion masses and mixings, the charged-scalar couplings of the A2HDM are fully characterized by three complex parameters  $\varsigma_f$ . In the previous sections, we have analyzed the impact of the  $H^\pm$  contribution to different observables, where it is expected to be the dominant new-physics effect. Using conservatively estimated hadronic parameters and up-to-date data, we have inferred the present constraints on the new-physics parameters involved in these processes.

Leptonic tau decays provide a direct bound on the leptonic Yukawa coupling:  $|\varsigma_l|/M_{H^\pm} \leq 0.40 \text{ GeV}^{-1}$  (95% CL). From semileptonic processes constraints on the products  $\varsigma_l^* \varsigma_u/M_{H^\pm}^2$  and  $\varsigma_l^* \varsigma_d/M_{H^\pm}^2$  are derived. The leptonic decays of heavy-light mesons allow us to disentangle the effects from  $\varsigma_u$  and  $\varsigma_d$ . Thus, from  $B \rightarrow \tau\nu$  we derive an annular constraint on the complex plane  $\varsigma_l^* \varsigma_d/M_{H^\pm}^2$  (figure 6.1a), implying the absolute bound  $|\varsigma_l^* \varsigma_d/M_{H^\pm}^2| < 0.108 \text{ GeV}^{-2}$  (95% CL). For real Yukawa couplings there is a two-fold sign ambiguity generating two possible solutions, the expected one around  $\Delta_{ij} = 0$  (the SM amplitude dominates) and its mirror around  $\Delta_{ij} = 2$ , corresponding to a new-physics contribution twice as large as the SM one and of opposite sign. The real solutions are  $\varsigma_l^* \varsigma_d/M_{H^\pm}^2 \in [-0.036, 0.008] \text{ GeV}^{-2}$  or  $[0.065, 0.108] \text{ GeV}^{-2}$ .

Similar, but slightly weaker, constraints on  $\varsigma_l^* \varsigma_u/M_{H^\pm}^2$  are obtained from the decays  $D \rightarrow \mu\nu$  (figure 6.1b) and  $D_s \rightarrow (\tau, \mu)\nu$  (figure 6.2); in the last case the bounds from  $B \rightarrow \tau\nu$  are used to get rid of the small  $\varsigma_d$  contamination proportional to the strange quark mass. The resulting absolute bound  $|\varsigma_l^* \varsigma_u/M_{H^\pm}^2| < 0.6 \text{ GeV}^{-2}$  (95% CL) is rather weak, but the upper limit corresponds to a new-physics contribution twice as large as the SM one, a very unlikely situation. The annular form of these constraints results in much stronger limits, once this possibility is excluded by other processes. For real Yukawa couplings, one finds  $\varsigma_l^* \varsigma_u/M_{H^\pm}^2 \in [-0.005, 0.037] \text{ GeV}^{-2}$  or  $[0.511, 0.535] \text{ GeV}^{-2}$ , at 95% CL.

Owing to the quark-mass suppression, the absolute constraints obtained from leptonic decays of light mesons (figure 6.4) are obviously much weaker. However, the excellent experimental precision achieved in  $\pi$  and  $K$  decays implies a narrow allowed annular region. For real Yukawa couplings this translates into quite stringent bounds:  $\varsigma_l^* \varsigma_d/M_{H^\pm}^2 \in [-0.07, 0.07] \text{ GeV}^{-2}$  or  $[8.14, 8.28] \text{ GeV}^{-2}$  (95% CL). The uncertainties are dominated by the present theoretical knowledge of the ratio  $f_K/f_\pi$ .

Independent information is obtained from the semileptonic decays of pseudoscalar mesons, through the scalar form-factor contribution. One needs, however, to disentangle the dominant vector form-factor amplitude, which does not contain any charged-scalar effect and is correlated with the usual measurement of the corresponding CKM mixing factor. The present constraints from the ratio  $\text{Br}(B \rightarrow D\tau\nu_\tau)/\text{Br}(B \rightarrow D\ell\nu_\ell)$ , shown in figures 6.5 and 6.6, are not very strong by themselves, but allow in combination with

other processes the exclusion of the second real solutions in the  $\varsigma_{u,d}\varsigma_l^*/M_H^2$  planes. A future measurement of the differential distribution in  $B \rightarrow D\tau\nu_\tau$  would obviously increase the sensitivity to the scalar contribution. In spite of the strange-mass suppression, the much higher experimental accuracy achieved in the analysis of  $K \rightarrow \pi l\nu$  decays allows to derive the bound  $\text{Re}(\varsigma_l^*\varsigma_d/M_{H^\pm}^2) \in [-0.16, 0.30]$  GeV $^{-2}$  (95% CL). This already excludes the second real solution (a scalar amplitude larger than the SM one) obtained from  $K_{\mu 2}/\pi_{\mu 2}$ .

Combining the information from all leptonic and semileptonic decays analyzed, one gets the constraints shown in figure 6.8.

The flavour-conserving decay  $Z \rightarrow b\bar{b}$  provides a very stringent constraint on  $|\varsigma_u|$ . Since  $V_{tb} \approx 1$ , the one-loop contributions involving virtual top quarks completely dominate both the SM ( $W^\pm$ ) and the new-physics ( $H^\pm$ ) radiative corrections. In contrast to leptonic and semileptonic processes, where the charged-scalar effects are necessarily proportional to  $\varsigma_l$ , the  $Z \rightarrow b\bar{b}$  amplitude gives direct access to  $\varsigma_u$  and  $\varsigma_d$ . Owing to the relative factor  $m_b/m_t$  which suppresses the  $\varsigma_d$  contribution, one gets finally the constraints on  $|\varsigma_u|$  shown in figure 6.9 (assuming  $|\varsigma_d| \leq 50$ ). At 95% CL, we obtain  $|\varsigma_u| < 0.75$  (1.6), for  $M_{H^\pm} = 80$  (500) GeV. The upper bound increases linearly with  $M_{H^\pm}$ , implying  $|\varsigma_u|/M_{H^\pm} < 0.0020$  GeV $^{-1} + \frac{0.59}{M_{H^\pm}} < 0.010$  GeV $^{-1}$ , where we have used the LEP lower bound on the charged-scalar mass  $M_{H^\pm} > 78.6$  GeV (95% CL) [41, 74]. Together with the tau-decay constraint on  $|\varsigma_l|/M_{H^\pm}$ , this gives the limit  $|\varsigma_u\varsigma_l^*/M_{H^\pm}^2 < 0.004$  GeV $^{-2}$ , which is much stronger than the information extracted from the global fit to leptonic and semileptonic decays.

Quite similar information can be extracted from  $B^0$  mixing, which is also dominated by one-loop contributions involving virtual top quarks. The smallness of the  $m_s/M_W$  ratio implies that SU(3)-breaking corrections are negligible; therefore, the charged-scalar contributions cancel in the ratio  $\Delta m_{B_s^0}/\Delta m_{B_d^0}$ , which can be used in the CKM fit. Only two  $\Delta B = 2$  four-quark operators are numerically relevant; the one generating the leading SM amplitude gets new-physics contributions proportional to  $|\varsigma_u|^2$ , while the other operator generates subleading corrections proportional to  $(\varsigma_u^*\varsigma_d)^{1,2}m_b^2/M_W^2$ . Scanning the parameter ranges  $|\varsigma_d| < 50$  and  $\varphi \in [0, 2\pi]$ , where  $\varphi$  is the relative phase between  $\varsigma_u$  and  $\varsigma_d$ , the measured  $B_s^0$  mixing amplitude implies the constraints shown in figure 6.10, in the plane  $M_{H^\pm} - |\varsigma_u|$ . At 95% CL, one gets  $|\varsigma_u| < 0.00301 M_{H^\pm} - 0.12 + 130/M_{H^\pm}$ , for  $M_{H^\pm} \in [80, 500]$ , in GeV units. The charged-scalar contribution could accommodate a  $B_s^0$  mixing phase, without spoiling the agreement in the  $B_d$  system, although not as large as the present D0 central value, which is at odds with the rate being unaffected by new physics.

The radiative decay  $\bar{B} \rightarrow X_s\gamma$  provides another important source of information. There are two different charged-scalar contributions, proportional again to  $|\varsigma_u|^2$  and  $\varsigma_u^*\varsigma_d$ , but in this case the two have similar sizes. Their combined effect can be quite different depending on the value of the relative phase  $\varphi$ . This results in rather weak limits because a destructive interference can be adjusted through this phase. The resulting constraints on  $|\varsigma_u|$  and  $|\varsigma_d|$  are shown in figure 6.12, varying the charged-scalar mass in the range  $M_{H^\pm} \in [80, 500]$  GeV. Scanning the phase  $\varphi$  in the whole range from 0 to  $2\pi$ , and imposing  $|\varsigma_u| < 3$ , one finds roughly  $|\varsigma_d||\varsigma_u| < 20$  (95% CL). Much stronger bounds are obtained at fixed values of the

relative phase. Assuming real values of  $\varsigma_u$  and  $\varsigma_d$  (i.e.  $\varphi = 0$  or  $\pi$ ), one finds that couplings of different sign are excluded, except at very small values, while a broad region of large equal-sign couplings is allowed, reflecting again the possibility of a destructive interference. Figures 6.13, 6.14 and 6.15 show the sensitivity of the  $\bar{B} \rightarrow X_s \gamma$  constraints to the different unknown parameters:  $M_{H^\pm}$ ,  $|\varsigma_u|$ ,  $|\varsigma_d|$  and  $\varphi$ . The strong constraints on the model parameters e.g. in type II models are not visible in the A2HDM, due to the presence of additional parameters. They are replaced by correspondingly strong correlations, which we analyzed in some detail above, and which play an important role when combining other constraints with this observable. An example for their influence is given by the LDCA in  $B^0$ -decays, whose most recent measurement was given by the D0 experiment. The con-

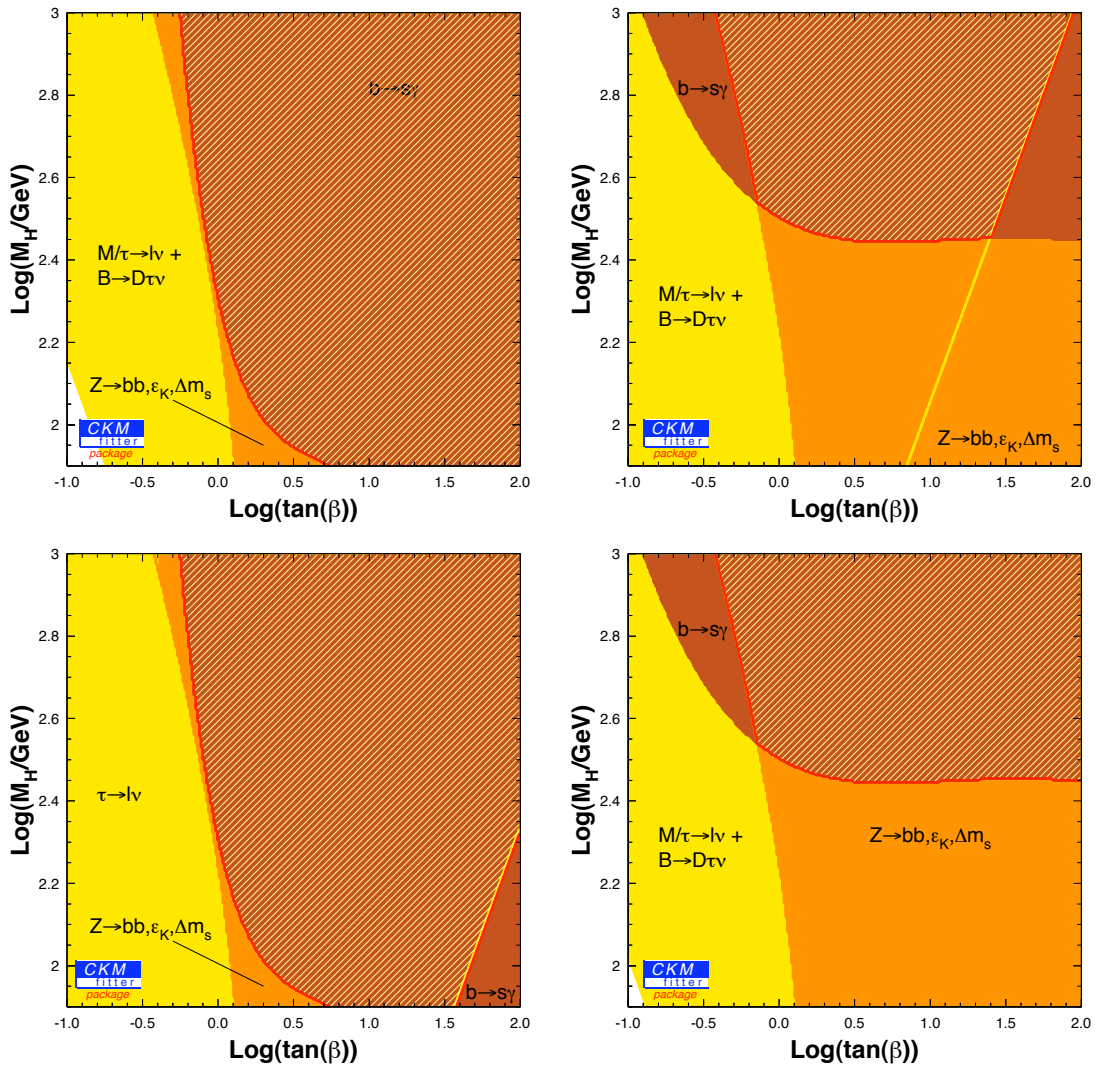


Figure 6.24: Constraints on  $M_{H^\pm}$  (in GeV) versus  $\tan\beta$  (95% CL), in the 2HDM models of types I (upper-left), II (upper-right), X (lower-left) and Y (lower-right).

straints discussed so far apply to the general A2HDM framework, with three arbitrary complex parameters  $\zeta_f$ . The limits become of course much stronger in particular models where these parameters are correlated. Figures 6.24 show the combined constraints on the  $\tan\beta$ - $M_{H^\pm}$  plane for the different  $\mathcal{Z}_2$  models. The bounds from  $Z \rightarrow b\bar{b}$ ,  $\Delta m_{B_s}$  and  $\bar{B} \rightarrow X_s\gamma$  are obviously identical for the models of type I and X and also for type II and Y. In the type I/X case,  $\zeta_u^2 = \zeta_d^2 = \zeta_u\zeta_d = \cot^2\beta$  and the scalar amplitudes grow for decreasing values of  $\tan\beta$ . For type II/Y, this behaviour is only observed in the  $\zeta_u^2$  term, while  $\zeta_d^2 = \tan^2\beta$  and  $\zeta_u\zeta_d = -1$ ; the decay  $\bar{B} \rightarrow X_s\gamma$  provides then a very strong lower bound on the scalar mass,  $M_{H^\pm} > 277$  GeV (95% CL), due to the constructive interference of the two contributing amplitudes. The  $\zeta_l$  coupling gives rise to different constraints from leptonic and semileptonic decays in each of the four models. Our results agree with the qualitative behaviour found in previous analyses [73, 130–133, 216, 239–244], the small differences originating from the slightly different inputs adopted.

Another obvious question to address is the phenomenologically allowed size for the new phases, which should be constrained by the measured CP-violating observables in flavour physics. Of these, the  $b \rightarrow s\gamma$  asymmetry is known to have both a very small SM contribution and a high sensitivity to new physics. Unfortunately, although the  $b \rightarrow s\gamma$  rate is known at NNLO in the SM, the 2HDM contributions have been only computed at NLO. Since a non-zero rate asymmetry requires absorptive contributions leading to a strong-phase difference, it first appears at NLO. Therefore, the theoretical uncertainties are much larger than for the branching ratio. On the other hand, some of the parametric uncertainties cancel in the asymmetry.

We have analyzed the predicted  $b \rightarrow s\gamma$  rate asymmetry within the A2HDM, scanning the parameter space of the model over the full domain allowed by known constraints from other processes. We have shown that, while  $a_{CP}$  could be enhanced for some particular values of the parameters, it remains compatible with its present measurement when considering parameters leading to acceptable values for the branching ratio. Sizable CP asymmetries at the 1-5% level, close to the present experimental bound, seem possible for Yukawa phases around  $\arg(\zeta_u^*\zeta_d) \sim \pm 0.7$  rad, making a future measurement of this quantity very interesting. Such a measurement would be possible at a Super- $B$  factory, where precisions better than 1% could be achieved [245, 246]. However, the presently large theoretical uncertainty from scale and mass dependence makes necessary a complete NNLO calculation for the SM and the A2HDM contributions to fully exploit such a measurement. At the 1% level, one also needs to analyze the small corrections induced by  $|V_{ub}V_{us}^*| \neq 0$ , which have been neglected up to now. An exception is given by potential experimental information on the quadrant of the new-physics weak phase  $\varphi$ : once a measurement is available which determines the sign of the asymmetry unambiguously, two quadrants are excluded.

The A2HDM is not the most general version of a 2HDM without tree-level FCNCs. To avoid the unwanted FCNCs one just needs diagonal Yukawa matrices  $Y_f$  in the fermion mass-eigenstate basis, i.e.  $Y_d = \text{diag}(y_d, y_s, y_b)$ ,  $Y_u = \text{diag}(y_u, y_c, y_t)$  and  $Y_l = \text{diag}(y_e, y_\mu, y_\tau)$ ,

with arbitrary parameters  $y_i$ . This more general scenario can be formally described by the Lagrangian (5.3) with the substitution  $\varsigma_f M_f \rightarrow Y_f$ . One could still use nine dimensionless parameters  $\varsigma_f \equiv y_f/m_f$ , one for each charged fermion [247], but in this case this is just a redefinition of the Yukawa couplings  $y_f$  because a priori nothing relates them to the fermion masses [248]. The hierarchy of couplings characteristic of the A2HDM ansatz is lost and one cannot longer justify that the leading charged-scalar effects originate in the heavier fermion couplings (it becomes an assumption). With this caveat in mind, our results can still be applied in this case, but most correlations among different processes disappear because the associated constraints correspond now to different  $\varsigma_f$  parameters. For instance, the constraint in (6.4) refers to  $\varsigma_\mu$  and figures 6.1 to  $\varsigma_\tau^* \varsigma_b$  (left) and  $\varsigma_\mu^* \varsigma_c$  (right).

The A2HDM provides a general setting to discuss the phenomenology of 2HDMs, satisfying in a natural way the requirement of very suppressed FCNC effects. The alignment conditions imply Yukawa couplings proportional to the corresponding fermion masses, which is supported by the data (bounds of order 1 for the  $\varsigma_f$  parameters). While including as limiting cases all  $\mathcal{Z}_2$  models, the A2HDM incorporates possible new sources of CP violation through the  $\varsigma_f$  phases. The additional freedom introduced by these phases makes easier to avoid some low-energy constraints, resulting in weaker limits than in the usual scenarios with discrete  $\mathcal{Z}_2$  symmetries. A detailed analysis of CP-violating observables is clearly needed to investigate the allowed ranges for these phases and their potential phenomenological relevance.

At the moment, the data does not show any clear deviation from the SM. Therefore, we have derived upper limits on the Yukawa parameters. Nevertheless, we have already pointed out that the A2HDM could account for a sizeable  $B_s^0$  mixing phase, as suggested by the present  $B_s \rightarrow J/\psi\phi$  and like-sign dimuon data. Our bounds could be made stronger, adopting more aggressive estimates for the hadronic parameters entering the analysis, but we have preferred to be on the conservative side and infer solid limits for later use. Improvements are to be expected on one hand from better theoretical determinations of the hadronic inputs, and on the other hand from more accurate measurements at NA62 (kaons), LHCb ( $\Delta m_{d,s}, B_s \rightarrow J/\psi\phi$ ), a future Super-B factory ( $\tau, b \rightarrow s\gamma, \Delta m_d, B \rightarrow \ell\nu, B \rightarrow D\ell\nu$ ), or a linear collider with Giga-Z option ( $R_b$ ). The agreement of the different bounds in the vicinity of zero is trivial, when the SM agrees with the data. If signals for new-physics are found at LHC, the analysis presented here will be capable of quantifying the agreement (or disagreement) of the data with the A2HDM, and with the different implementations of the 2HDM based on  $\mathcal{Z}_2$  symmetries, in one step.



# Chapter 7

## The two-Higgs-doublet model in the presence of an extra $U(1)$ gauge boson

### 7.1 Introduction

The Standard Model of Particle Physics (SM) (for reviews see e.g. [1, 249]) has been extremely successful in describing all low energy phenomena, being in excellent agreement with a vast amount of experimental data. The only missing part of the SM today is the Higgs boson that gives masses to fermions and to  $W^\pm$  and  $Z$  bosons. The Stueckelberg mechanism [250] gives mass to abelian vector bosons without breaking gauge invariance on the Lagrangian, and thus provides an alternative to the Higgs mechanism [251–255] to achieve gauge symmetry breaking without spoiling renormalizability. A Stueckelberg extension of the SM was studied in [256, 257] (see also [258] for a generalization with a kinetic mixing), where the neutral electroweak gauge bosons acquire a mass via both the Higgs and the Stueckelberg mechanism.

Most of the well motivated extensions of the SM, which have been developed to address its open issues, involve an extra  $U(1)$  in the gauge group. A new heavy gauge boson,  $Z'$ , is predicted which would have profound implications for particle physics and cosmology. Such gauge bosons occur naturally in  $SO(10)$  grand unified models, extra dimensional models with a hidden sector brane, and string theoretic models with intersecting branes. For a nice recent review see e.g. [259]. In general, in models with an additional abelian factor in the gauge group the fermions are charged under the extra  $U(1)$ , and furthermore there is a mixing between the SM boson  $Z$  and the new gauge boson  $Z'$ . A  $Z'$  boson that mixes with the SM  $Z$  boson distorts its properties, such as couplings to fermions and mass relative to electroweak inputs. One thus has to worry about the cancellation of all anomalies, and remain in agreement with the LEP and SLC data [260].

Another famous minimal extension of the SM consists in the addition of one scalar doublet to the theory [16], as it is discussed in this thesis. We have seen already the rich phenomenology that generates, being able to introduce new dynamical possibilities, like different sources of CP violation or dark matter candidates, helps to solve some of

the SM problems. In the most general version of the two-Higgs-doublet model (2HDM), the fermionic couplings of the neutral scalars are not diagonal in flavour, which generates dangerous flavour-changing neutral current (FCNC) phenomena. Since these are tightly constrained by the experimental data, it is necessary to implement ad-hoc dynamical restrictions to guarantee their absence at the required level. For that aim, several versions of the 2HDM based in different ideas have been developed (see Chapter 3). In this chapter we present another framework for the 2HDM with flavour conservation in the neutral sector, without any discrete symmetry or flavour symmetry, the presence of an extra  $U(1)$  gauge symmetry plays a crucial role [261]. The only possible 2HDM in this context has not FCNC terms and the scalar potential results CP invariant.

Many attempts have been made in order to embed the SM in open string theory, with some success [262–271]. They consider the SM particles as open string states attached on different stacks of D-branes.  $N$  coincident D-branes typically generate a unitary group  $U(N) \sim SU(N) \times U(1)$ . Therefore, every stack of branes supplies the model with an extra abelian factor in the gauge group. Such  $U(1)$  fields have generically four-dimensional anomalies [272, 273]. These anomalies are cancelled via the Green-Schwarz mechanism [274–277] where a scalar axionic field is responsible for the anomaly cancellation. This mechanism gives a mass to the anomalous  $U(1)$  fields and breaks the associated gauge symmetry. If the string scale is around a few TeV, observation of such anomalous  $U(1)$  gauge bosons becomes a realistic possibility [278–280]. The structure of the Minimal Low Scale Orientifold Model has been presented in detail in [281].

This class of models is characterized by i) the existence of two Higgs doublets necessary to give masses to all fermions, and ii) the massive gauge bosons acquire their mass from two sources, namely the usual Higgs mechanism, as well as the stringy mechanism related to the generalized Green-Schwarz mechanism, which is very similar to the Stueckelberg mechanism. In the light of these developments, it becomes clear that it is natural to study the 2HDM with additional  $U(1)$ s and the Stueckelberg mechanism together with the Higgs mechanism. In the present work we wish to study the phenomenology of a simple four-dimensional, non-GUT, non-supersymmetric model with an additional Higgs doublet, and just one extra  $U(1)$  factor in the gauge group for simplicity. In a similar spirit, albeit in a different set-up, possible signatures at colliders of new invisible physics and Stueckelberg axions have been analyzed in [282–286].

Our work is summarized as follows. In the next section we present the model, in section 3 we discuss the physics of the heavy gauge boson, and finally we conclude in section 4.

## 7.2 The model

Here we shall present the ingredients of the model, the electroweak symmetry breaking, and the mass spectrum at tree level, while the relevant interaction vertices will be given in the next section.

The gauge group of the model is the SM gauge group times an extra abelian factor  $U(1)_X$ , with a coupling constant  $g_X$  and a gauge boson  $C_\mu$  associated with it. We have

three generations of quarks and leptons with the usual quantum numbers under the SM gauge group, and they are assumed to be neutral under the extra  $U(1)$ . This is a simple choice that ensures that there are no anomalies in the model. We consider the presence of two Higgs doublets,  $H_1$  and  $H_2$ , with the same quantum numbers under the SM gauge group, the only difference being is that  $H_1$  is assumed to be neutral under  $U(1)_X$ , while  $H_2$  is charged under the additional abelian factor with charge  $Y_X = \pm 1$ <sup>1</sup>. As a consequence no Yukawa terms including  $H_2$  are allowed by the symmetry, and therefore the FCNC problem is avoided. The gauge interactions are thus completely specified, and the Yukawa couplings are the same as in the SM. The most general Higgs potential which is renormalizable and compatible with the symmetries in this framework is the following:

$$V = \mu_1^2 H_1^\dagger H_1 + \mu_2^2 H_2^\dagger H_2 + \frac{1}{2} \lambda_1 (H_1^\dagger H_1)^2 + \frac{1}{2} \lambda_2 (H_2^\dagger H_2)^2 + \lambda_3 (H_1^\dagger H_1) (H_2^\dagger H_2) + \lambda_4 (H_1^\dagger H_2) (H_2^\dagger H_1), \quad (7.1)$$

where  $\mu_{1,2}$  and  $\lambda_{1-4}$  are real parameters. This corresponds to an *inert* approach, with the potential similar to the one generated by imposing a  $\mathcal{Z}_2$  discrete symmetry in the *Higgs basis* of a general two-Higgs-doublet model with the SM gauge group [42–45], but in this case, resulting from a gauge symmetry which additionally forbids the  $\lambda_5$  term. From the three possible solutions given by the minimization conditions of the potential [31], we choose for analogy the one where the second Higgs doublet vacuum expectation value (VEV) is zero,  $\langle 0|H_2|0 \rangle = 0$ , and only the first Higgs doublet,  $H_1$ , acquires a VEV,  $v$ . As in the  $\mathcal{Z}_2$ -inert model, the nonexistence of a VEV for  $H_2$  ensures the absence of mixing between the components of  $H_1$  and those of  $H_2$ . Hence,  $H_1$  closely corresponds to the ordinary SM Higgs doublet, and the fields belonging to  $H_2$  are inert in the sense that they do not couple directly to fermions, but they have gauge interactions and self-interactions.

Finally, the Stueckelberg contribution is [256]

$$\mathcal{L}_{\text{St}} = -\frac{1}{4} C_{\mu\nu} C^{\mu\nu} - \frac{1}{2} (\partial_\mu \sigma + M_1 C_\mu + M_2 B_\mu)^2, \quad (7.2)$$

where  $C_\mu$  is the gauge boson associated with the  $U(1)_X$ ,  $C_{\mu\nu}$  is the corresponding field strength,  $\sigma$  is the scalar axionic field which is assumed to couple both to  $B_\mu$  and  $C_\mu$ , and  $M_1$  and  $M_2$  are two mass scales which serve as two extra parameters of the model.

After giving masses to the gauge bosons, the doublets are of the form [44]

$$H_1 = \begin{bmatrix} 0 \\ \frac{1}{\sqrt{2}}(v+h) \end{bmatrix}, \quad H_2 = \begin{bmatrix} H^+ \\ \frac{1}{\sqrt{2}}(H+iA) \end{bmatrix}, \quad (7.3)$$

where  $H_1$  has one physical degree of freedom left: the neutral scalar field  $h$ . Since  $h$  closely resembles the Higgs particle of the SM it will be called here the SM Higgs boson. In

<sup>1</sup>In intersecting brane models one naturally obtains two Higgs doublets, with three possibilities arising regarding their charges under the  $U(1)$  factors: i) both are neutral, ii) one is neutral and one charged, and iii) both are charged with opposite charges [262, 271, 278]. The first possibility is not interesting, while in the third one no Yukawa couplings are allowed.

addition,  $H_2$  includes the neutral  $CP$ -even  $H$ , the neutral  $CP$ -odd  $A$  (with defined  $CP$  parities because the parameters of the scalar potential are real), and two charged  $H^\pm$  inert scalars. The masses of the particles are (at tree level) given by

$$\begin{aligned} M_h^2 &= \lambda_1 v^2, \\ M_{H^\pm}^2 &= \mu_2^2 + \frac{1}{2} \lambda_3 v^2, \\ M_H^2 &= \mu_2^2 + \frac{1}{2} (\lambda_3 + \lambda_4) v^2, \\ M_A^2 &= \mu_2^2 + \frac{1}{2} (\lambda_3 + \lambda_4) v^2. \end{aligned} \quad (7.4)$$

Notice that in our model the neutral inert Higgs bosons are exactly degenerate in mass, and this should be true also at loop level, since  $A$  and  $H$  couple to the same fields with the same coupling constants. If  $H$  and  $A$  are exactly degenerate in mass, there is not a good dark matter candidate because of direct detection limits [45]. In direct detection searches the dark matter particle scatters off a nucleus of the material in the detector. What is seen is the recoil of the nucleus, while the dark matter particle is not observed. Analysing the data an upper bound on the nucleon/dark matter particle cross section for a given dark matter particle mass is obtained [287]. If the masses of  $H, A$  are different, the lightest of the two Higgs bosons, say  $H$ , is supposed to play the role of dark matter in the universe, and the scattering off a nucleus takes place via an exchange of the SM Higgs boson (see the first Feynman diagram in the Figure 7 below). If, however, the two inert Higgs bosons are degenerate in mass, the scattering of  $H$  off a nucleus can take place also via a  $Z$  boson exchange (see the second Feynman diagram in the Figure 7 below). In this case there is an unsuppressed coupling with the  $Z$  boson, and the elastic scattering  $Hq \rightarrow Aq$  through a  $Z$  boson exchange has a cross section orders of magnitude larger than the allowed ones [45]. The components of the inert scalar doublet interact with  $h$  and

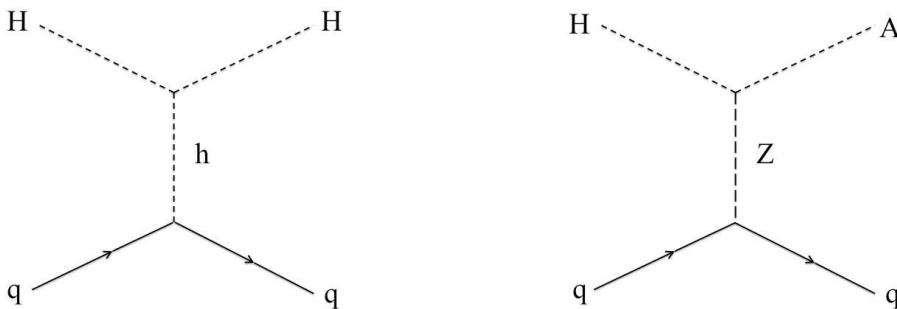


Figure 7.1: Feynman diagrams corresponding to the elastic scatterings  $H q \rightarrow H q$  and  $H q \rightarrow A q$  respectively.

among themselves as follows:

$$\begin{aligned}
V_{int} &= \frac{1}{2}\lambda_2 \left[ H^+ H^- + \frac{1}{2}H^2 + \frac{1}{2}A^2 \right]^2 \\
&+ \lambda_3 \left( vh + \frac{1}{2}h^2 \right) \left[ H^+ H^- + \frac{1}{2}H^2 + \frac{1}{2}A^2 \right] \\
&+ \frac{1}{2}\lambda_4 \left( vh + \frac{1}{2}h^2 \right) H^2 + \frac{1}{2}\lambda_4 \left( vh + \frac{1}{2}h^2 \right) A^2 .
\end{aligned} \tag{7.5}$$

With the Stueckelberg extension, and after the standard spontaneous electroweak symmetry breaking the mass terms in the neutral vector boson sector take the form  $-\frac{1}{2}V_{a\mu}M_{ab}^2V_b^\mu$ , using  $(V_\mu^T)_a = (C_\mu, B_\mu, W_\mu^3)_a$ , with mass matrix [256]

$$M_{ab}^2 = \begin{bmatrix} M_1^2 & M_1 M_2 & 0 \\ M_1 M_2 & M_2^2 + \frac{1}{4}g_Y^2 v^2 & -\frac{1}{4}g_Y g_2 v^2 \\ 0 & -\frac{1}{4}g_Y g_2 v^2 & \frac{1}{4}g_2^2 v^2 \end{bmatrix} , \tag{7.6}$$

where  $v = 2M_W/g_2 = (\sqrt{2}G_F)^{-\frac{1}{2}} = 246$  GeV,  $g_2$  and  $g_Y$  are the  $SU(2)_L \times U(1)_Y$  gauge coupling constants,  $M_W$  is the mass of the  $W^\pm$  boson and  $G_F$  is the Fermi constant. From  $\det(M_{ab}^2) = 0$  it is easily seen that one eigenvalue is zero, whose eigenvector corresponds to the photon  $A_\mu^\gamma$ . Among the remaining two eigenvalues  $M_\pm^2$ , we identify the lighter mass eigenstate with mass  $M_-$  as the  $Z$  boson, and the heavy eigenstate with mass  $M_+$  as the  $Z'$  boson. Using an orthogonal transformation  $O$  to diagonalize  $M_{ab}^2$ ,  $O^T M_{ab}^2 O = M_D^2$ , we go to the eigenstates basis  $E_\mu^T = (Z'_\mu, Z_\mu, A_\mu^\gamma)$ , where  $M_D^2 = \text{diag}(M_{Z'}^2, M_Z^2, 0)$ ,  $V_\mu = O E_\mu$  and  $O$  is parametrized as

$$O = \begin{bmatrix} \cos \psi \cos \phi - \sin \theta \sin \phi \sin \psi & -\sin \psi \cos \phi - \sin \theta \sin \phi \cos \psi & -\cos \theta \sin \phi \\ \cos \psi \sin \phi + \sin \theta \cos \phi \sin \psi & -\sin \psi \sin \phi + \sin \theta \cos \phi \cos \psi & \cos \theta \cos \phi \\ -\cos \theta \sin \psi & -\cos \theta \cos \psi & \sin \theta \end{bmatrix} . \tag{7.7}$$

The mixing angles  $\theta$ ,  $\phi$  and  $\psi$  are given by [256]

$$\tan \theta = \frac{g_Y}{g_2} \cos \phi , \quad \tan \phi = \frac{M_2}{M_1} , \quad \tan \psi = \frac{\tan \theta \tan \phi M_W^2}{\cos \theta (M_{Z'}^2 - (1 + \tan^2 \theta) M_W^2)} , \tag{7.8}$$

and we can again define the weak angle to be the same as in the SM,  $\tan \theta_w = g_Y/g_2$ . In this model, there are some extra free parameters apart from the SM ones, which are: i) the mass parameters and couplings in the Higgs potential, and ii) the coupling constant  $g_X$  and the mass scales  $M_1, M_2$  (or  $M_2/M_1$  and  $M_{Z'}$ ) from the Stueckelberg contribution. Usually, to be consistent with the LEP data on the  $Z$  boson, the mixing between the  $Z$  and  $Z'$  bosons has to be small,  $|\epsilon| \leq 0.001$  [260], which is satisfied when either the  $Z'$  boson is heavy or the new coupling constant  $g_X$  is very small. In the model discussed here, the couplings of  $Z'$  to the fermions (see the relevant formulas in the next section) do not deviate significantly from the SM values if we take a small ratio  $M_2/M_1 \leq (0.05 - 0.06)$  [257]. We

have considered mainly the case in which  $M_2/M_1 = 0.03$ , but later on we will also make a comment on what the effect of varying the ratio is. Since  $M_2/M_1$  is taken to be small, the new gauge boson is allowed to be relatively light, and if not very heavy it is within future experimental reach. Therefore in the following we shall take the mass of the heavy gauge boson to be in the range between 200 GeV and 1 – 2 TeV.

The interactions between the fermions, the SM Higgs and the charged  $W^\pm$  bosons are the same as in the SM, and the electromagnetic interactions of charged particles have the usual form, where now the electric charge is given by

$$e = \frac{g_2 g_Y \cos(\phi)}{\sqrt{g_2^2 + g_Y^2 \cos(\phi)^2}}. \quad (7.9)$$

Furthermore, the interactions of the inert bosons with  $W^\pm$  are the same as in the inert 2HDM. However, due to the existence of  $C_\mu$  and the new mixing between the mass eigenstates and the gauge eigenstates, the couplings to the  $Z$  boson are different, and there are also similar couplings to the  $Z'$ . In the model discussed here, the photon is a linear combination of  $W_\mu^3$ ,  $C_\mu$ ,  $B_\mu$ , and we find the relation

$$Q = T_3 + \frac{Y}{2} - \frac{g_X Y_X M_2}{2g_Y M_1} \quad (7.10)$$

which generalizes the usual SM formula  $Q = T_3 + Y/2$ . For the particles that are neutral under the extra  $U(1)$  factor the third term vanishes and we recover the formula valid in the SM, while for the inert Higgs bosons, assuming that  $Y_X = \pm 1$ , we find

$$Y = 1 \pm \frac{g_X}{g_Y} \frac{M_2}{M_1} \quad (7.11)$$

and therefore for a coupling constant  $g_X$  similar to the SM coupling constants  $g_2$ ,  $g_Y$  or lower, the usual hypercharge for the inert Higgs bosons is slightly different than one.

### 7.3 Heavy gauge boson searches

The LHC is designed to collide protons with a center-of-mass energy 14 TeV. Since the center-of-mass energy of proton-proton collisions at LHC is 14 TeV, the particle cascades coming from the collisions might contain  $Z'$  if its mass is of the order of 1 TeV. Therefore a heavy gauge boson can be discovered at LHC, and in fact new gauge bosons are perhaps the next best motivated new physics, after the Higgs and supersymmetric particles, to be searched for at future experiments. The mass, total decay width as well as branching ratios for various decay modes are some of the properties of  $Z'$  that should be accurately measurable, and could be used to distinguish between various models at colliders. Thus, in this section we discuss the phenomenology of the model as far as the physics of the new gauge boson is concerned. In the following we shall be interested in two-body decays,  $M \rightarrow m_1 m_2$ , of a heavy particle with mass  $M$  into two lighter particles with masses

$m_1, m_2$ , provided of course that in the Lagrangian there is the corresponding three-point vertex, and that the decay is kinematically allowed, namely that  $M > m_1 + m_2$ . The general formula for the decay width is given by

$$\Gamma(M \rightarrow m_1 m_2) = \frac{\lambda^{1/2}(M^2, m_1^2, m_2^2)}{16\pi M^3} |\mathcal{M}_{fi}|^2, \quad (7.12)$$

where  $\mathcal{M}_{fi}$  is the transition amplitude from the initial to final state and the function  $\lambda(a, b, c) \equiv a^2 + b^2 + c^2 - 2ab - 2ac - 2bc$ . In particular, we are here interested in the decays of the heavy gauge boson  $Z'$  into fermions,  $W^\pm$ ,  $Z$  and Higgs bosons:

$$\begin{aligned} Z' &\rightarrow f\bar{f}, \\ Z' &\rightarrow W^+W^-, \\ Z' &\rightarrow H^+H^-, \\ Z' &\rightarrow HA, \\ Z' &\rightarrow hZ. \end{aligned} \quad (7.13)$$

### 7.3.1 $Z'$ to fermions

For the first decay channel in (7.13), the Lagrangian interaction between fermions and a massive neutral gauge boson  $V$  has the form

$$\mathcal{L}_{Vff} = -g_{Vff} \bar{f} \gamma^\mu (c_V + c_A \gamma^5) f V_\mu, \quad (7.14)$$

and the corresponding decay width is given by

$$\Gamma(V \rightarrow f\bar{f}) = N_c \frac{g_{Vff}^2 M_V}{12\pi} \left[ c_V^2 + c_A^2 + 2(c_V^2 - 2c_A^2) \frac{m_f^2}{M_V^2} \right] \sqrt{1 - 4 \frac{m_f^2}{M_V^2}}, \quad (7.15)$$

which in the massless fermion limit ( $M_V \gg m_f$ ) is simplified to

$$\Gamma(V \rightarrow f\bar{f}) = N_c \frac{g_{Vff}^2 (c_V^2 + c_A^2) M_V}{12\pi}, \quad (7.16)$$

where the number of colors  $N_c$  is one for leptons and three for quarks. In the model discussed here  $V$  corresponds to the  $Z'$  boson and the coupling  $g_{Z'ff}$  is given by

$$g_{Z'ff} = \frac{g_2}{4 \cos(\theta_w)}, \quad (7.17)$$

while  $c_V$  and  $c_A$  are given by

$$\begin{aligned} c_V &= 2T_3 \cos(\theta_w) O_{31} + (Y_L + Y_R) \sin(\theta_w) O_{21}, \\ c_A &= -2T_3 \cos(\theta_w) O_{31} - (Y_L - Y_R) \sin(\theta_w) O_{21}, \end{aligned} \quad (7.18)$$

and can be also found in [288]. In Table 7.1 we recall the quantum number of the fermions.

	$T_3$	$Y_L$	$Y_R$
Neutrinos	$\frac{1}{2}$	-1	0
Charged leptons	$-\frac{1}{2}$	-1	-2
Up quarks	$\frac{1}{2}$	$\frac{1}{3}$	$\frac{4}{3}$
Down quarks	$-\frac{1}{2}$	$\frac{1}{3}$	$-\frac{2}{3}$

Table 7.1: Fermion quantum numbers.

### 7.3.2 $Z'$ to bosons

For the decay channels of  $Z'$  into Higg bosons the Lagrangian interaction has the usual structure as in [289]. Departing from the neutral gauge eigenstates  $V_\mu = \{C_\mu, B_\mu, W_\mu^3\}$  Lagrangians,

$$\begin{aligned}
i\mathcal{L}_{VH^+H^-} &= \frac{1}{2}g_Y \left( H^+ \overleftrightarrow{\partial}_\mu H^- \right) B^\mu + \frac{Y_X}{2}g_X \left( H^+ \overleftrightarrow{\partial}_\mu H^- \right) C^\mu + \frac{1}{2}g_2 \left( H^+ \overleftrightarrow{\partial}_\mu H^- \right) W_3^\mu \\
\mathcal{L}_{VHA} &= \frac{g_Y}{2} \left( H \overleftrightarrow{\partial}_\mu A \right) B^\mu + \frac{g_X}{2} \left( H \overleftrightarrow{\partial}_\mu A \right) C^\mu - \frac{g_2}{2} \left( H \overleftrightarrow{\partial}_\mu A \right) W_3^\mu \\
\mathcal{L}_{VVh} &= \frac{1}{v} h M_Z^2 \left( \cos(\theta_w)W_\mu^3 - \sin(\theta_w)B_\mu \right) \left( \cos(\theta_w)W_3^\mu - \sin(\theta_w)B^\mu \right), \quad (7.19)
\end{aligned}$$

one can derive the interaction between the new gauge boson  $Z'$  rotating the fields as in Eq. (7.7). Therefore, from the mass eigenstates basis  $E_\mu = \{Z'_\mu, Z_\mu, A_\mu^\gamma\}$ , the contributions describing these interactions are,

$$\begin{aligned}
\mathcal{L}_{Z'H^+H^-} &= -i g_{Z'H^+H^-} Z'^\mu \left( H^+ \overleftrightarrow{\partial}_\mu H^- \right), \\
\mathcal{L}_{Z'HA} &= g_{Z'HA} Z'^\mu \left( H \overleftrightarrow{\partial}_\mu A \right), \\
\mathcal{L}_{Z'Zh} &= g_{Z'Zh} Z'^\mu Z_\mu h, \quad (7.20)
\end{aligned}$$

given the corresponding couplings,

$$\begin{aligned}
g_{Z'HA} &= \frac{1}{2}(-g_2 O_{31} + g_Y Y O_{21} + g_X Y_X O_{11}), \\
g_{Z'H^+H^-} &= \frac{1}{2}(g_2 O_{31} + g_Y Y O_{21} + g_X Y_X O_{11}), \\
g_{Z'Zh} &= \frac{M_Z^2}{v} (2 \cos^2(\theta_w) O_{31} O_{32} + 2 \sin^2(\theta_w) O_{21} O_{22} \\
&\quad - \sin(2\theta_w)(O_{31} O_{22} + O_{32} O_{21})), \quad (7.21)
\end{aligned}$$

where  $g_{Z'Zh}$  can be also found in [288]. Thus, the decay rates (7.12) corresponding to these processes can be easily obtained from the following amplitudes squared

$$\begin{aligned}
|\mathcal{M}_{Z'\rightarrow HA}|^2 &= \frac{1}{3}g_{Z'HA}^2 \left[ \frac{(M_H^2 - M_A^2)^2}{M_{Z'}^2} + M_{Z'}^2 \left( 1 - \frac{2(M_H^2 + M_A^2)}{M_{Z'}^2} \right) \right], \\
|\mathcal{M}_{Z'\rightarrow H^+H^-}|^2 &= \frac{1}{3}g_{Z'H^+H^-}^2 M_{Z'}^2 \left( 1 - \frac{4M_{H^\pm}^2}{M_{Z'}^2} \right), \\
|\mathcal{M}_{Z'\rightarrow Zh}|^2 &= \frac{1}{3}g_{Z'Zh}^2 \left[ \frac{(M_{Z'}^2 + M_Z^2 - M_h^2)^2}{4M_Z^2 M_{Z'}^2} \right].
\end{aligned} \tag{7.22}$$

Finally, for the decay of  $Z'$  into  $W^\pm$  bosons, we have obtained a formula similar to that of [289], with the coupling in the model discussed here being different by the SM coupling between  $Z$  and  $W^\pm$  bosons by a factor  $\frac{O_{31}}{\cos(\theta_w)}$ . Suppression by  $O_{31}$  of the decay  $Z' \rightarrow W^+W^-$ , resulting in a branching ratio of a few percent for this mode, is seen in [290].

### 7.3.3 Results

Our results are summarized in the figures below. We have fixed the Higgs boson masses (Set 1 and Set 2 as can be seen in Table 2), as well as the coupling constant  $g_X$  considering two cases, one in which the coupling is small,  $g_X = 0.001$ , and one in which the coupling is comparable to the SM couplings,  $g_X = 0.1$ . Then the only free parameter left is the heavy gauge boson mass. Therefore, in the figures shown below the independent variable is the mass of  $Z'$ . First we focus on the case where  $g_X = 0.001$ . Figures 7.2 and 7.3 show the total decay width of  $Z'$  (in GeV) as a function of its mass for Set 1, with  $M_2/M_1 = 0.03$  and  $0.05$ , respectively. In the rest of the figures the impact of changing the value for the ratio  $M_2/M_1$  is negligible, so it is fixed at  $0.03$ . Figures 7.4 and 7.5 show all branching ratios as a function of  $M_{Z'}$  (for Set 1 and Set 2 respectively). All the decay channels into quarks have been considered together as a single quark channel. However, we have checked that  $Z'$  decay into quarks is dominated by the up quark contributions, as in Figure 1 of [290]. The straight vertical lines correspond to the thresholds, one for the top quark ( $\sim 346$  GeV), one for the neutral Higgs bosons (600 GeV for Set 2 only) and one for the charged Higgs bosons (400 GeV for Set 1 and 1000 GeV for Set 2). We remind the reader that in the SM, the branching ratio of the  $Z$  boson to electrons or muons or tau leptons is 0.034 for each of them, to all neutrino species (invisible channel) is 0.2, and to hadrons is 0.7. To compare with the Stueckelberg extension of the SM with just one Higgs doublet, we show for that model the branching ratios of  $Z'$  in Figure 7.9 (for Set 1), and the total decay width in Figures 7.2 and 7.3 together with the total width for our model with two Higgs doublets. In the model with one Higgs doublet there are no decay channels to inert Higgs bosons, and for a large enough  $M_{Z'}$ , where the branching ratios of  $Z'$  to the inert Higgs bosons become significant, the decay widths in the two models tend to differ. However, the difference is small since the dominant contribution to the decay width is from  $Z'$  to fermions, which scales as  $M_{Z'}g_Y^2(M_2/M_1)^2$  [291]. Furthermore, in the model with one Higgs doublet only, there is just the SM neutral Higgs boson, while in the model

	Set 1	Set 2
$M_{H^\pm}$ (GeV)	200	500
$M_{H,A}$ (GeV)	100	300
$M_h$ (GeV)	100	250

Table 7.2: The two sets of Higgs boson masses used in the analysis.

with two Higgs doublets there are both neutral and charged Higgs bosons. Clearly, if a charged Higgs boson is seen at colliders, this would be a direct evidence of physics beyond the SM. Without Yukawa couplings the charged Higgs bosons cannot directly decay into fermions, and therefore the dominant decay channels of the charged Higgs bosons are just two,  $H^\pm \rightarrow W^\pm H$  and  $H^\pm \rightarrow W^\pm A$ . Taking into account that  $H$  and  $A$  are degenerate in mass, the model discussed here predicts that there are two main decay channels for  $H^\pm$  with the two branching ratios being equal to  $1/2$ . We can also mention here in passing that if the decay channel  $h \rightarrow ZZ$  is kinematically allowed, the SM Higgs boson can be easily found through the so-called four-lepton golden Higgs channel,  $h \rightarrow ZZ \rightarrow l^+l^-l^+l^-$  [15].

As in the case with one Higgs doublet, the total decay width is much smaller than in other models [292, 293], and therefore a heavy gauge boson is expected to show up at colliders as a sharp resonance. Finally, in Figure 7.8 we show ratios of decay widths of two channels as a function of  $M_{Z'}$ , and in particular we have chosen to show the following ratios: Leptons to hadrons, leptons to neutrinos, charged Higgs to neutral Higgs, and  $W^\pm$  bosons to SM Higgs and  $Z$  boson. Recall that in the SM the ratio of leptons to neutrinos is 0.17, and the ratio of leptons to hadrons is 0.05.

Finally, notice that in Figures 7.2 and 7.3, although they look very similar, the scale is different. When the ratio  $M_2/M_1$  is increased from 0.03 to 0.05, the total decay width also increases by a factor  $\sim 3$ , because the couplings of the new gauge boson are now larger. We have also checked that the plot with larger mass ratio showing the branching fractions cannot be distinguished from the one with smaller mass ratio.

We now consider the case where  $g_X = 0.1$  for Set 1 and  $M_2/M_1 = 0.03$ . Most of the decay modes remain the same, apart from the ones into the inert Higgs bosons, for which the coupling now is larger, leading to larger partial decay widths. Figure 7.7 shows the effect of increasing the coupling constant  $g_X$  in the total decay width, while Figure 7.6 shows the effect on the branching ratios. The curves corresponding to the decays into the inert Higgs bosons preserve their shape, but now they are above the rest. The sign of  $Y_X$  has been taken to be positive. If we change the sign of  $Y_X$  we obtain a similar plot where the branching ratios for the inert Higgs bosons are slightly larger.

## 7.4 Conclusions

A model with an extra  $U(1)$  and a second Higgs doublet has been investigated. It is assumed that the fermions and the SM Higgs are neutral under the extra  $U(1)$ , while the

dark Higgs is charged. Thus, Yukawa couplings for the additional Higgs are not allowed, and the FCNC problem is avoided. From this point of view the model is similar to the inert 2HDM, although the gauge symmetry is more restrictive than the  $\mathcal{Z}_2$  discrete symmetry. The massive gauge bosons obtain their masses from two separate mechanisms, namely from the usual Higgs mechanism, as well as from the Stueckelberg mechanism. The interplay between the heavy gauge boson and the extended Higgs sector makes the phenomenology of this model very rich. We have computed the total decay width and all the branching ratios of  $Z'$  as a function of its mass for two different sets of the Higgs bosons masses. We find that two distinct features of the model are a) a sharp decay width for the heavy gauge boson, characteristic of the Stueckelberg mechanism like in the corresponding model with just one Higgs doublet, and b) a pair of charged Higgs bosons with no Yukawa couplings decaying dominantly into a  $W^\pm$  boson and a neutral Higgs boson  $H$  or  $A$ , with the two branching ratios being equal to  $1/2$  each.

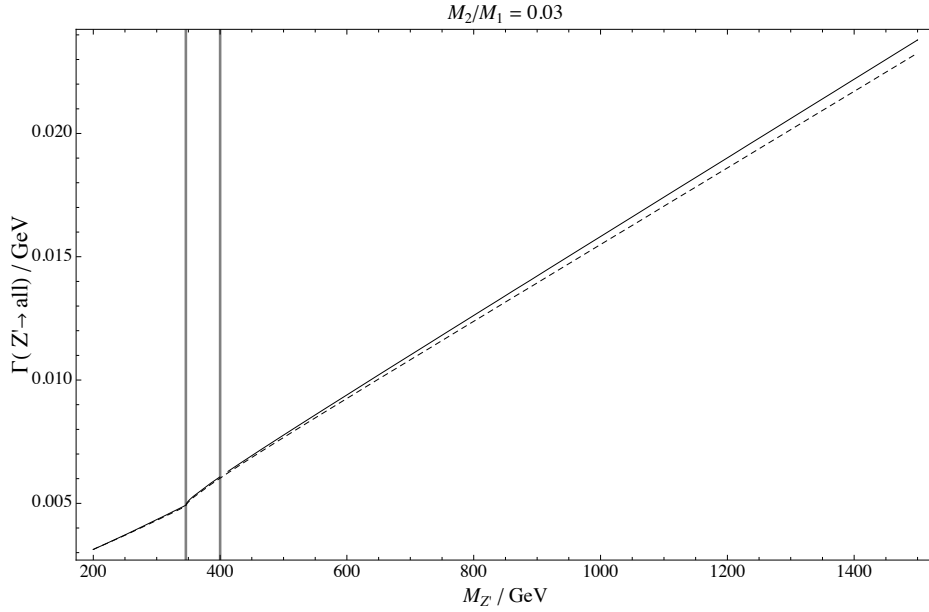


Figure 7.2: Total  $\Gamma$  of  $Z'$  depending on  $M_{Z'}$  for one Higgs doublet (dashed) and two Higgs doublet model (for Set 1 and  $M_2/M_1 = 0.03$ ). The vertical lines are kinematic thresholds corresponding to twice the masses of the top quark and charged Higgs of Set 1.

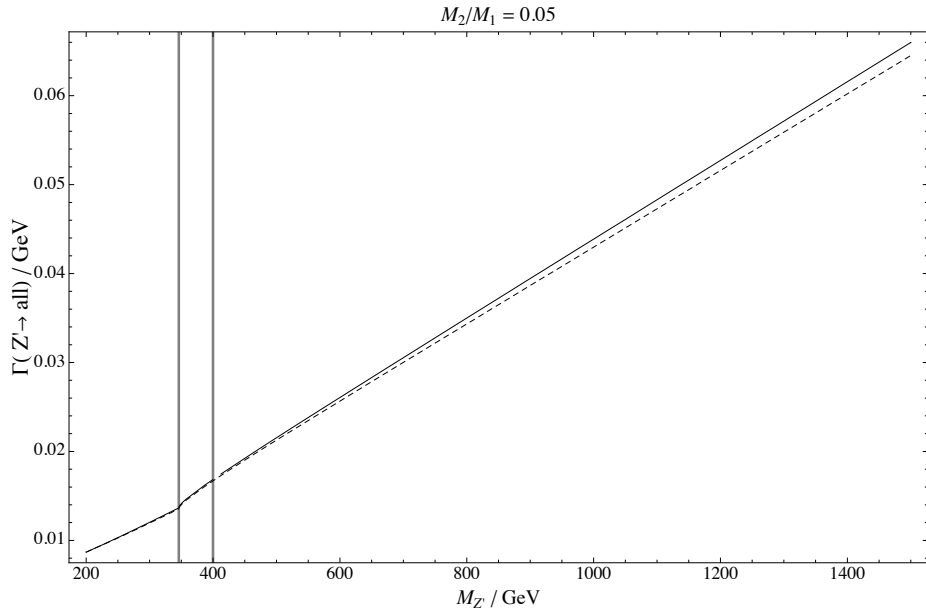


Figure 7.3: Total  $\Gamma$  of  $Z'$  depending on  $M_{Z'}$  for one Higgs doublet (dashed) and two Higgs doublet model (for Set 1 and  $M_2/M_1 = 0.05$ ). The vertical lines are kinematic thresholds corresponding to twice the masses of the top quark and charged Higgs of Set 1.

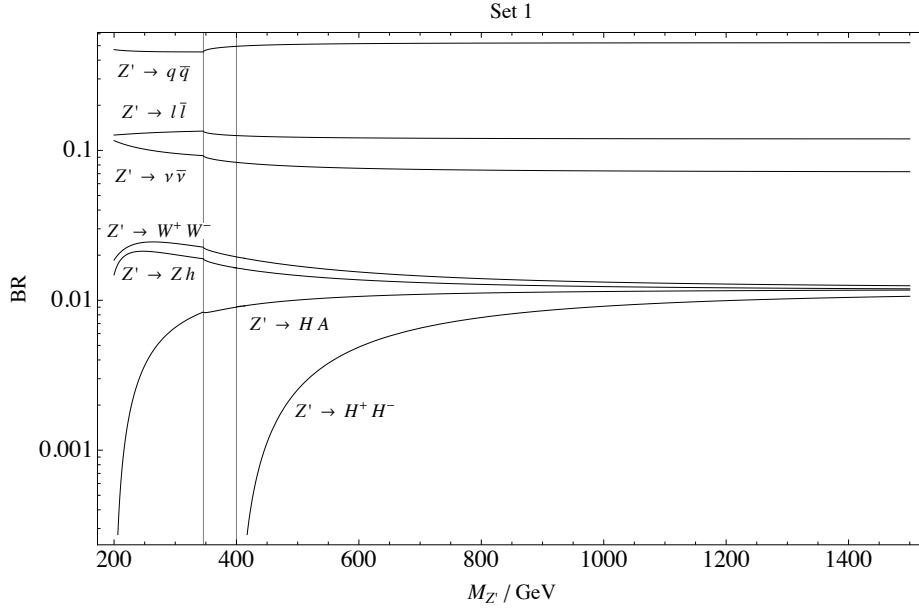


Figure 7.4: Branching ratios depending on  $M_{Z'}$  for Set 1. All the decay channels into quarks have been considered together as a single quark channel. The vertical lines are kinematic thresholds corresponding to twice the masses of the top quark and charged Higgs of Set 1.

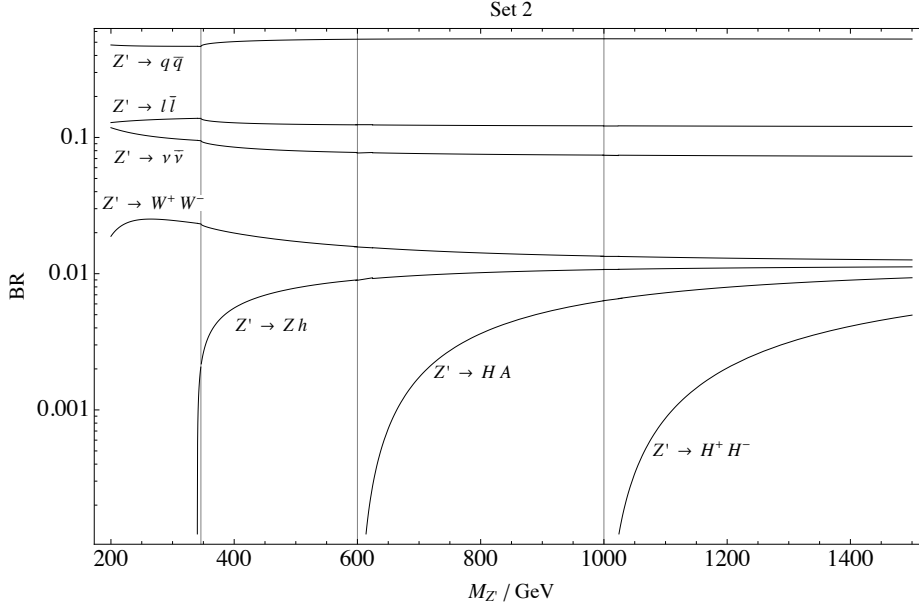


Figure 7.5: Branching ratios depending on  $M_{Z'}$  for Set 2. All the decay channels into quarks have been considered together as a single quark channel. The vertical lines are kinematic thresholds corresponding to twice the masses of the top quark, the neutral Higgs and charged Higgs of Set 2.

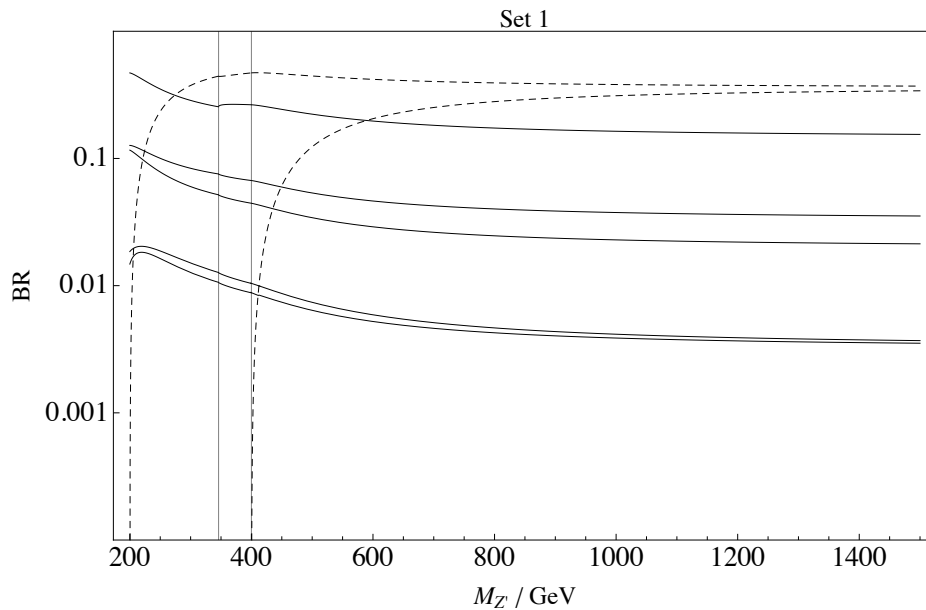


Figure 7.6: Same as Figure 7.4 but only changing the value of  $Y_X g_X$  to  $+0.1$ . Apart from the total decay rate, which is larger, the only relevant difference is for the branching ratios of  $Z'$  decaying into inert Higgs (dashed lines), that increase significantly.

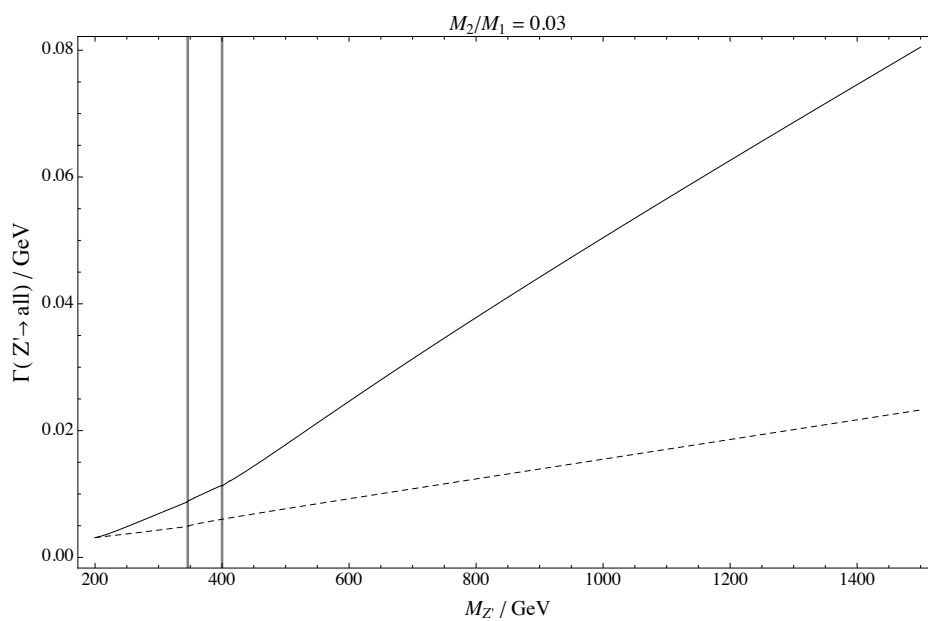


Figure 7.7: Same as Figure 7.2 but only changing the value of  $Y_X g_X$  to  $+0.1$ . The total decay rate when the inert Higgs are present (two-Higgs-doublet model) increases.

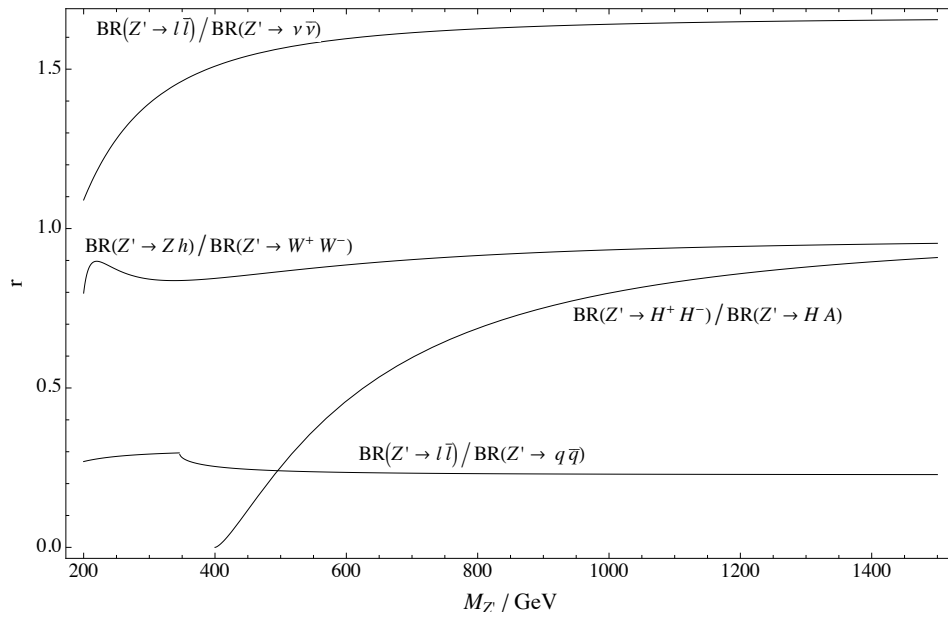


Figure 7.8: Ratios  $r$  of partial decay widths depending on  $M_{Z'}$  (for Set 1).

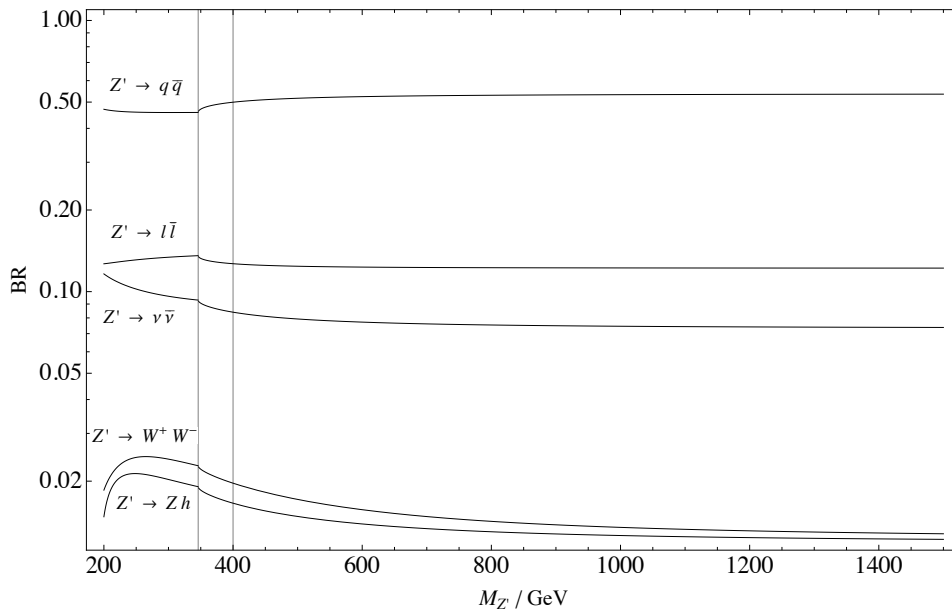


Figure 7.9: Branching ratios depending on  $M_{Z'}$  in the case of one Higgs doublet model (for Set 1). The vertical lines are kinematic thresholds corresponding to twice the masses of the top quark and charged Higgs of Set 1.



# Conclusions

The Two-Higgs-Doublet Model (2HDM) provides new interesting features in the flavour sector of the Electroweak theory; some of them have been analyzed in this thesis and the main conclusions are summarized in the following:

The most general 2HDM generates flavour-changing neutral current (FCNC) interactions at tree level, which are very constrained by the experimental data, however, the possibility of having these flavour-violating sources makes the model a perfect framework to describe them, in the case they are observed. The simplest FCNC effect within the general model is lepton flavour violation (LFV). Due to the absence of righ-handed neutrinos there is only one Yukawa matrix,  $Y_l$ , in the lepton sector of the model, instead of the two that are present in the quark sector,  $Y_{u,d}$ , which decreases the number of free parameters to deal with. Also, LFV experimental constraints are easier to accommodate than the FCNC effects in the quark sector. With all that in mind, we presented a general analysis about LFV, taking advantage of some possible low-energy experiments that could easily discriminate among different underlying dynamics, scalar, vector or dipole operators. Those experiments would study the  $\mu \rightarrow e$  conversion in different nuclei. Our main conclusions after this analysis are, first, that hadronic uncertainties are not a limiting factor when measuring LFV rates, since we have always taken ratios of branching ratios (either  $\mu \rightarrow e$  in different nuclei or  $\mu \rightarrow e$  over  $\mu \rightarrow e\gamma$ ) so the theoretical uncertainties largely cancel. Also, we have given the accuracy at which the experiment should be done. In the case of single-operator dominance the ratio of the conversion rates in light nuclei (e.g. Titanium) should be measured at least at the level of 5%, while in heavy nuclei (e.g. Lead) the level of accuracy should be 20%, given the rates normalized to the rate in Aluminum. Similar requirements appear for more than one operator dominance. Once these accuracies are reached by the experiments, a discrimination among the different models will be possible, which would be specially interesting for the general 2HDM.

The Aligned Two-Higgs-Doublet Model (A2HDM) assumes that the Yukawa matrices of the two scalars are aligned in flavour space. With this simple condition FCNC structures automatically disappear at tree level and all the dynamics gets parametrized by only three complex parameters,  $\varsigma_u$ ,  $\varsigma_d$  and  $\varsigma_l$ , which are possible sources of CP violation. Therefore, this model preserves flavour conservation in neutral interactions and keeps the possibility of having CP violation in the flavour sector. Moreover, it contains as particular cases

all the models based on the implementation of a discrete  $\mathcal{Z}_2$  symmetry, which makes the A2HDM a convenient approach where to study the phenomenology of this kind of models. This alignment is not protected by a symmetry, and some misalignment is generated at one-loop level. However, due to a flavour symmetry present in the Lagrangian, those FCNC structures are minimal flavour violation like and result very constrained. The alignment conditions imply the Yukawa couplings proportional to the masses of the corresponding fermions, which is in agreement with the data and gives bounds of order 1 for the  $\varsigma_{u,d,l}$  parameters. The additional freedom introduced by the phases of these complex parameters makes easier to avoid the electroweak precision constraints, resulting in weaker limits than in the scenarios where these parameters are correlated ( $\mathcal{Z}_2$  models). In this sense, the A2HDM parameter space could accommodate larger deviations from the SM than other models. These conclusions arise from the phenomenological analysis of the processes with charged Higgs contributions presented here. On one hand, we obtained limits on  $\varsigma_{u,d} \varsigma_l^* / M_{H^\pm}^2$  from leptonic and semileptonic meson decays and direct upper limits on  $\varsigma_{u,d}$  from loop-induced processes,  $Z \rightarrow b\bar{b}$ ,  $\epsilon_K$ ,  $\bar{B}^0 - B^0$  and  $\bar{B} \rightarrow X_s \gamma$ . We have also analyzed two CP violating observables present in  $B$  systems, the  $\bar{B} \rightarrow X_s \gamma$  rate asymmetry and the  $B_s^0$  mixing phase. In the first case, we have shown that although the asymmetry could be enhanced for some particular values of the parameters, it is still compatible with the current measurements when considering parameters that lead to acceptable values of the branching ratio. The theoretical errors play a crucial role in this “compatibility”, making the accurate calculation of the branching ratio at NNLO very important, and also a future more precise measurement of this quantity very interesting. A sizeable  $B_s^0$  mixing phase can be accommodated by the A2HDM, without spoiling the agreement in the  $B_d$  system, although not as large as the one detected in the D0 experiment, which is at odds with the rate having no contributions from new physics. The  $\bar{B} \rightarrow X_s \gamma$  bounds give strong correlations among the parameters, which reduce the enhanced  $B_s^0$  mixing phase given by the  $B_s^0$  system itself. If signals of new physics are detected at the LHC, this analysis will be capable to show the agreement or disagreement of the A2HDM.

The study of a new gauge boson in a Stueckelberg extension of the 2HDM gives rise automatically to an “inert” approach, where the second doublet does not interact with fermions. The model is similar to the inert 2HDM, although the gauge symmetry is more restrictive than the  $\mathcal{Z}_2$ . In this model, the masses of the gauge bosons come from both the Higgs sector and the Stueckelberg mechanism, and the interplay between the new gauge boson and the extended scalar sector makes the phenomenology very rich. In the analysis, we have shown all the possible branching ratios of the heavy boson  $Z'$  as a function of its mass. A sharp decay width is observed, which is characteristic of the Stueckelberg mechanism also in the case of one Higgs doublet.

As we have seen, the 2HDM is a versatile extension of the SM that provides many new dynamical features. In this thesis, we exploited that fact and presented three different studies of the Electroweak model with this non-minimal realization of the scalar sector, in the way to look for new physics at the time of the LHC.

# Conclusions

El Model de Dos Doblets de Higgs (2HDM) dóna lloc a nous i interessants trets en el sector de sabor de la teoria Electrofeble; en aquesta tesi hem analitzat alguns d'ells i a continuació resumim les conclusions més importants:

El 2HDM més general genera corrents neutres amb canvi de sabor (FCNC) a nivell arbre, les quals estan molt retringides experimentalment, malgrat això, la possibilitat de tenir aquestes fonts de violació de sabor fa del model un context perfecte per tal de descriure-les, en cas de què foren observades. L'efecte més simple de FCNC en el model general és la violació de sabor leptònic (LFV). Degut a l'absència de neutrins dextrogirs només hi ha una matriu de Yukawa,  $Y_l$ , en el sector leptònic del model, en lloc de les dues que hi ha en el sector de quarks,  $Y_{u,d}$ , fet que decreix el nombre de paràmetres lliures amb què treballar. A més, les restriccions experimentals de LFV són més fàcils d'acomodar que els efectes de FCNC en el sector de quarks. Amb tot això al cap, hem presentat una anàlisi general sobre LFV, aprofitant els possibles experiments a baixa energia que podrien discriminar fàcilment entre diferents dinàmiques subjacents, operadors escalars, vectorials o dipolars. Eixos experiments estudiarien la conversió  $\mu \rightarrow e$  en diferents nuclis. Les nostres conclusions principals després de l'anàlisi són, primer, que els errors hadrònics no són un factor limitador per mesurar amplades de LFV, ja que sempre hem pres quocients de *branching ratios* (bé en la conversió  $\mu \rightarrow e$  en nuclis diferents o bé en la conversió  $\mu \rightarrow e$  normalitzada a  $\mu \rightarrow e\gamma$ ), de manera que els errors teòrics cancel·len. A més, hem donat la precisió a la que caldria fer els experiments. En el cas de domini d'un únic operador els quocients entre les amplades en nuclis lleugers (e.g. Titani) haurien de ser mesurades almenys al nivell del 5%, mentre que en nuclis pesats (e.g. Plom) el nivell de precisió hauria d'estar al voltant del 20%, on totes les amplades estan normalitzades a l'amplada en Alumini. Per a més d'un operador dominant els requisits que s'obtenen són similars. Una vegada assolides aquestes precisions per part dels experiments, es podrà fer una discriminació entre els models, que seria especialment interessant per al 2HDM general.

El Model Alineat de Dos Doblets de Higgs (A2HDM) assumeix que les matrius de Yukawa dels dos escalars estan alineades en l'espai de sabor. Amb aquesta simple condició, les estructures FCNC desapareixen automàticament a nivell arbre i tota la dinàmica queda parametritzada per, només, tres paràmetres complexos,  $\varsigma_u$ ,  $\varsigma_d$  i  $\varsigma_l$ , que són possibles fonts de violació de CP. Per tant, aquest model preserva conservació de sabor en inter-

accions neutres i manté la possibilitat de tenir violació de CP en el sector de sabor. A més, conté com a casos particulars tots els models basats en la implementació de simetria discreta  $\mathcal{Z}_2$ , el que fa del A2HDM un marc adient per l'estudi de la fenomenologia d'aquest tipus de models. Aquest alineament no està protegit per una simetria, i cert desalineament es pot generar a 1-loop. Malgrat això, la presència d'una simetria de sabor en el Lagrangià, fa que eixes estructures FCNC siguin del tipus *violació mínima de sabor* i resulten estar molt suprimides. Les condicions d'alineament impliquen que els acoblaments de Yukawa siguin proporcionals a les masses dels fermions corresponents, la qual cosa està d'acord amb les dades experimentals i imposa límits d'ordre 1 per als paràmetres  $\zeta_{u,d,l}$ . La llibertat adicional introduïda per les fases d'aquests paràmetres complexos facilita l'ajust del model a les restriccions experimentals electrofebles de precisió, donant lloc a límits menys forts que en escenaris on els paràmetres entan correlacionats (models tipus  $\mathcal{Z}_2$ ). En aquest sentit, l'espai de paràmetres del A2HDM podria tenir més lloc que altres models per a desviacions del SM. Aquestes conclusions venen de l'anàlisi fenomenològica dels processos amb contribucions de Higgs carregats presentada ací. Per una part, hem obtingut límits en  $\zeta_{u,d}\zeta_l^*/M_{H^\pm}^2$  de desintegracions leptòniques i semileptòniques de mesons i límits directes en  $\zeta_{u,d}$  de processos induïts per loop,  $Z \rightarrow b\bar{b}$ ,  $\epsilon_K$ ,  $\bar{B}^0 - B^0$  i  $\bar{B} \rightarrow X_s\gamma$ . També hem analitzat dos observables de violació de CP presents en sistemes de  $B$ , l'assimetria en l'amplada del  $\bar{B} \rightarrow X_s\gamma$  i la fase de mescla en  $B_s^0$ . En el primer cas, hem mostrat que malgrat que l'assimetria podria estar amplificada per a certs valors del paràmetres, és encara compatible amb les mesures actuals quan els valors dels paràmetres que es consideren són aquells compatibles amb valors acceptables per al *branching ratio*. El A2HDM pot donar lloc a una fase de mescla en  $B_s^0$  no menyspreable, tot i sent consistent amb el sistema  $B_d$ , encara que no tan gran com la detectada a l'experiment D0, la qual és incompatible amb el fet de considerar l'amplada lliure de contribucions de nova física. El  $\bar{B} \rightarrow X_s\gamma$  imposa fortes correlacions entre els paràmetres, cosa que redueix la grandària de la fase de mescla en  $B_s^0$  que tenia lloc només considerant aquest mateix sistema. Si l'LHC detecta senyals de nova física, aquest anàlisi serà capaç de mostrar l'acord o desacord del A2HDM.

L'estudi d'un nou bosó de *gauge* en una extensió tipus Stueckelberg del 2HDM dóna lloc automàticament a un context "*inert*", on el segon doblet no interacciona amb els fermions. El model és semblant al 2HDM *inert*, sent la simetria *gauge* més restrictiva que la  $\mathcal{Z}_2$ . En aquest model, les masses dels bosons de *gauge* venen d'ambdós sectors, el de Higgs i el del mecanisme d'Stueckelberg; la interacció entre el nou bosó de *gauge* i el sector escalar està dóna una fenomenologia molt rica. En aquesta anàlisi, hem mostrat tots els possibles *branching ratios* del bosó pesat  $Z'$  en funció de la seua massa. L'amplada de desintegració observada és pronunciada, cosa que també és característica del mecanisme d'Stueckelberg en el cas d'un doblet de Higgs.

Com hem vist, el 2HDM resulta ser una extensió del SM certament versàtil, que proporciona diverses característiques dinàmiques noves. En aquesta tesi, hem explotat aquest fet, tot i presentant tres estudis diferents del model Electrofeble amb aquesta realització no mínima del sector escalar, en el camí de cercar nova física en el temps de l'LHC.

# Appendix A

## Higgs potential formulae

### A.1 Basis dependent potential parameters

The potential in the general basis  $(\phi_1, \phi_2)$  (3.7) can be expressed as

$$\begin{aligned}
 \mathcal{V} &= \mu'_1 \phi_1^\dagger \phi_1 + \mu'_2 \phi_2^\dagger \phi_2 + [\mu'_{12} \phi_1^\dagger \phi_2 + h.c.] \\
 &+ \lambda'_1 (\phi_1^\dagger \phi_1)^2 + \lambda'_2 (\phi_2^\dagger \phi_2)^2 + \lambda'_3 (\phi_1^\dagger \phi_1) (\phi_2^\dagger \phi_2) + \lambda'_4 (\phi_1^\dagger \phi_2) (\phi_2^\dagger \phi_1) \\
 &+ [(\lambda'_5 \phi_1^\dagger \phi_2 + \lambda'_6 \phi_1^\dagger \phi_1 + \lambda'_7 \phi_2^\dagger \phi_2) (\phi_1^\dagger \phi_2) + h.c.] ,
 \end{aligned} \tag{A.1}$$

where the quadratic and quartic couplings are

$$\begin{aligned}
 Y_{11} &= \mu'_1 & Y_{12} &= \mu'_{12} \\
 Y_{21} &= \mu'_{12}{}^* & Y_{22} &= \mu'_2 ,
 \end{aligned} \tag{A.2}$$

and,

$$\begin{aligned}
 Z_{1111} &= \lambda'_1 & Z_{2222} &= \lambda'_2 \\
 Z_{1122} &= Z_{2211} = \frac{\lambda'_3}{2} & Z_{1221} &= Z_{2112} = \frac{\lambda'_4}{2} \\
 Z_{1212} &= \lambda'_5 & Z_{2121} &= \lambda'_{5}{}^* \\
 Z_{1112} &= Z_{1211} = \frac{\lambda'_6}{2} & Z_{1121} &= Z_{2111} = \frac{\lambda'_{6}{}^*}{2} \\
 Z_{2212} &= Z_{1222} = \frac{\lambda'_7}{2} & Z_{2221} &= Z_{2122} = \frac{\lambda'_{7}{}^*}{2} ,
 \end{aligned} \tag{A.3}$$

respectively. The parameters corresponding to the general basis  $\phi_a$  (with prime) in (A.1) are related to the ones in the Higgs basis  $\Phi_a$  of (3.9) as,

$$\begin{aligned}
 \mu_1 &= \mu'_1 \cos^2 \beta + \mu'_2 \sin^2 \beta + 2\mu'_{12}{}^R \sin \beta \cos \beta , \\
 \mu_2 &= \mu'_1 \sin^2 \beta + \mu'_2 \cos^2 \beta - 2\mu'_{12}{}^R \sin \beta \cos \beta , \\
 \mu_{12} &= e^{-i\theta} [(\mu'_1 - \mu'_2) \sin \beta \cos \beta - \mu'_{12} \cos^2 \beta + \mu'_{12}{}^* \sin^2 \beta] ,
 \end{aligned} \tag{A.4}$$

$$\begin{aligned}
\lambda_1 &= \lambda'_1 \cos^4 \beta + \lambda'_2 \sin^4 \beta + \lambda'_3 \sin^2 \beta \cos^2(\beta) + \lambda'_4 \sin^2 \beta \cos^2 \beta \\
&\quad + 2\lambda_5'^R \sin^2 \beta \cos^2 \beta + 2\lambda_6'^R \sin \beta \cos^3 \beta + 2\lambda_7'^R \sin^3 \beta \cos \beta , \\
\lambda_2 &= \lambda'_1 \sin^4 \beta + \lambda'_2 \cos^4 \beta + \lambda'_3 \sin^2 \beta \cos^2(\beta) + \lambda'_4 \sin^2 \beta \cos^2 \beta \\
&\quad + 2\lambda_5'^R \sin^2 \beta \cos^2 \beta - 2\lambda_6'^R \sin^3 \beta \cos \beta - 2\lambda_7'^R \sin \beta \cos^3 \beta , \\
\lambda_3 &= \frac{1}{4} [(\lambda'_1 + \lambda'_2 - \lambda'_4 - 2\lambda_5'^R)(1 - \cos(4\beta)) + \lambda'_3(3 + \cos(4\beta)) \\
&\quad - 2\lambda_6'^R \sin(4\beta) + 2\lambda_7'^R \sin(4\beta)] , \\
\lambda_4 &= \frac{1}{4} [(\lambda'_1 + \lambda'_2 - \lambda'_3 - 2\lambda_5'^R)(1 - \cos(4\beta)) + \lambda'_4(3 + \cos(4\beta)) \\
&\quad - 2\lambda_6'^R \sin(4\beta) + 2\lambda_7'^R \sin(4\beta)] , \\
\lambda_5 &= e^{-2i\theta} [(\lambda'_1 + \lambda'_2 - \lambda'_3 - \lambda'_4) \sin^2 \beta \cos^2 \beta + \lambda'_5 \cos^4 \beta + \lambda_5'^* \sin^4 \beta \\
&\quad + (\lambda'_7 - \lambda'_6) \sin \beta \cos^3 \beta + (\lambda_6'^* - \lambda_7'^*) \sin^3 \beta \cos \beta] , \\
\lambda_6 &= e^{-i\theta} [\cos \beta (\sin \beta \cos^2 \beta (2\lambda'_1 - \lambda'_3 - \lambda'_4 - 2\lambda_5') + \sin^3 \beta (-2\lambda'_2 + \lambda'_3 + \lambda'_4) \\
&\quad + \sin^2 \beta \cos \beta (\lambda'_6 - 2\lambda_7') - \lambda_6' \cos^3 \beta + 2 \sin^3 \beta \lambda_5'^*) \\
&\quad + 2 \sin^2 \beta \cos^2 \beta \lambda_6'^* - \sin^2 \beta \cos(2\beta) \lambda_7'^*] , \\
\lambda_7 &= \frac{1}{4} e^{-i\theta} [2(\lambda'_1 - \lambda'_2 + \lambda'_5) \sin(2\beta) - (\lambda'_1 + \lambda'_2 - \lambda'_3 - \lambda'_4 - \lambda'_5) \sin(4\beta) \\
&\quad + (\lambda'_6 - \lambda'_7) \cos(4\beta) - 2\lambda_7' \cos(2\beta) - \lambda_6' - \lambda_7' \\
&\quad - 8\lambda_5'^* \sin^3 \beta \cos \beta - 4\lambda_6'^* \sin^2 \beta \cos(2\beta) + 2\lambda_7'^* \sin^2(2\beta)] . \tag{A.5}
\end{aligned}$$

## A.2 Higgs self-couplings

The self-couplings of the Higgs fields are described by the potential (3.9), where the parameters are encoded in the Higgs basis. Tables A.1 and A.2 summarize the couplings for all possible scalar self-interactions. The neutral Higgs couplings do not refer the mass eigenstates interactions yet, but to the fields  $S_1$ ,  $S_2$  and  $S_3$ . As is discussed in Section 3.2.1, these fields are related to the mass eigenstates  $\varphi_i^0$  through an orthogonal matrix  $\mathcal{R}$ , which is defined by (3.14). Then,  $\varphi_i^0 = \mathcal{R}_{ij} S_j$  with  $\varphi_i^0 = \{h_1, h_2, h_3\}$  for the most general potential where CP is explicitly violated. If CP is preserved, then the form of  $\mathcal{R}$  changes and  $\varphi_i^0 = \{h, H, A\}$ . These relations among the fields can be easily translated for the self-couplings in the following way:

$$g_{h_i h_j h_k} = \mathcal{R}_{il} \mathcal{R}_{jm} \mathcal{R}_{kn} g_{S_l S_m S_n} , \tag{A.6}$$

where the sum over equal indices is understood,  $i, j, k, l, m, n = 1, 2, 3$ . Of course, CP violating interactions coming from the elements of the same doublet are forbidden, therefore  $S_2 S_2 S_2 S_3$ ,  $S_2 S_3 S_3 S_3$  and  $H^+ H^- S_2 S_3$  do not exist. Since the most general potential of the 2HDM violates CP, all the other possible self-interactions are allowed.

$g_{S_1 S_1 S_1}$	$v \lambda_1$	$g_{S_3 S_3 S_3}$	$-\frac{1}{2} v \lambda_7^I$
$g_{S_1 S_1 S_2}$	$\frac{3}{2} v \lambda_6^R$	$g_{S_3 S_3 S_1}$	$\frac{1}{2} v (\lambda_3 + \lambda_4 - 2\lambda_5^R)$
$g_{S_1 S_2 S_2}$	$\frac{1}{2} v (\lambda_3 + \lambda_4 + 2\lambda_5^R)$	$g_{S_3 S_1 S_1}$	$-\frac{3}{2} v \lambda_6^I$
$g_{S_2 S_2 S_2}$	$\frac{1}{2} v \lambda_7^R$	$g_{S_1 S_2 S_3}$	$-2v \lambda_5^I$
$g_{S_2 S_2 S_3}$	$-\frac{1}{2} v \lambda_7^I$	$g_{H^+ H^- S_1}$	$v \lambda_3$
$g_{S_2 S_3 S_3}$	$\frac{1}{2} v \lambda_7^R$	$g_{H^+ H^- S_2}$	$v \lambda_7^R$
		$g_{H^+ H^- S_3}$	$-v \lambda_7^I$

Table A.1: Self-couplings of three Higgs.

$g_{S_1 S_1 S_1 S_1}$	$\frac{1}{4} \lambda_1$	$g_{S_3 S_1 S_1 S_1}$	$-\frac{1}{2} \lambda_6^I$
$g_{S_1 S_1 S_1 S_2}$	$\frac{1}{2} \lambda_6^R$	$g_{S_1 S_1 S_2 S_3}$	$-\lambda_5^I$
$g_{S_1 S_1 S_2 S_2}$	$\frac{1}{4} (\lambda_3 + \lambda_4 + 2i\lambda_5^R)$	$g_{S_1 S_2 S_2 S_3}$	$-\frac{1}{2} \lambda_7^I$
$g_{S_1 S_2 S_2 S_2}$	$\frac{1}{2} \lambda_7^R$	$g_{S_1 S_2 S_3 S_3}$	$\frac{1}{2} \lambda_7^R$
$g_{S_2 S_2 S_2 S_2}$	$\frac{1}{4} \lambda_2$	$g_{H^+ H^- S_1 S_1}$	$\frac{1}{2} \lambda_3$
$g_{S_2 S_2 S_2 S_3}$	—	$g_{H^+ H^- S_1 S_2}$	$\lambda_7^R$
$g_{g_{S_2 S_2 S_3 S_3}}$	$\frac{1}{2} \lambda_2$	$g_{H^+ H^- S_1 S_3}$	$-\lambda_7^I$
$g_{g_{S_2 S_3 S_3 S_3}}$	—	$g_{H^+ H^- S_2 S_3}$	—
$g_{g_{S_3 S_3 S_3 S_3}}$	$\frac{1}{4} \lambda_2$	$g_{H^+ H^- S_2 S_2}$	$\lambda_2$
$g_{g_{S_3 S_3 S_3 S_1}}$	$-\frac{1}{2} \lambda_7^I$	$g_{H^+ H^- S_3 S_3}$	$\lambda_2$
$g_{S_3 S_3 S_1 S_1}$	$\frac{1}{4} (\lambda_3 + \lambda_4 - 2i\lambda_5^R)$	$g_{H^+ H^- H^+ H^-}$	$\lambda_2$

Table A.2: Self-couplings of four Higgs.



# Appendix B

## $\Delta F = 2$ effective Hamiltonian

### B.1 $\Delta B = 2$

At lowest order, the  $\Delta F = 2$  transitions are mediated by box diagrams with exchanges of  $W^\pm$  and/or  $H^\pm$  propagators. Performing the matching between the A2HDM amplitude and the low-energy effective Hamiltonian  $\mathcal{H}_{\text{eff}}^{\Delta F=2}$ , at the scale  $\mu_{tW} \sim M_W, m_t$ , one obtains the Wilson coefficients  $C_i(\mu)$ . We have derived the LO results given in table B.1, where  $x_W \equiv m_t^2/M_W^2$  and  $x_H \equiv m_t^2/M_{H^\pm}^2$ . They can be expressed in terms of the two four-point functions [294]:

$$\begin{aligned}
 D_0(m_1, m_2, M_1, M_2) &\equiv \frac{m_2^2 \log\left(\frac{m_2^2}{m_1^2}\right)}{(m_2^2 - m_1^2)(m_2^2 - M_1^2)(m_2^2 - M_2^2)} \\
 &+ \frac{M_1^2 \log\left(\frac{M_1^2}{m_1^2}\right)}{(M_1^2 - m_1^2)(M_1^2 - m_2^2)(M_1^2 - M_2^2)} \\
 &+ \frac{M_2^2 \log\left(\frac{M_2^2}{m_1^2}\right)}{(M_2^2 - m_1^2)(M_2^2 - m_2^2)(M_2^2 - M_1^2)}, \tag{B.1}
 \end{aligned}$$

$$\begin{aligned}
 D_2(m_1, m_2, M_1, M_2) &\equiv \frac{m_2^4 \log\left(\frac{m_2^2}{m_1^2}\right)}{(m_2^2 - m_1^2)(m_2^2 - M_1^2)(m_2^2 - M_2^2)} \\
 &+ \frac{M_1^4 \log\left(\frac{M_1^2}{m_1^2}\right)}{(M_1^2 - m_1^2)(M_1^2 - m_2^2)(M_1^2 - M_2^2)} \\
 &+ \frac{M_2^4 \log\left(\frac{M_2^2}{m_1^2}\right)}{(M_2^2 - m_1^2)(M_2^2 - m_2^2)(M_2^2 - M_1^2)},
 \end{aligned}$$

$\mathcal{O}_i$	$C_i(\mu_{tW})$
$\mathcal{O}^{\text{VLL}}$	$(4x_W + x_W^2)M_W^2 D_2(m_t, M_W) - 8x_W^2 M_W^4 D_0(m_t, M_W) +$ $+ 2 \zeta_u ^2 x_W^2 [M_W^2 D_2(m_t, M_W, M_H) - 4M_W^4 D_0(m_t, M_W, M_H)] +$ $+  \zeta_u ^4 x_W^2 M_W^2 D_2(m_t, M_H)$
$\mathcal{O}^{\text{VRR}}$	$\frac{m_d^2 m_b^2}{M_W^4} [ \zeta_d ^4 x_H M_W^2 D_2(m_t, M_H) +  \zeta_d ^2 M_W^2 \overline{D}_2(m_t, M_W, M_H)]$
$\mathcal{O}_1^{\text{LR}}$	$2\frac{m_d m_b}{M_W^2} x_W [ \zeta_d ^2  \zeta_u ^2 M_W^2 D_2(m_t, M_H) + 2\text{Re}(\zeta_d^* \zeta_u) M_W^2 D_2(m_t, M_W, M_H)]$
$\mathcal{O}_2^{\text{LR}}$	$2\frac{m_d m_b}{M_W^2} [4 \zeta_d ^2  \zeta_u ^2 x_W M_W^4 D_0(m_t, M_H) - 4 \zeta_d ^2 M_W^2 \overline{D}_2(m_t, M_W, M_H) +$ $+ ( \zeta_d ^2 +  \zeta_u ^2) x_W M_W^2 D_2(m_t, M_W, M_H)]$
$\mathcal{O}_1^{\text{SLL}}$	$4\frac{m_d^2}{M_W^2} x_W^2 [(\zeta_u \zeta_d^*)^2 M_W^4 D_0(m_t, M_H) + 2\zeta_u \zeta_d^* M_W^4 D_0(m_t, M_W, M_H)]$
$\mathcal{O}_2^{\text{SLL}}$	0
$\mathcal{O}_1^{\text{SRR}}$	$4\frac{m_d^2}{M_W^2} x_W^2 [(\zeta_d \zeta_u^*)^2 M_W^4 D_0(m_t, M_H) + 2\zeta_d \zeta_u^* M_W^4 D_0(m_t, M_W, M_H)]$
$\mathcal{O}_2^{\text{SRR}}$	0

Table B.1: Leading-order Wilson coefficients for the  $\Delta B = 2$  operators given above. The quark masses from the scalar couplings are to be taken at the matching scale  $\mu_{tW}$ .

through ( $i = 0, 2$ )

$$D_i(m, M_1, M_2) \equiv \lim_{m_2 \rightarrow m} D_i(m, m_2, M_1, M_2), \quad (\text{B.2})$$

$$D_i(m, M) \equiv \lim_{M_2 \rightarrow M} D_i(m, M, M_2), \quad (\text{B.3})$$

$$\overline{D}_2(m, M_1, M_2) \equiv D_2(m, M_1, M_2) - D_2(0, M_1, M_2). \quad (\text{B.4})$$

These one-loop contributions involve virtual propagators of up-type quarks ( $u, c, t$ ). Once the GIM cancellation is taken into account, the up and charm contributions vanish in the limit  $m_{u,c} \rightarrow 0$ , which we have adopted. Thus, the B meson mixing is completely dominated by the top-quark contributions (the different CKM factors have all a similar size for  $B_d^0$  mixing,  $V_{ud}^* V_{ub} \sim V_{cd}^* V_{cb} \sim V_{td}^* V_{tb} \sim A\lambda^3$ , while in the  $B_s^0$  case  $V_{us}^* V_{ub} \sim A\lambda^4$  and  $V_{cs}^* V_{cb} \sim V_{ts}^* V_{tb} \sim A\lambda^2$ ). Since the scalar couplings are proportional to quark masses, we have maintained the masses of the external down-type quarks. In the limit  $m_d \rightarrow 0$ , we reproduce the results given in [207]. The only Wilson coefficients which are not suppressed by powers of  $m_d$  are  $C_{\text{VLL}}$  and  $C_{\text{SRR}}^1$ . Therefore, for all practical purposes, one can neglect the remaining operators.

The running for  $\mathcal{O}_1^{\text{SRR}}$  is performed using the results of [205],

$$\begin{pmatrix} C_{\text{SRR}}^1(\mu_b) \\ C_{\text{SRR}}^2(\mu_b) \end{pmatrix} = \begin{pmatrix} [\eta_{11}(\mu_b)]_{\text{SRR}} & [\eta_{12}(\mu_b)]_{\text{SRR}} \\ [\eta_{21}(\mu_b)]_{\text{SRR}} & [\eta_{22}(\mu_b)]_{\text{SRR}} \end{pmatrix} \begin{pmatrix} C_{\text{SRR}}^1(\mu_{tW}) \\ C_{\text{SRR}}^2(\mu_{tW}) \end{pmatrix}, \quad (\text{B.5})$$

	$B_d^0$	$B_s^0$
$B_2^{MS}(m_b)$	$0.83 \pm 0.03 \pm 0.06$	$0.84 \pm 0.02 \pm 0.06$
$B_3^{MS}(m_b)$	$0.90 \pm 0.06 \pm 0.12$	$0.91 \pm 0.03 \pm 0.12$

Table B.2:  $B$ -parameters for  $B_{d,s}^0$  mixing from [295]. Systematic errors added linearly.

with

$$[\eta_{11}(\mu_b)]_{\text{SRR}} = 1.0153 \eta_5^{-0.6315} - 0.0153 \eta_5^{0.7184}, \quad (\text{B.6})$$

$$[\eta_{12}(\mu_b)]_{\text{SRR}} = 1.9325 (\eta_5^{-0.6315} - \eta_5^{0.7184}), \quad (\text{B.7})$$

$$[\eta_{21}(\mu_b)]_{\text{SRR}} = 0.0081 (\eta_5^{0.7184} - \eta_5^{-0.6315}), \quad (\text{B.8})$$

$$[\eta_{22}(\mu_b)]_{\text{SRR}} = 1.0153 \eta_5^{0.7184} - 0.0153 \eta_5^{-0.6315}. \quad (\text{B.9})$$

These are leading-order expressions, but they have been evaluated with the two-loop expression for  $\alpha_s$  in  $\eta_5 = \frac{\alpha_s^{(5)}(\mu_{tW})}{\alpha_s^{(5)}(\mu_b)} \sim 0.7$ .

The corresponding matrix elements are given by

$$\langle \mathcal{O}^{\text{VLL}} \rangle(\mu) = \frac{1}{3} m_{B_d^0} f_{B_d^0}^2 B^{\text{VLL}}(\mu), \quad (\text{B.10})$$

$$\langle \mathcal{O}_1^{\text{SRR}} \rangle(\mu) = -\frac{5}{24} \left( \frac{m_{B_d^0}}{m_b(\mu) + m_d(\mu)} \right)^2 m_{B_d^0} f_{B_d^0}^2 B_1^{\text{SRR}}(\mu), \quad (\text{B.11})$$

$$\langle \mathcal{O}_2^{\text{SRR}} \rangle(\mu) = -\frac{1}{2} \left( \frac{m_{B_d^0}}{m_b(\mu) + m_d(\mu)} \right)^2 m_{B_d^0} f_{B_d^0}^2 B_2^{\text{SRR}}(\mu), \quad (\text{B.12})$$

the  $B_i(\mu)$  parametrizing the deviation from the naive factorization limit. These  $B_i(\mu)$  factors have been evaluated in the quenched approximation on the lattice in [295], using a different operator basis. The connection reads (see again [205], given here with both operators in the same scheme)

$$B_1^{\text{SRR}}(\mu) = B_2(\mu), \quad B_2^{\text{SRR}}(\mu) = \frac{5}{3} B_2(\mu) - \frac{2}{3} B_3(\mu). \quad (\text{B.13})$$

From [295] we arrive at the values given in table B.2 by adding again all systematic uncertainties linearly.

The wanted  $B_d^0$ - $\bar{B}_d^0$  mixing amplitude is given by

$$\begin{aligned} \langle B^0 | \mathcal{H}_{\text{eff}}^{\Delta B=2} | \bar{B}^0 \rangle &= \frac{G_F^2 M_W^2}{16\pi^2} (V_{td}^* V_{tb})^2 f_{B_d^0}^2 M_{B_d^0}^2 \\ &\times \left[ \frac{2}{3} \hat{B}_{B_d^0} \eta_B(x_W, x_H) C_{\text{VLL}}(\mu_{tW}) \right. \\ &\left. + \frac{m_{B_d^0}^2}{(m_b(\mu_b) + m_d(\mu_b))^2} [\eta_{\text{SRR}}(\mu_b, \mu_{tW}) \mathbf{C}_{\text{SRR}}(\mu_{tW})]^T \mathbf{B}_{\text{SRR}}(\mu_b) \right], \end{aligned} \quad (\text{B.14})$$

with

$$\mathbf{B}_{\text{SRR}}(\mu_b) = \begin{pmatrix} -\frac{5}{12}B_{2,d}(\mu_b) \\ \frac{2}{3}B_{3,d}(\mu_b) - \frac{5}{3}B_{2,d}(\mu_b) \end{pmatrix}. \quad (\text{B.15})$$

From this, we get the relevant observables as

$$\Delta m_{B_d^0} = \frac{1}{m_{B_d^0}} |\langle B_d^0 | \mathcal{H}_{\text{eff}}^{\Delta B=2} | \bar{B}_d^0 \rangle|, \quad (\text{B.16})$$

$$\phi_{B_d^0} = -\text{Arg} [\langle B_d^0 | \mathcal{H}_{\text{eff}}^{\Delta B=2} | \bar{B}_d^0 \rangle]. \quad (\text{B.17})$$

The analogous expressions for  $B_s^0$ - $\bar{B}_s^0$  mixing are trivially obtained changing the label  $d$  to  $s$  everywhere.

## B.2 $\Delta S = 2$

For the Kaon mixing amplitude, we have calculated the LO matching coefficients completely analogous to the  $\Delta B = 2$  coefficients, keeping the charm mass finite. Due to the strong suppression of all other operators by light quark masses we can choose the LO matching coefficients to be

$$\begin{aligned} C_{\mathcal{O}_{\text{VLL}}}^{cc} &= (4x_W^{cc} + x_W^{cc2})M_W^2 D_2(m_c, M_W) - 8x_W^{cc2}M_W^4 D_0(m_c, M_W), \\ C_{\mathcal{O}_{\text{VLL}}}^{ct} &= (4x_W^{ct} + x_W^{ct2})M_W^2 D_2(m_c, m_t, M_W) - 8x_W^{ct2}M_W^4 D_0(m_c, m_t, M_W) \\ &\quad + 2|\zeta_u|^2 x_W^{ct2} [M_W^2 D_2(m_c, m_t, M_W, M_H) - 4M_W^4 D_0(m_c, m_t, M_W, M_H)] \\ &\quad + |\zeta_u|^4 x_W^{ct2} M_W^2 D_2(m_c, m_t, M_H), \\ C_{\mathcal{O}_{\text{VLL}}}^{tt} &= (4x_W^{tt} + x_W^{tt2})M_W^2 D_2(m_t, M_W) - 8x_W^{tt2}M_W^4 D_0(m_t, M_W) \\ &\quad + 2|\zeta_u|^2 x_W^{tt2} [M_W^2 D_2(m_t, M_W, M_H) - 4M_W^4 D_0(m_t, M_W, M_H)] \\ &\quad + |\zeta_u|^4 x_W^{tt2} M_W^2 D_2(m_t, M_H), \\ C_{\mathcal{O}_i} &= 0 \quad (i \neq \text{VLL}), \end{aligned} \quad (\text{B.18})$$

where the loop functions  $D_{0,2}$  have been defined already, and  $x_W^{ct} = m_c m_t / M_W^2$ . In the calculation, we use the NLO results for the SM which have been calculated in [296, 297], while the NLO charged Higgs contributions to the top contribution are again taken from [207], corrected and applied to our scenario.

# Bibliography

- [1] Antonio Pich. The Standard model of electroweak interactions. *arXiv:0705.4264 [hep-ph]*, 2007.
- [2] S. L. Glashow, J. Iliopoulos, and L. Maiani. Weak Interactions with Lepton-Hadron Symmetry. *Phys. Rev.*, D2:1285–1292, 1970.
- [3] Nicola Cabibbo. Unitary Symmetry and Leptonic Decays. *Phys. Rev. Lett.*, 10:531–533, 1963.
- [4] Makoto Kobayashi and Toshihide Maskawa. CP Violation in the Renormalizable Theory of Weak Interaction. *Prog. Theor. Phys.*, 49:652–657, 1973.
- [5] K. Nakamura et al. Review of particle physics. *J. Phys.*, G37:075021, 2010.
- [6] Lincoln Wolfenstein. Parametrization of the Kobayashi-Maskawa Matrix. *Phys. Rev. Lett.*, 51:1945, 1983.
- [7] Gustavo C. Branco, Luis Lavoura, and Joao P. Silva. *CP violation*, volume 103. 1999.
- [8] J. Charles et al. CP violation and the CKM matrix: Assessing the impact of the asymmetric B factories. *Eur. Phys. J.*, C41:1–131, 2005.
- [9] Andreas Hocker, H. Lacker, S. Laplace, and F. Le Diberder. A New approach to a global fit of the CKM matrix. *Eur. Phys. J.*, C21:225–259, 2001.
- [10] G. P. Dubois-Felsmann, D. G. Hitlin, F. C. Porter, and G. Eigen. Sensitivity of CKM fits to theoretical uncertainties and their representation. *arXiv:hep-ph/0308262*, 2003.
- [11] Marcella Bona et al. The 2004 UTfit Collaboration report on the status of the unitarity triangle in the standard model. *JHEP*, 07:028, 2005.
- [12] M. Bona et al. Model-independent constraints on Delta F=2 operators and the scale of new physics. *JHEP*, 03:049, 2008.
- [13] Olivier Deschamps. CKM global fit and constraints on New Physics in the B meson mixing. *arXiv:0810.3139 [hep-ph]*, 2008.

- 
- [14] Victor Mukhamedovich Abazov et al. Evidence for an anomalous like-sign dimuon charge asymmetry. *Phys. Rev.*, D82:032001, 2010.
- [15] G. Kane J. Gunion, H. Haber and S. Dawson. *The Higgs Hunters Guide*. 1990.
- [16] T. D. Lee. A Theory of Spontaneous T Violation. *Phys. Rev.*, D8:1226–1239, 1973.
- [17] Howard E. Haber and Deva O’Neil. Basis-independent methods for the two-Higgs-doublet model. II: The significance of  $\tan(\beta)$ . *Phys. Rev.*, D74:015018, 2006.
- [18] L. Lavoura and Joao P. Silva. Fundamental CP violating quantities in a  $SU(2) \times U(1)$  model with many Higgs doublets. *Phys. Rev.*, D50:4619–4624, 1994.
- [19] F. J. Botella and Joao P. Silva. Jarlskog - like invariants for theories with scalars and fermions. *Phys. Rev.*, D51:3870–3875, 1995.
- [20] Sacha Davidson and Howard E. Haber. Basis-independent methods for the two-Higgs-doublet model. *Phys. Rev.*, D72:035004, 2005.
- [21] John F. Gunion and Howard E. Haber. Conditions for CP-violation in the general two-Higgs- doublet model. *Phys. Rev.*, D72:095002, 2005.
- [22] Gustavo C. Branco, M. N. Rebelo, and J. I. Silva-Marcos. CP-odd invariants in models with several Higgs doublets. *Phys. Lett.*, B614:187–194, 2005.
- [23] Ilya F. Ginzburg and Maria Krawczyk. Symmetries of two Higgs doublet model and CP violation. *Phys. Rev.*, D72:115013, 2005.
- [24] C. C. Nishi. Physical parameters and basis transformations in the Two-Higgs-Doublet model. *Phys. Rev.*, D77:055009, 2008.
- [25] Celso C. Nishi. The structure of potentials with  $N$  Higgs doublets. *Phys. Rev.*, D76:055013, 2007.
- [26] C. C. Nishi. CP violation conditions in N-Higgs-doublet potentials. *Phys. Rev.*, D74:036003, 2006.
- [27] Igor P. Ivanov. Minkowski space structure of the Higgs potential in 2HDM: II. Minima, symmetries, and topology. *Phys. Rev.*, D77:015017, 2008.
- [28] I. P. Ivanov. Minkowski space structure of the Higgs potential in 2HDM. *Phys. Rev.*, D75:035001, 2007.
- [29] I. P. Ivanov. Two-Higgs-doublet model from the group-theoretic perspective. *Phys. Lett.*, B632:360–365, 2006.
- [30] M. Maniatis, A. von Manteuffel, and O. Nachtmann. CP Violation in the General Two-Higgs-Doublet Model: a Geometric View. *Eur. Phys. J.*, C57:719–738, 2008.

- 
- [31] Nilendra G. Deshpande and Ernest Ma. Pattern of Symmetry Breaking with Two Higgs Doublets. *Phys. Rev.*, D18:2574, 1978.
- [32] Boris M. Kastening. Bounds from stability and symmetry breaking on parameters in the two Higgs doublet potential. *arXiv:hep-ph/9307224*, 1992.
- [33] Howard E. Haber. Nonminimal Higgs sectors: The Decoupling limit and its phenomenological implications. *hep-ph/9501320*, 1994.
- [34] John F. Gunion and Howard E. Haber. The CP-conserving two-Higgs-doublet model: The approach to the decoupling limit. *Phys. Rev.*, D67:075019, 2003.
- [35] I. F. Ginzburg and I. P. Ivanov. Tree-level unitarity constraints in the 2HDM with CP- violation. *arXiv:hep-ph/0312374*, 2003.
- [36] Sheldon L. Glashow and Steven Weinberg. Natural Conservation Laws for Neutral Currents. *Phys. Rev.*, D15:1958, 1977.
- [37] Benjamin W. Lee, C. Quigg, and H. B. Thacker. Weak Interactions at Very High-Energies: The Role of the Higgs Boson Mass. *Phys. Rev.*, D16:1519, 1977.
- [38] Andrew G. Akeroyd, Abdesslam Arhrib, and El-Mokhtar Naimi. Note on tree-level unitarity in the general two Higgs doublet model. *Phys. Lett.*, B490:119–124, 2000.
- [39] I. F. Ginzburg and I. P. Ivanov. Tree-level unitarity constraints in the most general 2HDM. *Phys. Rev.*, D72:115010, 2005.
- [40] Howard E. Haber and Deva O’Neil. Basis-independent methods for the two-Higgs-doublet model III: The CP-conserving limit, custodial symmetry, and the oblique parameters S, T, U. *arXiv:1011.6188 [hep-ph]*, 2010.
- [41] Search for charged Higgs bosons: Preliminary combined results using LEP data collected at energies up to 209 GeV. *arXiv:hep-ex/0107031*, 2001.
- [42] Ernest Ma. Utility of a Special Second Scalar Doublet. *Mod. Phys. Lett.*, A23:647–652, 2008.
- [43] Ernest Ma. Verifiable radiative seesaw mechanism of neutrino mass and dark matter. *Phys. Rev.*, D73:077301, 2006.
- [44] Riccardo Barbieri, Lawrence J. Hall, and Vyacheslav S. Rychkov. Improved naturalness with a heavy Higgs: An alternative road to LHC physics. *Phys. Rev.*, D74:015007, 2006.
- [45] Laura Lopez Honorez, Emmanuel Nezri, Josep F. Oliver, and Michel H. G. Tytgat. The inert doublet model: An archetype for dark matter. *JCAP*, 0702:028, 2007.

- [46] G. Abbiendi et al. Search for Charged Higgs Bosons in  $e^+e^-$  Collisions at  $\sqrt{s}=189\text{--}209$  GeV. *arXiv:0812.0267 [hep-ph]*, 2008.
- [47] T. Aaltonen et al. Search for charged Higgs bosons in decays of top quarks in  $p - \bar{p}$  collisions at  $\sqrt{s} = 1.96$  TeV. *Phys. Rev. Lett.*, 103:101803, 2009.
- [48] V. M. Abazov et al. Search for charged Higgs bosons in decays of top quarks. *Phys. Rev.*, D80:051107, 2009.
- [49] T. Aaltonen et al. Search for Higgs bosons predicted in two-Higgs-doublet models via decays to tau lepton pairs in 1.96 TeV proton- antiproton collisions. *Phys. Rev. Lett.*, 103:201801, 2009.
- [50] G. Abbiendi et al. Search for Yukawa production of a light neutral Higgs boson at LEP. *Eur. Phys. J.*, C23:397–407, 2002.
- [51] G. Abbiendi et al. Flavour independent search for Higgs bosons decaying into hadronic final states in  $e^+ e^-$  collisions at LEP. *Phys. Lett.*, B597:11–25, 2004.
- [52] J. Abdallah et al. Final results from DELPHI on the searches for SM and MSSM neutral Higgs bosons. *Eur. Phys. J.*, C32:145–183, 2004.
- [53] J. Abdallah et al. Flavour independent searches for hadronically decaying neutral Higgs bosons. *Eur. Phys. J.*, C44:147–159, 2005.
- [54] V. M. Abazov et al. Search for NMSSM Higgs bosons in the  $h \rightarrow aa \rightarrow \mu\mu\mu\mu, \mu\mu\tau\tau$  channels using  $p\bar{p}$  collisions at  $\sqrt{s}=1.96$  TeV. *Phys. Rev. Lett.*, 103:061801, 2009.
- [55] Steven Weinberg. Gauge Theory of CP Violation. *Phys. Rev. Lett.*, 37:657, 1976.
- [56] C. D. Froggatt and Holger Bech Nielsen. Hierarchy of Quark Masses, Cabibbo Angles and CP Violation. *Nucl. Phys.*, B147:277, 1979.
- [57] T. P. Cheng and Marc Sher. Mass Matrix Ansatz and Flavor Nonconservation in Models with Multiple Higgs Doublets. *Phys. Rev.*, D35:3484, 1987.
- [58] David Atwood, Laura Reina, and Amarjit Soni. Phenomenology of two Higgs doublet models with flavor changing neutral currents. *Phys. Rev.*, D55:3156–3176, 1997.
- [59] G. C. Branco, W. Grimus, and L. Lavoura. Relating the scalar flavour changing neutral couplings to the CKM matrix. *Phys. Lett.*, B380:119–126, 1996.
- [60] J. L. Diaz-Cruz, R. Noriega-Papaqui, and A. Rosado. Measuring the fermionic couplings of the Higgs boson at future colliders as a probe of a non-minimal flavor structure. *Phys. Rev.*, D71:015014, 2005.
- [61] Alakabha Datta. Suppressed FCNC in New Physics with Shared Flavor Symmetry. *Phys. Rev.*, D78:095004, 2008.

- [62] J. L. Diaz-Cruz, J. Hernandez-Sanchez, S. Moretti, R. Noriega-Papaqui, and A. Rosado. Yukawa Textures and Charged Higgs Boson Phenomenology in the 2HDM-III. *Phys. Rev.*, D79:095025, 2009.
- [63] F. J. Botella, G. C. Branco, and M. N. Rebelo. Minimal Flavour Violation and Multi-Higgs Models. *Phys. Lett.*, B687:194–200, 2010.
- [64] H. E. Haber, Gordon L. Kane, and T. Sterling. The Fermion Mass Scale and Possible Effects of Higgs Bosons on Experimental Observables. *Nucl. Phys.*, B161:493, 1979.
- [65] Lawrence J. Hall and Mark B. Wise. Flavor changing Higgs boson couplings. *Nucl. Phys.*, B187:397, 1981.
- [66] John F. Donoghue and Ling Fong Li. Properties of Charged Higgs Bosons. *Phys. Rev.*, D19:945, 1979.
- [67] Vernon D. Barger, J. L. Hewett, and R. J. N. Phillips. New Constraints on the Charged Higgs Sector in Two Higgs Doublet Models. *Phys. Rev.*, D41:3421, 1990.
- [68] Martin J. Savage. Constraining flavor changing neutral currents with  $B \rightarrow \mu^+ \mu^-$ . *Phys. Lett.*, B266:135–141, 1991.
- [69] Yuval Grossman. Phenomenology of models with more than two Higgs doublets. *Nucl. Phys.*, B426:355–384, 1994.
- [70] A. G. Akeroyd. Fermiophobic and other non-minimal neutral Higgs bosons at the LHC. *J. Phys.*, G24:1983–1994, 1998.
- [71] A. G. Akeroyd. Non-minimal neutral Higgs bosons at LEP2. *Phys. Lett.*, B377:95–101, 1996.
- [72] A. G. Akeroyd and W. James Stirling. Light charged Higgs scalars at high-energy  $e^+ e^-$  colliders. *Nucl. Phys.*, B447:3–17, 1995.
- [73] Mayumi Aoki, Shinya Kanemura, Koji Tsumura, and Kei Yagyu. Models of Yukawa interaction in the two Higgs doublet model, and their collider phenomenology. *Phys. Rev.*, D80:015017, 2009.
- [74] Antonio Pich and Paula Tuzon. Yukawa Alignment in the Two-Higgs-Doublet Model. *Phys. Rev.*, D80:091702, 2009.
- [75] R. Diaz, R. Martinez, and Jairo Alexis Rodriguez. Lepton flavor violation in the two Higgs doublet model type III. *Phys. Rev.*, D63:095007, 2001.
- [76] Rodolfo A. Diaz, R. Martinez, and Carlos E. Sandoval. Constraints on lepton flavor violation in the two Higgs doublet model. *arXiv:hep-ph/0311201*, 2003.

- [77] Rodolfo A. Diaz, R. Martinez, and Carlos E. Sandoval. Flavor changing neutral currents from lepton and B decays in the two Higgs doublet model. *Eur. Phys. J.*, C41:305–310, 2005.
- [78] A. E. Carcamo Hernandez, R. Martinez, and Jairo Alexis Rodriguez. Different kind of textures of Yukawa coupling matrices in the two Higgs doublet model type III. *Eur. Phys. J.*, C50:935–948, 2007.
- [79] Wen-Jun Li, Ying-Ying Fan, Gong-Wei Liu, and Lin-Xia Lu. Lepton Flavor Violating  $\tau$  Decays in Two Higgs Doublet Model III. *Int. J. Mod. Phys.*, A25:4827–4837, 2010.
- [80] Vincenzo Cirigliano, Ryuichiro Kitano, Yasuhiro Okada, and Paula Tuzon. On the model discriminating power of  $\mu \rightarrow e$  conversion in nuclei. *Phys. Rev.*, D80:013002, 2009.
- [81] M. L. Brooks et al. New Limit for the Family-Number Non-conserving Decay  $\mu^+ \rightarrow e^+ \gamma$ . *Phys. Rev. Lett.*, 83:1521–1524, 1999.
- [82] U. Bellgardt et al. Search for the Decay  $\mu^+ \rightarrow e^+ e^+ e^-$ . *Nucl. Phys.*, B299:1, 1988.
- [83] Wilhelm H. Bertl et al. Search for muon - electron conversion on gold. Prepared for International Europhysics Conference on High- Energy Physics (HEP 2001), Budapest, Hungary, 12-18 Jul 2001.
- [84] C. Dohmen et al. Test of lepton flavor conservation in  $\mu \rightarrow e$  conversion on titanium. *Phys. Lett.*, B317:631–636, 1993.
- [85] W. Honecker et al. Improved limit on the branching ratio of  $\mu \rightarrow e$  conversion on lead. *Phys. Rev. Lett.*, 76:200–203, 1996.
- [86] Ryuichiro Kitano, Masafumi Koike, and Yasuhiro Okada. Detailed calculation of lepton flavor violating muon electron conversion rate for various nuclei. *Phys. Rev.*, D66:096002, 2002.
- [87] Oruganti U. Shanker.  $Z$  dependence of coherent  $\mu e$  conversion rate in anomalous neutrinoless muon capture. *Phys. Rev.*, D20:1608, 1979.
- [88] Andrzej Czarnecki, William J. Marciano, and Kirill Melnikov. Coherent muon electron conversion in muonic atoms. *AIP Conf. Proc.*, 435:409–418, 1998.
- [89] T. S. Kosmas, Sergey Kovalenko, and Ivan Schmidt.  $\mu^- - e^-$  conversion in strange quark sea. *Phys. Lett.*, B511:203, 2001.
- [90] Mikhail A. Shifman, A. I. Vainshtein, and Valentin I. Zakharov. Remarks on Higgs Boson Interactions with Nucleons. *Phys. Lett.*, B78:443, 1978.
- [91] Achille Corsetti and Pran Nath. Gaugino Mass Nonuniversality and Dark Matter in SUGRA, Strings and D Brane Models. *Phys. Rev.*, D64:125010, 2001.

- 
- [92] H. Ohki et al. Nucleon sigma term and strange quark content from lattice QCD with exact chiral symmetry. *Phys. Rev.*, D78:054502, 2008.
- [93] J. Gasser, H. Leutwyler, M. P. Locher, and M. E. Sainio. Extracting the pion - nucleon sigma term from data. *Phys. Lett.*, B213:85–90, 1988.
- [94] J. Gasser, H. Leutwyler, and M. E. Sainio. Sigma term update. *Phys. Lett.*, B253:252–259, 1991.
- [95] M. M. Pavan, I. I. Strakovsky, R. L. Workman, and R. A. Arndt. The pion nucleon Sigma term is definitely large: Results from a GWU analysis of pi N scattering data. *PiN Newslett.*, 16:110–115, 2002.
- [96] B. Borasoy and Ulf-G. Meissner. Chiral expansion of baryon masses and sigma-terms. *Annals Phys.*, 254:192–232, 1997.
- [97] Massimiliano Procura, Thomas R. Hemmert, and Wolfram Weise. Nucleon mass, sigma term and lattice QCD. *Phys. Rev.*, D69:034505, 2004.
- [98] M. Procura, B. U. Musch, T. Wollenweber, T. R. Hemmert, and W. Weise. Nucleon mass: From lattice QCD to the chiral limit. *Phys. Rev.*, D73:114510, 2006.
- [99] Hai-Yang Cheng. Low-energy interactions of scalar and pseudoscalar Higgs bosons with baryons. *Phys. Lett.*, B219:347, 1989.
- [100] H. Leutwyler. The ratios of the light quark masses. *Phys. Lett.*, B378:313–318, 1996.
- [101] Riccardo Barbieri and L. J. Hall. Signals for supersymmetric unification. *Phys. Lett.*, B338:212–218, 1994.
- [102] Riccardo Barbieri, Lawrence J. Hall, and Alessandro Strumia. Violations of lepton flavor and CP in supersymmetric unified theories. *Nucl. Phys.*, B445:219–251, 1995.
- [103] J. Hisano, T. Moroi, K. Tobe, and Masahiro Yamaguchi. Exact event rates of lepton flavor violating processes in supersymmetric SU(5) model. *Phys. Lett.*, B391:341–350, 1997.
- [104] Francesca Borzumati and Antonio Masiero. Large Muon and electron Number Violations in Supergravity Theories. *Phys. Rev. Lett.*, 57:961, 1986.
- [105] J. Hisano, T. Moroi, K. Tobe, and Masahiro Yamaguchi. Lepton-Flavor Violation via Right-Handed Neutrino Yukawa Couplings in Supersymmetric Standard Model. *Phys. Rev.*, D53:2442–2459, 1996.
- [106] V. Cirigliano, A. Kurylov, M. J. Ramsey-Musolf, and P. Vogel. Lepton flavor violation without supersymmetry. *Phys. Rev.*, D70:075007, 2004.

- [107] Ryuichiro Kitano, Masafumi Koike, Shinji Komine, and Yasuhiro Okada. Higgs-mediated muon electron conversion process in supersymmetric seesaw model. *Phys. Lett.*, B575:300–308, 2003.
- [108] Jihn E. Kim, Pyungwon Ko, and Dae-Gyu Lee. More on R-parity and lepton-family number violating couplings from muon(ium) conversion, and tau and pi0 decays. *Phys. Rev.*, D56:100–106, 1997.
- [109] K. Huitu, J. Maalampi, M. Raidal, and A. Santamaria. New constraints on R-parity violation from mu e conversion in nuclei. *Phys. Lett.*, B430:355–362, 1998.
- [110] A. Faessler, T. S. Kosmas, S. Kovalenko, and J. D. Vergados. Exotic mu e conversion in nuclei and R-parity violating supersymmetry. *Nucl. Phys.*, B587:25–44, 2000.
- [111] Andre de Gouvea, Smaragda Lola, and Kazuhiro Tobe. Lepton flavor violation in supersymmetric models with trilinear R-parity violation. *Phys. Rev.*, D63:035004, 2001.
- [112] H. De Vries, C. W. De Jager, and C. De Vries. Nuclear charge and magnetization density distribution parameters from elastic electron scattering. *Atom. Data Nucl. Data Tabl.*, 36:495–536, 1987.
- [113] G. Fricke et al. Nuclear Ground State Charge Radii from Electromagnetic Interactions. *Atom. Data Nucl. Data Tabl.*, 60:177, 1995.
- [114] Mu2e Collaboration website. <http://mu2e.fnal.gov>.
- [115] COMET. <http://comet.phys.sci.osaka-u.ac.jp/internal/publications/main.pdf>.
- [116] Martin Jung, Antonio Pich, and Paula Tuzon. Charged-Higgs phenomenology in the Aligned two-Higgs- doublet model. *JHEP*, 11:003, 2010.
- [117] P. M. Ferreira, L. Lavoura, and Joao P. Silva. Renormalization-group constraints on Yukawa alignment in multi-Higgs-doublet models. *Phys. Lett.*, B688:341–344, 2010.
- [118] G. D’Ambrosio, G. F. Giudice, G. Isidori, and A. Strumia. Minimal flavour violation: An effective field theory approach. *Nucl. Phys.*, B645:155–187, 2002.
- [119] R. Sekhar Chivukula and Howard Georgi. Composite Technicolor Standard Model. *Phys. Lett.*, B188:99, 1987.
- [120] L. J. Hall and Lisa Randall. Weak scale effective supersymmetry. *Phys. Rev. Lett.*, 65:2939–2942, 1990.
- [121] A. J. Buras, P. Gambino, M. Gorbahn, S. Jager, and L. Silvestrini. Universal unitarity triangle and physics beyond the standard model. *Phys. Lett.*, B500:161–167, 2001.

- [122] Vincenzo Cirigliano, Benjamin Grinstein, Gino Isidori, and Mark B. Wise. Minimal flavor violation in the lepton sector. *Nucl. Phys.*, B728:121–134, 2005.
- [123] Alexander L. Kagan, Gilad Perez, Tomer Volansky, and Jure Zupan. General Minimal Flavor Violation. *Phys. Rev.*, D80:076002, 2009.
- [124] Andrzej J. Buras, Maria Valentina Carlucci, Stefania Gori, and Gino Isidori. Higgs-mediated FCNCs: Natural Flavour Conservation vs. Minimal Flavour Violation. *JHEP*, 10:009, 2010.
- [125] Andrzej J. Buras, Gino Isidori, and Paride Paradisi. EDMs vs. CPV in  $B_{s,d}$  mixing in two Higgs doublet models with MFV. *Phys. Lett.*, B694:402–409, 2011.
- [126] G. Cvetič, C. S. Kim, and S. S. Hwang. Higgs-mediated flavor-changing neutral currents in the general framework with two Higgs doublets: An RGE analysis. *Phys. Rev.*, D58:116003, 1998.
- [127] Bogdan A. Dobrescu, Patrick J. Fox, and Adam Martin. CP violation in  $B_s$  mixing from heavy Higgs exchange. *Phys. Rev. Lett.*, 105:041801, 2010.
- [128] Carolin B. Braeuninger, Alejandro Ibarra, and Cristoforo Simonetto. Radiatively induced flavour violation in the general two- Higgs doublet model with Yukawa alignment. *Phys. Lett.*, B692:189–195, 2010.
- [129] H. Serodio. Yukawa Alignment in a Multi Higgs Doublet Model: An effective approach. *Phys. Lett.*, B700:133–138, 2011.
- [130] Abdul Wahab El Kaffas, Per Osland, and Odd Magne Ogreid. Constraining the Two-Higgs-Doublet-Model parameter space. *Phys. Rev.*, D76:095001, 2007.
- [131] O. Deschamps et al. The Two Higgs Doublet of Type II facing flavour physics data. *Phys. Rev.*, D82:073012, 2010.
- [132] Henning Flacher et al. Gfitter - Revisiting the Global Electroweak Fit of the Standard Model and Beyond. *Eur. Phys. J.*, C60:543–583, 2009.
- [133] Farvah Mahmoudi and Oscar Stal. Flavor constraints on the two-Higgs-doublet model with general Yukawa couplings. *arXiv:0907.1791 [hep-ph]*, 2009.
- [134] The CKMfitter Group. Average of lattice QCD inputs for CKM fits. [http://ckmfitter.in2p3.fr/plots\\_Beauty09/latticeinputs280809.pdf](http://ckmfitter.in2p3.fr/plots_Beauty09/latticeinputs280809.pdf), 2009.
- [135] Gilberto Colangelo. The FLAG working group: status report. In *EuroFlavour09 - Bari*, 2009.
- [136] Vittorio Lubicz. Kaon physics from lattice QCD. *PoS*, LAT2009:013, 2009.

- [137] P. A. Boyle et al.  $K \rightarrow \pi$  form factors with reduced model dependence. *Eur. Phys. J.*, C69:159–167, 2010.
- [138] P. A. Boyle et al.  $K_{l3}$  semileptonic form factor from 2+1 flavour lattice QCD. *Phys. Rev. Lett.*, 100:141601, 2008.
- [139] V. Lubicz, F. Mescia, S. Simula, C. Tarantino, and for the ETM Collaboration.  $K \rightarrow \pi l \nu$  Semileptonic Form Factors from Two-Flavor Lattice QCD. *Phys. Rev.*, D80:111502, 2009.
- [140] H. Leutwyler and M. Roos. Determination of the Elements  $V_{us}$  and  $V_{ud}$  of the Kobayashi-Maskawa Matrix. *Z. Phys.*, C25:91, 1984.
- [141] Johan Bijnens and Pere Talavera.  $K_{l3}$  decays in chiral perturbation theory. *Nucl. Phys.*, B669:341–362, 2003.
- [142] Matthias Jamin, Jose Antonio Oller, and Antonio Pich. Order  $p^6$  chiral couplings from the scalar  $K\pi$  form-factor. *JHEP*, 02:047, 2004.
- [143] V. Cirigliano et al. The  $\langle SPP \rangle$  Green function and SU(3) breaking in  $K_{l3}$  decays. *JHEP*, 04:006, 2005.
- [144] A. Kastner and H. Neufeld. The  $K_{l3}$  scalar form factors in the standard model. *Eur. Phys. J.*, C57:541–556, 2008.
- [145] Matthew Wingate, Christine T. H. Davies, Alan Gray, G. Peter Lepage, and Junko Shigemitsu. The  $B_s$  and  $D_s$  decay constants in 3 flavor lattice QCD. *Phys. Rev. Lett.*, 92:162001, 2004.
- [146] Elvira Gamiz, Christine T. H. Davies, G. Peter Lepage, Junko Shigemitsu, and Matthew Wingate. Neutral  $B$  Meson Mixing in Unquenched Lattice QCD. *Phys. Rev.*, D80:014503, 2009.
- [147] C. Bernard et al. B and D Meson Decay Constants. *PoS*, LATTICE2008:278, 2008.
- [148] E. Follana, C. T. H. Davies, G. P. Lepage, and J. Shigemitsu. High Precision determination of the  $\pi$ ,  $K$ ,  $D$  and  $D_s$  decay constants from lattice QCD. *Phys. Rev. Lett.*, 100:062002, 2008.
- [149] C. Bernard et al. Status of the MILC light pseudoscalar meson project. *PoS*, LAT2007:090, 2007.
- [150] S. Durr et al. The ratio  $F_K/F_\pi$  in QCD. *Phys. Rev.*, D81:054507, 2010.
- [151] C. Aubin, Jack Laiho, and Ruth S. Van de Water. The neutral kaon mixing parameter  $B_K$  from unquenched mixed-action lattice QCD. *Phys. Rev.*, D81:014507, 2010.

- [152] C. Kelly, P. A. Boyle, and C. T. Sachrajda. Continuum results for light hadrons from 2+1 flavor DWF ensembles. *PoS*, LAT2009:087, 2009.
- [153] J. C. Hardy and I. S. Towner. Superaligned  $0^+$  to  $0^+$  nuclear beta decays: A new survey with precision tests of the conserved vector current hypothesis and the standard model. *Phys. Rev.*, C79:055502, 2009.
- [154] Mario Antonelli et al. Flavor Physics in the Quark Sector. *Phys. Rept.*, 494:197–414, 2010.
- [155] E. Barberio et al. Averages of  $b$ -hadron and  $c$ -hadron Properties at the End of 2007. *arXiv:0808.1297 [hep-ex]*, 2008.
- [156] Claude Amsler et al. Review of particle physics. *Phys. Lett.*, B667:1, 2008.
- [157] Combination of CDF and D0 Results on the Mass of the Top Quark. *arXiv:0903.2503 [hep-ex]*, 2009.
- [158] William J. Marciano. Precise determination of  $|V_{us}|$  from lattice calculations of pseudoscalar decay constants. *Phys. Rev. Lett.*, 93:231803, 2004.
- [159] Vincenzo Cirigliano and Ignasi Rosell.  $\pi/K \rightarrow e\nu$  branching ratios to  $O(e^2 p^4)$  in Chiral Perturbation Theory. *JHEP*, 10:005, 2007.
- [160] Vincenzo Cirigliano and Ignasi Rosell. Two-loop effective theory analysis of  $\pi (K) \rightarrow e\bar{\nu}_e [\gamma]$  branching ratios. *Phys. Rev. Lett.*, 99:231801, 2007.
- [161] M. Antonelli et al. An evaluation of  $|V_{us}|$  and precise tests of the Standard Model from world data on leptonic and semileptonic kaon decays. *Eur. Phys. J.*, C69:399–424, 2010.
- [162] Roger Decker and Markus Finkemeier. Short and long distance effects in the decay  $\tau \rightarrow \pi\nu_\tau (\gamma)$ . *Nucl. Phys.*, B438:17–53, 1995.
- [163] Roger Decker and Markus Finkemeier. Radiative corrections to the decay  $\tau \rightarrow \pi\nu_\tau$ . *Nucl. Phys. Proc. Suppl.*, 40:453–461, 1995.
- [164] William J. Marciano and A. Sirlin. Radiative corrections to  $\pi_{l2}$  decays. *Phys. Rev. Lett.*, 71:3629–3632, 1993.
- [165] G. M. de Divitiis, R. Petronzio, and N. Tantalo. Quenched lattice calculation of semileptonic heavy-light meson form factors. *JHEP*, 10:062, 2007.
- [166] Precision electroweak measurements on the Z resonance. *Phys. Rept.*, 427:257–454, 2006.
- [167] G. Degrandi and P. Slavich. QCD Corrections in two-Higgs-doublet extensions of the Standard Model with Minimal Flavor Violation. *Phys. Rev.*, D81:075001, 2010.

- [168] Andrzej J. Buras, Diego Guadagnoli, and Gino Isidori. On  $\epsilon_K$  beyond lowest order in the Operator Product Expansion. *Phys. Lett.*, B688:309–313, 2010.
- [169] Bernard Aubert et al. Measurements of Charged Current Lepton Universality and  $|V_{us}|$  using Tau Lepton Decays to  $e^-\bar{\nu}_e\nu_\tau$ ,  $\mu^-\bar{\nu}_\mu\nu_\tau$ ,  $\pi^-\nu_\tau$ , and  $K^-\nu_\tau$ . *Phys. Rev. Lett.*, 105:051602, 2010.
- [170] B. I. Eisenstein et al. Precision Measurement of  $B(D^+ \rightarrow \mu^+\nu)$  and the Pseudoscalar Decay Constant  $f_{D^+}$ . *Phys. Rev.*, D78:052003, 2008.
- [171] J. P. Alexander et al. Measurement of  $B(D_s^+ \rightarrow \ell^+\nu)$  and the Decay Constant  $f_{D_s^+}$  From 600  $/pb^{-1}$  of  $e^\pm$  Annihilation Data Near 4170 MeV. *Phys. Rev.*, D79:052001, 2009.
- [172] P. U. E. Onyisi et al. Improved Measurement of Absolute Branching Fraction of  $D_s \rightarrow \tau\nu$ . *Phys. Rev.*, D79:052002, 2009.
- [173] P. Naik et al. Measurement of the Pseudoscalar Decay Constant  $f_{D_s}$  Using  $D_s^+ \rightarrow \tau^+\nu$ ,  $\tau^+ \rightarrow \rho^+\bar{\nu}$  Decays. *Phys. Rev.*, D80:112004, 2009.
- [174] J. P. Lees et al. Measurement of the Branching Fraction for  $D_s^+ \rightarrow \tau^+\nu_\tau$  and Extraction of the Decay Constant  $f_{D_s}$ . *arXiv:1003.3063 [hep-ex]*, 2010.
- [175] Jonathan L. Rosner and Sheldon Stone. Leptonic Decays of Charged Pseudoscalar Mesons. *arXiv:1002.1655 [hep-ex]*, 2010.
- [176] L. Widhalm et al. Measurement of  $B(D_s \rightarrow \mu\nu)$ . *Phys. Rev. Lett.*, 100:241801, 2008.
- [177] F. Ambrosino et al. Measurement of the  $K_L \rightarrow \pi\mu\nu$  form factor parameters with the KLOE detector. *JHEP*, 12:105, 2007.
- [178] E. Abouzaid et al. Dispersive analysis of  $K_{L\mu 3}$  and  $K_{Le 3}$  scalar and vector form factors using KTeV data. *Phys. Rev.*, D81:052001, 2010.
- [179] B. Aubert et al. Measurement of the Semileptonic Decays  $B \rightarrow D\tau^-\bar{\mu}_\tau$  and  $B \rightarrow D^*\tau^-\bar{\nu}_\tau$ . *Phys. Rev.*, D79:092002, 2009.
- [180] A. Bozek et al. Observation of  $B^+ \rightarrow \bar{D}^{*0}\tau + \nu_\tau$  and Evidence for  $B^+ \rightarrow \bar{D}^0\tau + \nu_\tau$  at Belle. *Phys. Rev.*, D82:072005, 2010.
- [181] I. Adachi et al. Measurement of  $B \rightarrow D^*\tau\nu$  using full reconstruction tags. *arXiv:0910.4301 [hep-ex]*, 2009.
- [182] J. Alcaraz. Precision Electroweak Measurements and Constraints on the Standard Model. *arXiv:0911.2604 [hep-ex]*, 2009.
- [183] A. Pich. Tau Physics: Theory Overview. *Nucl. Phys. Proc. Suppl.*, 181-182:300–305, 2008.

- [184] A. Pich. Tau physics. *Adv. Ser. Direct. High Energy Phys.*, 15:453–492, 1998.
- [185] Antonio Pich and Joao P. Silva. Constraining new interactions with leptonic  $\tau$  decays. *Phys. Rev.*, D52:4006–4018, 1995.
- [186] W. J. Marciano and A. Sirlin. Electroweak Radiative Corrections to tau Decay. *Phys. Rev. Lett.*, 61:1815–1818, 1988.
- [187] Andrzej J. Buras, Piotr H. Chankowski, Janusz Rosiek, and Lucja Slawianowska.  $\Delta M_{d,s}, B_{d,s}^0 \rightarrow \mu^+ \mu^-$  and  $B \rightarrow X_s \gamma$  in supersymmetry at large  $\tan \beta$ . *Nucl. Phys.*, B659:3, 2003.
- [188] A. G. Akeroyd and S. Recksiegel. The effect of  $H^\pm$  on  $B^\pm \rightarrow \tau^\pm \nu_\tau$  and  $B^\pm \rightarrow \mu^\pm \nu_\mu$ . *J. Phys.*, G29:2311–2317, 2003.
- [189] Gustavo Burdman, J. Terrance Goldman, and Daniel Wyler. Radiative Leptonic Decays of Heavy Mesons. *Phys. Rev.*, D51:111–117, 1995.
- [190] Jernej F. Kamenik and Federico Mescia.  $B \rightarrow D\tau\nu$  Branching Ratios: Opportunity for Lattice QCD and Hadron Colliders. *Phys. Rev.*, D78:014003, 2008.
- [191] Ulrich Nierste, Stephanie Trine, and Susanne Westhoff. Charged-Higgs effects in a new  $B \rightarrow D\tau\nu$  differential decay distribution. *Phys. Rev.*, D78:015006, 2008.
- [192] C. G. Callan and S. B. Treiman. Equal Time Commutators and K Meson Decays. *Phys. Rev. Lett.*, 16:153–157, 1966.
- [193] Roger F. Dashen and M. Weinstein. Theorem on the form-factors in  $K_{l3}$  decay. *Phys. Rev. Lett.*, 22:1337–1340, 1969.
- [194] J. Gasser and H. Leutwyler. Low-Energy Expansion of Meson Form-Factors. *Nucl. Phys.*, B250:517–538, 1985.
- [195] Emilie Passemar. Precision SM calculations and theoretical interests beyond the SM in  $K_{l2}$  and  $K_{l3}$  decays. *PoS*, KAON09:024, 2009.
- [196] Veronique Bernard, Micaela Oertel, Emilie Passemar, and Jan Stern.  $K_{\mu 3}^L$  decay: A stringent test of right-handed quark currents. *Phys. Lett.*, B638:480–486, 2006.
- [197] A. Lai et al. Measurement of  $K_{\mu 3}^0$  form factors. *Phys. Lett.*, B647:341–350, 2007.
- [198] J. Bernabeu, A. Pich, and A. Santamaria.  $\Gamma(Z \rightarrow B\bar{B})$ : A Signature of Hard Mass Terms for a Heavy Top. *Phys. Lett.*, B200:569, 1988.
- [199] J. Bernabeu, A. Pich, and A. Santamaria. Top quark mass from radiative corrections to the  $Z \rightarrow b\bar{b}$  decay. *Nucl. Phys.*, B363:326–344, 1991.

- [200] Howard E. Haber and Heather E. Logan. Radiative corrections to the  $Zb\bar{b}$  vertex and constraints on extended Higgs sectors. *Phys. Rev.*, D62:015011, 2000.
- [201] J. H. Field. Indications for an anomalous righthanded coupling of the b-quark from a model independent analysis of LEP and SLD data on Z decays. *Mod. Phys. Lett.*, A13:1937–1954, 1998.
- [202] K. G. Chetyrkin, Johann H. Kuhn, and A. Kwiatkowski. QCD corrections to the  $e^+e^-$  cross-section and the Z boson decay rate: Concepts and results. *Phys. Rept.*, 277:189–281, 1996.
- [203] J. M. Gerard, W. Grimus, Amitava Raychaudhuri, and G. Zoupanos. Super Kobayashi-Maskawa CP Violation. *Phys. Lett.*, B140:349, 1984.
- [204] F. Gabbiani, E. Gabrielli, A. Masiero, and L. Silvestrini. A complete analysis of FCNC and CP constraints in general SUSY extensions of the standard model. *Nucl. Phys.*, B477:321–352, 1996.
- [205] Andrzej J. Buras, Sebastian Jager, and Jorg Urban. Master formulae for  $\Delta F = 2$  NLO-QCD factors in the standard model and beyond. *Nucl. Phys.*, B605:600–624, 2001.
- [206] D. Becirevic et al.  $B_d - \bar{B}_d$  mixing and the  $B_d \rightarrow J/\psi K_s$  asymmetry in general SUSY models. *Nucl. Phys.*, B634:105–119, 2002.
- [207] J. Urban, F. Krauss, U. Jentschura, and G. Soff. Next-to-leading order QCD corrections for the  $B^0\bar{B}^0$  mixing with an extended Higgs sector. *Nucl. Phys.*, B523:40–58, 1998.
- [208] Andrzej J. Buras and Diego Guadagnoli. Correlations among new CP violating effects in  $\Delta F = 2$  observables. *Phys. Rev.*, D78:033005, 2008.
- [209] Marco Ciuchini, G. Degrassi, P. Gambino, and G. F. Giudice. Next-to-leading QCD corrections to  $B \rightarrow X_s\gamma$ : Standard model and two-Higgs doublet model. *Nucl. Phys.*, B527:21–43, 1998.
- [210] Francesca Borzumati and Christoph Greub. 2HDMs predictions for  $\bar{B} \rightarrow X_s\gamma$  in NLO QCD. *Phys. Rev.*, D58:074004, 1998.
- [211] Paolo Ciafaloni, Andrea Romanino, and Alessandro Strumia. Two-loop QCD corrections to charged-Higgs-mediated  $b \rightarrow s\gamma$  decay. *Nucl. Phys.*, B524:361–376, 1998.
- [212] Christoph Greub, Tobias Hurth, and Daniel Wyler. Virtual corrections to the decay  $b \rightarrow s\gamma$ . *Phys. Lett.*, B380:385–392, 1996.
- [213] M. Misiak. QCD challenges in radiative B decays. *arXiv:1010.4896 [hep-ph]*, 2010.

- [214] Gil Paz. Theory of Inclusive Radiative B Decays. *arXiv:1011.4953 [hep-ph]*, 2010.
- [215] Tobias Hurth and Mikihiro Nakao. Radiative and Electroweak Penguin Decays of B Mesons. *Ann. Rev. Nucl. Part. Sci.*, 60:645, 2010.
- [216] M. Misiak et al. The first estimate of  $B(\bar{B} \rightarrow X_s \gamma)$  at  $O(\alpha_s^2)$ . *Phys. Rev. Lett.*, 98:022002, 2007.
- [217] D. Asner et al. Averages of b-hadron, c-hadron, and tau-lepton Properties. *arXiv:1010.1589 [hep-ex]*, 2010. Online update available at <http://www.slac.stanford.edu/xorg/hfag>.
- [218] Thomas Becher and Matthias Neubert. Analysis of  $Br(B \rightarrow X_s \gamma)$  at NNLO with a cut on photon energy. *Phys. Rev. Lett.*, 98:022003, 2007.
- [219] Jeppe R. Andersen and Einan Gardi. Radiative B decay spectrum: DGE at NNLO. *JHEP*, 01:029, 2007.
- [220] Zoltan Ligeti, Iain W. Stewart, and Frank J. Tackmann. Treating the b quark distribution function with reliable uncertainties. *Phys. Rev.*, D78:114014, 2008.
- [221] Mikolaj Misiak. QCD Calculations of Radiative B Decays. *arXiv:0808.3134 [hep-ph]*, 2008.
- [222] Michael Benzke, Seung J. Lee, Matthias Neubert, and Gil Paz. Factorization at Subleading Power and Irreducible Uncertainties in  $\bar{B} \rightarrow X_s \gamma$  Decay. *JHEP*, 08:099, 2010.
- [223] Mikolaj Misiak and Matthias Steinhauser. NNLO QCD corrections to the  $B \rightarrow X_s \gamma$  matrix elements using interpolation in mc. *Nucl. Phys.*, B764:62–82, 2007.
- [224] Christian W. Bauer, Zoltan Ligeti, Michael Luke, Aneesh V. Manohar, and Michael Trott. Global analysis of inclusive B decays. *Phys. Rev.*, D70:094017, 2004.
- [225] Paolo Gambino and Mikolaj Misiak. Quark mass effects in  $B \rightarrow X_s \gamma$ . *Nucl. Phys.*, B611:338–366, 2001.
- [226] Christian W. Bauer. Corrections to moments of the photon spectrum in the inclusive decay  $B \rightarrow X_s \gamma$ . *Phys. Rev.*, D57:5611–5619, 1998.
- [227] Matthias Neubert. Renormalization-group improved calculation of the  $B \rightarrow X_s \gamma$  branching ratio. *Eur. Phys. J.*, C40:165–186, 2005.
- [228] Martin Jung, Antonio Pich, and Paula Tuzon. The  $B \rightarrow X_s \gamma$  Rate and CP Asymmetry within the Aligned Two-Higgs-Doublet Model. *Phys. Rev.*, D83:074011, 2011.

- [229] Ahmed Ali, H. Asatrian, and C. Greub. Inclusive decay rate for  $B \rightarrow X_d \gamma$  in next-to-leading logarithmic order and CP asymmetry in the standard model. *Phys. Lett.*, B429:87–98, 1998.
- [230] Tobias Hurth, Enrico Lunghi, and Werner Porod. Untagged  $B \rightarrow X_{s+d} \gamma$  CP asymmetry as a probe for new physics. *Nucl. Phys.*, B704:56–74, 2005.
- [231] Alexander L. Kagan and Matthias Neubert. Direct CP violation in  $B \rightarrow X_s \gamma$  decays as a signature of new physics. *Phys. Rev.*, D58:094012, 1998.
- [232] L. Wolfenstein and Y. L. Wu. CP violation in the decay  $b \rightarrow s \gamma$  in the two Higgs doublet model. *Phys. Rev. Lett.*, 73:2809–2812, 1994.
- [233] G. M. Asatrian, G. K. Egüian, and A. N. Ioannisian. CP-violation in b quark radiative inclusive decays. *Phys. Lett.*, B399:303–311, 1997.
- [234] Alexander Lenz and Ulrich Nierste. Theoretical update of  $B_s - \bar{B}_s$  mixing. *JHEP*, 06:072, 2007.
- [235] V. M. Abazov et al. Search for CP violation in semileptonic  $B_s$  decays. *Phys. Rev.*, D82:012003, 2010.
- [236] V. M. Abazov et al. Lifetime difference and CP-violating phase in the  $B_s^0$  system. *Phys. Rev. Lett.*, 98:121801, 2007.
- [237] T. Aaltonen et al. First Flavor-Tagged Determination of Bounds on Mixing-Induced CP Violation in  $B_s^0 \rightarrow J/\psi \phi$  Decays. *Phys. Rev. Lett.*, 100:161802, 2008.
- [238] V. M. Abazov et al. Measurement of  $B_s^0$  mixing parameters from the flavor-tagged decay  $B_s^0 \rightarrow J/\psi \phi$ . *Phys. Rev. Lett.*, 101:241801, 2008.
- [239] Heather E. Logan and Deanna MacLennan. Charged Higgs phenomenology in the lepton-specific two Higgs doublet model. *Phys. Rev.*, D79:115022, 2009.
- [240] Heather E. Logan and Deanna MacLennan. Charged Higgs phenomenology in the flipped two Higgs doublet model. *Phys. Rev.*, D81:075016, 2010.
- [241] A. G. Akeroyd, Chuan Hung Chen, and S. Recksiegel. Measuring  $B^\pm \rightarrow \tau^\pm \nu$  and  $B_c^\pm \rightarrow \tau^\pm \nu$  at the Z peak. *Phys. Rev.*, D77:115018, 2008.
- [242] A. G. Akeroyd and F. Mahmoudi. Constraints on charged Higgs bosons from  $D_s^\pm \rightarrow \mu^\pm \nu$  and  $D_s^\pm \rightarrow \tau^\pm \nu$ . *JHEP*, 04:121, 2009.
- [243] Gabriela Barenboim, Paride Paradisi, Oscar Vives, Enrico Lunghi, and Werner Porod. Light charged Higgs at the beginning of the LHC era. *JHEP*, 04:079, 2008.

- [244] Rick S. Gupta and James D. Wells. Next Generation Higgs Bosons: Theory, Constraints and Discovery Prospects at the Large Hadron Collider. *Phys. Rev.*, D81:055012, 2010.
- [245] M. Bona et al. SuperB: A High-Luminosity Asymmetric  $e^+e^-$  Super Flavor Factory. Conceptual Design Report. *arXiv:0709.0451 [hep-ex]*, 2007.
- [246] A. G. Akeroyd et al. Physics at super  $B$  factory. *arXiv:hep-ex/0406071*, 2004.
- [247] Y. H. Ahn and Chuan-Hung Chen. New charged Higgs effects on  $\Gamma_{K_{e2}}/\Gamma_{K_{\mu 2}}$ ,  $f_{D_s}$  and  $\mathcal{B}(B^+ \rightarrow \tau^+\nu)$  in the Two-Higgs-Doublet model. *Phys. Lett.*, B690:57–61, 2010.
- [248] Anjan S. Joshipura and Bhavik P. Kodrani. Fermion number conservation and two Higgs doublet models without tree level flavour changing neutral currents. *Phys. Rev.*, D82:115013, 2010.
- [249] Paul Langacker. Structure of the standard model. *arXiv:HEP-PH/0304186*, 1995.
- [250] E. C. G. Stueckelberg. Interaction forces in electrodynamics and in the field theory of nuclear forces. *Helv. Phys. Acta*, 11:299–328, 1938.
- [251] Peter W. Higgs. Broken symmetries, massless particles and gauge fields. *Phys. Lett.*, 12:132–133, 1964.
- [252] Peter W. Higgs. Broken symmetries and the masses of gauge bosons. *Phys. Rev. Lett.*, 13:508–509, 1964.
- [253] Peter W. Higgs. Spontaneous Symmetry Breakdown without Massless Bosons. *Phys. Rev.*, 145:1156–1163, 1966.
- [254] G. S. Guralnik, C. R. Hagen, and T. W. B. Kibble. Global conservation laws and massless particles. *Phys. Rev. Lett.*, 13:585–587, 1964.
- [255] F. Englert and R. Brout. Broken symmetry and the mass of gauge vector mesons. *Phys. Rev. Lett.*, 13:321–322, 1964.
- [256] Boris Kors and Pran Nath. A Stueckelberg extension of the standard model. *Phys. Lett.*, B586:366–372, 2004.
- [257] Daniel Feldman, Zuowei Liu, and Pran Nath. Probing a Very Narrow  $Z'$  Boson with CDF and D0 Data. *Phys. Rev. Lett.*, 97:021801, 2006.
- [258] Daniel Feldman, Zuowei Liu, and Pran Nath. The Stueckelberg  $Z'$  extension with kinetic mixing and milli-charged dark matter from the hidden sector. *Phys. Rev.*, D75:115001, 2007.
- [259] Paul Langacker. The Physics of Heavy  $Z'$  Gauge Bosons. *Rev. Mod. Phys.*, 81:1199–1228, 2009.

- [260] Marcela S. Carena, Alejandro Daleo, Bogdan A. Dobrescu, and Timothy M. P. Tait.  $Z'$  gauge bosons at the Tevatron. *Phys. Rev.*, D70:093009, 2004.
- [261] Grigoris Panotopoulos and Paula Tuzon. The physics of a new gauge boson in a Stueckelberg extension of the two-Higgs-doublet model. *arXiv:1102.5726 [hep-ph]*, 2011.
- [262] Ignatios Antoniadis, E. Kiritsis, and T. N. Tomaras. A D-brane alternative to unification. *Phys. Lett.*, B486:186–193, 2000.
- [263] D. Bailin, G. V. Kraniotis, and A. Love. Supersymmetric standard models on D-branes. *Phys. Lett.*, B502:209–215, 2001.
- [264] Luis E. Ibanez, F. Marchesano, and R. Rabadan. Getting just the standard model at intersecting branes. *JHEP*, 11:002, 2001.
- [265] Christos Kokorelis. GUT model hierarchies from intersecting branes. *JHEP*, 08:018, 2002.
- [266] Christos Kokorelis. New standard model vacua from intersecting branes. *JHEP*, 09:029, 2002.
- [267] Mirjam Cvetič, Paul Langacker, and Gary Shiu. Phenomenology of a three-family standard-like string model. *Phys. Rev.*, D66:066004, 2002.
- [268] D. Bailin, G. V. Kraniotis, and A. Love. New standard-like models from intersecting D4-branes. *Phys. Lett.*, B547:43–50, 2002.
- [269] Christos Kokorelis. Exact standard model structures from intersecting branes. *arXiv:hep-th/0210004*, 2002.
- [270] D. Bailin, G. V. Kraniotis, and A. Love. Standard-like models from intersecting D5-branes. *Phys. Lett.*, B553:79–86, 2003.
- [271] I. Antoniadis, E. Kiritsis, J. Rizos, and T. N. Tomaras. D-branes and the standard model. *Nucl. Phys.*, B660:81–115, 2003.
- [272] Pascal Anastasopoulos. 4D anomalous  $U(1)$ 's, their masses and their relation to 6D anomalies. *JHEP*, 08:005, 2003.
- [273] Pascal Anastasopoulos. Anomalous  $U(1)$ s masses in non-supersymmetric open string vacua. *Phys. Lett.*, B588:119–126, 2004.
- [274] Michael B. Green and John H. Schwarz. Anomaly Cancellation in Supersymmetric D=10 Gauge Theory and Superstring Theory. *Phys. Lett.*, B149:117–122, 1984.
- [275] Michael B. Green and John H. Schwarz. The Hexagon Gauge Anomaly in Type I Superstring Theory. *Nucl. Phys.*, B255:93–114, 1985.

- [276] Augusto Sagnotti. A Note on the Green-Schwarz mechanism in open string theories. *Phys. Lett.*, B294:196–203, 1992.
- [277] Luis E. Ibanez, R. Rabadan, and A. M. Uranga. Anomalous U(1)’s in type I and type IIB  $D = 4$ ,  $N = 1$  string vacua. *Nucl. Phys.*, B542:112–138, 1999.
- [278] E. Kiritsis and Pascal Anastasopoulos. The anomalous magnetic moment of the muon in the D-brane realization of the standard model. *JHEP*, 05:054, 2002.
- [279] D. M. Ghilencea, L. E. Ibanez, N. Irges, and F. Quevedo. TeV-Scale  $Z'$  Bosons from D-branes. *JHEP*, 08:016, 2002.
- [280] D. M. Ghilencea. U(1) masses in intersecting  $D^-$  brane SM - like models. *Nucl. Phys.*, B648:215–230, 2003.
- [281] Claudio Coriano', Nikos Irges, and Elias Kiritsis. On the effective theory of low scale orientifold string vacua. *Nucl. Phys.*, B746:77–135, 2006.
- [282] Nikos Irges, Claudio Coriano, and Simone Morelli. Stueckelberg axions and the effective action of anomalous Abelian models. II: A  $SU(3)_C \times SU(2)_W \times U(1)_Y \times U(1)_B$  model and its signature at the LHC. *Nucl. Phys.*, B789:133–174, 2008.
- [283] Jason Kumar, Arvind Rajaraman, and James D. Wells. Probing the Green-Schwarz Mechanism at the Large Hadron Collider. *Phys. Rev.*, D77:066011, 2008.
- [284] Roberta Armillis, Claudio Coriano', Marco Guzzi, and Simone Morelli. An Anomalous Extra Z Prime from Intersecting Branes with Drell-Yan and Direct Photons at the LHC. *Nucl. Phys.*, B814:156–179, 2009.
- [285] Ignatios Antoniadis, Alexey Boyarsky, Sam Espahbodi, Oleg Ruchayskiy, and James D. Wells. Anomaly driven signatures of new invisible physics at the Large Hadron Collider. *Nucl. Phys.*, B824:296–313, 2010.
- [286] Claudio Coriano and Marco Guzzi. Axions from Intersecting Branes and Decoupled Chiral Fermions at the Large Hadron Collider. *Nucl. Phys.*, B826:87–147, 2010.
- [287] CDMS et al. Combined Limits on WIMPs from the CDMS and EDELWEISS Experiments. 2011.
- [288] Kingman Cheung, Kuo-Hsing Tsao, and Tzu-Chiang Yuan. Hidden Sector Dirac Dark Matter, Stueckelberg  $Z'$  Model and the CDMS and XENON Experiments. 2010.
- [289] Vernon D. Barger and K. Whisnant. Heavy Z boson decays to two bosons in E(6) superstring models. *Phys. Rev.*, D36:3429, 1987.
- [290] Daniel Feldman, Zuowei Liu, and Pran Nath. The Stueckelberg Z Prime at the LHC: Discovery Potential, Signature Spaces and Model Discrimination. *JHEP*, 11:007, 2006.

- 
- [291] Boris Kors and Pran Nath. Aspects of the Stueckelberg extension. *JHEP*, 07:069, 2005.
- [292] O. C. Anoka, K. S. Babu, and I. Gogoladze. Constraining  $Z'$  from supersymmetry breaking. *Nucl. Phys.*, B687:3–30, 2004.
- [293] A. Aydemir, H. Arslan, and A. K. Topaksu. The estimation of the  $Z'$  gauge boson mass in  $E_6$  models. *Phys. Part. Nucl. Lett.*, 6:304–308, 2009.
- [294] Andrzej J. Buras, Piotr H. Chankowski, Janusz Rosiek, and Lucja Slawianowska.  $\Delta M_s/\Delta M_d$ ,  $\sin 2\beta$  and the angle  $\gamma$  in the presence of new  $\Delta F = 2$  operators. *Nucl. Phys.*, B619:434–466, 2001.
- [295] D. Becirevic, V. Gimenez, G. Martinelli, M. Papinutto, and J. Reyes. B-parameters of the complete set of matrix elements of  $\Delta B = 2$  operators from the lattice. *JHEP*, 04:025, 2002.
- [296] Andrzej J. Buras, Matthias Jamin, and Peter H. Weisz. Leading and next-to-leading QCD corrections to  $\epsilon$ -parameter and  $B^0 - \bar{B}^0$  mixing in the presence of a heavy top quark. *Nucl. Phys.*, B347:491–536, 1990.
- [297] Stefan Herrlich and Ulrich Nierste. The Complete  $|\Delta S| = 2$  Hamiltonian in the Next-To- Leading Order. *Nucl. Phys.*, B476:27–88, 1996.

# Acknowledgements

Primer vull agrair al meu director de tesi, Toni Pich, la seua dedicació i confiança; per compartir amb mi tant de coneixement (que no és poc) i de tanta qualitat, una visió de la física tan simple només la pot assolir aquell que ha passat fonament per tot allò complexe. De manera anecdòtica, vull deixar també constància ara i ací que, a banda d'haver adquirit, gràcies a ell, certa habilitat en la fenomenologia de partícules, també he desenvolupat, a força de supervivència, un agut sentit de l'oïda capaç de diferenciar el soroll que fa la porta de Jorge quan s'obri de la seua. Per tot i per més, gràcies. Second, I would like to thank Martin Jung, who worked very hard over my work and did the “dirty job” of being my super-supervisor (a super-hero employment). Thank you also for the personal side, for treating me always as “an equal” and discuss almost everything assuming that I am capable to do it (while sometimes actually I was not). Thank you for the discussions in the blackboard and by Skype, for the tensions, the euphoria, the mistakes, the “discoveries” and (mis)understandings, because only that means research and you have been a wonderful partner.

Vull agrair també a la resta del grup per haver-me acompanyat aquestos anys. Gràcies, Jorge Portolés, per estar sempre disponible i disposat a respondre a les meues preguntes; pels consells i la implicació. Als companys, a Julia, Paola, amiga i companya de tasques divulgatives, per ser tan propera, Martín i Fabio; a Pablo Roig, Natxo, Vicent Mateu i Juanjo, per aparicions espontànies, veus de l'experiència i dubtes resolt; a Francisco, Tracey, Xing Qiang, Petros, Sebastian and (speaking of which) Alenjandro, Isabella and Emilie, great friends, Òscar y Zahara, por las tardes de cotilleos interminables, Alberto, la constante de estos cuatro años. A todos vosotros, gracias por hacer de las comidas ratos imprescindibles.

Fora del grup però dins l'IFIC o el Departament, vull mencionar també a algunes persones. First of all, thanks to Greg Panotopoulos, for our work together, product of a fruitful collaboration. The discussions in my office were really interesting and instructive. We made it! Gràcies a Pepe Bernabéu, pel que fa a l'inici d'aquesta “aventura”, per haver confiat i apostat per mi, per haver-me endinsat on estic ara. A Quico Botella, per l'interés en el nostre treball i els comentaris adients. A Carlos Peña, Germán Rodrigo, Nuria Rius i Pilar, per l'interés.

En la part un poc més personal però sense eixir encara de l'IFIC, vull agrair també: A Joel y Selim, sin duda alguna, las grandes adquisiciones personales de mi doctorado (os disecaré y os pondré en mi vitrina); gracias por los infinitos ratos de ocio y conversaciones, y también, por compartir conmigo vuestra extrema madurez científica, sois excepcionales. Joel, gracias por dedicarme tanto tiempo. Guo, who answered many times many questions I had about Chiral Perturbation Theory, for his friendship and happiness. Esther, a quien arrastré vilmente (junto con algunos otros mencionados aquí) a estresantes ejercicios de teatro, por apoyarme en todas mis propuestas.

Carlos Mayoral, por compartir conmigo las crudas realidades y la necesidad de celebrarlas con cervezas. A los compañeros del máster, por aquel “gran” Sexto de Física.

Outside IFIC, I'd like to thank the people I met during my short stays. First of all, thanks to Vincenzo Cirigliano and Ryuichiro Kitano for giving me the opportunity of writing my first paper with them, I had a great time in Los Alamos. Thanks to Gustavo C. Branco and Margarida Rebelo, for the hospitality during my stay in Lisbon; where I met wonderful people, my friends Nicolás, Catalina, Nuno, Albert, Sergio and David. Finally, I would like to thank Howard Haber, for my stay in Santa Cruz last winter, for the starting collaboration, for being so kind and offering me different opportunities. I also enjoyed my stay with friends from the department, specially, John, Lorenzo and Sebastian, thanks for the good times close to the Pacific.

Antes de pasar a un terreno puramente personal, he de agradecer a dos personas de suma importancia en mi vida, que ajenos a la física, han hecho grandes aportaciones a esta tesis: A Guillermo García por intensos momentos de programación, sin ti esto habría salido unos meses más tarde; gracias por la disponibilidad y por entender estas fórmulas raras tan rápido. Y por supuesto, a Javier Montero, por la programación del día a día, por las dudas compartidas, por las discusiones y la dedicación, por aconsejarme mucho antes de saber que necesitaba consejo, porque contigo todo es mejor y más fácil.

Ja fora del que ha sigut la tesi en sí mateixa, vull començar per esmentar als amics de la carrera, protagonistes dels meus inicis (i jo dels seus) en (intentar) entendre la física (el punt de fusió de l'argent), a eixa família ultra-cohesionada que en sap tant de tot i, de vegades, tan *tautològicament*. Pels sopars dels dijous i les discussions de política, pels comentaris absurds, per a mi sou una retroalimentació imprescindible: Pablo, Alabau, Pere, Carles, Tito, Arnau, Cristóbal, Picó, Aureli, i més... I en especial, a Montse i Regina, perquè tres no són multitud. I a Marina.

Als meus amics no físics, i amb això no vull dir que siguen imaginaris sinó que, de fet, fan de la meua realitat una necessitat molt més completa. A los Andaneros Abueloides, uno por uno, Willy, Lucía, Josemi, Leticia, Elena, Haru, porque vuestra *paranormal* es fundamental en mi vida. A la gent de La Vall, en especial a Nuria, per guardar sempre el seu interès per mi i per tot el que faça sense importar la freqüència en què ens vegem. Al sector Campillos, en especial a Elena y María. A los amigos de Pau, amigos míos también, por los martes o jueves o lunes de pirridos entre chinos y cervezas, por las *friki-series* y las gracias interminables (a Palomitas, por humanizar un poco mis horas de trabajo). A Cecilia, por reírse de mis miserias y hacerme reír a mí también. A Idus o la Tartuguita que come hierba a las orillas del río Ladón, por ponerme siempre los pies en el suelo.

A Marisa y Enrique, por ayudar a nuestra subsistencia con sabrosas comidas, por ser tan humanos y por tener siempre tantas ganas de escucharnos. A Kike y a Noe, por los viajes y las excursiones, por tratarnos las lesiones que este duro trabajo deja en nuestras espaldas, por la cercanía, el interès y los ánimos. A los cuatro, por cuidarnos tanto, por ser tan próximos, a nosotros y a mí.

A la meua família. A ma mare, per la confiança i la força extrema, per la vitalitat i la constància, per ser la primera. A mon pare, per estar-hi sempre, per les xerrades i l'interès enorgullit, a Marisa, per ser partícip de tot això i fer-ne força. A Carlos, la base de muchas de mis decisiones,

por la fuerza que (me) transmites. A mis hermanos Carlos y Elena, por ser eso, mis hermanos. Als meus *tios* Ximo i Sílvia, i a Anna i a Pol, per ser més que família. A la part Tuzón i a la Domínguez, per envoltar-me amb calidesa. Als meus avis, que sempre duré a dintre.

I finalment vull agrair a Pau la seua companyia, amb extraordinària estima, indispensable, insubstituïble, impagable.

Aquesta tesi, en sí mateixa i tot el seu el procés, m'ha ensenyat el que vol dir investigar, m'ha obert portes i m'ha fet adquirir aptituds de comunicació, redacció i estructura de pensament que, de segur, no només em serviran en el context de la ciència. També he desmitificat alguns mites i n'he creat uns altres, com ara la necessitat d'aprendre del que no sabem, transformant la sensació d'estupidesa en un repte de coneixement. He après de la ciència, de la física, la dignitat d'argumentar racionalment i la humilitat de reconèixer els propis límits, la no infal·libilitat, l'honradesa i que, malauradament per a alguns, no és infusa. Gràcies a tots aquells que heu contribuït a que escollira aquest camí.